A Prominent Couple

A Prominent Couple

The *TMPRSS2:ERG* Gene Fusion in Aggressive Prostate Cancer

A Prominent Couple – The *TMPRSS2:ERG* Gene Fusion in Aggressive Prostate Cancer
Leonie Ratz

ISBN 978 94 6159 776 2
Cover design and layout by Leonie Ratz
Printed by Datawyse | Universitaire Pers Maastricht

Cover illustration: collection of silhouettes of men (from shutterstock.inc)

A Prominent Couple

The *TMPRSS2:ERG* Gene Fusion in Aggressive Prostate Cancer

DISSERTATION

to obtain the degree of Doctor at Maastricht University,
on the authority of the Rector Magnificus, Prof. Dr. Rianne M. Letschert
in accordance with the decision of the Board of Deans,
to be defended in public
on Friday, 15th of December 2017, at 13:30 hours

by

Leonie Ratz
born on 23rd of March 1987 in Cologne

SUPERVISORS

Prof. Dr. F. C. S. Ramaekers
Prof. Dr. H. Sültmann (German Cancer Research Center and National Center of Tumor Diseases, Heidelberg)

CO-SUPERVISORS

Privatdozentin Dr. S. M. Klauck (German Cancer Research Center, Heidelberg)
Prof. Dr. P. Altevogt (German Cancer Research Center, Heidelberg)

ASSESSMENT COMMITTEE

Prof. Dr. M. van Engeland (chair)
Prof. Dr. J. Schalken (Radboud University Medical Center, Nijmegen)
Prof. Dr. S. Pahernik (Nuremberg General Hospital, Paracelsus Medical University, Nuremberg)
Prof. Dr. M. Vooijs

FUNDING

This project was supported through intramural funding by the German Cancer Research Center.

CONTENTS

LIST OF ABBREVIATIONS

ACPP	acid phosphatase, prostate
ADT	androgen deprivation therapy
AKT	AKT serine/threonine kinase 1
ALK1	activin receptor like kinase 1
AMACR	alpha-methylacyl-CoA racemase
AR	androgen receptor
AR-V7	androgen receptor splice variant 7
ASCL1	achaete-scute homolog 1
BAMBI	BMP and activin membrane-bound inhibitor
BCA	bicinchoninic acid
BMP	bone morphogenetic protein
bp	base pair
BPH	benign prostate hyperplasia
BSA	bovine serum albumin
CD24	cluster of differentiation 24
CDH1	E-cadherin
CDH2	N-cadherin
CDK1	cyclin-dependent kinase 1
cDNA	complementary DNA
CFU	colony forming units
CHD1	chromodomain helicase DNA binding protein 1
CHGA and B	chromogranin A and B
CK	cytokeratin
CNA	Copy number alteration
Cp	crossing point
CRPC	castration-resistant prostate cancer
CTC	circulating tumor cell
DHT	dihydrotestosterone
DMSO	dimethyl sulfoxide
DNA	deoxyribonucleic acid
DNase	deoxyribunuclease
DNMT	DNA methyltransferase
Dox	doxycycline
EGFR	epidermal growth factor receptor
EMT	epithelial-to-mesenchymal transition
ERG	V-ets erythroblastosis virus E26 homolog (avian)
ERK2	extracellular signal-regulated kinases, alias of MAPK1
Ev	empty vector

FC	fold change
FN1	fibronectin 1
FPKM	fragments per kilobase of exon per million fragments mapped
FZD4	frizzled 4
GAPDH	glyceraldehyde-3-phosphate dehydrogenase
GO	gene ontology
HGPIN	high-grade prostatic intraepithelial neoplasia
HLA-DMB	major histocompatibility complex, class II, DM beta
ICGC-EOPC	International Cancer Genome Consortium-Early Onset PCa project
ID1 and 2	inhibitor of differentiation (1 and 2)
IGP	NGFN IG Prostate Cancer project
INSM1	insulinoma associated-1
IPA	Ingenuity Pathway Analysis
JNK	c-Jun N-terminal kinases
L1CAM	L1 cell adhesion molecule
LRP5 and 6	low-density lipoprotein receptor-related protein 5 and 6
MAPK	mitogen-activated protein kinase
MET	mesenchymal-to-epithelial transition
miR	micro-RNA
MMP	matrix metalloproteinase
MSMB	microseminoprotein beta
MYCN	N-myc proto-oncogene
NCAM	neuronal cell adhesion molecule
NED	neuroendocrine differentiation
NEPC	neuroendocrine prostate cancer
NSE	neuron specific enolase
ORF	open reading frame
p38	alias of MAPK14, mitogen-activated protein kinase 14
pAKT	phospho-AKT
PAP	prostatic acid phosphatase
PCa	prostate cancer
PI3K	phosphatidylinositol 3-kinase
PIN	prostatic intraepithelial neoplasia
PLA1A	phospholipase A1 member A
PLAT	plasminogen activator, tissue type
p-p38	phospho-p38
PSA	prostate specific antigen
pSMAD	phospho-SMAD
qPCR	quantitative reverse transcription PCR
RELN	reelin

REST	RE-1 silencing transcription factor/neuron-restrictive silencer factor (NRSF)
rhALK1	recombinant decoy receptor ALK1
rhFZD4	recombinant decoy receptor FZD4
RPKM	reads per kilobase per million mapped reads
RT-PCR	reverse transcription PCR
SCG3	secretogranin III
siRNA	small interfering RNA
SLC45A3	solute carrier family 45 member 3
SMAD	SMAD family protein
SNAI2	snail family transcriptional repressor 2
SYP	synaptophysin
TCF7L2	T cell factor/lymphoid enhancer 2
TCF/LEF-1	transcription factor/lymphoid enhancer binding factor 1
TCGA	The Cancer Genome Atlas
TDRD1	tudor domain containing 1
T/E	TMPRSS2:ERG
TGF-β	transforming growth factor beta
TGFB1 and 2	TGF-β 1 and 2
TMPRSS2	transmembrane protease, serine 2
TUBB3	tubulin beta 3
VIM	vimentin
VTN	vitronectin
WNT	wingless-type family member
ZEB1	zinc finger E-box binding homeobox 1

General introduction

THE EPIDEMIOLOGY OF PROSTATE CANCER

Prostate cancer (PCa) is the most prevalent non-cutaneous malignancy accounting for 15% of the cancers diagnosed in men [1]. It is the second leading cause of cancer-related death in men in Western countries with 417,000 new cases and 92,000 deaths in 2012 in Europe [1, 2]. Only few risk determinants for the development of PCa have been defined, such as increasing age, ethnic or geographical origin, and family history, while the influence of lifestyle factors is less well-established [3-5]. Increasing age is by far the most important risk factor. Only 30% of all cases are diagnosed under the age of 65 years in the US [6]. The 10-years risk to develop PCa for men aged 30 years is 0.01%, increases to 4.77% for men aged 60 years and to 5.50% for men aged 70 years [6].

In 2014, the highest incidence rates for PCa in the US were in the age group of 65-74 years, while between 1975-1995 the incidence rates were in the group of 75 years or older indicating that the diagnosis is currently made at younger age [7]. The incidence rates for PCa are highly variable between different geographical areas, with highest incidence in industrialized countries [6]. Since autopsy-based detection of PCa revealed similar prevalence rates among different geographical areas, the increasing incidence is significantly associated with the widespread implementation of PSA testing leading to elevated biopsy-based detection rates in asymptomatic patients [8, 9]. The mortality pattern has largely remained unchanged and shows less variation worldwide, as PSA testing has a greater impact on incidence than on mortality [6, 8]. Family history is an important contributing factor for the incidence of PCa (men with affected first-degree relatives are diagnosed 2.48 times (95% confidence interval: 2.25-2.74) more often compared to men with unaffected relatives), and has a higher impact on the incidence rate for men aged <65 years [10].

THE PROSTATIC GLAND

The adult prostatic tissue consists of pseudostratified epithelium with basal, luminal and neuroendocrine (NE) cells, together forming the glandular acini surrounded by a fibro-muscular stromal network. The basal cell layer forms the proliferating compartment characterized by high expression of p63, cytokeratin (CK) 5, 6, 14, 19, glutathione-S-transferase-pi (GSTpi), B-cell lymphoma 2 (Bcl-2), and epidermal growth factor receptor (EGFR) [11, 12]. The basal layer also contains pluripotent stem cells or transit amplifying (TA) cells with limited proliferative capacity that can differentiate into the functional distinct cell types of the prostate and give rise to phenotypically intermediate cells re-presenting different states in the differentiation process [11, 12]. Pluripotent stem cells are maintained by different signaling mechanisms including Notch/Delta, TGF-β and integrin signaling [13]. The differentiation compartment contains secretory luminal

cells, which are the major cell type of the prostate, characterized by expression of CK8 and CK18 [12]. Luminal cells are positive for prostate specific antigen (PSA) and prostatic acid phosphatase (PAP) and show high expression of androgen receptor (AR). The NE cells, that are assumed to derive from the periurogenital paraganglia from the neural crest and invade the developing prostate by week 10 of gestational age, are localized disseminated throughout the prostate epithelium and display dendritic-like extensions [14, 15]. Electron microscopic analysis has revealed a granular morphology of NE cells correlating with the detection of various neurosecretory products including serotonin, histamine and members of the chromogranin/secretogranin peptide family, as well as the NE markers synaptophysin and CD56 (NCAM) [16, 17].

The development of the prostatic gland depends on AR signaling. In the absence of androgens, AR, a steroid hormone receptor, is sequestered in the cytoplasm and bound to a heat shock protein chaperone complex that protects it from proteolysis and maintains a conformational state that is accessible to ligand binding [18]. Androgen signaling is initiated by entering of testosterone into the cell and its conversion to the more potent dihydrotestosterone (DHT) by the enzyme 5α-reductase [19]. Upon binding of DHT to the AR ligand-binding domain, receptor dissociation from the heat shock protein complex, phosphorylation and translocation to the nucleus is induced. Translocation enables binding of the nuclear receptor to androgen response elements (ARE) within target genes by its DNA-binding domain and subsequent recruitment of co-regulatory transcription factors, including histone modifiers (e.g. CBP/p300, NCoR) [20], transcription regulators (e.g. TRAP/DRIP/ARC) and DNA structural modifiers (e.g. SWI/SNF/BRG1) [21]. Assembly of the transcriptional complex initiates gene expression of AR target genes including PSA [22]. Under physiologic conditions, AR signaling is terminated by cyclic assembly/disassembly of the AR-transcription factor complex mediated by the heat shock protein complex [18].

CHALLENGES IN CURRENT DIAGNOSTIC AND THERAPEUTIC MANAGEMENT OF PROSTATE CANCER

PCa is usually suspected based on an elevated PSA value and abnormal digital rectal examination (DRE), but PSA level is not a direct surrogate for tumor stage. Definitive diagnosis requires histopathological evaluation of prostate specimens obtained by systematic transrectal ultrasound (TRUS)-guided biopsy cores [23] (Figure 1). The sensitivity of this technique is limited to 53% and repeat biopsy is recommended to one third of patients with a persistently suspected PCa, which can be very stressful to patients [24, 25]. Prostate biopsies are classified according to the Gleason grading system based on glandular architectural pattern, scored from 1 to 5 with decreasing differentiation, and combining primary and secondary patterns taking into account the morphologic hete-

rogeneity of PCa [26]. The dilemma with the Gleason score is that different histological foci can harbor distinct genetic aberrations leading to heterogeneous clinical outcomes among patients with the same histological pattern [27].

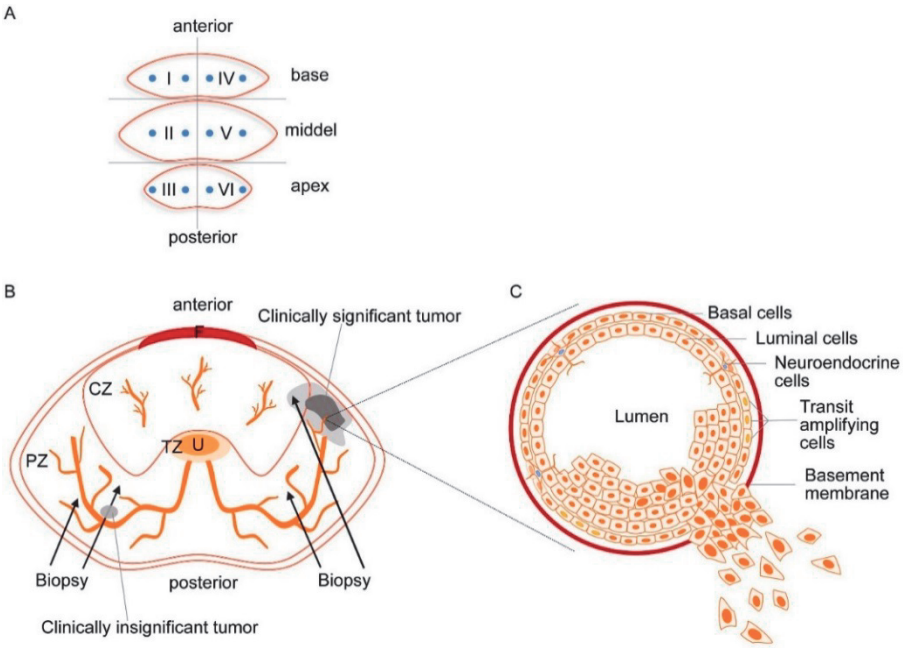

Figure 1: Schematic illustration of the prostate gland. (A) Scheme of prostate biopsy practice. The most commonly used biopsy scheme includes 12 systematically obtained tissue cores covering all parts of the prostate gland. Blue dots represent biopsy cores. (B) Axial cross-section of the prostate. Black arrows indicating ultrasound-guided biopsy. Thirty percent of patients undergoing prostate biopsy will have positive results, of the remaining 70% with negative biopsy 20-30% will have false-negative biopsy due to the systematically yet random biopsy pattern that may miss a clinically significant tumor. In 15% of cases random biopsy cores underscore the tumor grade by detecting clinically insignificant lesion with low Gleason score or by missing the actual extent of the aggressive lesion leading to understaging of the disease. (C) Different cell types within a prostatic duct displaying invading metastatic cancer cells. U – urethra, TZ – transitional zone, CZ – central zone, PZ - peripheral zone, F – fibromuscular stroma.

PCa frequently shows an indolent clinical course with a 2.5-3% lifetime risk of dying from PCa and risk stratification remains a major clinical question [6]. Patients with histologically confirmed PCa are assigned to risk groups based on stage, grade, and PSA value used to predict the probability of biochemical failure after treatment and determine treatment recommendations. Eighty percent of newly diagnosed PCa cases are detected as clinically local disease that can be effectively treated with surgery and radiotherapy or hormone therapy [28, 29]. The 5-year relative survival rate for localized PCa

is 100% [6]. Five percent of men are diagnosed at stage IV PCa or will progress after primary therapy to treatment refractory metastatic disease, with a 5-years survival rate of 29.8% [6]. However, there is uncertainty about the risk of disease progression, since clinicopathologic criteria are insufficient to efficiently distinguish between slow growing and aggressive non-indolent tumors. Identifying biomarkers that predict clinically aggressive PCa and metastatic dissemination is a current challenge for PCa translational research to reduce overtreatment of insignificant disease on the one hand and select patients that are at risk of progressive disease and need aggressive treatment on the other hand.

Characterization of the cancer genome, epigenome and transcriptome of prostate cancer patients can provide important insights into the biological properties of PCa cells. PCa is a genomically complex disease and the molecular mechanisms and implications for disease outcome of distinct genomic aberrations are poorly understood. Identification of the specific molecular profiles that promote tumor aggressiveness is essential to predict the risk of clinically significant disease. Functional characterization of biological processes involved in therapy resistance could identify novel targets to improve therapy management.

AIM AND OUTLINE OF THE THESIS

My work aims to identify novel molecular mechanisms of aggressive PCa and to functionally characterize promising driver genes. The focus is on the role of the *TMPRSS2:ERG* gene fusion, the most prevalent genomic alteration in PCa present in approximately 50% of all PCa cases. The *TMPRSS2:ERG* gene fusion, resulting from the fusion of *ERG* (v-ets erythroblastosis virus E26 homolog (avian)) to the androgen responsive gene *TMPRSS2*, leads to upregulation of ERG protein and activation of downstream target genes [30]. The expression of fusion mRNAs from distinct *TMPRSS2:ERG* variants is associated with clinicopathological parameters, while the underlying molecular processes resulting from expression of T/E gene fusion variants remain unclear.

Chapter 1 provides an overview of the diverse molecular alterations that have been identified in the aggressive prostate cancer genome. Further, the progress towards the clinical implementation of selected molecular targets will be highlighted. In chapter 2, the gene expression and signaling alterations and their functional implications caused by the *TMPRSS2:ERG* gene fusion will be analysed. Using a doxycycline (Dox)-inducible overexpression cell model, we show that the TGF-β/BMP as well as the WNT/β-catenin signaling pathways are the molecular determinants underlying *TMPRSS2:ERG*-mediated epithelial-to-mesenchymal transition (EMT) in PCa cells. The global epigenetic alterations induced by the *TMPRSS2:ERG* gene fusion will be explored in chapter 3. Hy-

pomethylation correlates with upregulation of *FZD4* and *HLA-DMB*. In chapter 4, a candidate gene selection approach from expression profiling and RNA-sequencing data of PCa patient tumor samples is used to identify and functionally characterize PCa-relevant genes. The neuronal transcription factor insulinoma-associated 1 (*INSM1*) is identified as a regulator of a NE network in prostate cancer cell lines. Neuroendocrine prostate cancer (NEPC) is considered as a highly aggressive manifestation of advanced PCa. We show that the *TMPRSS2:ERG* gene fusion is associated with NE characteristics in prostate cancer cell lines. We further show that a regulatory network of neuronal transcription factors promotes a NE phenotype in PCa cell lines that could be mediated by the Reelin signaling pathway. We suggest that the *INSM1* could be an important driver of this NE network and should be considered for future biomarker studies or drug development.

REFERENCES

1. Ferlay J, Steliarova-Foucher E, Lortet-Tieulent J, Rosso S, Coebergh JW, Comber H, Forman D and Bray F. Cancer incidence and mortality patterns in Europe: estimates for 40 countries in 2012. Eur J Cancer. 2013; 49(6):1374-1403.
2. Torre LA, Bray F, Siegel RL, Ferlay J, Lortet-Tieulent J and Jemal A. Global cancer statistics, 2012. CA Cancer J Clin. 2015; 65(2):87-108.
3. Cuzick J, Thorat MA, Andriole G, Brawley OW, Brown PH, Culig Z, Eeles RA, Ford LG, Hamdy FC, Holmberg L, Ilic D, Key TJ, La Vecchia C, Lilja H, Marberger M, Meyskens FL, et al. Prevention and early detection of prostate cancer. Lancet Oncol. 2014; 15(11):e484-492.
4. Loeb S and Schaeffer EM. Risk factors, prevention and early detection of prostate cancer. Prim Care. 2009; 36(3):603-621.
5. Williams SB, Salami S, Regan MM, Ankerst DP, Wei JT, Rubin MA, Thompson IM and Sanda MG. Selective detection of histologically aggressive prostate cancer: an Early Detection Research Network Prediction model to reduce unnecessary prostate biopsies with validation in the Prostate Cancer Prevention Trial. Cancer. 2012; 118(10):2651-2658.
6. Howlader N NA, Krapcho M, Miller D, Bishop K, Kosary CL, Yu M, Ruhl J, Tatalovich Z, Mariotto A, Lewis DR, Chen HS, Feuer EJ, Cronin KA (eds). (2017). SEER Cancer Statistics Review, 1975-2014. National Cancer Institute. Bethesda, MD, USA).
7. Stanford JL, Stephenson RA, Coyle LM, Cerhan J, Correa R, Eley JW, Gilliland F, Hankey B, Kolonel LN, Kosary C, Ross R, Severson R and D. W. (1999). Prostate Cancer Trends 1973-1995, SEER Program National Cancer Institute. (Bethesda, USA: National Cancer Institute (NCI)).
8. Center MM, Jemal A, Lortet-Tieulent J, Ward E, Ferlay J, Brawley O and Bray F. International variation in prostate cancer incidence and mortality rates. Eur Urol. 2012; 61(6):1079-1092.
9. Breslow N, Chan CW, Dhom G, Drury RA, Franks LM, Gellei B, Lee YS, Lundberg S, Sparke B, Sternby NH and Tulinius H. Latent carcinoma of prostate at autopsy in seven areas. The International Agency for Research on Cancer, Lyons, France. Int J Cancer. 1977; 20(5):680-688.
10. Kicinski M, Vangronsveld J and Nawrot TS. An epidemiological reappraisal of the familial aggregation of prostate cancer: a meta-analysis. PLoS One. 2011; 6(10):e27130.
11. Letellier G, Perez MJ, Yacoub M, Levillain P, Cussenot O and Fromont G. Epithelial phenotypes in the developing human prostate. J Histochem Cytochem. 2007; 55(9):885-890.
12. Wang Y, Hayward S, Cao M, Thayer K and Cunha G. Cell differentiation lineage in the prostate. Differentiation. 2001; 68(4-5):270-279.
13. Hudson DL. Epithelial stem cells in human prostate growth and disease. Prostate Cancer Prostatic Dis. 2004; 7(3):188-194.
14. Epstein JI, Amin MB, Beltran H, Lotan TL, Mosquera JM, Reuter VE, Robinson BD, Troncoso P and Rubin MA. Proposed morphologic classification of prostate cancer with neuroendocrine differentiation. Am J Surg Pathol. 2014; 38(6):756-767.
15. Aumuller G, Leonhardt M, Janssen M, Konrad L, Bjartell A and Abrahamsson PA. Neurogenic origin of human prostate endocrine cells. Urology. 1999; 53(5):1041-1048.
16. Szczyrba J, Niesen A, Wagner M, Wandernoth PM, Aumuller G and Wennemuth G. Neuroendocrine Cells of the Prostate Derive from the Neural Crest. J Biol Chem. 2017; 292(5):2021-2031.
17. Abbas F, Civantos F, Benedetto P and Soloway MS. Small cell carcinoma of the bladder and prostate. Urology. 1995; 46(5):617-630.
18. Prescott J and Coetzee GA. Molecular chaperones throughout the life cycle of the androgen receptor. Cancer Lett. 2006; 231(1):12-19.
19. Feldman BJ and Feldman D. The development of androgen-independent prostate cancer. Nat Rev Cancer. 2001; 1(1):34-45.

20. Chakravarti D, LaMorte VJ, Nelson MC, Nakajima T, Schulman IG, Juguilon H, Montminy M and Evans RM. Role of CBP/P300 in nuclear receptor signalling. Nature. 1996; 383(6595):99-103.
21. Chmelar R, Buchanan G, Need EF, Tilley W and Greenberg NM. Androgen receptor coregulators and their involvement in the development and progression of prostate cancer. Int J Cancer. 2007; 120(4):719-733.
22. McKenna NJ, Lanz RB and O'Malley BW. Nuclear receptor coregulators: cellular and molecular biology. Endocr Rev. 1999; 20(3):321-344.
23. Hendriks RJ, van Oort IM and Schalken JA. Blood-based and urinary prostate cancer biomarkers: a review and comparison of novel biomarkers for detection and treatment decisions. Prostate Cancer Prostatic Dis. 2017; 20(1):12-19.
24. Nevoux P, Ouzzane A, Ahmed HU, Emberton M, Montironi R, Presti JC, Jr. and Villers A. Quantitative tissue analyses of prostate cancer foci in an unselected cystoprostatectomy series. BJU Int. 2012; 110(4):517-523.
25. Haas GP, Delongchamps NB, Jones RF, Chandan V, Serio AM, Vickers AJ, Jumbelic M, Threatte G, Korets R, Lilja H and de la Roza G. Needle biopsies on autopsy prostates: sensitivity of cancer detection based on true prevalence. J Natl Cancer Inst. 2007; 99(19):1484-1489.
26. Gordetsky J and Epstein J. Grading of prostatic adenocarcinoma: current state and prognostic implications. Diagn Pathol. 2016; 11:25.
27. Andreoiu M and Cheng L. Multifocal prostate cancer: biologic, prognostic, and therapeutic implications. Hum Pathol. 2010; 41(6):781-793.
28. Penney KL, Stampfer MJ, Jahn JL, Sinnott JA, Flavin R, Rider JR, Finn S, Giovannucci E, Sesso HD, Loda M, Mucci LA and Fiorentino M. Gleason grade progression is uncommon. Cancer Res. 2013; 73(16):5163-5168.
29. Miller DC, Hafez KS, Stewart A, Montie JE and Wei JT. Prostate carcinoma presentation, diagnosis, and staging: an update form the National Cancer Data Base. Cancer. 2003; 98(6):1169-1178.
30. Tomlins SA, Laxman B, Varambally S, Cao X, Yu J, Helgeson BE, Cao Q, Prensner JR, Rubin MA, Shah RB, Mehra R and Chinnaiyan AM. Role of the TMPRSS2-ERG gene fusion in prostate cancer. Neoplasia. 2008; 10(2):177-188.

Chapter 1

The biology of aggressive prostate cancer: Implications for innovative diagnostics and therapy

Partly published in:

Novel RNA markers in prostate cancer: functional considerations and clinical translation. Pickl JM, Heckmann D, Ratz L, Klauck SM, Sültmann H. Biomed Res Int. 2014;2014:765207. doi: 10.1155/2014/765207.

In preparation for submission as review by:

Ratz L, Klauck SM, Sültmann H

THE PATHOGENESIS AND PROGRESSION OF PROSTATE CANCER

The human prostate can be divided into distinct anatomical zones (peripheral, central, and periurethral transitional zone, and the non-glandular anterior fibromuscular stroma). The histological division of the prostate into the different zones is of clinical relevance since the majority of prostate cancers are located in the peripheral zone (PZ), while benign prostate hyperplasia (BPH), a condition in which proliferation of prostatic cells causes significant discomfort and complications, occurs mainly in the transitional zone (TZ) [1, 2]. Tumors in the PZ have been found to be less differentiated with higher Gleason scores, and more invasive showing capsule infiltration at a smaller tumor volume [1]. Local variation in intercellular signaling and gene expression might play a role in this zonal occurrence [3].

The majority of prostate cancers are adenocarcinomas arising from multifocal hyperplasia of luminal secretory cells within acinar or ductal structures [4]. Luminal cancerous cells display aberrant morphological characteristics including nuclear enlargement, hyperchromasia, and prominent nucleoli that gradually increase during malignant transition [5]. The continuum of morphological changes, ranging from low-grade dysplasia to carcinoma in situ, are collectively described as prostatic intraepithelial neoplasia (PIN) [6]. High-grade PIN (HGPIN), occurring with increased incidence and severity with increasing age, is considered as a premalignant condition of most prostate adenocarcinomas and was found as histological predictor of PCa [7-9]. The morphological, immunohistochemical and molecular changes observed in HGPIN are similar to those in prostate adenocarcinomas [10], such as staining of luminal cell specific CK7, 8, 18 [11], and alpha-methylacyl-CoA racemase (AMACR) [10], allelic loss of chromosome 8p12-21 [12], loss of telomere length [13], and gain of chromosomes 7, 8, 10, and 12 [14], while the basal cell layer and the basement membrane are mostly preserved. Staining for basal cell specific antigens, such as high molecular weight keratins or p63, is therefore a useful diagnostic tool to distinguish between HGPIN and PCa [15].

PCa is characterized by a complex pathology with multiple histologically heterogeneous foci that are classified according to the Gleason score [16, 17]. Different histological foci can harbor distinct genetic aberrations reflecting molecular subtypes with independent clonal origin, leading to heterogeneous clinical outcomes among patients with the same histological pattern [18]. PCa frequently shows an indolent clinical course indicating that many cancer foci arise from a pathogenic program that is insufficient to promote aggressiveness [18]. The acquisition of critical activating events may induce aggressive cell characteristics leading to a dominant tumor focus and clinically relevant disease [19]. The presence of multiple genetic aberrations within a tumor focus is challenging for the analysis of tumor promoting mutations and its predictive value [20]. However, the detection of shared molecular aberrations in metastatic tumor samples has led to the

hypothesis that most metastatic prostate cancers have monoclonal origins arising from a single precursor cancer cell by a selective advantage of individual clones or by therapy-induced selection pressure [19, 21].

A complex spectrum of somatic genomic alterations is seen in PCa including point mutations, copy number alterations (CNA), structural rearrangements, and changes in DNA methylation (Table 1.1) [22, 23]. Major signaling pathways that are most commonly altered in PCa, including AR, PTEN-PI3K/AKT, Ras/Raf/MEK/ERK and the retinoblastoma protein (pRB) signaling pathway, are affected in 34-43% of primary PCa and 74-100% of metastatic tumors [23, 24]. In primary PCa, focal genomic deletions are seen, while in metastatic PCa they can affect a large portion of the genome suggesting increased genomic instability with disease progression [25]. Highly altered cancer genomes with extensive CNAs have been associated with higher Gleason score, unfavourable disease prognosis and early biochemical relapse [23, 26]. Deletion of chromosome 8p21-22 involving *NKX3-1* (8p21) is the most frequently reported allelic loss in primary PCa. *NKX3-1* is a prostate-specific homeobox gene having growth-suppressive and differentiating effects on prostatic epithelium. Genomic deletion of *NKX3-1* occurs early during prostatic carcinogenesis, its loss has been reported in PIN and was suggested to be related to the progression to PCa [27]. Deletions of tumor suppressors such as *PTEN* (10q23), *RB1* (13q14), *BRCA2* (13q13), and *TP53* (17p31) are recurrently seen in PCa subsets [23, 25]. Loss of *PTEN*, an inhibitor of PI3K/AKT signaling and negative regulator of cell migration and cell survival, is considered as a late event in cancer progression, since it is more prevalent in PCa and less frequent in PIN lesions [28]. Gene amplifications including *MYC* (8q24), *NCOA2* (8q13), *PIK3CA* (3q26), and *ELK4* (1q32) are commonly seen in primary and advanced PCa [25], while focal amplification of *AR* (Xq12) is restricted to metastatic PCa [23].

Table 1.1: Molecular targets for PCa diagnosis. This table encompasses established as well as novel targets in the progression towards aggressive PCa.

Stage	Normal prostate epithelium →	PIN →	PCa	mCRPC →	NEPC *
Molecular alterations		Deletion: 8p12-21 (*NKX3-1*) Telomere shortening Gain: 7q (*MET*), 7p (*EGFR*) 8q (*MYC*, *PSCA*) *GSTP1* hypermethylation	Deletion: *PTEN* (10q23) *RB1* (13q14) *BRCA2* (13q13) *TP53* (17p31) *CDKN1B* (12p) *CDKN2A* (9p21) Gain: *MYC* (8q24) *NCOA2* (8q13) *PIK3CA* (3q26) *ELK4* (1q32) *TMPRSS2:ERG* *SPOP* mutation *CHD1 deletion* Methylation-induced hyperactivity of developmental pathways Genomic instability (135, 137)	*AR* amplification (Xq12) *AR-V7*	*MYCN, AURKA* (113) *REST* inactivity *BRN2* (88) *PEG10* (90) *SRRM4* (89)
Biomarkers	Age Family history Environment Germline variants	Histologic appearance IHC: AMACR, absent p63 and CK5/14 LB: *AR-V7* (144-146) LB: CD56 (148) LB: *PCA3*/*TMPRSS2:ERG* (142)			
Clinical signs			Asymptomatic PSA, DRE	Rising PSA Symptomatic metastasis	Failure of ADT Visceral metastasis
Clinical management			Surveillance versus local therapy LHRH agonists Antiandrogens Docetaxel	Arbiraterone Enzalutamide	Docetaxel Cabazitaxel

*PIN - prostatic intraepithelial neoplasia, mCRPC – metastatic castration resistant PCa, NEPC – neuroendocrine PCa, IHC – immunohistochemistry, LB - liquid biopsy

Androgens play a central role in PCa development and progression to metastatic disease. Genetic variations and mutations within the *AR* gene or the androgen biosynthesis and metabolism pathways can affect the response to androgen signaling. The length of polymorphic CAG nucleotide sequence repeats in exon 1 of the *AR* gene, encoding a polyglutamine chain in the DNA-binding domain, inversely affects the AR-induced transcriptional activity [29, 30]. In a limited number of studies, ethnicity-based differences in CAG nucleotide repeat length correlated with the ethnical variation in PCa incidence and mortality [31-33].

Long-term AR signaling can induce DNA double-strand breaks driving the generation of chromosomal rearrangements [34]. Chromosomal translocations involving the ETS transcription factor family (e.g. *ERG*, *ETV1*, *ETV4*, and *ETV5*) are high-frequency rearrangement events in PCa [35]. The AR-responsive protease *TMPRSS2* is the most frequent fusion partner, but *SLC45A3* and *NDRG1* among others have also been reported as partner genes [36, 37]. The *TMPRSS2:ERG* gene fusion is the most prevalent genomic

alteration in PCa resulting from the fusion of *ERG* to *TMPRSS2* by intrachromosomal deletion and translocation events, leading to overexpression of the transcription factor from the androgen-regulated *TMPRSS2* promoter [38, 39]. The ETS gene family is the largest group of transcriptional regulators consisting of 28 members in the human genome and can be further subclassified based on sequence similarities in the ETS DNA binding domain [40]. ETS proteins can act as activator or repressor of transcription by regulating genes that are involved in cellular architecture, migration, invasion, and permeability. Therefore, ETS transcription factors play a role in embryogenesis, vasculogenesis, angiogenesis, haematopoiesis and neuronal development in a wide range of tissues [41]. During development, ERG is involved in the formation of the vascular system, the urogenital tract, in bone development, and in migration of embryonic neural crest cells [41]. In adult tissue, ERG expression is found in endothelial cells of various tissues maintaining vascular integrity and regulating vascular inflammatory response by regulating VE-cadherin, von Willebrand factor, endoglin, *VEGF*, *IL8*, *ICAM-1*, and *VCAM* [41].

AR activity promotes the spatial proximity of distant genomic regions and recruitment of enzymes facilitating double-strand breaks (e.g. TOP2B) and subsequent recombination suggesting a non-random chromosomal rearrangement in PCa [40, 42, 43]. In response to genotoxic stress, AR also recruits activation-induced cytidine deaminase (AID) and the LINE-1 encoded endonuclease ORF2 that promote genomic rearrangements [42]. Exposure of androgen-sensitive fusion-negative LNCaP cells to DHT and irradiation, etoposide or doxorubicin, led to the induction of *TMPRSS2:ERG* and *TMPRSS2:ETV1* gene fusions that corresponded to the identified gene fusion variants in PCa tissue [42]. Regarding the role of AR signaling in the development of gene fusion events, the *TMPRSS2:ERG* rearrangement is considered as an early event in PCa development [34]. Bastus et al. found shorter length of the CAG repeat in the *AR* gene in fusion-positive cases (n=20) compared to fusion-negative cases (n=20), however, this finding was not statistically significant [44].

Blocking of the AR signaling pathway by androgen deprivation therapy (ADT) in combination with chemotherapy belongs to the initial treatment options of advanced-stage PCa [45, 46]. ADT is achieved by luteinizing hormone-releasing hormone (LHRH) analoga or LHRH antagonists, combined with antiandrogens such as bicalutamide. However, most cancers will relapse and progress to castration-resistant prostate cancer (CRPC), a condition in which PCa cells do not respond to ADT [45], defined by low serum testosterone together with rising PSA levels or radiological progression of metastatic lesions on ADT [47]. Increasing PSA level is a significant predictor of survival in patients who have newly diagnosed, metastatic PCa treated with continuous ADT [48]. CRPC can initially be treated by blocking AR signaling activity with the second-generation AR antagonist enzalutamide, and androgen synthesis inhibitors such as abiraterone [49, 50]. The development of CRPC is driven by the genomic instability of PCa cells and multiple me-

chanisms lead to the aberrant reactivation of AR signaling, including receptor promiscuity allowing alternative ligand binding, *AR* gene amplification [51, 52], recruitment of alternating transcriptional coregulators [53-56] and *AR* splice variants. C-terminal truncated splice variants constitutively drive AR signaling under castrate conditions [57, 58]. Of note is that *AR* splice variants were shown to regulate a distinct transcriptional program [59]. The most commonly expressed *AR* splice variant is *AR-V7*, resulting from splicing of exon 3 to a cryptic exon in the intron between exon 3 and 4 generating a truncated AR protein lacking the ligand-binding domain, but retaining transcriptional activity [60, 61]. *AR-V7* could be detected in primary untreated PCa at low levels, but showed an increased ratio relative to full length *AR* in metastatic CRPC (mCRPC) [24, 62]. *AR-V7* has been implicated in abiraterone and enzalutamide resistance and correlated to disease progression and mortality [24, 62, 63]. In VCaP cells, androgen deprivation using enzalutamide induced expression of *AR-V7* [64]. The molecular effects of ADT using a second-generation AR antagonist are also under investigation with respect to neuroendocrine differentiation and increased immune check-point signaling, highlighting the diverse mutational complexity of CRPC [65, 66].

NEUROENDOCRINE PROSTATE CANCER

Among patients with advanced disease, manifestation of a high-grade neuroendocrine PCa (NEPC) phenotype is detected, distinguished from prostatic acinar carcinoma by unique clinical and ultrastructural characteristics and immunohistochemical staining for various neuroendocrine elements and polypeptide hormones [67]. NE cells containing neurosecretory granules by electron microscopy, are immunohistochemically detected by positive staining for synaptophysin (SYP) (Figure 1.1A), chromogranins A and B (CHGA, CHGB), neuron-specific enolase (NSE/ENO2), or neuronal cell adhesion molecule (NCAM1/CD56) [67] [68]. NEPC is the most significant histological subtype of PCa compared to other rare categories such as ductal adenocarcinoma, mucinous carcinoma, and signet ring carcinoma [69].

Clinically, NEPC appears as a highly aggressive variant of advanced CRPC defined by unresponsiveness to hormone therapy, rapid disease progression, poor prognosis, lytic bone lesions, visceral metastases, and marked prostatic enlargement [70, 71]. Absent AR expression and disproportional low PSA levels are hallmarks of NEPC [70, 71]. NE foci exist within virtually all human prostate adenocarcinomas, reported incidence rates range from 25-90% [67, 72, 73]. It was suggested that the different morphologic manifestations of NEPC, i.e. carcinoid tumors, large cell neuroendocrine carcinomas and small cell carcinomas, represent a continuum characterized by gradual expression of molecular aberrations [74]. Small cell carcinoma of the prostate (Figure 1.1B), the most

aggressive form of NEPC, where transformation towards a predominantly neuroendocrine histology occurred, is rare with a reported frequency of less than 1% [72].

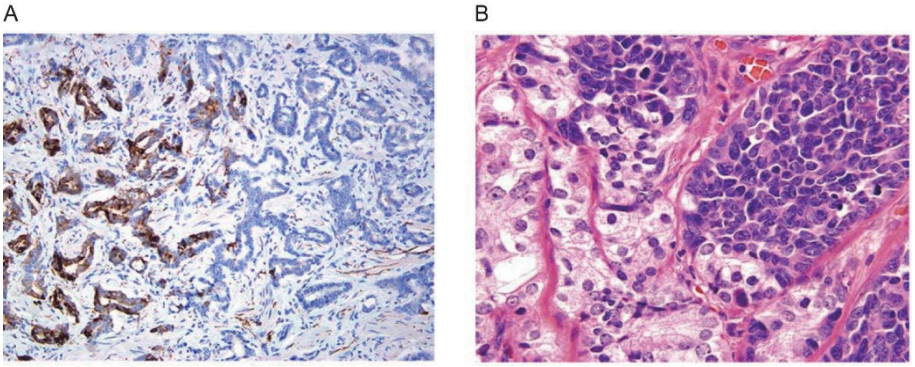

Figure 1.1: Prostate cancer biopsy core with NE differentiation. (A) Adenocarcinoma of the prostate Gleason score 3+3 = 6. Areas with positive SYP staining (left) showing same glandular morphology as negative stained SYP areas (right). (B) Mixed usual adenocarcinoma of the prostate (left) with small cell carcinoma (right) (adapted from Epstein et al. [67]).

The increasing incidence of NEPC (about 6.8% per year between 2004-2011) can be partly attributed to prolonged patients' life expectancy and aggressive rebiopsy practice of metastatic CRPC [71, 75]. The median survival rate after NEPC diagnosis is 7 months [70] and the 5-years survival rates are low (17%), mirroring the lack of a specific detection method and effective therapy for NEPC [76]. NEPC can arise de novo, however, it is more prevalent in previously treated adenocarcinomas. There is a growing body of evidence that the extent of neuroendocrine differentiation (NED) correlates with exposure to ADT and represents an adaptive clinical phenotype, which is of special significance regarding the advent of novel highly potent AR-targeted therapies [75, 77-86]. Androgen-deprived culture conditions were shown to induce a neuronal morphology and expression of NSE and CHGA in LNCaP cells [87]. Intriguing molecular mechanisms of ADT-induced NED in PCa have recently been elucidated (Table 1.1). On enzalutamide treatment, AR-targeted inhibition *in vitro* released the repressive activity of AR signaling on the neuronal transcription factor *BRN2*, thereby enabling induction of a NE program and promoting tumor aggressiveness [88]. Overexpression of the RNA splicing factor *SRRM4* in prostate tumors was found to drive progression to NEPC by regulating splicing of the RE-1 silencing transcription factor (*REST*) and reducing functional REST protein [89]. REST is known to mediate restriction of neuronal gene expression and is involved in AR-mediated control of cell differentiation [65]. Androgen deprivation reduced the expression of REST that coincided with increased expression of CHGA and a NE-like morphology in LNCaP cells [65]. Loss of REST in NEPC in association with a NE phenotype was a crucial discovery in the emerging mechanisms of NEPC [81]. By identifying an additive effect of *SRRM4* and AR pathway inhibition to induce NEPC, the researchers

proposed a role for ADT as prerequisite condition to release a lineage-specific differentiation program and preparing transformation to NEPC [89]. The placental gene *PEG10* was identified as driver of NEPC in a dynamic progression xenograft model revealing a biphasic expression pattern during distinct stages of NEPC development [90]. *PEG10* expression increased during enzalutamide-mediated AR inhibition in the initial progression phase. A second increase was detected at the emergence of NEPC promoting cell cycle progression in the context of *RB1* and *TP53* loss, and triggering invasion by increased *SNAIL* expression via TGF-β signaling [90].
It was initially assumed that NEPC developed from outgrowth of normal prostatic NE cells, promoted by the selective pressure of androgen-independent growth [91]. Current evidence suggests a common origin of adenocarcinoma and NEPC supported by concordant molecular alterations, involving *TMPRSS2:ERG* gene fusion and *TP53* mutations [92-94]. This concept assumes evolution of NED from adenocarcinoma cells into NE cells, underpinned by the detection of epithelial characteristics in NE cells such as expression of CK8, CK18, and AMACR [84, 95, 96]. Several signaling mediators have been implicated in NED including neuropeptides (bombesin/gastrin-releasing peptide, calcitonin, serotonin, and vasoactive intestinal peptide) [97], cytokines (IL-6, IL-1β, IL-8) [98-100], ionizing irradiation [101], and stimuli elevating intra-cellular cAMP (such as forskolin) [102]. LNCaP cells cultured with cAMP or charcoal-stripped fetal bovine serum acquired a NE phenotype [103, 104]. cAMP further induced G1 growth arrest in LNCaP cell [104] and synergized with IL-6, a prominent inducer of NED [105]. IL-6 triggered REST repression and STAT3-induced NED in LNCaP cells [106-108]. Neuropeptides and IL-8 activated the nonreceptor tyrosine kinases ETK, Src and FAK resulting in androgen-independent AR activation [100, 109]. In a transgenic adenocarcinoma of the mouse prostate (TRAMP) model, cooperativity between the NE-specific forkhead transcription factor FoxA2 and the hypoxia-induced transcription factor HIF1α induced target genes that were required for a NE phenotype in PCa [110]. FoxA2/HIF1α complex formation was promoted by the ubiquitin ligase Siah2 that regulated HIF1α activity thus enabling complexation with FoxA2 [110]. Hypoxia-mediated NED of LNCaP cells was shown to be facilitated by decreased Notch signaling, which is known for its role in cell fate and differentiation by inhibiting neurogenesis and maintaining a progenitor cell state [111].

Amplification of Aurora kinase A (*AURKA*) and N-myc (*MYCN*), also frequently occurring in neuroblastoma and small cell lung cancer, was identified in 40% of patients that clinically had developed NEPC [112, 113]. AURKA, involved in G2-to-M transition during the cell cycle, and the transcription factor N-myc were shown to physically interact and function in reciprocal stabilization [112]. Overexpression of either *AURKA* or *MYCN* in RWPE-1 cells induced expression of the NE markers *NSE* and *SYP* [112]. *MYCN* overexpression in LNCaP cells revealed direct binding of N-myc to the promoter of *NSE* and *SYP* [112]. AURKA inhibition led to a reduced cell viability in *MYCN*-overexpressing LNCaP and NCI-H660 cells, and induced tumor shrinkage by 50-87% in NE-tumor xeno-

graft models accompanied by reduced *SYP* expression [112]. In a mouse model transplanted with N-myc overexpressing human prostate basal epithelial cells, activated AKT1 downstream of N-myc was sufficient to induce NEPC detected by histological NE attributes and positive IHC stain for NE markers (CHGA, SYP, NCAM1, NSE), accompanied by negative AR stain [114]. Detection of *AURKA* amplification and overexpression in primary PCa specimens suggested its role as marker to identify patients that are more likely to develop NEPC [112]. Together, these finding indicate molecular parallels to the well-studied NE tumor models of neuroblastoma and small cell lung cancer and announce a crucial step towards a better understanding of the molecular pathogenesis of NEPC promoting the development of therapeutic strategies and identification of potential biomarkers [112-115].

MOLECULAR TARGETS AND NOVEL APPROACHES TO DIAGNOSIS AND TREATMENT

The majority of PCa is diagnosed as locoregional disease [116, 117]. Since clinicopathologic criteria are insufficient to efficiently discriminate between slow growing versus non-indolent biologically aggressive tumors, there is uncertainty about the risk of disease progression. Although Gleason scoring together with clinical data is used for stratification of treatment modalities according to risk category today, genomic features rather than histopathological grading may determine the clinical course of the disease in future. Molecular subtypes may determine distinct genomic pathways of progression. At a molecular level, 74% of primary PCa could be assigned to a mutational subtype defined by distinct oncogenic drivers involving *SPOP*, *FOXA1*, and *IDH1* or gene fusions involving *ERG*, *ETV1*, *ETV4* or *FLI1* [118]. Deletion of three genomic regions have been shown to co-occur with the *TMPRSS2:ERG* fusion spanning the *PTEN* and *TP53* locus, and a multigenic region located at 3p14 including *FOXP1* [23]. *PTEN* deletion is associated with advanced PCa, decreased time to metastasis and poor prognosis [119]. *TMPRSS2:ERG* expression can be used for confirmation of PCa diagnosis in morphologically suspicious biopsy cores [120]. Its detection also discriminates between NE tumors of the prostate and small cell carcinoma of other organs [121]. The stratification of molecular subtypes may further have important treatment implications. The enzyme poly [ADP-ribose] polymerase 1 (PARP1) is a required cofactor for ERG, and PARP1 inhibition induced increased vulnerability of PCa cells to low-dose radiation [122, 123] suggesting that tumors may respond to treatment by PARP1-inhibitors. Recent studies showed that PCa patients with inherited mutations in *BRCA1/2* and ataxia-telangiectasia mutated (*ATM*), who have a shorter survival time, clinically respond to the PARP1 inhibitor olaparib [124, 125]. *SPOP* (Speckle-type POZ protein), a substrate recognition component of an E3 ubiquitin ligase, is the gene with the most common point mutations in primary PCa. However, the occurrence of *SPOP* mutations was not further increased in

CRPC [24]. Tumors of the *SPOP* mutant subtype were recently demonstrated to activate PI3K and AR signaling, suggesting a mechanism of signaling convergence between *SPOP* mutant and *TMPRSS2:ERG* positive tumors with potential implications for androgen-targeting therapy [126]. *SPOP*-mutant tumors often show deletion of the *CHD1* locus (5q21), encoding the chromodomain helicase DNA binding protein 1, a tumor suppressor functioning in genome stability and maintenance of chromatin architecture. *SPOP*-mutation and *CHD1*-deletion sensitizes tumors to increased genomic instability by deficient DNA mismatch repair processes [127]. Functional studies suggest a synergistic effect of *SPOP*-mutant and *CHD1*-deleted tumors [128]. *SPOP*-mutant tumors are further characterized by recurrent overexpression of *SPINK1* (a serine peptidase inhibitor Kazal type 1), that occurred mutually exclusive from *ERG* rearrangements [129, 130]. *SPINK1* overexpression was shown to be associated with earlier clinical recurrence [129]. Due to its high homology with the epidermal growth factor receptor (EGFR), SPINK1 overexpressing tumors could respond to cetuximab, a monoclonal antibody against EGFR currently tested in the preclinical setting [131].

The genomic alterations within these molecular subtypes also showed an association with altered DNA methylation, potentially representing different epigenetic mechanisms between these subtypes with yet unresolved functional consequences suggesting DNA methylation as biomarker in PCa [26]. Promoter-associated hypermethylated CpG islands were highly enriched for differentiation and developmental processes, and associated with reduced gene expression (e.g. *PTEN*, *TP53*, *GSTP1*), suggesting that DNA hypermethylation may change differentiation states and activity of carcinogenic pathways [132, 133]. CpG island hypermethylation of a gene-panel (*GSTP1*, *APC*, *RASSF1A*, *PTGS2*, *MDR1*) could discriminate primary PCa from benign prostate tissue [134]. Hypermethylation of the transcriptional elongation regulator (*TCERG1L*) in combination with other genomic markers could predict disease relapse in localized PCa [135]. The DNA methylation profile has also been found to be subject specific and maintained within metastatic subclones, suggesting a role as longitudinal marker [132, 136].

Genomic instability leading to complex rearrangements are frequently found in PCa [135] [137]. Chromothripsis, the extensive DNA rearrangement involving few chromosomal loci, occurring most likely by an initial error in chromosome segregation of incompletely replicated DNA during mitosis, has been proposed as marker of an aggressive non-indolent course in initially localized PCa that requires aggressive treatment [135, 137-139]. Chained genomic rearrangements, called chromoplexy, were frequently found in *ERG* fusion-positive genomes and affect regions that are highly expressed in PCa, suggesting an association with AR-driven transcriptional processes [137]. Chromoplexy induced deletion of *PTEN*, *NKX3-1*, *CDKN1B*, *TP53*, and *RB1*, and may thereby simultaneously deregulate PCa pathways, potentially leading to a rapid punctuated progression of PCa [137].

PCa is usually suspected based on PSA value and digital rectal examination (DRE), but PSA level is not a direct surrogate for tumor stage. Definitive diagnosis requires histopathological confirmation of the disease on prostate biopsy [140]. Tumor heterogeneity often precludes precise staging and histopathological grading and therefore weakens the power of current diagnostic management in PCa. Analysis of genetic changes evolving within metastatic PCa is challenged by the poor availability of samples from bone metastases, the major location of PCa dissemination. Liquid biopsies, circulating genetic material or proteins detected in different body fluids, could provide a highly valuable easily accessible source of tumor markers to detect clinically significant PCa and to obtain a faithful representation of tumor aggressiveness that could lead to an improved therapy decision. Several blood-based and urinary prostate cancer biomarkers are currently evaluated. The Prostate Health Index (PHI) is a test recently approved by the US Food and Drug Administration (FDA) using serum PSA isoforms in men with PSA levels ranging from 4–10 ng/mL to support decision-making regarding prostate biopsies [141]. The diagnostic and prognostic value of the prostate cancer gene 3 (*PCA3*), a non-coding RNA highly overexpressed in PCa, and the *TMPRSS2:ERG* gene fusion in liquid biopsies are under investigation in different trials (reviewed in [140]). The detection of urinary *PCA3* could potentially reduce the number of biopsies in men with increased PSA level (>10 ng/mL). The combined detection of *PCA3* and *TMPRSS2:ERG* in urinary exosomes was used for improved risk stratification of men with elevated serum PSA levels to guide further disease management [142]. Exosomes are nanosized (40–100nm) extracellular vesicles secreted from cells via the endosomal pathway. Tumor cells release exosomes at increased levels, which are then detectable in different body fluids. Exosomal cargo reflects the genetic and proteomic signature of the tumor rendering them as suitable target for biomarker detection in PCa [143]. Exosomes and circulating tumor cells (CTCs) could overcome the shortcoming of metastatic biopsies in PCa to obtain insights in aggressive mechanisms with implications for treatment adjustment. Detection of *AR* splice variant *AR-V7* in exosomes and CTCs from CRPC patients was shown to be a predictive biomarker of resistance to AR-targeting agents [58, 144-146]. Molecular profiling of CTCs was demonstrated as dynamic approach to monitor AR signaling during treatment and to predict response to arbiraterone [147]. For the histologic evaluation of small cell neuroendocrine PCa, rebiopsy often reveals mixed features of both adenocarcinoma and neuroendocrine carcinoma and the diagnosis of NEPC is predominantly based on clinical characteristics. CTCs in blood samples from patients with confirmed small cell carcinoma were shown to be positive for CD56 and were of smaller size than CTCs from CRPC patients. This study highlights the phenotypic similarities between tumor and CTCs and suggests potential use of CTCs in the early detection of PCa transforming towards NEPC [148]. However, so far only increased CTC count was prospectively validated in two phase III randomized trials, showing association with reduced overall survival [149, 150].

Blood mRNA signatures are also investigated as biomarker source. Two studies suggested the detection of transcript levels of selected mRNAs in whole-blood samples of patients with CRPC as improved prognostic markers [151, 152]: a panel consisting of six circulating mRNA markers (*ABL2*, *C1QA*, *SEMA4D*, *TIMP1*, *ITGAL*, and *CDKN1A*) predicted survival in CRPC patients [151]. Poor overall survival of patients with CRPC was associated with a nine-gene model (*RHAG*, *CA1*, *HEPACAM2*, *SNCA*, *HEMGN*, *SOX6*, *TMEM56*, *OSBP2*, and *RHD*) [152]. However, the biological relevance of these gene signatures remains unresolved.

SUMMARY

At the time of diagnosis, PCa will frequently present as organ-confined disease and most tumors will persist as indolent clinical conditions [116, 117]. The individual risk to develop clinically significant, and potentially lethal disease is not recognized by histological grading alone. The heterogeneous clinical course that is observed among PCa cases is determined by complex and dynamic genomic aberrations. Novel markers for refined risk stratification of progressive disease outcome and prediction of treatment response are needed. Several tissue-based multigene expression assays for the prediction of aggressive PCa are available for clinical application [153, 154]. Their routine implementation is currently hampered by intrinsic challenges of PCa research, such as heterogeneity, multifocality, and a small sample volume in prostate biopsy. Genetic instability increases the complexity of somatic genomic alterations leading to a specific combination of driver mutations in a tumor. However, molecular pathology is an emerging field in PCa as a growing number of targets with known correlation to tumor biology are recognized, such as *AR* splice variants (Table 1.1). Further, differentiation markers of neuroendocrine manifestation may predict poor responsiveness to ADT. Individual genetic aberrations could be interrogated by next generation sequencing and may find application for a personalized approach in clinical practice. Molecular and genetic analysis of biopsy cores is currently not included in the PCa guidelines. In future, it may complement the diagnosis of PCa as it has already been implemented in other tumor entities, such as breast cancer, melanoma and, most recently, lung cancer [155-157]. Simultaneously, a broader spectrum of therapeutic targets in addition to ADT is required to improve the clinical management of metastatic PCa [158]. The functional and mechanistic evaluation of genetic markers is the basis for the development of novel drug targets and treatment strategies, and could guide the emphasis of future research.

REFERENCES

1. Greene DR, Wheeler TM, Egawa S, Dunn JK and Scardino PT. A comparison of the morphological features of cancer arising in the transition zone and in the peripheral zone of the prostate. J Urol. 1991; 146(4):1069-1076.
2. McNeal JE, Redwine EA, Freiha FS and Stamey TA. Zonal distribution of prostatic adenocarcinoma. Correlation with histologic pattern and direction of spread. Am J Surg Pathol. 1988; 12(12):897-906.
3. Sinnott JA, Rider JR, Carlsson J, Gerke T, Tyekucheva S, Penney KL, Sesso HD, Loda M, Fall K, Stampfer MJ, Mucci LA, Pawitan Y, Andersson SO and Andren O. Molecular differences in transition zone and peripheral zone prostate tumors. Carcinogenesis. 2015; 36(6):632-638.
4. Kendal WS and Mai KT. Histological subtypes of prostatic cancer: a comparative survival study. Can J Urol. 2010; 17(5):5355-5359.
5. Ayala AG and Ro JY. Prostatic intraepithelial neoplasia: recent advances. Arch Pathol Lab Med. 2007; 131(8):1257-1266.
6. Bostwick DG and Brawer MK. Prostatic intra-epithelial neoplasia and early invasion in prostate cancer. Cancer. 1987; 59(4):788-794.
7. McNeal JE and Bostwick DG. Intraductal dysplasia: a premalignant lesion of the prostate. Hum Pathol. 1986; 17(1):64-71.
8. Kronz JD, Allan CH, Shaikh AA and Epstein JI. Predicting cancer following a diagnosis of high-grade prostatic intraepithelial neoplasia on needle biopsy: data on men with more than one follow-up biopsy. Am J Surg Pathol. 2001; 25(8):1079-1085.
9. Davidson D, Bostwick DG, Qian J, Wollan PC, Oesterling JE, Rudders RA, Siroky M and Stilmant M. Prostatic intraepithelial neoplasia is a risk factor for adenocarcinoma: predictive accuracy in needle biopsies. J Urol. 1995; 154(4):1295-1299.
10. Zynger DL and Yang X. High-grade prostatic intraepithelial neoplasia of the prostate: the precursor lesion of prostate cancer. Int J Clin Exp Pathol. 2009; 2(4):327-338.
11. Brawer MK, Peehl DM, Stamey TA and Bostwick DG. Keratin immunoreactivity in the benign and neoplastic human prostate. Cancer Res. 1985; 45(8):3663-3667.
12. Emmert-Buck MR, Vocke CD, Pozzatti RO, Duray PH, Jennings SB, Florence CD, Zhuang Z, Bostwick DG, Liotta LA and Linehan WM. Allelic loss on chromosome 8p12-21 in microdissected prostatic intraepithelial neoplasia. Cancer Res. 1995; 55(14):2959-2962.
13. Vukovic B, Park PC, Al-Maghrabi J, Beheshti B, Sweet J, Evans A, Trachtenberg J and Squire J. Evidence of multifocality of telomere erosion in high-grade prostatic intraepithelial neoplasia (HPIN) and concurrent carcinoma. Oncogene. 2003; 22(13):1978-1987.
14. Bostwick DG and Qian J. Atypical adenomatous hyperplasia of the prostate. Relationship with carcinoma in 217 whole-mount radical prostatectomies. Am J Surg Pathol. 1995; 19(5):506-518.
15. Novis DA, Zarbo RJ and Valenstein PA. Diagnostic uncertainty expressed in prostate needle biopsies. A College of American Pathologists Q-probes Study of 15,753 prostate needle biopsies in 332 institutions. Arch Pathol Lab Med. 1999; 123(8):687-692.
16. Gordetsky J and Epstein J. Grading of prostatic adenocarcinoma: current state and prognostic implications. Diagn Pathol. 2016; 11:25.
17. Arora R, Koch MO, Eble JN, Ulbright TM, Li L and Cheng L. Heterogeneity of Gleason grade in multifocal adenocarcinoma of the prostate. Cancer. 2004; 100(11):2362-2366.
18. Andreoiu M and Cheng L. Multifocal prostate cancer: biologic, prognostic, and therapeutic implications. Hum Pathol. 2010; 41(6):781-793.
19. Shen MM and Abate-Shen C. Molecular genetics of prostate cancer: new prospects for old challenges. Genes Dev. 2010; 24(18):1967-2000.
20. Verhagen PC, Tilanus MG, de Weger RA, van Moorselaar RJ, van den Tweel JG and Boon TA. Prognostic factors in localised prostate cancer with emphasis on the application of molecular techniques. Eur Urol. 2002; 41(4):363-371.

21. Liu W, Laitinen S, Khan S, Vihinen M, Kowalski J, Yu G, Chen L, Ewing CM, Eisenberger MA, Carducci MA, Nelson WG, Yegnasubramanian S, Luo J, Wang Y, Xu J, Isaacs WB, et al. Copy number analysis indicates monoclonal origin of lethal metastatic prostate cancer. Nat Med. 2009; 15(5):559-565.
22. Beroukhim R, Mermel CH, Porter D, Wei G, Raychaudhuri S, Donovan J, Barretina J, Boehm JS, Dobson J, Urashima M, Mc Henry KT, Pinchback RM, Ligon AH, Cho YJ, Haery L, Greulich H, et al. The landscape of somatic copy-number alteration across human cancers. Nature. 2010; 463(7283):899-905.
23. Taylor BS, Schultz N, Hieronymus H, Gopalan A, Xiao Y, Carver BS, Arora VK, Kaushik P, Cerami E, Reva B, Antipin Y, Mitsiades N, Landers T, Dolgalev I, Major JE, Wilson M, et al. Integrative genomic profiling of human prostate cancer. Cancer Cell. 2010; 18(1):11-22.
24. Robinson D, Van Allen EM, Wu YM, Schultz N, Lonigro RJ, Mosquera JM, Montgomery B, Taplin ME, Pritchard CC, Attard G, Beltran H, Abida W, Bradley RK, Vinson J, Cao X, Vats P, et al. Integrative clinical genomics of advanced prostate cancer. Cell. 2015; 161(5):1215-1228.
25. Schoenborn JR, Nelson P and Fang M. Genomic profiling defines subtypes of prostate cancer with the potential for therapeutic stratification. Clin Cancer Res. 2013; 19(15):4058-4066.
26. Cancer Genome Atlas Research N. The Molecular Taxonomy of Primary Prostate Cancer. Cell. 2015; 163(4):1011-1025.
27. Bowen C, Bubendorf L, Voeller HJ, Slack R, Willi N, Sauter G, Gasser TC, Koivisto P, Lack EE, Kononen J, Kallioniemi OP and Gelmann EP. Loss of NKX3.1 expression in human prostate cancers correlates with tumor progression. Cancer Res. 2000; 60(21):6111-6115.
28. Morais CL, Han JS, Gordetsky J, Nagar MS, Anderson AE, Lee S, Hicks JL, Zhou M, Magi-Galluzzi C, Shah RB, Epstein JI, De Marzo AM and Lotan TL. Utility of PTEN and ERG immunostaining for distinguishing high-grade PIN from intraductal carcinoma of the prostate on needle biopsy. Am J Surg Pathol. 2015; 39(2):169-178.
29. Chamberlain NL, Driver ED and Miesfeld RL. The length and location of CAG trinucleotide repeats in the androgen receptor N-terminal domain affect transactivation function. Nucleic Acids Res. 1994; 22(15):3181-3186.
30. La Spada AR, Wilson EM, Lubahn DB, Harding AE and Fischbeck KH. Androgen receptor gene mutations in X-linked spinal and bulbar muscular atrophy. Nature. 1991; 352(6330):77-79.
31. Giovannucci E, Stampfer MJ, Krithivas K, Brown M, Dahl D, Brufsky A, Talcott J, Hennekens CH and Kantoff PW. The CAG repeat within the androgen receptor gene and its relationship to prostate cancer. Proc Natl Acad Sci U S A. 1997; 94(7):3320-3323.
32. Bennett CL, Price DK, Kim S, Liu D, Jovanovic BD, Nathan D, Johnson ME, Montgomery JS, Cude K, Brockbank JC, Sartor O and Figg WD. Racial variation in CAG repeat lengths within the androgen receptor gene among prostate cancer patients of lower socioeconomic status. J Clin Oncol. 2002; 20(17):3599-3604.
33. Buchanan G, Irvine RA, Coetzee GA and Tilley WD. Contribution of the androgen receptor to prostate cancer predisposition and progression. Cancer Metastasis Rev. 2001; 20(3-4):207-223.
34. Bastus NC, Boyd LK, Mao X, Stankiewicz E, Kudahetti SC, Oliver RT, Berney DM and Lu YJ. Androgen-induced TMPRSS2:ERG fusion in nonmalignant prostate epithelial cells. Cancer Res. 2010; 70(23):9544-9548.
35. Tomlins SA, Rhodes DR, Perner S, Dhanasekaran SM, Mehra R, Sun XW, Varambally S, Cao X, Tchinda J, Kuefer R, Lee C, Montie JE, Shah RB, Pienta KJ, Rubin MA and Chinnaiyan AM. Recurrent fusion of TMPRSS2 and ETS transcription factor genes in prostate cancer. Science. 2005; 310(5748):644-648.
36. Esgueva R, Perner S, C JL, Scheble V, Stephan C, Lein M, Fritzsche FR, Dietel M, Kristiansen G and Rubin MA. Prevalence of TMPRSS2-ERG and SLC45A3-ERG gene fusions in a large prostatectomy cohort. Mod Pathol. 2010; 23(4):539-546.
37. Pflueger D, Rickman DS, Sboner A, Perner S, LaFargue CJ, Svensson MA, Moss BJ, Kitabayashi N, Pan Y, de la Taille A, Kuefer R, Tewari AK, Demichelis F, Chee MS, Gerstein MB and Rubin MA. N-myc downstream regulated gene 1 (NDRG1) is fused to ERG in prostate cancer. Neoplasia. 2009; 11(8):804-811.
38. Perner S, Demichelis F, Beroukhim R, Schmidt FH, Mosquera JM, Setlur S, Tchinda J, Tomlins SA, Hofer MD, Pienta KG, Kuefer R, Vessella R, Sun XW, Meyerson M, Lee C, Sellers WR, et al. TMPRSS2:ERG fusion-

associated deletions provide insight into the heterogeneity of prostate cancer. Cancer Res. 2006; 66(17):8337-8341.
39. Attard G, Clark J, Ambroisine L, Fisher G, Kovacs G, Flohr P, Berney D, Foster CS, Fletcher A, Gerald WL, Moller H, Reuter V, De Bono JS, Scardino P, Cuzick J, Cooper CS, et al. Duplication of the fusion of TMPRSS2 to ERG sequences identifies fatal human prostate cancer. Oncogene. 2008; 27(3):253-263.
40. Sharrocks AD. The ETS-domain transcription factor family. Nat Rev Mol Cell Biol. 2001; 2(11):827-837.
41. Adamo P and Ladomery MR. The oncogene ERG: a key factor in prostate cancer. Oncogene. 2016; 35(4):403-414.
42. Lin C, Yang L, Tanasa B, Hutt K, Ju BG, Ohgi K, Zhang J, Rose DW, Fu XD, Glass CK and Rosenfeld MG. Nuclear receptor-induced chromosomal proximity and DNA breaks underlie specific translocations in cancer. Cell. 2009; 139(6):1069-1083.
43. Haffner MC, Aryee MJ, Toubaji A, Esopi DM, Albadine R, Gurel B, Isaacs WB, Bova GS, Liu W, Xu J, Meeker AK, Netto G, De Marzo AM, Nelson WG and Yegnasubramanian S. Androgen-induced TOP2B-mediated double-strand breaks and prostate cancer gene rearrangements. Nat Genet. 2010; 42(8):668-675.
44. Mangelsdorf PC and Galinat WC. The Tunicate Locus in Maize Dissected and Reconstituted. Proc Natl Acad Sci U S A. 1964; 51(2):147-150.
45. Nouri M, Ratther E, Stylianou N, Nelson CC, Hollier BG and Williams ED. Androgen-targeted therapy-induced epithelial mesenchymal plasticity and neuroendocrine transdifferentiation in prostate cancer: an opportunity for intervention. Front Oncol. 2014; 4:370.
46. Huggins C and Hodges CV. Studies on prostatic cancer. I. The effect of castration, of estrogen and androgen injection on serum phosphatases in metastatic carcinoma of the prostate. CA Cancer J Clin. 1972; 22(4):232-240.
47. Mottet N, Bellmunt J, Bolla M, Briers E, Cumberbatch MG, De Santis M, Fossati N, Gross T, Henry AM, Joniau S, Lam TB, Mason MD, Matveev VB, Moldovan PC, van den Bergh RC, Van den Broeck T, et al. EAU-ESTRO-SIOG Guidelines on Prostate Cancer. Part 1: Screening, Diagnosis, and Local Treatment with Curative Intent. Eur Urol. 2017; 71(4):618-629.
48. Hussain M, Goldman B, Tangen C, Higano CS, Petrylak DP, Wilding G, Akdas AM, Small EJ, Donnelly BJ, Sundram SK, Burch PA, Dipaola RS and Crawford ED. Prostate-specific antigen progression predicts overall survival in patients with metastatic prostate cancer: data from Southwest Oncology Group Trials 9346 (Intergroup Study 0162) and 9916. J Clin Oncol. 2009; 27(15):2450-2456.
49. Wadosky KM and Koochekpour S. Therapeutic Rationales, Progresses, Failures, and Future Directions for Advanced Prostate Cancer. Int J Biol Sci. 2016; 12(4):409-426.
50. Massard C and Fizazi K. Targeting continued androgen receptor signaling in prostate cancer. Clin Cancer Res. 2011; 17(12):3876-3883.
51. Visakorpi T, Hyytinen E, Koivisto P, Tanner M, Keinanen R, Palmberg C, Palotie A, Tammela T, Isola J and Kallioniemi OP. In vivo amplification of the androgen receptor gene and progression of human prostate cancer. Nat Genet. 1995; 9(4):401-406.
52. Urbanucci A, Sahu B, Seppala J, Larjo A, Latonen LM, Waltering KK, Tammela TL, Vessella RL, Lahdesmaki H, Janne OA and Visakorpi T. Overexpression of androgen receptor enhances the binding of the receptor to the chromatin in prostate cancer. Oncogene. 2012; 31(17):2153-2163.
53. Chen CD, Welsbie DS, Tran C, Baek SH, Chen R, Vessella R, Rosenfeld MG and Sawyers CL. Molecular determinants of resistance to antiandrogen therapy. Nat Med. 2004; 10(1):33-39.
54. Han G, Buchanan G, Ittmann M, Harris JM, Yu X, Demayo FJ, Tilley W and Greenberg NM. Mutation of the androgen receptor causes oncogenic transformation of the prostate. Proc Natl Acad Sci U S A. 2005; 102(4):1151-1156.
55. Shah S and Small E. Emerging biological observations in prostate cancer. Expert Rev Anticancer Ther. 2010; 10(1):89-101.
56. Feldman BJ and Feldman D. The development of androgen-independent prostate cancer. Nat Rev Cancer. 2001; 1(1):34-45.

57. Dehm SM, Schmidt LJ, Heemers HV, Vessella RL and Tindall DJ. Splicing of a novel androgen receptor exon generates a constitutively active androgen receptor that mediates prostate cancer therapy resistance. Cancer Res. 2008; 68(13):5469-5477.
58. Antonarakis ES, Lu C, Wang H, Luber B, Nakazawa M, Roeser JC, Chen Y, Mohammad TA, Chen Y, Fedor HL, Lotan TL, Zheng Q, De Marzo AM, Isaacs JT, Isaacs WB, Nadal R, et al. AR-V7 and resistance to enzalutamide and abiraterone in prostate cancer. N Engl J Med. 2014; 371(11):1028-1038.
59. Hu R, Lu C, Mostaghel EA, Yegnasubramanian S, Gurel M, Tannahill C, Edwards J, Isaacs WB, Nelson PS, Bluemn E, Plymate SR and Luo J. Distinct transcriptional programs mediated by the ligand-dependent full-length androgen receptor and its splice variants in castration-resistant prostate cancer. Cancer Res. 2012; 72(14):3457-3462.
60. Hu R, Dunn TA, Wei S, Isharwal S, Veltri RW, Humphreys E, Han M, Partin AW, Vessella RL, Isaacs WB, Bova GS and Luo J. Ligand-independent androgen receptor variants derived from splicing of cryptic exons signify hormone-refractory prostate cancer. Cancer Res. 2009; 69(1):16-22.
61. Guo Z, Yang X, Sun F, Jiang R, Linn DE, Chen H, Chen H, Kong X, Melamed J, Tepper CG, Kung HJ, Brodie AM, Edwards J and Qiu Y. A novel androgen receptor splice variant is up-regulated during prostate cancer progression and promotes androgen depletion-resistant growth. Cancer Res. 2009; 69(6):2305-2313.
62. Sun M and Abdollah F. Re: AR-V7 and Resistance to Enzalutamide and Abiraterone in Prostate Cancer. Eur Urol. 2015; 68(1):162-163.
63. Lokhandwala PM, Riel SL, Haley L, Lu C, Chen Y, Silberstein J, Zhu Y, Zheng G, Lin MT, Gocke CD, Partin AW, Antonarakis ES, Luo J and Eshleman JR. Analytical Validation of Androgen Receptor Splice Variant 7 Detection in a Clinical Laboratory Improvement Amendments (CLIA) Laboratory Setting. J Mol Diagn. 2017; 19(1):115-125.
64. Liu LL, Xie N, Sun S, Plymate S, Mostaghel E and Dong X. Mechanisms of the androgen receptor splicing in prostate cancer cells. Oncogene. 2014; 33(24):3140-3150.
65. Svensson C, Ceder J, Iglesias-Gato D, Chuan YC, Pang ST, Bjartell A, Martinez RM, Bott L, Helczynski L, Ulmert D, Wang Y, Niu Y, Collins C and Flores-Morales A. REST mediates androgen receptor actions on gene repression and predicts early recurrence of prostate cancer. Nucleic Acids Res. 2014; 42(2):999-1015.
66. Bishop JL, Sio A, Angeles A, Roberts ME, Azad AA, Chi KN and Zoubeidi A. PD-L1 is highly expressed in Enzalutamide resistant prostate cancer. Oncotarget. 2015; 6(1):234-242.
67. Epstein JI, Amin MB, Beltran H, Lotan TL, Mosquera JM, Reuter VE, Robinson BD, Troncoso P and Rubin MA. Proposed morphologic classification of prostate cancer with neuroendocrine differentiation. Am J Surg Pathol. 2014; 38(6):756-767.
68. Qi J, Pellecchia M and Ronai ZA. The Siah2-HIF-FoxA2 axis in prostate cancer - new markers and therapeutic opportunities. Oncotarget. 2010; 1(5):379-385.
69. Grignon DJ. Unusual subtypes of prostate cancer. Mod Pathol. 2004; 17(3):316-327.
70. Wang HT, Yao YH, Li BG, Tang Y, Chang JW and Zhang J. Neuroendocrine Prostate Cancer (NEPC) progressing from conventional prostatic adenocarcinoma: factors associated with time to development of NEPC and survival from NEPC diagnosis-a systematic review and pooled analysis. J Clin Oncol. 2014; 32(30):3383-3390.
71. Gillessen S, Omlin A, Attard G, de Bono JS, Efstathiou E, Fizazi K, Halabi S, Nelson PS, Sartor O, Smith MR, Soule HR, Akaza H, Beer TM, Beltran H, Chinnaiyan AM, Daugaard G, et al. Management of patients with advanced prostate cancer: recommendations of the St Gallen Advanced Prostate Cancer Consensus Conference (APCCC) 2015. Ann Oncol. 2015; 26(8):1589-1604.
72. di Sant'Agnese PA and Cockett AT. Neuroendocrine differentiation in prostatic malignancy. Cancer. 1996; 78(2):357-361.
73. Aparicio A, Logothetis CJ and Maity SN. Understanding the lethal variant of prostate cancer: power of examining extremes. Cancer Discov. 2011; 1(6):466-468.
74. Tzelepi V, Zhang J, Lu JF, Kleb B, Wu G, Wan X, Hoang A, Efstathiou E, Sircar K, Navone NM, Troncoso P, Liang S, Logothetis CJ, Maity SN and Aparicio AM. Modeling a lethal prostate cancer variant with small-cell carcinoma features. Clin Cancer Res. 2012; 18(3):666-677.

75. Parimi V, Goyal R, Poropatich K and Yang XJ. Neuroendocrine differentiation of prostate cancer: a review. Am J Clin Exp Urol. 2014; 2(4):273-285.
76. Alanee S, Moore A, Nutt M, Holland B, Dynda D, El-Zawahry A and McVary KT. Contemporary Incidence and Mortality Rates of Neuroendocrine Prostate Cancer. Anticancer Res. 2015; 35(7):4145-4150.
77. Beltran H, Tagawa ST, Park K, MacDonald T, Milowsky MI, Mosquera JM, Rubin MA and Nanus DM. Challenges in recognizing treatment-related neuroendocrine prostate cancer. J Clin Oncol. 2012; 30(36):e386-389.
78. Wright ME, Tsai MJ and Aebersold R. Androgen receptor represses the neuroendocrine transdifferentiation process in prostate cancer cells. Mol Endocrinol. 2003; 17(9):1726-1737.
79. Wang W and Epstein JI. Small cell carcinoma of the prostate. A morphologic and immunohistochemical study of 95 cases. Am J Surg Pathol. 2008; 32(1):65-71.
80. Guate JL, Escaf S, Menendez CL, del Valle M and Vega JA. Neuroendocrine cells in benign prostatic hyperplasia and prostatic carcinoma: effect of hormonal treatment. Urol Int. 1997; 59(3):149-153.
81. Lapuk AV, Wu C, Wyatt AW, McPherson A, McConeghy BJ, Brahmbhatt S, Mo F, Zoubeidi A, Anderson S, Bell RH, Haegert A, Shukin R, Wang Y, Fazli L, Hurtado-Coll A, Jones EC, et al. From sequence to molecular pathology, and a mechanism driving the neuroendocrine phenotype in prostate cancer. J Pathol. 2012; 227(3):286-297.
82. Miyoshi Y, Uemura H, Kitami K, Satomi Y, Kubota Y and Hosaka M. Neuroendocrine differentiated small cell carcinoma presenting as recurrent prostate cancer after androgen deprivation therapy. BJU Int. 2001; 88(9):982-983.
83. Burchardt T, Burchardt M, Chen MW, Cao Y, de la Taille A, Shabsigh A, Hayek O, Dorai T and Buttyan R. Transdifferentiation of prostate cancer cells to a neuroendocrine cell phenotype in vitro and in vivo. J Urol. 1999; 162(5):1800-1805.
84. Germann M, Wetterwald A, Guzman-Ramirez N, van der Pluijm G, Culig Z, Cecchini MG, Williams ED and Thalmann GN. Stem-like cells with luminal progenitor phenotype survive castration in human prostate cancer. Stem Cells. 2012; 30(6):1076-1086.
85. Stratton M, Evans DJ and Lampert IA. Prostatic adenocarcinoma evolving into carcinoid: selective effect of hormonal treatment? J Clin Pathol. 1986; 39(7):750-756.
86. Sasaki T, Komiya A, Suzuki H, Shimbo M, Ueda T, Akakura K and Ichikawa T. Changes in chromogranin a serum levels during endocrine therapy in metastatic prostate cancer patients. Eur Urol. 2005; 48(2):224-229; discussion 229-230.
87. Yuan TC, Veeramani S, Lin FF, Kondrikou D, Zelivianski S, Igawa T, Karan D, Batra SK and Lin MF. Androgen deprivation induces human prostate epithelial neuroendocrine differentiation of androgen-sensitive LNCaP cells. Endocr Relat Cancer. 2006; 13(1):151-167.
88. Bishop JL, Thaper D, Vahid S, Davies A, Ketola K, Kuruma H, Jama R, Nip KM, Angeles A, Johnson F, Wyatt AW, Fazli L, Gleave ME, Lin D, Rubin MA, Collins CC, et al. The Master Neural Transcription Factor BRN2 Is an Androgen Receptor-Suppressed Driver of Neuroendocrine Differentiation in Prostate Cancer. Cancer Discov. 2017; 7(1):54-71.
89. Li Y, Donmez N, Sahinalp C, Xie N, Wang Y, Xue H, Mo F, Beltran H, Gleave M, Wang Y, Collins C and Dong X. SRRM4 Drives Neuroendocrine Transdifferentiation of Prostate Adenocarcinoma Under Androgen Receptor Pathway Inhibition. Eur Urol. 2017; 71(1):68-78.
90. Akamatsu S, Wyatt AW, Lin D, Lysakowski S, Zhang F, Kim S, Tse C, Wang K, Mo F, Haegert A, Brahmbhatt S, Bell R, Adomat H, Kawai Y, Xue H, Dong X, et al. The Placental Gene PEG10 Promotes Progression of Neuroendocrine Prostate Cancer. Cell Rep. 2015; 12(6):922-936.
91. Bonkhoff H, Stein U and Remberger K. Endocrine-paracrine cell types in the prostate and prostatic adenocarcinoma are postmitotic cells. Hum Pathol. 1995; 26(2):167-170.
92. Sauer CG, Roemer A and Grobholz R. Genetic analysis of neuroendocrine tumor cells in prostatic carcinoma. Prostate. 2006; 66(3):227-234.
93. Lotan TL, Gupta NS, Wang W, Toubaji A, Haffner MC, Chaux A, Hicks JL, Meeker AK, Bieberich CJ, De Marzo AM, Epstein JI and Netto GJ. ERG gene rearrangements are common in prostatic small cell carcinomas. Mod Pathol. 2011; 24(6):820-828.

94. Hansel DE, Nakayama M, Luo J, Abukhdeir AM, Park BH, Bieberich CJ, Hicks JL, Eisenberger M, Nelson WG, Mostwin JL and De Marzo AM. Shared TP53 gene mutation in morphologically and phenotypically distinct concurrent primary small cell neuroendocrine carcinoma and adenocarcinoma of the prostate. Prostate. 2009; 69(6):603-609.
95. Huang J, Yao JL, di Sant'Agnese PA, Yang Q, Bourne PA and Na Y. Immunohistochemical characterization of neuroendocrine cells in prostate cancer. Prostate. 2006; 66(13):1399-1406.
96. Bonkhoff H, Stein U and Remberger K. Multidirectional differentiation in the normal, hyperplastic, and neoplastic human prostate: simultaneous demonstration of cell-specific epithelial markers. Hum Pathol. 1994; 25(1):42-46.
97. Jongsma J, Oomen MH, Noordzij MA, Romijn JC, van Der Kwast TH, Schroder FH and van Steenbrugge GJ. Androgen-independent growth is induced by neuropeptides in human prostate cancer cell lines. Prostate. 2000; 42(1):34-44.
98. Mori S, Murakami-Mori K and Bonavida B. Interleukin-6 induces G1 arrest through induction of p27(Kip1), a cyclin-dependent kinase inhibitor, and neuron-like morphology in LNCaP prostate tumor cells. Biochem Biophys Res Commun. 1999; 257(2):609-614.
99. Albrecht M, Doroszewicz J, Gillen S, Gomes I, Wilhelm B, Stief T and Aumuller G. Proliferation of prostate cancer cells and activity of neutral endopeptidase is regulated by bombesin and IL-1beta with IL-1beta acting as a modulator of cellular differentiation. Prostate. 2004; 58(1):82-94.
100. Lee LF, Louie MC, Desai SJ, Yang J, Chen HW, Evans CP and Kung HJ. Interleukin-8 confers androgen-independent growth and migration of LNCaP: differential effects of tyrosine kinases Src and FAK. Oncogene. 2004; 23(12):2197-2205.
101. Deng X, Liu H, Huang J, Cheng L, Keller ET, Parsons SJ and Hu CD. Ionizing radiation induces prostate cancer neuroendocrine differentiation through interplay of CREB and ATF2: implications for disease progression. Cancer Res. 2008; 68(23):9663-9670.
102. Bang YJ, Pirnia F, Fang WG, Kang WK, Sartor O, Whitesell L, Ha MJ, Tsokos M, Sheahan MD, Nguyen P, Niklinski WT, Myers CE and Trepel JB. Terminal neuroendocrine differentiation of human prostate carcinoma cells in response to increased intracellular cyclic AMP. Proc Natl Acad Sci U S A. 1994; 91(12):5330-5334.
103. Shen R, Dorai T, Szaboles M, Katz AE, Olsson CA and Buttyan R. Transdifferentiation of cultured human prostate cancer cells to a neuroendocrine cell phenotype in a hormone-depleted medium. Urol Oncol. 1997; 3(2):67-75.
104. Cox ME, Deeble PD, Lakhani S and Parsons SJ. Acquisition of neuroendocrine characteristics by prostate tumor cells is reversible: implications for prostate cancer progression. Cancer Res. 1999; 59(15):3821-3830.
105. Deeble PD, Murphy DJ, Parsons SJ and Cox ME. Interleukin-6- and cyclic AMP-mediated signaling potentiates neuroendocrine differentiation of LNCaP prostate tumor cells. Mol Cell Biol. 2001; 21(24):8471-8482.
106. Zhu Y, Liu C, Cui Y, Nadiminty N, Lou W and Gao AC. Interleukin-6 induces neuroendocrine differentiation (NED) through suppression of RE-1 silencing transcription factor (REST). Prostate. 2014; 74(11):1086-1094.
107. Lou W, Ni Z, Dyer K, Tweardy DJ and Gao AC. Interleukin-6 induces prostate cancer cell growth accompanied by activation of stat3 signaling pathway. Prostate. 2000; 42(3):239-242.
108. Spiotto MT and Chung TD. STAT3 mediates IL-6-induced neuroendocrine differentiation in prostate cancer cells. Prostate. 2000; 42(3):186-195.
109. Lee LF, Guan J, Qiu Y and Kung HJ. Neuropeptide-induced androgen independence in prostate cancer cells: roles of nonreceptor tyrosine kinases Etk/Bmx, Src, and focal adhesion kinase. Mol Cell Biol. 2001; 21(24):8385-8397.
110. Qi J, Nakayama K, Cardiff RD, Borowsky AD, Kaul K, Williams R, Krajewski S, Mercola D, Carpenter PM, Bowtell D and Ronai ZA. Siah2-dependent concerted activity of HIF and FoxA2 regulates formation of neuroendocrine phenotype and neuroendocrine prostate tumors. Cancer Cell. 2010; 18(1):23-38.

111. Danza G, Di Serio C, Rosati F, Lonetto G, Sturli N, Kacer D, Pennella A, Ventimiglia G, Barucci R, Piscazzi A, Prudovsky I, Landriscina M, Marchionni N and Tarantini F. Notch signaling modulates hypoxia-induced neuroendocrine differentiation of human prostate cancer cells. Mol Cancer Res. 2012; 10(2):230-238.
112. Beltran H, Rickman DS, Park K, Chae SS, Sboner A, MacDonald TY, Wang Y, Sheikh KL, Terry S, Tagawa ST, Dhir R, Nelson JB, de la Taille A, Allory Y, Gerstein MB, Perner S, et al. Molecular characterization of neuroendocrine prostate cancer and identification of new drug targets. Cancer Discov. 2011; 1(6):487-495.
113. Mosquera JM, Beltran H, Park K, MacDonald TY, Robinson BD, Tagawa ST, Perner S, Bismar TA, Erbersdobler A, Dhir R, Nelson JB, Nanus DM and Rubin MA. Concurrent AURKA and MYCN gene amplifications are harbingers of lethal treatment-related neuroendocrine prostate cancer. Neoplasia. 2013; 15(1):1-10.
114. Lee JK, Phillips JW, Smith BA, Park JW, Stoyanova T, McCaffrey EF, Baertsch R, Sokolov A, Meyerowitz JG, Mathis C, Cheng D, Stuart JM, Shokat KM, Gustafson WC, Huang J and Witte ON. N-Myc Drives Neuroendocrine Prostate Cancer Initiated from Human Prostate Epithelial Cells. Cancer Cell. 2016; 29(4):536-547.
115. Tsai H, Morais CL, Alshalalfa M, Tan HL, Haddad Z, Hicks J, Gupta N, Epstein JI, Netto GJ, Isaacs WB, Luo J, Mehra R, Vessella RL, Karnes RJ, Schaeffer EM, Davicioni E, et al. Cyclin D1 Loss Distinguishes Prostatic Small-Cell Carcinoma from Most Prostatic Adenocarcinomas. Clin Cancer Res. 2015; 21(24):5619-5629.
116. Penney KL, Stampfer MJ, Jahn JL, Sinnott JA, Flavin R, Rider JR, Finn S, Giovannucci E, Sesso HD, Loda M, Mucci LA and Fiorentino M. Gleason grade progression is uncommon. Cancer Res. 2013; 73(16):5163-5168.
117. Miller DC, Hafez KS, Stewart A, Montie JE and Wei JT. Prostate carcinoma presentation, diagnosis, and staging: an update form the National Cancer Data Base. Cancer. 2003; 98(6):1169-1178.
118. Cancer Genome Atlas Research Network. Electronic address scmo and Cancer Genome Atlas Research N. The Molecular Taxonomy of Primary Prostate Cancer. Cell. 2015; 163(4):1011-1025.
119. Yoshimoto M, Cunha IW, Coudry RA, Fonseca FP, Torres CH, Soares FA and Squire JA. FISH analysis of 107 prostate cancers shows that PTEN genomic deletion is associated with poor clinical outcome. Br J Cancer. 2007; 97(5):678-685.
120. Tomlins SA, Palanisamy N, Siddiqui J, Chinnaiyan AM and Kunju LP. Antibody-based detection of ERG rearrangements in prostate core biopsies, including diagnostically challenging cases: ERG staining in prostate core biopsies. Arch Pathol Lab Med. 2012; 136(8):935-946.
121. Scheble VJ, Braun M, Wilbertz T, Stiedl AC, Petersen K, Schilling D, Reischl M, Seitz G, Fend F, Kristiansen G and Perner S. ERG rearrangement in small cell prostatic and lung cancer. Histopathology. 2010; 56(7):937-943.
122. Brenner JC, Ateeq B, Li Y, Yocum AK, Cao Q, Asangani IA, Patel S, Wang X, Liang H, Yu J, Palanisamy N, Siddiqui J, Yan W, Cao X, Mehra R, Sabolch A, et al. Mechanistic rationale for inhibition of poly(ADP-ribose) polymerase in ETS gene fusion-positive prostate cancer. Cancer Cell. 2011; 19(5):664-678.
123. Chatterjee P, Choudhary GS, Sharma A, Singh K, Heston WD, Ciezki J, Klein EA and Almasan A. PARP inhibition sensitizes to low dose-rate radiation TMPRSS2-ERG fusion gene-expressing and PTEN-deficient prostate cancer cells. PLoS One. 2013; 8(4):e60408.
124. Na R, Zheng SL, Han M, Yu H, Jiang D, Shah S, Ewing CM, Zhang L, Novakovic K, Petkewicz J, Gulukota K, Helseth DL, Jr., Quinn M, Humphries E, Wiley KE, Isaacs SD, et al. Germline Mutations in ATM and BRCA1/2 Distinguish Risk for Lethal and Indolent Prostate Cancer and are Associated with Early Age at Death. Eur Urol. 2017; 71(5):740-747.
125. Fong PC, Boss DS, Yap TA, Tutt A, Wu P, Mergui-Roelvink M, Mortimer P, Swaisland H, Lau A, O'Connor MJ, Ashworth A, Carmichael J, Kaye SB, Schellens JH and de Bono JS. Inhibition of poly(ADP-ribose) polymerase in tumors from BRCA mutation carriers. N Engl J Med. 2009; 361(2):123-134.
126. Blattner M, Liu D, Robinson BD, Huang D, Poliakov A, Gao D, Nataraj S, Deonarine LD, Augello MA, Sailer V, Ponnala L, Ittmann M, Chinnaiyan AM, Sboner A, Chen Y, Rubin MA, et al. SPOP Mutation Drives Prostate Tumorigenesis In Vivo through Coordinate Regulation of PI3K/mTOR and AR Signaling. Cancer Cell. 2017; 31(3):436-451.

127. Boysen G, Barbieri CE, Prandi D, Blattner M, Chae SS, Dahija A, Nataraj S, Huang D, Marotz C, Xu L, Huang J, Lecca P, Chhangawala S, Liu D, Zhou P, Sboner A, et al. SPOP mutation leads to genomic instability in prostate cancer. Elife. 2015; 4.
128. Shenoy TR, Boysen G, Wang MY, Xu QZ, Guo W, Koh FM, Wang C, Zhang LZ, Wang Y, Gil V, Aziz S, Christova R, Rodrigues DN, Crespo M, Rescigno P, Tunariu N, et al. CHD1 loss sensitizes prostate cancer to DNA damaging therapy by promoting error-prone double-strand break repair. Ann Oncol. 2017.
129. Tomlins SA, Rhodes DR, Yu J, Varambally S, Mehra R, Perner S, Demichelis F, Helgeson BE, Laxman B, Morris DS, Cao Q, Cao X, Andren O, Fall K, Johnson L, Wei JT, et al. The role of SPINK1 in ETS rearrangement-negative prostate cancers. Cancer Cell. 2008; 13(6):519-528.
130. Barbieri CE, Baca SC, Lawrence MS, Demichelis F, Blattner M, Theurillat JP, White TA, Stojanov P, Van Allen E, Stransky N, Nickerson E, Chae SS, Boysen G, Auclair D, Onofrio RC, Park K, et al. Exome sequencing identifies recurrent SPOP, FOXA1 and MED12 mutations in prostate cancer. Nat Genet. 2012; 44(6):685-689.
131. Ateeq B, Tomlins SA, Laxman B, Asangani IA, Cao Q, Cao X, Li Y, Wang X, Feng FY, Pienta KJ, Varambally S and Chinnaiyan AM. Therapeutic targeting of SPINK1-positive prostate cancer. Sci Transl Med. 2011; 3(72):72ra17.
132. Aryee MJ, Liu W, Engelmann JC, Nuhn P, Gurel M, Haffner MC, Esopi D, Irizarry RA, Getzenberg RH, Nelson WG, Luo J, Xu J, Isaacs WB, Bova GS and Yegnasubramanian S. DNA methylation alterations exhibit intraindividual stability and interindividual heterogeneity in prostate cancer metastases. Sci Transl Med. 2013; 5(169):169ra110.
133. Brocks D, Assenov Y, Minner S, Bogatyrova O, Simon R, Koop C, Oakes C, Zucknick M, Lipka DB, Weischenfeldt J, Feuerbach L, Cowper-Sal Lari R, Lupien M, Brors B, Korbel J, Schlomm T, et al. Intratumor DNA methylation heterogeneity reflects clonal evolution in aggressive prostate cancer. Cell Rep. 2014; 8(3):798-806.
134. Yegnasubramanian S, Kowalski J, Gonzalgo ML, Zahurak M, Piantadosi S, Walsh PC, Bova GS, De Marzo AM, Isaacs WB and Nelson WG. Hypermethylation of CpG islands in primary and metastatic human prostate cancer. Cancer Res. 2004; 64(6):1975-1986.
135. Fraser M, Sabelnykova VY, Yamaguchi TN, Heisler LE, Livingstone J, Huang V, Shiah YJ, Yousif F, Lin X, Masella AP, Fox NS, Xie M, Prokopec SD, Berlin A, Lalonde E, Ahmed M, et al. Genomic hallmarks of localized, non-indolent prostate cancer. Nature. 2017; 541(7637):359-364.
136. Mundbjerg K, Chopra S, Alemozaffar M, Duymich C, Lakshminarasimhan R, Nichols PW, Aron M, Siegmund KD, Ukimura O, Aron M, Stern M, Gill P, Carpten JD, Orntoft TF, Sorensen KD, Weisenberger DJ, et al. Identifying aggressive prostate cancer foci using a DNA methylation classifier. Genome Biol. 2017; 18(1):3.
137. Baca SC, Prandi D, Lawrence MS, Mosquera JM, Romanel A, Drier Y, Park K, Kitabayashi N, MacDonald TY, Ghandi M, Van Allen E, Kryukov GV, Sboner A, Theurillat JP, Soong TD, Nickerson E, et al. Punctuated evolution of prostate cancer genomes. Cell. 2013; 153(3):666-677.
138. Holland AJ and Cleveland DW. Chromoanagenesis and cancer: mechanisms and consequences of localized, complex chromosomal rearrangements. Nat Med. 2012; 18(11):1630-1638.
139. Wu C, Wyatt AW, McPherson A, Lin D, McConeghy BJ, Mo F, Shukin R, Lapuk AV, Jones SJ, Zhao Y, Marra MA, Gleave ME, Volik SV, Wang Y, Sahinalp SC and Collins CC. Poly-gene fusion transcripts and chromothripsis in prostate cancer. Genes Chromosomes Cancer. 2012; 51(12):1144-1153.
140. Hendriks RJ, van Oort IM and Schalken JA. Blood-based and urinary prostate cancer biomarkers: a review and comparison of novel biomarkers for detection and treatment decisions. Prostate Cancer Prostatic Dis. 2017; 20(1):12-19.
141. Catalona WJ, Partin AW, Sanda MG, Wei JT, Klee GG, Bangma CH, Slawin KM, Marks LS, Loeb S, Broyles DL, Shin SS, Cruz AB, Chan DW, Sokoll LJ, Roberts WL, van Schaik RH, et al. A multicenter study of [-2]pro-prostate specific antigen combined with prostate specific antigen and free prostate specific antigen for prostate cancer detection in the 2.0 to 10.0 ng/ml prostate specific antigen range. J Urol. 2011; 185(5):1650-1655.

142. Tomlins SA, Aubin SM, Siddiqui J, Lonigro RJ, Sefton-Miller L, Miick S, Williamsen S, Hodge P, Meinke J, Blase A, Penabella Y, Day JR, Varambally R, Han B, Wood D, Wang L, et al. Urine TMPRSS2:ERG fusion transcript stratifies prostate cancer risk in men with elevated serum PSA. Sci Transl Med. 2011; 3(94):94ra72.
143. Minciacchi VR, Zijlstra A, Rubin MA and Di Vizio D. Extracellular vesicles for liquid biopsy in prostate cancer: where are we and where are we headed? Prostate Cancer Prostatic Dis. 2017.
144. Del Re M, Biasco E, Crucitta S, Derosa L, Rofi E, Orlandini C, Miccoli M, Galli L, Falcone A, Jenster GW, van Schaik RH and Danesi R. The Detection of Androgen Receptor Splice Variant 7 in Plasma-derived Exosomal RNA Strongly Predicts Resistance to Hormonal Therapy in Metastatic Prostate Cancer Patients. Eur Urol. 2017; 71(4):680-687.
145. Steinestel J, Luedeke M, Arndt A, Schnoeller TJ, Lennerz JK, Wurm C, Maier C, Cronauer MV, Steinestel K and Schrader AJ. Detecting predictive androgen receptor modifications in circulating prostate cancer cells. Oncotarget. 2015.
146. Scher HI, Lu D, Schreiber NA, Louw J, Graf RP, Vargas HA, Johnson A, Jendrisak A, Bambury R, Danila D, McLaughlin B, Wahl J, Greene SB, Heller G, Marrinucci D, Fleisher M, et al. Association of AR-V7 on Circulating Tumor Cells as a Treatment-Specific Biomarker With Outcomes and Survival in Castration-Resistant Prostate Cancer. JAMA Oncol. 2016; 2(11):1441-1449.
147. Miyamoto DT, Lee RJ, Stott SL, Ting DT, Wittner BS, Ulman M, Smas ME, Lord JB, Brannigan BW, Trautwein J, Bander NH, Wu CL, Sequist LV, Smith MR, Ramaswamy S, Toner M, et al. Androgen receptor signaling in circulating tumor cells as a marker of hormonally responsive prostate cancer. Cancer Discov. 2012; 2(11):995-1003.
148. Beltran H, Jendrisak A, Landers M, Mosquera JM, Kossai M, Louw J, Krupa R, Graf RP, Schreiber NA, Nanus DM, Tagawa ST, Marrinucci D, Dittamore R and Scher HI. The Initial Detection and Partial Characterization of Circulating Tumor Cells in Neuroendocrine Prostate Cancer. Clin Cancer Res. 2016; 22(6):1510-1519.
149. Goldkorn A, Ely B, Quinn DI, Tangen CM, Fink LM, Xu T, Twardowski P, Van Veldhuizen PJ, Agarwal N, Carducci MA, Monk JP, 3rd, Datar RH, Garzotto M, Mack PC, Lara P, Jr., Higano CS, et al. Circulating tumor cell counts are prognostic of overall survival in SWOG S0421: a phase III trial of docetaxel with or without atrasentan for metastatic castration-resistant prostate cancer. J Clin Oncol. 2014; 32(11):1136-1142.
150. Scher HI, Heller G, Molina A, Attard G, Danila DC, Jia X, Peng W, Sandhu SK, Olmos D, Riisnaes R, McCormack R, Burzykowski T, Kheoh T, Fleisher M, Buyse M and de Bono JS. Circulating tumor cell biomarker panel as an individual-level surrogate for survival in metastatic castration-resistant prostate cancer. J Clin Oncol. 2015; 33(12):1348-1355.
151. Ross RW, Galsky MD, Scher HI, Magidson J, Wassmann K, Lee GS, Katz L, Subudhi SK, Anand A, Fleisher M, Kantoff PW and Oh WK. A whole-blood RNA transcript-based prognostic model in men with castration-resistant prostate cancer: a prospective study. Lancet Oncol. 2012; 13(11):1105-1113.
152. Olmos D, Brewer D, Clark J, Danila DC, Parker C, Attard G, Fleisher M, Reid AH, Castro E, Sandhu SK, Barwell L, Oommen NB, Carreira S, Drake CG, Jones R, Cooper CS, et al. Prognostic value of blood mRNA expression signatures in castration-resistant prostate cancer: a prospective, two-stage study. Lancet Oncol. 2012; 13(11):1114-1124.
153. Davis JW. Novel commercially available genomic tests for prostate cancer: a roadmap to understanding their clinical impact. BJU Int. 2014; 114(3):320-322.
154. Alshalalfa M, Schliekelman M, Shin H, Erho N and Davicioni E. Evolving transcriptomic fingerprint based on genome-wide data as prognostic tools in prostate cancer. Biol Cell. 2015; 107(7):232-244.
155. Hagemann IS. Molecular Testing in Breast Cancer: A Guide to Current Practices. Arch Pathol Lab Med. 2016; 140(8):815-824.
156. Jang S and Atkins MB. Which drug, and when, for patients with BRAF-mutant melanoma? Lancet Oncol. 2013; 14(2):e60-69.
157. Lindeman NI, Cagle PT, Beasley MB, Chitale DA, Dacic S, Giaccone G, Jenkins RB, Kwiatkowski DJ, Saldivar JS, Squire J, Thunnissen E, Ladanyi M, College of American Pathologists International Association for the

Study of Lung C and Association for Molecular P. Molecular testing guideline for selection of lung cancer patients for EGFR and ALK tyrosine kinase inhibitors: guideline from the College of American Pathologists, International Association for the Study of Lung Cancer, and Association for Molecular Pathology. J Mol Diagn. 2013; 15(4):415-453.

158. Georgi B, Korzeniewski N, Hadaschik B, Grullich C, Roth W, Sultmann H, Pahernik S, Hohenfellner M and Duensing S. Evolving therapeutic concepts in prostate cancer based on genome-wide analyses (review). Int J Oncol. 2014; 45(4):1337-1344.

Chapter 2

TMPRSS2:ERG gene fusion variants induce TGF-β signaling and epithelial to mesenchymal transition in human prostate cancer cells

Published as:

Leonie Ratz, Mark Laible, Lukasz A. Kacprzyk, Stephanie M. Wittig-Blaich, Yanis Tolstov, Stefan Duensing, Peter Altevogt, Sabine M. Klauck and Holger Sültmann
Oncotarget. 2017; 8(15):25115-25130. doi: 10.18632/oncotarget.15931

ABSTRACT

TMPRSS2:ERG (T/E) gene fusions are present in approximately 50% of all prostate cancer cases. The expression of fusion mRNAs from distinct T/E variants is associated with clinicopathological parameters, while the underlying molecular processes remain unclear. We characterized the molecular mechanisms and functional implications caused by doxycycline (Dox)-inducible overexpression of the frequent T/E III and VI fusion variants in LNCaP cells. Induction of T/E expression resulted in increased cellular migratory and invasive potential, and reduced proliferation caused by accumulation in G1 phase. T/E overexpressing cells showed epithelial-to-mesenchymal transition (EMT), as demonstrated by upregulation of TGF-β and WNT pathway genes, mesenchymal markers, and increased phosphorylation of the p38 MAPK. Augmented secretion of TGF-β1 and -β2, and T/E-mediated regulation of *ALK1*, a member of the TGF-β receptor family, was detected. ALK1 inhibition in T/E overexpressing cells blocked p38 phosphorylation and reduced the expression of the TGF-β target genes *VIM*, *MMP1*, *CDH2*, and *SNAI2*. We found a T/E variant VI-specific induction of *miR-503* associated with reduced expression of SMAD7 and CDH1. Overexpression of *miR-503* led to increased levels of *VIM* and *MMP1*. Our findings indicate that TGF-β signaling is a major determinant of EMT in T/E overexpressing LNCaP cells. We provide evidence that T/E VI-specific transcriptional modulation by *miR-503* accounts for differences in the activation of EMT pathway genes, promoting the aggressive phenotype of tumors expressing T/E variant VI. We suggest that ALK1-mediated TGF-β signaling is a novel oncogenic mechanism in T/E positive PCa.

INTRODUCTION

Prostate cancer (PCa) is the most frequently diagnosed cancer among men in Western countries and a major cause of cancer-related mortality [1, 2]. PCa is a heterogeneous disease with several molecular and clinicopathological subtypes. The *TMPRSS2:ERG* (T/E) gene fusion, resulting from a chromosomal rearrangement of *ERG* (v-ets erythroblastosis virus E26 homolog (avian)) to the androgen responsive gene *TMPRSS2* (transmembrane protease, serine 2), is the most frequent somatic alteration in PCa [3], and detectable in 50% of the tumors [4]. In those cases, *ERG* overexpression is driven by the androgen-responsive promoter of *TMPRSS2*, resulting in upregulation of ERG protein and activation of downstream target genes [5]. Ninety percent of prostate cancers overexpressing ERG harbor T/E fusions [5]. However, no consensus on the prognostic significance of T/E fusion-positive tumors has been reached so far [6, 7]. This may be due to differences in tumor characteristics and multiple T/E isoforms [6, 8, 9], which have been associated with clinicopathological parameters [10] and progression [11, 12]. The most common fusion mRNA variant III (T/E III), containing exon 1 of *TMPRSS2* (1-17bp) and exon 4-11 of *ERG* (T1/E4), is present in 86% of fusion-positive tumors [10]. Since exon 1 of *TMPRSS2* is noncoding, this mRNA is translated from an internal ATG site, resulting in a truncated ERG protein. The expression of T/E VI, resulting from fusion of exons 1-2 of *TMPRSS2* to exons 4-11 of *ERG* (T2/E4), has been associated with aggressive disease [10]. This mRNA is translated from a start codon within *TMPRSS2* exon 2 that is in frame with the *ERG* ORF. The resulting protein includes the first five amino acids of TMPRSS2 and lacks the first 12 amino acids of the full-length ERG protein.

Previously, we found T/E specific transcriptional upregulation of genes associated with activated TGF-β/BMP and WNT signaling in fusion-positive PCa compared to fusion-negative PCa [13]. TGF-β and WNT signaling regulate a diverse range of cellular processes related to cancer progression [14, 15] and are major inducers of epithelial-to-mesenchymal transition (EMT) [16]. Here, our aim was to characterize the molecular mechanisms and functional implications of T/E variant overexpression and their consequences on cellular and molecular phenotypes. We focused on the analysis of T/E III and T/E VI gene fusion variants based on their frequencies of occurrence and their association with clinical and pathological variables. We established LNCaP cells, featuring androgen-independency with high levels of androgen receptor (AR), stably overexpressing the T/E III and VI variants in an inducible promoter system (LNCaP-T/E), and examined the effects of overexpression on cellular properties and signal transduction pathways. To validate the observed transcriptional modulation upon *ERG* overexpression in LNCaP, the T/E-positive metastatic prostate cancer cell line NCI-H660 [17] was employed. This cell line harbors both T/E III and T/E VI fusions [17]. Complementary to the LNCaP-T/E model, *ERG* was silenced in NCI-H660 cells using an *ERG*-specific siRNA and mRNA levels of the targets previously measured in LNCaP-T/E clones were assessed. Overall, we found a large degree of commonality but also distinct transcriptional effects between T/E III and VI variants.

MATERIAL AND METHODS

Cell lines and culturing

LNCaP (CRL-1740) and NCI-H660 (CRL-5813) cells were purchased from American Type Culture Collection (ATCC, Manassas, VA, USA). Stably transfected acceptor LNCaP cells were maintained in RPMI1640 (Thermo Fisher Scientific, Waltham, MA, USA), supplemented with 10% of Tet System Approved FBS (tet-FBS, Clontech, Göteborg, Sweden) and 80 µg/mL hygromycin B (Thermo Fisher Scientific). NCI-H660 cells were maintained in HITES medium supplemented with 5% fetal bovine serum according to the provider's instructions. All cell lines were authenticated using Multiplex Cell Authentication by Multiplexion (Heidelberg, Germany) as described recently [61]. The SNP profiles matched known profiles or were unique. The purity of cell lines was validated using the Multiplex cell Contamination Test by Multiplexion (Heidelberg, Germany) as described recently [62]. No Mycoplasma, SMRV or interspecies contamination was detected.

Generation of LNCaP cell models stably expressing T/E variants

Establishment of the LNCaP-T/E variant cell model including T/E sequences is described in the Supplementary Methods, Supplementary Figure 2.1A and Supplementary Figure 2.2. Transgene expression was induced with 50 ng/mL Dox (Sigma-Aldrich, Munich, Germany) in RPMI1640 containing 10% tet-FBS. Medium of the uninduced cells was supplemented with the respective volume of PBS only.

RNA isolation, reverse transcription and quantitative real-time PCR

Total RNA was isolated from cell lines using the miRNeasy Mini Kit (Qiagen, Hilden, Germany) and quality controlled on the 2100 Bioanalyser (Agilent Technologies, Waldbronn, Germany) with RNA 6000 Nano Kit according to manufacturer's protocols. Total RNA was reverse transcribed using the RevertAid H Minus First Strand cDNA Synthesis Kit (Thermo Fisher Scientific). HotStarTaqDNA polymerase (Qiagen) was used for RT-PCR with 50 ng of cDNA template. Relative mRNA levels were assessed by quantitative RT-PCR on the Lightcycler 480 (Roche Diagnostics, Mannheim, Germany) using Universal Probe Library (UPL) assays and primers listed in Supplementary Table S2.1. Linear expression levels were normalized to *GAPDH* using the $2^{(-\Delta\Delta Ct)}$ method [63]. For miRNA quantification, TaqMan® Assays (*hsa-miR-503*, ID: 1048; *RNU6B*, ID: 1093, Thermo Fisher Scientific) were used according to the manufacturer's instruction.

Microarray gene expression profiling

RNA was isolated with the RNase-Free DNase Set (Qiagen) according to the manufacturer's protocol. After quality control, 500ng of total RNA with a concentration of 50 ng/µl were submitted to the DKFZ Genomics and Proteomics Core Facility (GPCF) for Illumina Whole-Genome Expression Beadchip Analysis (Human HT-12 Chip). The raw

data were quantile-normalized using the Bioconductor package preprocessCore in R. The microarray data reported in this study are available from the NCBI GEO database (GSE78032). Genes showing expression fold changes >|1.5| (p-value <0.05) were considered as differentially expressed and were analysed with Ingenuity Pathway Analysis (IPA) (see below). Genes involved in relevant biological processes obtained from microarray analysis were validated by qPCR in the same samples that were used for microarray profiling.

Luciferase reporter assay

Cells seeded in triplicate in 96-well plates at 5000 cells/well were treated with Dox and transfected with 100 ng of either wild-type TOPflash or mutant FOPflash reporter plasmid from the TCF Reporter Plasmid Kit (Merck Millipore, Darmstadt, Germany) using the jetPEI Polyplus transfection reagent (VWR International, Darmstadt, Germany). Firefly luciferase signals were determined 72h after transfection using the ONE-GloTM Luciferase Assay System (Promega, Mannheim, Germany). Activation of the WNT/β-catenin pathway was calculated by dividing wild-type TOPflash by mutant FOPflash activity.

siRNA-mediated gene knock-down

LNCaP-T/E cells were transfected with 20nM siRNA against *TGFB1* (Qiagen) using Lipofectamine RNAiMAX (Thermo Fisher Scientific) and OptiMEM® I (Thermo Fisher Scientific) according to the manufacturer's protocol. Cells transfected with nonsilencing AllStars Negative Control siRNA (Qiagen) were used as controls. Cells were treated for 48h, medium was changed, Dox-supplemented medium was added where indicated and siRNA treatment was repeated. Cells were incubated for 72h and processed for further analysis.

NCI-H660 cells were transfected with 50nM siRNA against *ERG* (Qiagen) using Lipofectamine RNAiMAX (Thermo Fisher Scientific) and OptiMEM® I (Thermo Fisher Scientific) according to the manufacturer's protocol. Cells transfected with nonsilencing AllStars Negative Control siRNA (Qiagen) were used as controls. Cells were incubated for 72h and processed for further analysis.

miRNA transfection

For transfection, cells were treated with Dox and transfected with *hsa-miR-503-5p* inhibitor (Exiqon, Vedbaek, Denmark) or *hsa-miR-503-5p* mimic (GE Healthcare, Rosersberg, Sweden) using Lipofectamine RNAiMAX transfection reagent (Thermo Fisher Scientific).

Pharmacological inhibitors

The ALK1 inhibitor K02288 (Biomol, Hamburg, Germany) was dissolved at a concentration of 100mM in DMSO. Further dilutions of K02288 were made in PBS to reduce the

final concentration of DMSO in the assay. Equal amounts of DMSO added to the cell culture medium served as negative control. RhALK1 (R&D, Wiesbaden, Germany) was dissolved in PBS at a concentration of 100 µg/mL, and rhFZD4 (R&D) was dissolved in PBS at a concentration of 400 µg/mL. Here, PBS was added to the cell culture medium as a negative control. Inhibitors or control solvents were diluted in Dox-containing tet-FBS medium and added to the cells for 48h.

Cell proliferation assay

Cells were treated with Dox for 48h and seeded into 96-well plates at 5000 cells/well in 90µl 10% tet-FBS-containing medium in triplicate. Ten µl of the colorimetric WST-1 reagent (Roche Diagnostics) was added to the medium and incubated at 37°C at the indicated time points. Absorbance was measured one hour after addition of WST-1 reagent using a Tecan Infinite® M200 microplate reader (Tecan Group Ltd., Männedorf, Switzerland).

Migration and invasion assays

In vitro cell migration assays were performed in duplicate using 24-well transwell chambers with 8µm pore size (Merck Millipore). Cells ($5x10^5$ cells/mL) were seeded in the upper chamber in 200µl serum-free medium. 700µl of medium supplemented with 10% FBS as chemoattractant was filled into the bottom well. After 48h of cultivation in 5% CO2 at 37°C, migrated cells attached to the lower surface of the insert were fixed with 100% methanol on ice and stained with 0.1% Crystal Violet (Sigma- Aldrich). Migrated cells were counted in four random fields under a light microscope (10x magnification).

Invasion assays were performed analogously after coating the transwell chambers with 100µl Matrigel (BD Biosciences, Heidelberg, Germany) per filter.

Cell cycle analysis

Twenty-four, 48 and 72h after Dox induction, trypsinized cells were fixed with 100% ice-cold ethanol and stained with propidium iodide (PI) solution (PBS containing 50 µg/mL PI, 0.1 mg/mL RNase A, 0.05% (v/v) Triton X-100). PI staining was analysed using a FACSCanto II flow cytometer (BD Biosciences). Data was analysed using the software Cyflogig, version 1.2.1 (CyFlo Ltd., Turku, Finland).

Cell lysis and Western blot analysis

Whole-cell lysates were prepared in RIPA lysis buffer (50mM Tris-HCl pH 8.0, 150mM NaCl, 1% NP-40, 0.5% sodium deoxycholate, 0.1% SDS), supplemented with 1x cOmplete Mini Protease Inhibitor Cocktail (Roche Diagnostics) and 1x PhosSTOP Phosphatase Inhibitor Cocktail (Roche Diagnostics). Lysates were boiled 5 min at 95°C with 4x reducing Roti-Load protein loading buffer (Roth, Karlsruhe, Germany). Samples were separated on a mini polyacrylamide gel (Bio-Rad, Munich, Germany) and transferred to

PVDF membranes using the Trans-Blot Turbo semi-dry blotting system (Bio-Rad) at 1.3A, 25V for 7-10 min. After blocking with 5% BSA in Tween-20/PBS, membranes were probed with primary antibodies prepared in blocking solution overnight at 4°C on a roller, followed by incubation with horseradish peroxidase-conjugated secondary antibody in blocking solution for 1h at room temperature and ECL detection (Thermo Fisher Scientific) by the ChemiDoc XRS+ system (Bio-Rad). Western blotting was performed using primary antibodies against ERG (Abcam, Cambridge, UK), and SMAD7 (Abcam), AR (Santa Cruz, Dallas, Texas, USA), p-SMAD1/5, SMAD1, p-p38, p38, p-AKT, AKT, CDH1, and GAPDH (all Cell Signaling Technology, Danvers, MA, USA) at 1:1000 dilution. Secondary antibodies used were anti-rabbit-HRP (at 1:25000 dilution; Dianova, Hamburg, Germany) and anti-mouse-HRP (at 1:10000 dilution; Cell Signaling). Quantitative analysis of protein expression relative to GAPDH was done using Image Lab software (Bio-Rad).

Luminex immunoassay

TGF-β signaling pathway components were analysed using the Milliplex Human TGF-β signaling 6-plex (Merck Millipore) and the Milliplex Human Multi-pathway 9-plex assay (Merck Millipore). Total TGF-β protein expression in cell lysates and cell culture supernatants were measured using the Milliplex Human TGF-β 1,2,3 assay (Merck Millipore). For Luminex analysis, the cells were treated with Dox to induce ERG expression. For collection, cell lysates and supernatants were centrifuged (15 min, 4000 rpm, 4°C) after 72h of induction. Immunoassays using Luminex® xMAP® technology were performed according to the manufacturer's instructions. The fluorescent reporter signals were analysed by a Bio-Plex 200 reader (Bio-Rad).

Ingenuity Pathway Analysis

Functional annotation and pathway enrichment of differentially regulated genes were identified using Ingenuity Pathway Analysis (IPA) software (Qiagen). IPA uses the Ingenuity knowledge base, a database of protein and gene interactions integrated from published biomedical literature and 3rd party sources. Analysis using IPA was performed between December 2015 and February 2016 (Ingenuity version 26127183). Genes showing an expression fold change >|1.5| were considered as differentially expressed and included in the analysis.

Functional annotations

Gene expression changes were categorized into functional annotations of molecular and cellular mechanisms. The Ingenuity knowledge base provides a predicted direction of change for the biological function (downstream effect analysis), represented by an activation z-score, where z >2.0 or <-2.0 is predictive for activation or reduction of the

process, respectively. A p-value <0.05 indicates a statistically significant association between a set of differentially expressed genes and a given process.

Pathway enrichment analysis

Ingenuity knowledge base provides an analysis of metabolic and cell signaling pathways that are significantly enriched in the gene expression signature. Significance values were calculated based on Fisher's right tailed exact test and the –log(p-value) by IPA. Pathways meeting the threshold p-value <0.05 were considered as significant. Using the 'Compare' tool, IPA identified the intersection and unique gene sets among T/E III and T/E VI versus empty vector datasets. Upstream regulator analysis can identify molecules upstream of the genes in the dataset that potentially explain the observed gene expression changes and molecular functions. It is based on prior knowledge of expected effects between transcriptional regulators and their target genes stored in the Ingenuity knowledge base.

Statistical testing

Expression differences between the induced and uninduced cells were analysed using a paired t-test and between induced cells of T/E III and VI by an unpaired t-test. Statistical significance of t-test depicted as *p<0.05, **p<0.01, ***p<0.001.

RESULTS

Characterization of T/E expressing LNCaP cells

To study the role of the T/E gene fusion variants (Figure 2.1A), we made use of a Flp recombinase based transfection system allowing stable and inducible expression of T/E variants III and VI in LNCaP cells. An empty expression vector served as a control. The expression of T/E variants (LNCaP-T/E) was verified using RT-PCR (Supplementary Figure S1B). QPCR analysis after Dox-induction showed ~50-fold and ~150-fold upregulation of *ERG* in T/E III and T/E VI cells, respectively (Figure 2.1B). Western blot analysis confirmed the expression of ERG protein in Dox-induced LNCaP-T/E cells only (Figure 2.1C). In line with previous reports that *ERG* expression leads to downregulation of androgen receptor (*AR*) transcripts [18], both LNCaP-T/E III and VI cell lines showed markedly decreased AR protein after *ERG* overexpression (Figure 2.1C), indicating that the cell lines faithfully reflect the *in vivo* situation. Concurrent with reports that lower AR expression is associated with reduced differentiation of PCa cells [19], we noticed morphological changes, including cellular rounding, spindle-like branching, and detachment from adjacent cells (Figure 2.1D), which resembled a fibroblast-like morphology. These results suggested that ERG affects processes controlling the morphology of LNCaP cells.

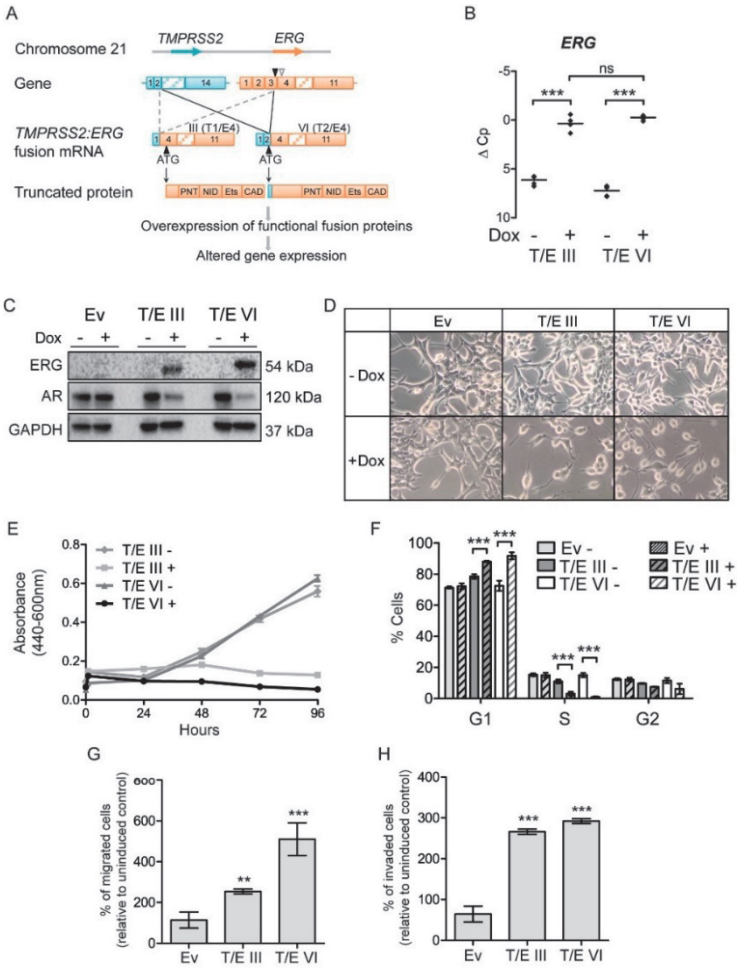

Figure 2.1: Stable T/E variant overexpression in LNCaP cells. (A) Structure of T/E gene fusion variants III and VI; *TMPRSS2* (RefSeq NM_005656), *ERG* (RefSeq NM_004449.4). Downward pointing arrowheads: position of *ERG* fusion break point in T/E III (white) and T/E VI (black). Upward black pointing arrowhead: translation initiation codon. Protein domains: PNT, pointed domain (a protein–protein interaction site); NID, N-terminal inhibitory domain; Ets, Ets-DNA binding domain; CAD, C-terminal activator domain. (B) qPCR of Dox-induced *ERG* expression in T/E III and T/E VI compared to uninduced cells. ΔCp values from three independent experiments are shown relative to *GAPDH*. (C) Western blot analysis of ERG and AR expression in empty vector (Ev), T/E III and T/E VI LNCaP cells, respectively. GAPDH served as protein loading control. (D) Morphological changes induced by Dox-mediated *ERG* overexpression in T/E III and T/E VI and control LNCaP cells. Pictures were taken at 20-fold magnification after 72h Dox induction. (E) Cell growth was measured by a WST-1 assay at the indicated time points after pre-treatment with Dox (three independent experiments). (F) Cell cycle analysis using flow cytometry with propidium iodide (PI) staining. T/E III, T/E VI and empty vector cells were either not treated (-) or treated with Dox (+) and analysed 72h post induction. Data are shown as percent positive staining cells ± s.d. of three independent experiments. (G-H) Quantification of (G) migrated, and (H) invaded T/E expressing cells with a transwell chamber assay. Eight microscopic fields per treatment were analysed and results of three independent experiments are shown. Ev – Empty vector; ns – not significant.

T/E overexpression confers oncogenic properties to LNCaP cells

The impact of T/E overexpression on LNCaP cells was analysed using proliferation, migration and invasion assays. T/E overexpressing cells showed reduced proliferation from 48h to 96h post induction (Figure 2.1E). After 72h, a decreased number of cells in S- and G2-phase and an increased number in G1-phase was observed (Figure 2.1F) for both T/E III and VI variants. No apoptotic cells were detectable in the sub-G1 fractions. Thus, T/E overexpression induced cell cycle changes leading to the accumulation of cells in G1 phase and reduced cell proliferation without evidence of apoptosis. T/E expressing LNCaP cells migrated and invaded significantly faster compared to uninduced or empty vector controls (Figure 2.1G and 1H). The migration rate was higher in T/E VI compared to T/E III cells (Figure 2.1G).

Overexpression of T/E III and VI variants reveal transcriptional programs associated with TGF-β signaling

The transcriptional programs regulated by T/E overexpression were investigated by microarray expression profiling on 48,107 genes (GEO accession GSE78032). Differentially expressed genes (>|1.5| fold change; $p<0.05$) compared to empty vector control (n=4,429; Supplementary Table S2.2) were selected for further analysis using the Ingenuity Pathway Analysis (IPA) program. Of the 2,205 genes, which were altered in both T/E III and VI variants (T/E intersection; Supplementary Table S2.2), 94% showed concordant expression changes, indicating a high degree of accordance between the variants. The number of distinct genes found after T/E III or VI overexpression (T/E III only and T/E VI only) was 418 and 1,806, respectively (Supplementary Table S2.2).

Comparison of differential mRNA expression between LNCaP-T/E cells and T/E-positive *ex vivo* tumors [13] revealed 30% (37/126) overlap, including the genes Tudor Domain Containing 1 (*TDRD1*), Cluster of Differentiation 24 (*CD24*), BMP And Activin Membrane-Bound Inhibitor (*BAMBI*), and Cyclin-Dependent Kinase 1 (*CDK1*) [13]. Furthermore, transcriptional changes in T/E overexpressing cells were consistent with the expected transcriptional response to *ERG* overexpression based on previous findings. For example, AR and the androgen-responsive genes *TMPRSS2* [5, 18], *SLC45A3* [5, 18, 19], *ACPP* [19], and *MSMB* [5, 19] were downregulated, whereas genes known to be activated by ERG, e.g. *PLAT* [18], *PLA1A* [5], and *MMP1* [20] were upregulated. These data indicated that our T/E expressing cell models faithfully reflected the transcriptional regulation in T/E-positive tumors and are suitable to study the biology of these fusion variants.

GO analysis in IPA using the T/E intersection (n=2,205) showed that genes associated with cell proliferation and interphase were downregulated (Supplementary Table S2.3), which was in agreement with the reduced proliferative ability of LNCaP-T/E cells (Figure

2.1E). 'Estrogen-mediated S-phase Entry' was identified among the top significantly enriched canonical pathways (Supplementary Table S2.4). This corresponded to the accumulation of the T/E overexpressing cells in G1 phase (Figure 2.1F). Consistent with the increased number of migrated and invaded cells found in the transwell assays (Figure 2.1G and 2.1H), genes belonging to the category 'Cell invasion' were primarily upregulated (Supplementary Table S2.3).

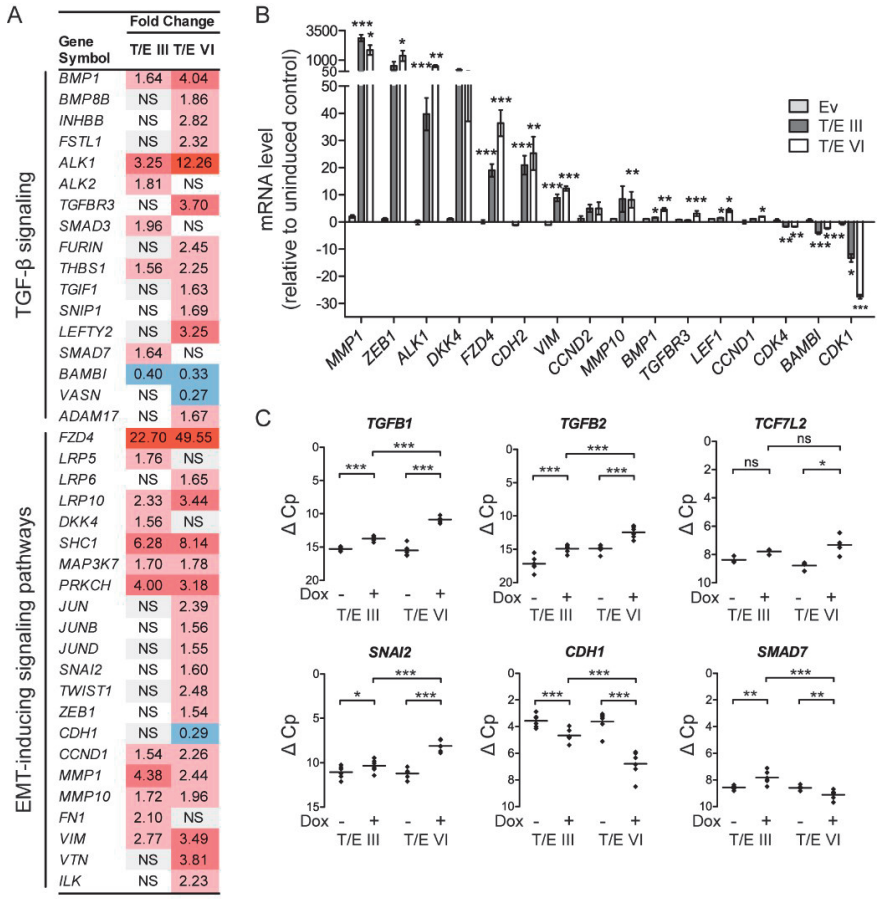

Figure 2.2: Transcriptional modulation in LNCaP-T/E cells. (A) Microarray gene expression data indicating activated TGF-β and EMT-inducing signaling pathways in T/E expressing cells. (B-C) qPCR validation of T/E-induced gene expression changes associated with an EMT profile. (B) mRNA expression after T/E induction relative to uninduced controls. (C) mRNA levels of selected targets showing prominent transcriptional modulation in T/E III and VI overexpressing cells. Data are shown as ΔCp values relative to *GAPDH* measured in the same samples, which had been used for the microarray analysis. Ev - Empty vector; Red - upregulated; blue - downregulated; NS - not significant.

To study potential mechanisms regulating transcriptional changes associated with increased migration and invasion in LNCaP-T/E cells, an upstream regulator analysis was performed with the T/E intersection dataset (Supplementary Table S2.2). The analysis revealed transforming growth factor beta 1 (*TGFB1*) as an upstream regulator of 284 genes that were directly associated with *TGFB1* regulation (Supplementary Table S2.4). These results indicated that TGF-β signaling plays a crucial role in T/E overexpressing cells as previously suggested by us [13]. Evidence for activated TGF-β signaling in the differentially expressed gene set (n=4,429) was provided by upregulation of several TGF-β pathway-specific genes, e.g. bone morphogenetic protein 1 (*BMP1*), or downregulation of negative regulators of TGF-β signaling, such as the pseudoreceptor *BAMBI* (Figure 2.2A). Activation of noncanonical TGF-β signaling was evident by upregulation of SMAD-independent molecules involved in the ERK, JNK/p38 and PI3K/AKT pathways (Figure 2.2A). We also found upregulation of EMT-inducing transcription factors (*SNAI2*, *ZEB1*), mesenchymal markers (*FN1*, *VIM*, *VTN*) and matrix metalloproteinases (*MMP1*, *MMP10*), and downregulation of E-cadherin (*CDH1*) (Figure 2.2A), again supporting our finding that T/E expressing cells lose epithelial characteristics and acquire a mesenchymal phenotype. Of note, the upregulated genes included the type I TGF-β receptor Activin A Receptor Like Type 1 (*ACVRL1*, also known as *ALK1*) (Figure 2.2A), as well as the WNT receptor Frizzled 4 (*FZD4*) and its co-receptors *LRP5* and *LRP6* (Figure 2.2A), suggesting that these receptors might be mediators of transcriptional changes leading to EMT in T/E overexpressing cells.

Validation of the microarray data by qPCR verified the strong upregulation of *ALK1* and *FZD4* in both LNCaP-T/E variants (Figure 2.2B) as well as upregulation of EMT-inducing components and downregulation of genes negatively associated with TGF-β signaling (Figure 2.2B). Notably, the validation confirmed the strong upregulation of the selected EMT inducing ligands (*TGFB1*, 7.3-fold; *TGFB2*, 5.5-fold) and downstream effector genes (*TCF7L2*, 5.1-fold; *SNAI2*, 4.7-fold) in T/E VI cells, whereas *CDH1* (4.3-fold) and *SMAD7* (2.3-fold) were downregulated in T/E VI compared to T/E III expressing cells (Figure 2.2C).

Distinct intracellular signaling molecules are regulated in T/E variants

TGF-β signaling is mediated by SMAD-dependent and -independent signaling pathways involving JNK/p38 MAPK and PI3K/AKT [21, 22]. Multiplex protein quantification using Luminex technology and Western blot (Figure 2.3) for TGF-β signaling analysis revealed increased phosphorylation of p38 MAPK (T/E VI cells only; Figure 2.3A and 3B), AKT (T/E III cells only; Figure 2.3C, 2.3D and 2.3E), JNK (Figure 2.3F), and SMAD1/5 (Figure 2.3G) upon T/E overexpression. Increased levels of p-SMAD1/5 and p-p38 were detectable 4h after T/E induction, concomitant with increasing ERG levels in T/E III and T/E VI cells. Increased phosphorylation of SMAD2 and 3 was not observed (data not shown). The increased AKT phosphorylation in T/E III, but not in T/E VI, expressing cells (Figure 2.3C, 2.3D and 2.3E) went along with the increasing ERG expression as confirmed by quantitative analysis showing the pAKT/AKT ratio in induced and uninduced cells, albeit this was not significant

(Figure 2.3E). High basal levels of pAKT were observed in T/E III cells (Figure 2.3D). Activation of survival-associated processes corresponded to the functional annotation of the T/E gene set (Supplementary Table S2.3). TGF-β-mediated AKT activation has previously been proposed to overcome the growth-inhibitory effects of TGF-β in BPH1 tumorigenic sublines [23]. Taken together, these findings provided evidence for increased TGF-β signaling in both T/E variants, as well as an activated AKT dependent survival network upon T/E III overexpression, that might act together to induce EMT in this PCa cell model.

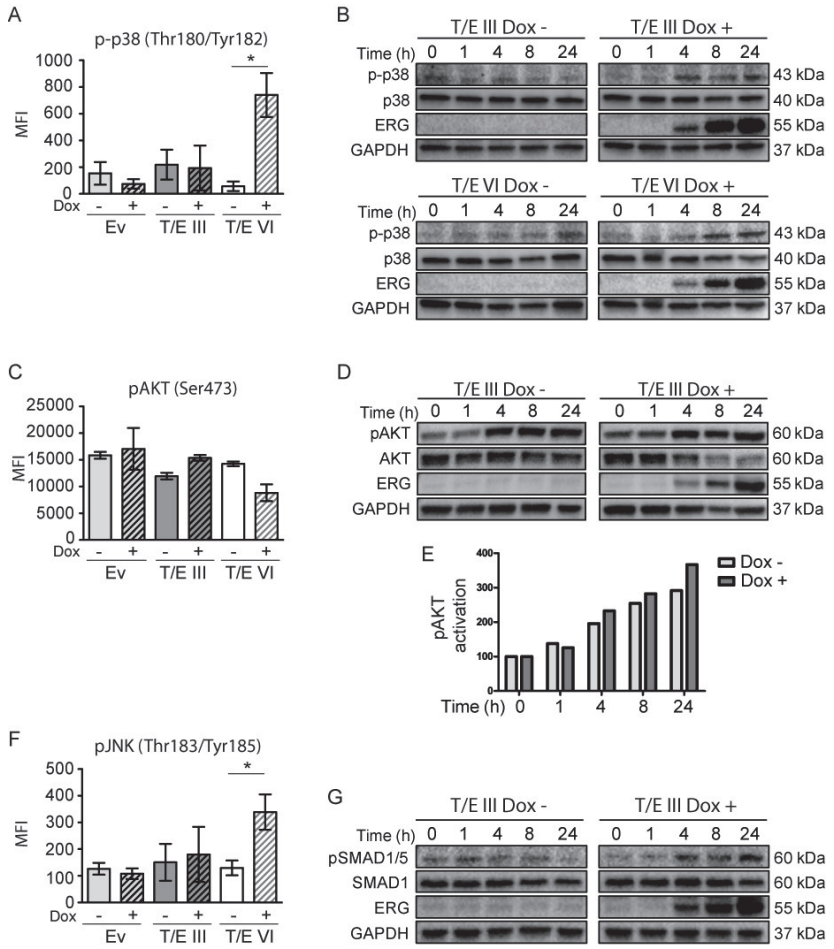

Figure 2.3: Signaling pathways in T/E expressing cells. Activation of signaling molecules (p38, AKT, JNK, and SMAD1/5) in T/E expressing cells measured by Luminex technology (A, C, F), and Western blot analysis (B, D, G). For Western blot analysis, GAPDH served as loading control. Increased p38 phosphorylation (Thr180/Tyr182) was evident in T/E III (B) and T/E VI (A, B) cells. T/E III cells showed increased AKT phosphorylation (Ser473) (C, D). (E) pAKT/AKT ratios after densitometric analysis of Western blot bands of (D). (F) Increased JNK phosphorylation (Thr183/Tyr185) was revealed in T/E VI cells. Increased pSMAD1/5 phosphorylation (Ser463/465) was evident in (G) T/E III cells.

Soluble TGF-β is produced by T/E overexpressing cells

Increased *TGFB1* and *-2* levels in T/E overexpressing cells motivated us to test whether TGF-β is secreted to act in an autocrine manner. Active TGF-β was measured in cell-free conditioned medium using Luminex immunoassays 72h after Dox induction. T/E III and VI overexpressing cells displayed considerably increased TGF-β1 (7-fold and 2-fold, respectively) and TGF-β2 (6-fold and 3-fold, respectively) protein compared to controls (Figure 2.4A). Thus, T/E overexpression induced secretion of TGF-β1 and TGF-β2. SiRNA-mediated *ERG* knockdown in the NCI-H660 PCa cell line carrying both T/E fusion variants III and VI [17] reduced *TGFB1* mRNA levels (Figure 2.5A), further supporting the T/E-mediated upregulation of TGF-β ligands. Moreover, siRNA-mediated *TGFB1* knockdown in T/E III and VI cells led to upregulation of the negative TGF-β regulators *BAMBI* (in T/E III and VI cells) and *SMAD7* (only in T/E VI cells, Figure 2.4B and 2.4C), indicating that *TGFB1* plays a role in T/E-induced TGF-β signaling.

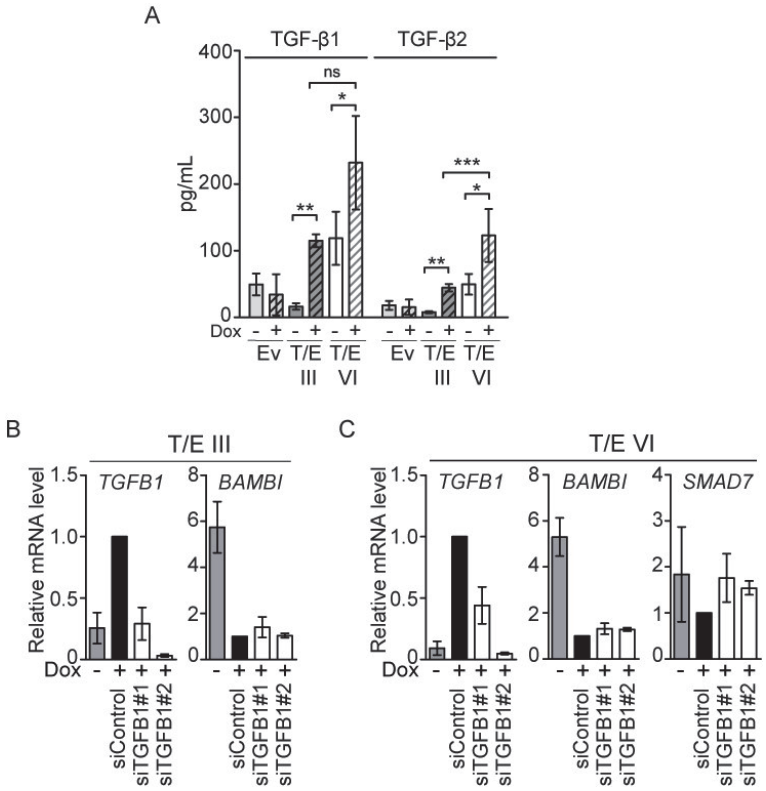

Figure 2.4: TGF-β signaling in LNCaP-T/E cells. (A) TGF-β1 and TGF-β2 released into the medium was determined in cell-free conditioned medium derived from Dox-induced (+) and uninduced (-) LNCaP-T/E cells, respectively. All Luminex results are presented as MFI (mean fluorescent intensity) values ± s.d. of three independent experiments. Ev - Empty vector. (B-C) siRNA-mediated knockdown of *TGFB1* using 20nM siRNA show upregulation of *BAMBI* in (B) T/E III and (C) T/E VI cells and additionally *SMAD7* in T/E VI cells (C) as determined by qPCR.

ALK1 signaling regulates p38 MAPK and EMT markers

Since *ALK1* mRNA was strongly upregulated in T/E overexpressing cells (40-fold in T/E III and 500-fold in T/E VI cells; Figure 2.2B), we analysed this pathway in more detail. *ERG* knockdown in NCI-H660 cells led to reduced *ALK1* mRNA levels (Figure 2.5A) confirming the association between *ERG* and *ALK1* expression. Next, Dox-induced LNCaP-T/E cells were incubated with a human recombinant decoy receptor (rhALK1) [24] or the ALK1 inhibitor K02288 [25]. Disruption of ALK1 signaling using rhALK1 (Figure 2.5B, and 2.5C) or K02288 (Figure 2.5F and 2.5G) resulted in reduced p38 phosphorylation. As expected [26, 27], the inhibitor of differentiation 1 (*ID1*), and *ID2* genes were upregulated after *ERG* induction, but reduced after rhALK1 (Figure 2.5D and 2.5E) or K02288 (Figure 2.5H and 2.5I) treatment. These data suggested that T/E overexpression induces ALK1-signaling and supported the concept that ALK1-mediated phosphorylation of p38 confers mesenchymal transformation of PCa cells. In line with this, rhALK1-mediated inhibition of ALK1 signaling led to reduced expression of *MMP1* (52% reduction) in T/E III (Figure 2.5D), and *MMP1*, *VIM*, and *SNAI2* (39%, 22%, and 5% reduction, respectively) in T/E VI cells (Figure 2.5E). ALK1 inhibition by K02288 also resulted in reduced expression of *MMP1* and *CDH2* (35% and 61% reduction, respectively) in T/E III (Figure 2.5H) and *MMP1*, *CDH2*, *VIM*, and *SNAI2* (72%, 50%, 40%, and 48% reduction, respectively) in T/E VI overexpressing cells (Figure 2.5I).

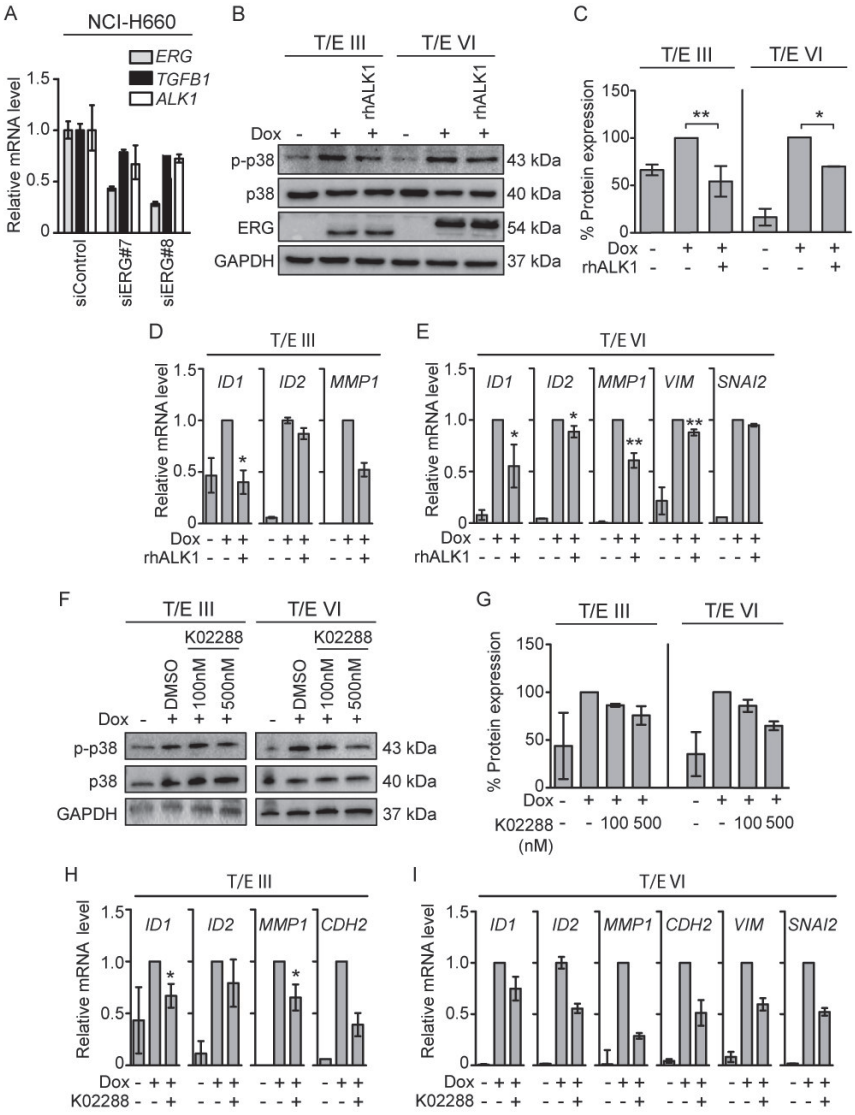

Figure 2.5: ALK1 inhibitors decrease T/E-induced ALK1 signaling. (A) *ERG* knockdown in NCI-H660 cells (50nM of siRNA) showed reduced levels of *TGFB1* and *ALK1*. (B) Western blot analysis in LNCaP-T/E cells revealed reduced p38 phosphorylation after treatment with rhALK1 (5 µg/mL) compared to PBS-treated control cells. (C) p-p38/p38 ratios after densitometric analysis of Western blot bands shown in (B) in T/E III and T/E VI cells, respectively. (D-E) Expression levels of TGF-β-responsive genes in (D) T/E III and (E) T/E VI expressing cells after rhALK1 treatment (5 µg/mL) determined by qPCR. (F) Western blot analysis of p38 phosphorylation after treatment with K02288 (at indicated concentrations) compared to DMSO-treated control cells. (G) p-p38/p38 ratios after densitometric analysis of Western blot bands shown in (F) of T/E III and T/E VI cells, respectively. (H-I) Expression levels of TGF-β/BMP-responsive genes in (H) T/E III and (I) T/E VI expressing cells after simultaneous treatment with Dox and K02288 (500nM) were determined by qPCR.

T/E overexpression activates β-catenin signaling in prostate cancer cells

WNT/β-catenin and TGF-β signaling pathways share key molecules (p38 MAPK, SNAI1/2, ZEB1/2 [16]) and can synergistically induce changes associated with EMT. Since we had identified an EMT transcriptional signature and upregulation of the WNT/β-catenin target genes in T/E overexpressing cells (Figure 2.2A, 2.2B and 2.2C), we characterized signaling downstream of WNT in more detail. Overexpression of both T/E variants led to increased β-catenin signaling (Figure 2.6A), which was 2.4-fold higher in T/E VI compared to T/E III overexpressing cells. To test whether induction of gene expression was mediated by *FZD4* upregulation, we incubated cells with rhFZD4. Disruption of FZD4-signaling showed a clear reduction of p38 phosphorylation in T/E III and T/E VI cells by Western blot (Figure 2.6B), and band quantification (Figure 2.6C). Further, we observed reduced *MMP1*, *VIM*, and *CDH2* levels in T/E III and VI (Figure 2.6D and 2.6E) and additionally reduced *SNAI2* in T/E VI cells (Figure 2.6E). These data suggest that FZD4-induced oncogenic effects of T/E overexpression are mediated by p38.

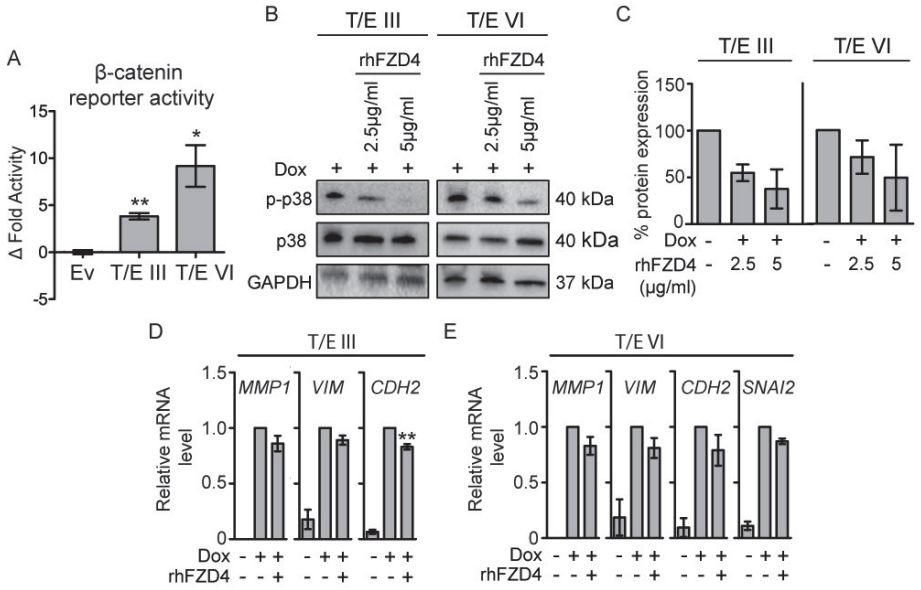

Figure 2.6: T/E expression induces FZD4-mediated β-catenin signaling in LNCaP cells. (A) TOPflash luciferase activity 72h post induction. Mean ± s.d. of three independent experiments are shown. TOPflash activity was normalized to mutant FOPflash activity and relative to uninduced clones. (B-E) Effects of FZD4-specific inhibition using rhFZD4 for 48h compared to PBS-treated control cells. (B) Phosphorylation of p38 was measured by Western blotting and p-p38/p38 (C) ratio was determined after band analysis of (B). (D-E) EMT target gene expression after rhFZD4 treatment (5 µg/mL) was assessed by qPCR in T/E III (D) and T/E VI (E) cells. Ev - Empty vector.

To dissect the sequence of transcriptional changes upon *ERG* overexpression, a time course experiment was performed in T/E expressing cells (Figure 2.7). *ERG* mRNA values showed a rapid increase (~10-fold after 1h, ~100-fold after 4h of Dox-induction) in T/E III (Figure 2.7A) and T/E VI cells (Figure 2.7D). A strong increase in *ALK1* mRNA, and to a lesser extent *FZD4* mRNA, were observed after 8h (Figure 2.7A and 2.7D) suggesting that ERG protein expression, which was detectable after 4h (Figure 2.3B, D, G), preceded mRNA expression of those receptors. The expression levels of *ZEB1* and *MMP1* showed a very strong upregulation after ~12h (*ZEB1*: 450-fold in T/E III and 1500-fold in T/E VI cells; *MMP1*: 35,000-fold in T/E III and 6,600-fold in T/E VI cells) (Figure 2.7B and 2.7E, respectively). The expression of *VIM* was induced after 24h of Dox-treatment (Figure 2.7A and 2.7D, respectively). These findings indicated that the dynamic transcriptional changes of EMT marker expression were preceded by a first wave of *ERG* overexpression and a second wave of increased *ALK1* and *FZD4* expression. Genes, that were negatively associated with TGF-β signaling (*BAMBI*) or associated with epithelial characteristics of LNCaP cells (*AR*, *CDH1*), showed a continuous decrease in expression after 4h of Dox-induction (Figure 2.7C and 2.7F). Of note, in T/E VI cells, *BAMBI* mRNA levels started to replenish after 48h of Dox-induction (Figure 2.7F), together with a declining *ALK1* level (Figure 2.7D). A similar effect was observed in T/E III cells, although at a lower level. By integrating the time course regulatory network with the previously modeled end-point measurements (Figure 2.3), we highlighted the dynamics of cellular activity leading to EMT upon *ERG* overexpression in LNCaP cells.

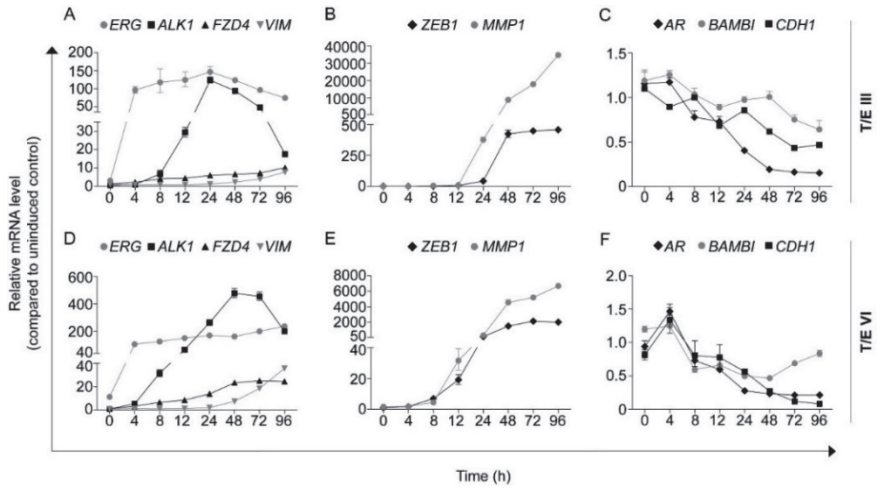

Figure 2.7: Time course experiment of selected ERG downstream targets. (A-C) T/E III and (D-F) T/E VI cells were treated with Dox for the indicated time points (0-96h). Samples were collected and mRNA expression was determined using qPCR. Expression levels are shown relative to uninduced controls at each time point. Upon Dox-induction, *ERG* mRNA levels show a rapid increase in (A) T/E III and (D) T/E VI cells. Subsequently, an increase in *ALK1* and *FZD4* mRNA levels are observed after 8h, followed by upregulation of the EMT marker (A, D) *VIM*, (B, E) *ZEB1* and *MMP1*. Genes that are negatively associated with EMT or TGF-β signaling are repressed upon Dox-induced *ERG* overexpression in (C) T/E III and (F) T/E VI expressing cells.

Upregulation of miR-503 in T/E VI cells promotes EMT by targeting SMAD7

We further aimed to identify determinants of the stronger activation of EMT regulating pathway genes in T/E VI expressing cells. We focused on *miR-503*, which was strongly upregulated in the T/E VI only (~7-fold), but not in the T/E III only microarray dataset (Supplementary Table S2.2). A search for potential *miR-503* targets using in silico prediction algorithms showed that *miR-503* can target *SMAD7* [28], which was downregulated in T/E VI, but upregulated in T/E III cells. We therefore hypothesized that *miR-503* might be a candidate modulating the biological activity of the T/E VI fusion variants. To test whether *miR-503* could augment EMT, we transiently overexpressed and inhibited *miR-503* in T/E III and T/E VI cells using *miR-503* mimics and inhibitors, respectively. Only induced T/E VI cells displayed significant upregulation of *miR-503*, which was further increased by simultaneous *miR-503* overexpression (Figure 2.8A). Key EMT markers like *VIM* and *MMP1* were upregulated in T/E-induced cells and were further increased after *miR-503* overexpression (Figure 2.8B). Inhibition of *miR-503* upon induction of T/E VI expression led to a reduction of *VIM* (Figure 2.8B). The consequences of *miR-503* overexpression, inhibition on SMAD7 and CDH1 quantities as surrogate for a mesenchymal phenotype, were examined by Western blot analysis. *MiR-503* overexpression led to decreased SMAD7 and CDH1 expression in T/E VI cells (Figure 2.8C and 2.8D). These results suggested that T/E VI-mediated overexpression of *miR-503* plays an important role in increasing EMT effectors and that *miR-503* can promote invasion of T/E VI expressing cells by affecting CDH1 expression. Furthermore, *TGFB1* knockdown in T/E VI cells showed reduced expression of *miR-503* (Figure 2.8E), suggesting that the expression of *miR-503* is regulated by TGF-β, thereby contributing to enhanced TGF-β signaling by inhibition of SMAD7 [29]. The varying SMAD7 levels are consistent with the observed differences in TGF-β and WNT/β-catenin signaling activity between T/E III and T/E VI cells.

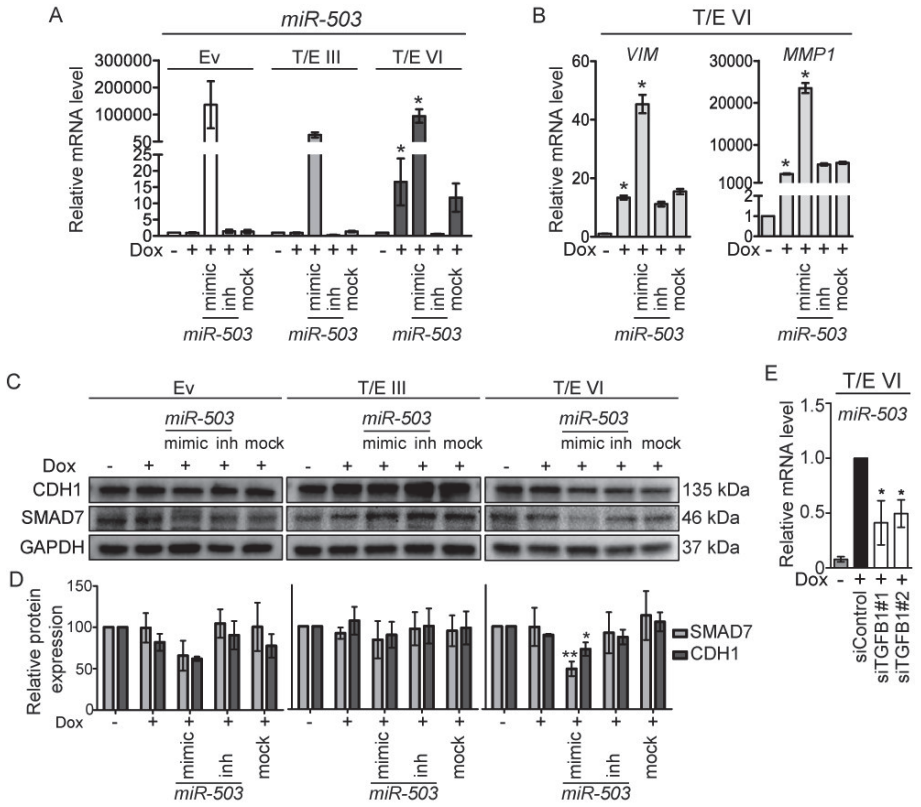

Figure 2.8: *MiR-503* overexpression in T/E VI cells inhibits SMAD7 and CDH1. (A) qPCR analysis of *miR-503* expression relative to *RNU6B*. Values are presented as mean ± s.d. of three independent experiments. (B) qPCR determination of *VIM* and *MMP1* expression in T/E VI expressing cells relative to *GAPDH*. (C) Western blot analysis of SMAD7 and CDH1 protein expression in T/E cells. Representative results of three independent Western blot experiments are shown. (D) Quantitative analysis of protein expression relative to GAPDH is presented as mean ± s.d. of three independent experiments. (E) *miR-503* expression upon siRNA-mediated knockdown of *TGFB1* (20nM) in T/E VI cells was determined by qPCR. Mimic - *hsa-miR-503-5p* mimic (used at 10nM), inh - *hsa-miR-503-5p* inhibitor (used at 100nM).

DISCUSSION

Previously, we reported that transcriptional changes in T/E-positive tumors are associated with deregulated TGF-β/BMP and WNT signaling pathways [13]. Here, by deploying inducible T/E overexpression in LNCaP cell models, we show that overexpression of two distinct T/E variants induce common as well as unique signaling programs that are able to lead the cells into EMT. Upon T/E overexpression, the cells acquire mesenchymal, fibroblast-like morphologies [30]. On the molecular level, this is accompanied

by downregulation of AR, suggesting that ERG disrupts a lineage-specific differentiation program of prostate cells [18, 19], and upregulation of EMT effector genes, like *MMP1* and *VIM*, which are correlated with poor PCa tissue differentiation [31] and metastasis formation [32]. Furthermore, upregulated EMT-associated genes included the transcription factors *ZEB1* [30] and *TCF*/*LEF-1* [33], as well as *TGFB1* and *-2* [34]. We also show that T/E overexpression significantly enhances the invasion capability of LNCaP cells. These results are in agreement with the role of T/E overexpression in promoting cell invasion via induction of matrix metalloproteinase and plasminogen activator genes [3, 5, 12]. Global gene expression analysis of T/E overexpressing cells led to significantly overrepresented GO categories (proliferation and invasion), which correlated with the observed cellular phenotype. We further found many components of known signaling pathways, including JNK/p38 MAPKs, AKT and SMAD1/5, to be deregulated (Figure 2.9). Importantly, *TGFB1* was identified as a regulator gene of T/E-induced transcriptional changes, which again supports our previous *ex vivo* data [13]. Increased TGF-β expression has been shown to induce a tumor-promoting phenotype [35] and metastatic dissemination [36]. TGF-β/BMP signaling is well known for its role in bone remodeling and metastasis formation in breast cancer [35] and could therefore play a similar role in PCa. Bone metastasis is common in PCa [37], and expression of TGF-β in PCa is correlated to metastasis and survival [38]. Intriguingly, serum TGF-β concentrations are elevated in PCa patients with bone metastases [39]. Furthermore, TGF-β protein and RNA expression was higher in bone metastases compared to visceral metastases in rapid autopsy specimens of patients who died of metastatic PCa and was associated with a fibroblast-like phenotype [40]. We therefore propose that T/E-induced TGF-β secretion could have autocrine effects promoting tumor progression.

The T/E variants III and VI deploy two routes of ERG-mediated oncogenic pathway activation (Figure 2.9). The first route is characterized by strong upregulation of the TGF-β receptor *ALK1*, which can be activated by various BMPs, in addition to TGF-β1 and TGF-β3 [41, 42]. Inhibition of ALK1 in our model led to reduced phosphorylation of p38, downregulation of the EMT-markers *VIM*, *MMP1*, *CDH2*, and *SNAI2*, as well as reduced expression of *ID1* and *ID2*, for which induction by ALK1 signaling is known [43]. ALK1-induced expression of ID1 promotes tumor cell metastasis [44]. ID1 was shown to be involved in mesenchymal-to-epithelial transition (MET) of breast cancer cells during lung colonization after having undergone TGF-β-induced EMT [45]. High levels of ALK1 protein in tumor blood vessels can serve as a prognostic marker for metastatic disease in breast cancer patients [45]. In addition, the pharmacological inhibition of ALK1 was able to prevent metastatic dissemination and lung colonization in mouse models of endocrine pancreatic and mammary carcinomas [45, 46]. The high upregulation of *ALK1* in T/E expressing cells in our study was accompanied by augmented levels of TGF-β1 and TGF-β2 mRNA and protein, suggesting that autocrine TGF-β signaling mediates ALK1 pathway activation and phenotypic cellular changes in T/E cells [47, 48].

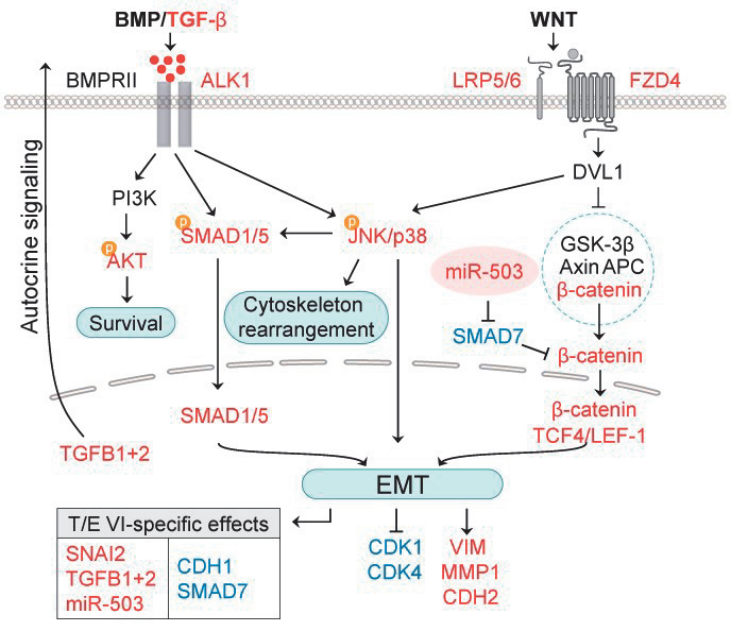

Figure 2.9: Working model for T/E-induced effects on BMP/TGF-β and WNT/β-catenin signaling pathways. T/E VI variant-specific transcriptional modulation of *miR-503* and SMAD7 leads to stronger activation of EMT-regulating genes compared to T/E variant III. Red - upregulation; blue - downregulation.

The second route of T/E-induced signaling pointed towards FZD4 receptor-mediated WNT/β-catenin signaling as an important element [49, 50]. Evidence for the role of WNT signaling was seen in the upregulation of transcription factors of the T cell factor/lymphoid enhancer family (*TCF7L2*, *LEF1*), increased β-catenin reporter activity and downregulation of the negative regulator *CDH1* [51]. These effects were more profound in T/E VI, compared to T/E III, expressing cells. Importantly, *FZD4* was upregulated upon T/E overexpression, and inhibition of *FZD4* led to reduced phosphorylation of p38. These results confirmed reports that loss of cell adhesion and EMT are associated with FZD4-induced activation of WNT signaling [49].

Our results further suggest that variant-specific transcriptional modulation is responsible for the differences in activation of EMT regulating pathway genes. Strikingly, we observed upregulation of *miR-503* exclusively in T/E VI overexpressing cells. Overexpression of *miR-503* was able to repress *SMAD7*, a known negative regulator of TGF-β and WNT/β-catenin signaling [52]. Thus, the *miR-503*-mediated downregulation of *SMAD7* in T/E VI, but not in T/E III cells, explains T/E VI variant-specific transcription. Recently, Li et al. could show that *miR-503* downregulates SMAD7 expression and thereby enhances TGF-β signaling and the metastatic capability of breast cancer cells

[28]. SMAD7-mediated stabilization of β-catenin binding to E-cadherin turned out to increase cell-cell adhesion and formation of adherens junctions [53], thereby potentially blocking metastasis. Reduced expression of SMAD7 might account for the stronger increase of TGF-β signaling and β-catenin reporter activity observed in T/E VI cells. Zhu et al. showed that stimulation of fibroblasts with recombinant TGF-β results in a decreased expression of SMAD7 [54]. In agreement with previous reports in MCF-10A breast cancer cells [55], *TGFB1* knockdown also decreased *miR-503* expression. *MiR-503*-mediated repression of *SMAD7* therefore appears to be a way to escape the inhibitory effect of SMAD7 on TGF-β and WNT/β-catenin signaling. Although *miR-503* expression was shown to be lower in metastatic compared to non-metastatic PCa xenografts [56], and several studies reported tumor suppressor properties of *miR-503* [57, 58], in the context of T/E-induced TGF-β signaling *miR-503* overexpression has tumor-promoting effects.

In conclusion, our study identifies the TGF-β/BMP and WNT/β-catenin signaling pathways as molecular determinants underlying T/E-mediated EMT in PCa cells (Figure 2.9). We confirm that WNT/β-catenin signaling in T/E cells is mediated by *FZD4* and propose that *miR-503* plays a crucial role in augmenting this process. We further demonstrate that TGF-β-ALK1-p38 signaling promotes EMT in T/E expressing cells. Our findings suggest that autocrine activation of ALK1 plays a role in PCa cells. This could provide a rational basis for ALK1-blocking agents (which are currently already tested in clinical studies in various malignancies [59, 60]) to inhibit progression of T/E fusion-positive PCa.

ACKNOWLEDGEMENTS

We thank Sabrina Gerhardt and Simon Ogrodnik for excellent technical assistance and Jan Mollenhauer for providing access to the LNCaP clones with modified Flp-In system. We thank the DKFZ Genomics and Proteomics Core Facility for performing Illumina Whole-Genome Expression Beadchips and associated statistical analyses.

FUNDING

This project was supported through intramural funding by the German Cancer Research Center.

SUPPLEMENTARY INFORMATION

Content

1. Supplementary material and methods

1.1. Supplementary Table S2.1: List of primer sequences

List of primers used for cloning

Name	Sequence 5' - 3'
attB1_universal	ggggacaagtttgtacaaaaaagcaggctccaccatg
attB2_universal	ggggaccactttgtacaagaaagctgggtc
ERG_T/E_III_For	ctcagcaggattggctgtct
ERG_T/E_III_Rev	tggttgagcagctttcgact
ERG_T/E_VI_For	gtgagtgaggaccagtcgtt
ERG_T/E_VI_Rev	tgatgcagctggagttggag

List of primers used for RT-PCR

Name	Sequence 5' - 3'
T/E_III_for	ctcagcaggattggctgtct
T/E_III_rev	tggttgagcagctttcgact
T/E VI_for	gtgagtgaggaccagtcgtt
T/E VI_rev	tgatgcagctggagttggag
vec_empty_for	gttttgacctccatagaagacac
vec_universal_rev	caacagatggctggcaacta

List of primer sequences and probes used for qPCR

Name	#UPL probe	Sequence forward 5' - 3'	Sequence reverse 5' – 3'
ACVRL1	71	agacccccaccatcccta	cgcatcatctgagctaggc
BAMBI	71	cgccactccagctacatctt	cacagtagcatcgaatttcacc
BMP1	18	ttcaaggcccacttcttctc	cataactgccgaacgtgttg
CCND1	17	gctgtgcatctacaccgaca	ttgagcttgttcaccaggag
CCND2	49	ggacatccaaccctacatgc	cgcacttctgttcctcacag
CDH1	84	tggaggaattcttgctttgc	cgctctcctccgaagaaac
CDH2	59	tcaacaatgagactggtgacatc	tatgtgggattgccttccat
CDK1	79	tggatctgaagaaatacttggattcta	caatcccctgtaggatttgg
CDK4	25	gtgcagtcggtggtacctg	ttcgcttgtgtgggttaaaa
DKK4	37	aggaggtgccagcgagat	tgcatcttccatcgtagtacaaa
ERG_T/E	64	ggttaatgcatgctagaaacaca	agatggttgagcagctttcg
FZD4	19	aactttcacaccgctcatcc	tgcacattggcacataaaca
GAPDH	60	agccacatcgctcagacac	gcccaatacgaccaaatcc
ID1	39	ccagaaccgcaaggtgag	ggtccctgatgtagtcgatga
ID2	5	atatcagcatcctgtccttgc	aaagaaatcatgaacaccgctta
LEF1	79	agatcaccccacctcttgg	atgagggatgccagttgtgt
MMP1	26	acgaatttgccgacagagat	gtccttggggtatccgtgta
MMP1	7	gctaacctttgatgctataactacga	tttgtgcgcatgtagaatctg
MMP10	61	gcaaaagaggaggactccaa	tcacatccttttcgaggttgta
SMAD7	69	acccgatggattttctcaaa	aggggccagataattcgttc
SNAI2	73	acagcgaactggacacacat	gatggggctgtatgctcct
TCF7L2	10	acgcctcttatcacgtacagc	gggtaatacggggatatatctgg
TGFB1	72	gcagcacgtggagctgta	cagccggttgctgaggta
TGFB2	67	ccaaagggtacaatgccaac	cagatgcttctggatttatggtatt
TGFBR3	82	gatttcatcttcggcttgaaa	gctcaggaggaatagtgtgga
VIM	13	tacaggaagctgctggaagg	accagagggagtgaatccag
ZEB1	3	cagtgaaagagaagggaatgct	cttcaggccccaggattt

1.2. Supplementary methods

Generation of LNCaP cell models stably expressing T/E variants

First, cDNA fragments of the two *TMPRSS2:ERG* variants were amplified by RT-PCR from the *ERG* ORF plasmid (RefSeq NM_004449.4) (provided by the DKFZ Genomics and Proteomics Core Facility (GPCF)) and cloned into a Gateway entry vector using BP Clonase Enzyme Mix (Thermo Fisher Scientific, Waltham, MA, USA). Sequences of cloning primer pairs are listed in Supplementary Table S5. DNA fragments were transferred from the entry vector to an expression vector carrying the tet repressor gene (tetR) as well as a doxycycline (Dox)-regulated CMV/Tet operator (TetO) promoter by LR Clonase Mix (Thermo Fisher Scientific). In a second step, the LNCaP acceptor clone #126 was generated by transfection with a vector carrying a Flp recombinase target (FRT) site. The single integration of the vector was verified by Southern blot hybridization, and the cells were selected for successful integration using neomycin resistance and green fluorescence as markers (Supplementary Figure S1A). Finally, LNCaP#126 cells were co-transfected with a plasmid encoding the Flp recombinase, and the expression vector construct carrying a FRT site and the different target genes under control of the Dox-regulated CMV/Tet operator (TetO) promoter. A HcRed expression construct served as proof for successive integration of transgenes into LNCaP#126 (Supplementary Figure S1A) by showing that upon disruption of the *EGFP* ORF green fluorescence was abolished. Induction of transgene expression by Dox for 72h activated the red fluorescence reporter gene in this case, compared to the uninduced state. Subsequently, the target T/E sequence variants III and VI (Supplementary Figure S2), respectively, under control of the Dox-regulated CMV/Tet operator (TetO) promoter were integrated into the LNCaP#126 cells in the same manner (LNCaP-T/E cells).

2. *Supplementary Figures*

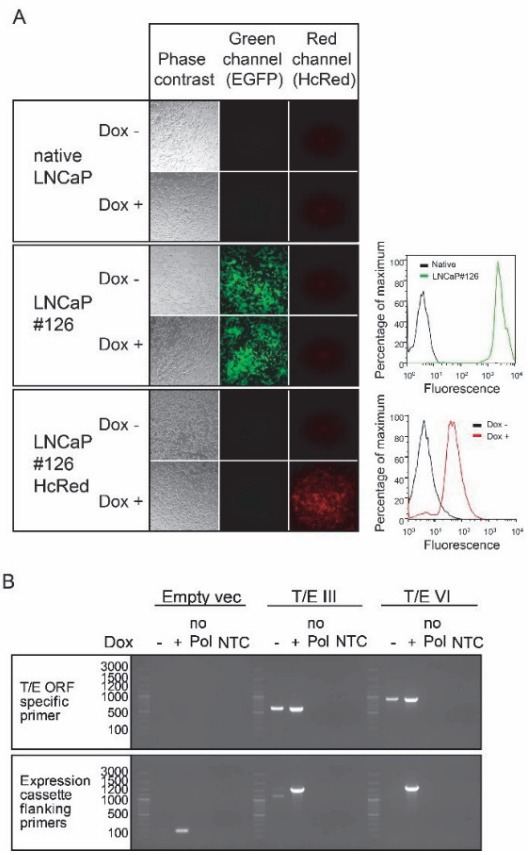

Supplementary Figure S2.1: Site-specific recombination-based system for generation of stably transfected LNCaP cells. (A) Fluorescence microscopy (left) and FACS analysis (right) of recombination events in LNCaP cells. Native LNCaP cells showing no fluorescence in both, green and red, channels (top left panel). LNCaP acceptor clone #126 after selection for neomycin resistance and green fluorescence: LNCaP cells successfully integrated the acceptor plasmid leading to expression of EGFP independent of Dox (left middle panel and upper right panel). LNCaP cells stably recombined with a HcRed expression plasmid after selection for hygromycin resistance. Successful recombination and integration of the expression plasmid disrupted the *EGFP* ORF and abolished green fluorescence of the LNCaP acceptor clone. Induction of transgene expression by Dox for 72h activated the red fluorescence reporter gene, compared to the uninduced state (left bottom panel). Fluorescence signal after induction depicts a homogeneous expression throughout the whole cell population (bottom right). Microscopic pictures were taken at 10-fold magnification. (B) Agarose gel electrophoresis of RT-PCR products after *ERG* overexpression in LNCaP empty vector and T/E clones III and VI, respectively. RT-PCR products from amplification with T/E specific primers for integrated sequences (upper panel) and from amplification with flanking primers for the complete ORF including parts of the expression cassette (lower panel) from induced (+) and uninduced (-) cells. Expected sizes of T/E specific PCR products are 599bp, and 866bp for the T/E inserts III and VI, respectively. Expected sizes of PCR products from flanking primers are 1481bp, 1559bp and 209bp for T/E III, VI and the empty vector, respectively. no Pol: no Polymerase negative control, NTC: no template negative control.

T/E III

ATGACCGCGTCCTCCTCCAGCGACTATGGACAGACTTCCAAGATGAGCCCACGCGTCCCTCAGCAGGATTGGCTGTCTCA
ACCCCCAGCCAGGGTCACCATCAAAATGGAATGTAACCCTAGCCAGGTGAATGGCTCAAGGAACTCTCCTGATGAATGC
AGTGTGGCCAAAGGCGGGAAGATGGTGGGCAGCCCAGACACCGTTGGGATGAACTACGGCAGCTACATGGAGGAGAA
GCACATGCCACCCCCAAACATGACCACGAACGAGCGCAGAGTTATCGTGCCAGCAGATCCTACGCTATGGAGTACAGAC
CATGTGCGGCAGTGGCTGGAGTGGGCGGTGAAAGAATATGGCCTTCCAGACGTCAACATCTTGTTATTCCAGAACATCG
ATGGGAAGGAACTGTGCAAGATGACCAAGGACGACTTCCAGAGGCTCACCCCCAGCTACAATGCCGACATCCTTCTCTC
ACATCTCCACTACCTCAGAGAGACTCCTCTTCCACATTTGACTTCAGATGATGTTGATAAAGCCTTACAAAACTCTCCACG
GTTAATGCATGCTAGAAACACAGATTTACCATATGAGCCCCCCAGGAGATCAGCCTGGACCGGTCACGGCCACCCCACG
CCCCAGTCGAAAGCTGCTCAACCATCTCCTTCCACAGTGCCCAAAACTGAAGACCAGCGTCCTCAGTTAGATCCTTATCAG
ATTCTTGGACCAACAAGTAGCCGCCTTGCAAATCCAGGCAGTGGCCAGATCCAGCTTTGGCAGTTCCTCCTGGAGCTCCT
GTCGGACAGCTCCAACTCCAGCTGCATCACCTGGGAAGGCACCAACGGGGAGTTCAAGATGACGGATCCCGACGAGGT
GGCCCGGCGCTGGGGAGAGCGGAAGAGCAAACCCAACATGAACTACGATAAGCTCAGCCGCGCCCTCCGTTACTACTA
TGACAAGAACATCATGACCAAGGTCCATGGGAAGCGCTACGCCTACAAGTTCGACTTCCACGGGATCGCCCAGGCCCTC
CAGCCCCACCCCCCGGAGTCATCTCTGTACAAGTACCCCTCAGACCTCCCGTACATGGGCTCCTATCACGCCCACCCACA
GAAGATGAACTTTGTGGCGCCCCACCCTCCAGCCCTCCCCGTGACATCTTCCAGTTTTTTTGCTGCCCCAAACCCATACTG
GAATTCACCAACTGGGGGTATATACCCCAACACTAGGCTCCCCACCAGCCATATGCCTTCTCATCTGGGCACTTACTACTA
A

T/E VI

ATGGCTTTGAACTCAGAAGCCTTATCAGTTGTGAGTGAGGACCAGTCGTTGTTTGAGTGTGCCTACGGAACGCCACACCT
GGCTAAGACAGAGATGACCGCGTCCTCCTCCAGCGACTATGGACAGACTTCCAAGATGAGCCCACGCGTCCCTCAGCAG
GATTGGCTGTCTCAACCCCCAGCCAGGGTCACCATCAAAATGGAATGTAACCCTAGCCAGGTGAATGGCTCAAGGAACT
CTCCTGATGAATGCAGTGTGGCCAAAGGCGGGAAGATGGTGGGCAGCCCAGACACCGTTGGGATGAACTACGGCAGCT
ACATGGAGGAGAAGCACATGCCACCCCCAAACATGACCACGAACGAGCGCAGAGTTATCGTGCCAGCAGATCCTACGCT
ATGGAGTACAGACCATGTGCGGCAGTGGCTGGAGTGGGCGGTGAAAGAATATGGCCTTCCAGACGTCAACATCTTGTT
ATTCCAGAACATCGATGGGAAGGAACTGTGCAAGATGACCAAGGACGACTTCCAGAGGCTCACCCCCAGCTACAATGCC
GACATCCTTCTCTCACATCTCCACTACCTCAGAGAGACTCCTCTTCCACATTTGACTTCAGATGATGTTGATAAAGCCTTAC
AAAACTCTCCACGGTTAATGCATGCTAGAAACACAGATTTACCATATGAGCCCCCCAGGAGATCAGCCTGGACCGGTCAC
GGCCACCCCACGCCCCAGTCGAAAGCTGCTCAACCATCTCCTTCCACAGTGCCCAAAACTGAAGACCAGCGTCCTCAGTT
AGATCCTTATCAGATTCTTGGACCAACAAGTAGCCGCCTTGCAAATCCAGGCAGTGGCCAGATCCAGCTTTGGCAGTTCC
TCCTGGAGCTCCTGTCGGACAGCTCCAACTCCAGCTGCATCACCTGGGAAGGCACCAACGGGGAGTTCAAGATGACGGA
TCCCGACGAGGTGGCCCGGCGCTGGGGAGAGCGGAAGAGCAAACCCAACATGAACTACGATAAGCTCAGCCGCGCCCT
CCGTTACTACTATGACAAGAACATCATGACCAAGGTCCATGGGAAGCGCTACGCCTACAAGTTCGACTTCCACGGGATC
GCCCAGGCCCTCCAGCCCCACCCCCCGGAGTCATCTCTGTACAAGTACCCCTCAGACCTCCCGTACATGGGCTCCTATCA
CGCCCACCCACAGAAGATGAACTTTGTGGCGCCCCACCCTCCAGCCCTCCCCGTGACATCTTCCAGTTTTTTTGCTGCCCC
AAACCCATACTGGAATTCACCAACTGGGGGTATATACCCCAACACTAGGCTCCCCACCAGCCATATGCCTTCTCATCTGG
GCACTTACTACTAA

Supplementary Figure S2.2: T/E sequences cloned into the expression vector. Underlined: sequence coding for the first five amino acids of *TMPRSS2* in T/E VI.

3. Supplementary tables

Supplementary Table S2.2: List of genes with expression fold change >|1.5| that were used in IPA

This table can be retrieved from the published version of this chapter, concordant with Supplementary Table 1 in Oncotarget. 2017; 8(15):25115-25130. doi: 10.18632/oncotarget.15931.

Supplementary Table S2.3: Functional annotation of genes differentially regulated upon T/E overexpression

Functional annotation	Genes	p-value	z-score*	# Genes†
Proliferation of cells	*SET, ATP5G1, STMN1, LILRB1, MYC, EIF4A1, ACTN4, S100P, LCP1, SCL19A1*	1.63E-34	-2.545	768
Cell proliferation of tumor cell lines	*CD24, IL24, IGFBP3, SLPI, GJA1, PLAT, SH2D3C, ZFP36, BCL6, SGK1*	9.02E-28	-1.640	372
Interphase	*MYC, FBXO5, CDKN1B, ERBB2, E2F2, PNPT1, BRCA1, CCNE1, BIRC5, CDKN3*	4.10E-19	-2.287	173
Invasion of cells	*CD24, CTNNAL1, GJA1, PLAT, TFF1, CTSK, SHC1, S100A9, MMP1, ETV6*	3.23E-13	1.316	197
Survival of organism	*PTGER4, PLAT, BCL6, ID2, MCL1, BCL2L1, CDKN2A, TRAF3IP2, LMNA, NOS3*	8.51E-05	1.540	130

Top 10 differentially expressed genes in our dataset that were annotated to a function. A gene was selected when its annotation to the indicated function was based on at least two findings in the Ingenuity knowledge base. *Activation z-score is a measure of predicted change (increase or decrease) of the process. †Total number of genes supporting a specific functional annotation.

Supplementary Table S2.4: Canonical pathway analysis of genes differentially regulated upon T/E overexpression

Ingenuity Canonical Pathways	p-value	z-score*	# Genes†
Cell Cycle: G2/M DNA Damage Checkpoint Regulation	1.02E-07	1.886	19 (49)
Molecular Mechanisms of Cancer	3.79E-06	NaN	65 (365)
Estrogen-mediated S-phase Entry	7.59E-06	-2.53	11 (24)
Sertoli Cell-Sertoli Cell Junction Signaling	1.51E-05	NaN	37 (178)
Mitotic Roles of Polo-Like Kinase	1.75E-05	-2.138	19 (66)

Significantly enriched canonical pathways across the dataset of commonly regulated genes between T/E III and VI are shown. *Activation z-score is a measure of predicted change (activated or reduced) of the process. NaN – not a number. †Number of genes in the dataset, which are represented in the pathway. Numbers in brackets depict the total number of genes in the pathway in the reference gene set.

Supplementary Table S2.5: Genes predicted to be regulated by TGF-β according to IPA

This table can be retrieved from the published version of this chapter, concordant with Supplementary Table 4 in Oncotarget. 2017; 8(15):25115-25130. doi: 10.18632/oncotarget.15931.

REFERENCES

1. Ferlay J, Steliarova-Foucher E, Lortet-Tieulent J, Rosso S, Coebergh JW, Comber H, Forman D and Bray F. Cancer incidence and mortality patterns in Europe: estimates for 40 countries in 2012. Eur J Cancer. 2013; 49(6):1374-1403.
2. Torre LA, Bray F, Siegel RL, Ferlay J, Lortet-Tieulent J and Jemal A. Global cancer statistics, 2012. CA Cancer J Clin. 2015; 65(2):87-108.
3. Tomlins SA, Rhodes DR, Perner S, Dhanasekaran SM, Mehra R, Sun XW, Varambally S, Cao X, Tchinda J, Kuefer R, Lee C, Montie JE, Shah RB, Pienta KJ, Rubin MA and Chinnaiyan AM. Recurrent fusion of TMPRSS2 and ETS transcription factor genes in prostate cancer. Science. 2005; 310(5748):644-648.
4. Tomlins SA, Bjartell A, Chinnaiyan AM, Jenster G, Nam RK, Rubin MA and Schalken JA. ETS gene fusions in prostate cancer: from discovery to daily clinical practice. Eur Urol. 2009; 56(2):275-286.
5. Tomlins SA, Laxman B, Varambally S, Cao X, Yu J, Helgeson BE, Cao Q, Prensner JR, Rubin MA, Shah RB, Mehra R and Chinnaiyan AM. Role of the TMPRSS2-ERG gene fusion in prostate cancer. Neoplasia. 2008; 10(2):177-188.
6. Perner S, Demichelis F, Beroukhim R, Schmidt FH, Mosquera JM, Setlur S, Tchinda J, Tomlins SA, Hofer MD, Pienta KG, Kuefer R, Vessella R, Sun XW, Meyerson M, Lee C, Sellers WR, et al. TMPRSS2:ERG fusion-associated deletions provide insight into the heterogeneity of prostate cancer. Cancer Res. 2006; 66(17):8337-8341.
7. Hu Y, Dobi A, Sreenath T, Cook C, Tadase AY, Ravindranath L, Cullen J, Furusato B, Chen Y, Thangapazham RL, Mohamed A, Sun C, Sesterhenn IA, McLeod DG, Petrovics G and Srivastava S. Delineation of TMPRSS2-ERG splice variants in prostate cancer. Clin Cancer Res. 2008; 14(15):4719-4725.
8. Linn DE, Penney KL, Bronson RT, Mucci LA and Li Z. Deletion of Interstitial Genes between TMPRSS2 and ERG Promotes Prostate Cancer Progression. Cancer Res. 2016.
9. Clark J, Merson S, Jhavar S, Flohr P, Edwards S, Foster CS, Eeles R, Martin FL, Phillips DH, Crundwell M, Christmas T, Thompson A, Fisher C, Kovacs G and Cooper CS. Diversity of TMPRSS2-ERG fusion transcripts in the human prostate. Oncogene. 2007; 26(18):2667-2673.
10. Wang J, Cai Y, Ren C and Ittmann M. Expression of variant TMPRSS2/ERG fusion messenger RNAs is associated with aggressive prostate cancer. Cancer Res. 2006; 66(17):8347-8351.
11. Wang J, Cai Y, Shao LJ, Siddiqui J, Palanisamy N, Li R, Ren C, Ayala G and Ittmann M. Activation of NF-{kappa}B by TMPRSS2/ERG Fusion Isoforms through Toll-Like Receptor-4. Cancer Res. 2011; 71(4):1325-1333.
12. Wang J, Cai Y, Yu W, Ren C, Spencer DM and Ittmann M. Pleiotropic biological activities of alternatively spliced TMPRSS2/ERG fusion gene transcripts. Cancer Res. 2008; 68(20):8516-8524.
13. Brase JC, Johannes M, Mannsperger H, Falth M, Metzger J, Kacprzyk LA, Andrasiuk T, Gade S, Meister M, Sirma H, Sauter G, Simon R, Schlomm T, Beissbarth T, Korf U, Kuner R, et al. TMPRSS2-ERG -specific transcriptional modulation is associated with prostate cancer biomarkers and TGF-beta signaling. BMC cancer. 2011; 11:507.
14. Oft M, Heider KH and Beug H. TGFbeta signaling is necessary for carcinoma cell invasiveness and metastasis. Curr Biol. 1998; 8(23):1243-1252.
15. Komiya Y and Habas R. Wnt signal transduction pathways. Organogenesis. 2008; 4(2):68-75.
16. Lamouille S, Xu J and Derynck R. Molecular mechanisms of epithelial-mesenchymal transition. Nat Rev Mol Cell Biol. 2014; 15(3):178-196.
17. Mertz KD, Setlur SR, Dhanasekaran SM, Demichelis F, Perner S, Tomlins S, Tchinda J, Laxman B, Vessella RL, Beroukhim R, Lee C, Chinnaiyan AM and Rubin MA. Molecular characterization of TMPRSS2-ERG gene fusion in the NCI-H660 prostate cancer cell line: a new perspective for an old model. Neoplasia. 2007; 9(3):200-206.
18. Yu J, Yu J, Mani RS, Cao Q, Brenner CJ, Cao X, Wang X, Wu L, Li J, Hu M, Gong Y, Cheng H, Laxman B, Vellaichamy A, Shankar S, Li Y, et al. An integrated network of androgen receptor, polycomb, and TMPRSS2-ERG gene fusions in prostate cancer progression. Cancer Cell. 2010; 17(5):443-454.

19. Sun C, Dobi A, Mohamed A, Li H, Thangapazham RL, Furusato B, Shaheduzzaman S, Tan SH, Vaidyanathan G, Whitman E, Hawksworth DJ, Chen Y, Nau M, Patel V, Vahey M, Gutkind JS, et al. TMPRSS2-ERG fusion, a common genomic alteration in prostate cancer activates C-MYC and abrogates prostate epithelial differentiation. Oncogene. 2008; 27(40):5348-5353.
20. Buttice G, Duterque-Coquillaud M, Basuyaux JP, Carrere S, Kurkinen M and Stehelin D. Erg, an Ets-family member, differentially regulates human collagenase1 (MMP1) and stromelysin1 (MMP3) gene expression by physically interacting with the Fos/Jun complex. Oncogene. 1996; 13(11):2297-2306.
21. Moustakas A and Heldin CH. Non-Smad TGF-beta signals. J Cell Sci. 2005; 118(Pt 16):3573-3584.
22. Zhang YE. Non-Smad pathways in TGF-beta signaling. Cell Res. 2009; 19(1):128-139.
23. Ao M, Williams K, Bhowmick NA and Hayward SW. Transforming growth factor-beta promotes invasion in tumorigenic but not in nontumorigenic human prostatic epithelial cells. Cancer Res. 2006; 66(16):8007-8016.
24. Weidle UH, Schneider B, Georges G and Brinkmann U. Genetically engineered fusion proteins for treatment of cancer. Cancer Genomics Proteomics. 2012; 9(6):357-372.
25. Sanvitale CE, Kerr G, Chaikuad A, Ramel MC, Mohedas AH, Reichert S, Wang Y, Triffitt JT, Cuny GD, Yu PB, Hill CS and Bullock AN. A new class of small molecule inhibitor of BMP signaling. PLoS One. 2013; 8(4):e62721.
26. Miyazono K and Miyazawa K. Id: a target of BMP signaling. Sci STKE. 2002; 2002(151):pe40.
27. Wiercinska E, Wickert L, Denecke B, Said HM, Hamzavi J, Gressner AM, Thorikay M, ten Dijke P, Mertens PR, Breitkopf K and Dooley S. Id1 is a critical mediator in TGF-beta-induced transdifferentiation of rat hepatic stellate cells. Hepatology. 2006; 43(5):1032-1041.
28. Li Y, Li W, Ying Z, Tian H, Zhu X, Li J and Li M. Metastatic heterogeneity of breast cancer cells is associated with expression of a heterogeneous TGFbeta-activating miR424-503 gene cluster. Cancer Res. 2014; 74(21):6107-6118.
29. Butz H, Racz K, Hunyady L and Patocs A. Crosstalk between TGF-beta signaling and the microRNA machinery. Trends Pharmacol Sci. 2012; 33(7):382-393.
30. Leshem O, Madar S, Kogan-Sakin I, Kamer I, Goldstein I, Brosh R, Cohen Y, Jacob-Hirsch J, Ehrlich M, Ben-Sasson S, Goldfinger N, Loewenthal R, Gazit E, Rotter V and Berger R. TMPRSS2/ERG promotes epithelial to mesenchymal transition through the ZEB1/ZEB2 axis in a prostate cancer model. PLoS One. 2011; 6(7):e21650.
31. Lang SH, Hyde C, Reid IN, Hitchcock IS, Hart CA, Bryden AA, Villette JM, Stower MJ and Maitland NJ. Enhanced expression of vimentin in motile prostate cell lines and in poorly differentiated and metastatic prostate carcinoma. Prostate. 2002; 52(4):253-263.
32. Wei J, Xu G, Wu M, Zhang Y, Li Q, Liu P, Zhu T, Song A, Zhao L, Han Z, Chen G, Wang S, Meng L, Zhou J, Lu Y, Wang S, et al. Overexpression of vimentin contributes to prostate cancer invasion and metastasis via src regulation. Anticancer Res. 2008; 28(1A):327-334.
33. Becker-Santos DD, Guo Y, Ghaffari M, Vickers ED, Lehman M, Altamirano-Dimas M, Oloumi A, Furukawa J, Sharma M, Wang Y, Dedhar S and Cox ME. Integrin-linked kinase as a target for ERG-mediated invasive properties in prostate cancer models. Carcinogenesis. 2012; 33(12):2558-2567.
34. Zhang Q, Helfand BT, Jang TL, Zhu LJ, Chen L, Yang XJ, Kozlowski J, Smith N, Kundu SD, Yang G, Raji AA, Javonovic B, Pins M, Lindholm P, Guo Y, Catalona WJ, et al. Nuclear factor-kappaB-mediated transforming growth factor-beta-induced expression of vimentin is an independent predictor of biochemical recurrence after radical prostatectomy. Clin Cancer Res. 2009; 15(10):3557-3567.
35. Owens P, Polikowsky H, Pickup MW, Gorska AE, Jovanovic B, Shaw AK, Novitskiy SV, Hong CC and Moses HL. Bone Morphogenetic Proteins stimulate mammary fibroblasts to promote mammary carcinoma cell invasion. PLoS One. 2013; 8(6):e67533.
36. Yang S, Pham LK, Liao CP, Frenkel B, Reddi AH and Roy-Burman P. A novel bone morphogenetic protein signaling in heterotypic cell interactions in prostate cancer. Cancer Res. 2008; 68(1):198-205.
37. Bubendorf L, Schopfer A, Wagner U, Sauter G, Moch H, Willi N, Gasser TC and Mihatsch MJ. Metastatic patterns of prostate cancer: an autopsy study of 1,589 patients. Hum Pathol. 2000; 31(5):578-583.

38. Wikstrom P, Stattin P, Franck-Lissbrant I, Damber JE and Bergh A. Transforming growth factor beta1 is associated with angiogenesis, metastasis, and poor clinical outcome in prostate cancer. Prostate. 1998; 37(1):19-29.
39. Shariat SF, Shalev M, Menesses-Diaz A, Kim IY, Kattan MW, Wheeler TM and Slawin KM. Preoperative plasma levels of transforming growth factor beta(1) (TGF-beta(1)) strongly predict progression in patients undergoing radical prostatectomy. J Clin Oncol. 2001; 19(11):2856-2864.
40. Haider M, Zhang X, Coleman I, Ericson N, True LD, Lam HM, Brown LG, Ketchanji M, Nghiem B, Lakely B, Coleman R, Montgomery B, Lange PH, Roudier M, Higano CS, Bielas JH, et al. Epithelial mesenchymal-like transition occurs in a subset of cells in castration resistant prostate cancer bone metastases. Clin Exp Metastasis. 2016; 33(3):239-248.
41. Goumans MJ, Valdimarsdottir G, Itoh S, Rosendahl A, Sideras P and ten Dijke P. Balancing the activation state of the endothelium via two distinct TGF-beta type I receptors. EMBO J. 2002; 21(7):1743-1753.
42. David L, Mallet C, Mazerbourg S, Feige JJ and Bailly S. Identification of BMP9 and BMP10 as functional activators of the orphan activin receptor-like kinase 1 (ALK1) in endothelial cells. Blood. 2007; 109(5):1953-1961.
43. Ota T, Fujii M, Sugizaki T, Ishii M, Miyazawa K, Aburatani H and Miyazono K. Targets of transcriptional regulation by two distinct type I receptors for transforming growth factor-beta in human umbilical vein endothelial cells. J Cell Physiol. 2002; 193(3):299-318.
44. Stankic M, Pavlovic S, Chin Y, Brogi E, Padua D, Norton L, Massague J and Benezra R. TGF-beta-Id1 signaling opposes Twist1 and promotes metastatic colonization via a mesenchymal-to-epithelial transition. Cell Rep. 2013; 5(5):1228-1242.
45. Cunha SI, Bocci M, Lovrot J, Eleftheriou N, Roswall P, Cordero E, Lindstrom L, Bartoschek M, Haller BK, Pearsall RS, Mulivor AW, Kumar R, Larsson C, Bergh J and Pietras K. Endothelial ALK1 Is a Therapeutic Target to Block Metastatic Dissemination of Breast Cancer. Cancer Res. 2015; 75(12):2445-2456.
46. Mitchell D, Pobre EG, Mulivor AW, Grinberg AV, Castonguay R, Monnell TE, Solban N, Ucran JA, Pearsall RS, Underwood KW, Seehra J and Kumar R. ALK1-Fc inhibits multiple mediators of angiogenesis and suppresses tumor growth. Mol Cancer Ther. 2010; 9(2):379-388.
47. Van Obberghen-Schilling E, Roche NS, Flanders KC, Sporn MB and Roberts AB. Transforming growth factor beta 1 positively regulates its own expression in normal and transformed cells. J Biol Chem. 1988; 263(16):7741-7746.
48. Zavadil J and Bottinger EP. TGF-beta and epithelial-to-mesenchymal transitions. Oncogene. 2005; 24(37):5764-5774.
49. Gupta S, Iljin K, Sara H, Mpindi JP, Mirtti T, Vainio P, Rantala J, Alanen K, Nees M and Kallioniemi O. FZD4 as a ediator of ERG oncogene-induced WNT signaling and epithelial-to-mesenchymal transition in human prostate cancer cells. Cancer Res. 2010; 70(17):6735-6745.
50. Wu L, Zhao JC, Kim J, Jin HJ, Wang CY and Yu J. ERG is a critical regulator of Wnt/LEF1 signaling in prostate cancer. Cancer Res. 2013; 73(19):6068-6079.
51. Herzig M, Savarese F, Novatchkova M, Semb H and Christofori G. Tumor progression induced by the loss of E-cadherin independent of beta-catenin/Tcf-mediated Wnt signaling. Oncogene. 2007; 26(16):2290-2298.
52. Kavsak P, Rasmussen RK, Causing CG, Bonni S, Zhu H, Thomsen GH and Wrana JL. Smad7 binds to Smurf2 to form an E3 ubiquitin ligase that targets the TGF beta receptor for degradation. Mol Cell. 2000; 6(6):1365-1375.
53. Tang Y, Liu Z, Zhao L, Clemens TL and Cao X. Smad7 stabilizes beta-catenin binding to E-cadherin complex and promotes cell-cell adhesion. J Biol Chem. 2008; 283(35):23956-23963.
54. Zhu H, Li Y, Qu S, Luo H, Zhou Y, Wang Y, Zhao H, You Y, Xiao X and Zuo X. MicroRNA expression abnormalities in limited cutaneous scleroderma and diffuse cutaneous scleroderma. J Clin Immunol. 2012; 32(3):514-522.
55. Llobet-Navas D, Rodriguez-Barrueco R, Castro V, Ugalde AP, Sumazin P, Jacob-Sendler D, Demircan B, Castillo-Martin M, Putcha P, Marshall N, Villagrasa P, Chan J, Sanchez-Garcia F, Pe'er D, Rabadan R, Iava-

rone A, et al. The miR-424(322)/503 cluster orchestrates remodeling of the epithelium in the involuting mammary gland. Genes Dev. 2014; 28(7):765-782.

56. Watahiki A, Wang Y, Morris J, Dennis K, O'Dwyer HM, Gleave M, Gout PW and Wang Y. MicroRNAs associated with metastatic prostate cancer. PLoS One. 2011; 6(9):e24950.
57. Oneyama C, Kito Y, Asai R, Ikeda J, Yoshida T, Okuzaki D, Kokuda R, Kakumoto K, Takayama K, Inoue S, Morii E and Okada M. MiR-424/503-mediated Rictor upregulation promotes tumor progression. PLoS One. 2013; 8(11):e80300.
58. Jiang X, Chen Y, Du E, Yang K, Zhang Z, Qi S and Xu Y. GATA3-driven expression of miR-503 inhibits prostate cancer rogression by repressing ZNF217 expression. Cell Signal. 2016; 28(9):1216-1224.
59. Vecchia L, Olivieri C and Scotti C. Activin Receptor-like kinase 1: a novel anti-angiogenesis target from TGF-beta family. Mini Rev Med Chem. 2013; 13(10):1398-1406.
60. Bendell JC, Gordon MS, Hurwitz HI, Jones SF, Mendelson DS, Blobe GC, Agarwal N, Condon CH, Wilson D, Pearsall AE, Yang Y, McClure T, Attie KM, Sherman ML and Sharma S. Safety, pharmacokinetics, pharmacodynamics, and antitumor activity of dalantercept, an activin receptor-like kinase-1 ligand trap, in patients with advanced cancer. Clin Cancer Res. 2014; 20(2):480-489.

Chapter 3

TMPRSS2:ERG overexpression induces changes in the epigenetic signature of human prostate cancer cells: Hypomethylation correlates with upregulation of *FZD4* and *HLA-DMB*

Leonie Ratz, Simone Bauer, Peter Altevogt, Sabine M Klauck, Holger Sültmann

In preparation

ABSTRACT

In prostate cancer, specific alterations of the DNA methylation profile of distinct molecular subtypes have been reported suggesting DNA methylation as potential biomarker. Distinct methylation patterns have also been observed in *TMPRSS2:ERG* (T/E) fusion-positive compared to fusion-negative samples. The T/E gene fusion has been associated with epigenetic reprogramming that could be mediated by recurrent overexpression of HDAC1, and cooperativity between ERG and the histone methyltransferase EZH2 leading to target gene silencing.

By using an inducible T/E overexpressing LNCaP cell model, we elucidated a global hypomethylation profile in T/E overexpressing cells that correlated with cell migration and neuron differentiation. Further, hypomethylation of *FZD4* and *HLA-DMB* was identified that correlated with increased expression levels of those genes. These findings were consistent with DNA methylation and gene expression data of the TCGA prostate cancer cohort (PRAD). Our results further corroborated the findings by Börno et al. who reported an increased global methylation in T/E fusion-negative tumors. In conclusion, we show that T/E overexpression affects the epigenetic and transcriptional profile in prostate cancer cells that are correlated with aggressive cell behavior on the global level and suggest that future research could reveal the mechanistic basis of those changes.

INTRODUCTION

Prostate cancer (PCa) is characterized by a low somatic mutation frequency [1, 2], and copy number variants are recurrently detected [3-5]. However, the identification of a definitive genomic driver event is lacking for many tumors [6]. DNA methylation changes occur at higher rates than copy number changes (10.5% vs. 2.1%) [5]. Specific alterations of the DNA methylation profile of distinct molecular subtypes of PCa have been described recently, potentially representing different epigenetic mechanisms with yet unresolved functional consequences proposing DNA methylation as a biomarker in PCa [7]. The DNA methylation profile has also been found to be subject-specific and maintained within metastatic subclones indicating a role as a longitudinal marker [8, 9]. Promoter-associated hypermethylated CpG islands were highly enriched for tumor suppressor genes [10] as well as differentiation and developmental processes, and associated with reduced gene expression (e.g. *PTEN*, *TP53*, *GSTP1*), implying that DNA hypermethylation may change the differentiation state and activity of carcinogenic pathways [8, 11]. Hypermethylation of the pi-class glutathione S-transferase 1 (*GSTP1*) promoter is among the most common somatic epigenomic changes. It is a well-known DNA methylation marker during the transformation from PIN to adenocarcinoma [12-14]. CpG island hypermethylation of a gene panel (*GSTP1*, *APC*, *RASSF1A*, *PTGS2*, *MDR1*) could discriminate primary PCa from benign prostate tissue [15]. Hypermethylation of the transcriptional elongation regulator (*TCERG1L*) in combination with other genomic markers could predict disease relapse in localized PCa [16]. Methylation signature analysis revealed recurrent hypermethylation in castration-resistant prostate cancer (CRPC) samples compared to benign prostate tissue [5, 17]. DNA methylation levels at CpG islands increased with disease severity [17] and occurred more often at genes with allelic deletion, e.g. *RB1* or *HSD17B2* [5]. In the same study, it was suggested that heterozygous deletion of *CYP17A1* could be compensated by *CYP17A1* gene body hypermethylation leading to gene upregulation and sustained androgen synthesis [5]. This implies that epigenetic aberrations could promote androgen signaling in CRPC [5, 18]. Lin et al. proposed a panel of 13 CpG islands that were increasingly methylated with disease severity and in PCa with NE differentiation [17] encompassing a potential clinical use of those CpG islands to detect advanced PCa. Analysis of the DNA methylation profile segregated NEPC from adenocarcinomas, which was not achieved by standard pathological assessment alone, suggesting that methylation analysis could improve clinical tumor classification [19]. It has further been shown that global hypomethylation leads to genomic instability at later stages of PCa, thereby increasing tumor heterogeneity [20, 21].

Only few studies have analysed the methylation profile associated with the T/E gene fusion. Some of these reported distinct methylation patterns in T/E-positive compared to T/E-negatives samples [17, 22, 23]. Since the T/E gene fusion has been detected in

PIN lesions, T/E-induced methylation changes can occur early during carcinogenesis before histological manifestation of PCa. Differentially methylated regions have been described to be specifically associated with T/E fusion-positive tumors [22]. Recurrent overexpression of the histone deacetylase 1 (*HDAC1*) and target gene silencing in T/E overexpressing PCa indicated a role of ERG in epigenetic reprogramming [24, 25]. ERG has been shown to interact with HDAC1 via the SETDB1 methyl transferase [26, 27]. A cooperativity between ERG and the histone methyltransferase enhancer of zeste homolog 2 (EZH2) was demonstrated to regulate shared target genes [28]. EZH2-mediated lysine methylation of *ERG* resulted in increased chromatin binding and ERG-induced transcriptional activity associated with a metastatic and dedifferentiation program [29]. Börno et al. observed increased global methylation in T/E fusion-negative tumors [23], in contrast to Kim et al. [22] and Lin et al. [17], who showed lower global methylation in T/E fusion-negative PCa. *EZH2* mRNA levels were significantly higher in fusion-negative than in fusion-positive tumors accompanied by hypermethylation of the *miR-26a* locus providing a mechanism for enhanced *EZH2* upregulation in those tumors [23]. We aim to obtain further insights into the T/E-induced epigenetic alterations in prostate cancer cell lines and to determine the molecular mechanism of ERG-mediated epigenetic alterations.

MATERIALS AND METHODS

Cell lines and culturing

LNCaP (CRL-1740) cells were purchased from American Type Culture Collection (ATCC, Manassas, VA, USA). Stably transfected acceptor LNCaP cells were maintained in RPMI1640 (Thermo Fisher Scientific, Waltham, MA, USA), supplemented with 10% of Tet System Approved FBS (tet-FBS, Clontech, Göteborg, Sweden) and 80 µg/mL hygromycin B (Thermo Fisher Scientific). The cells were authenticated using Multiplex Cell Authentication by Multiplexion (Heidelberg, Germany) as described recently [30]. The SNP profile matched known profiles. The purity of the cells was validated using the Multiplex cell Contamination Test by Multiplexion (Heidelberg, Germany) as described recently [31]. Neither Mycoplasma, SMRV nor interspecies contamination was detected.

Generation of LNCaP cell models stably expressing T/E variants

Establishment of the LNCaP-T/E variant cell model including T/E sequences has been described before [32]. Transgene expression was induced with 50 ng/mL Dox (Sigma-Aldrich, Munich, Germany) in RPMI1640 containing 10% tet-FBS. Medium of the uninduced cells was supplemented with the respective volume of PBS only. After 72h, cells were harvested and washed once with ice-cold 1x PBS. Cell suspensions were split, centrifuged and the pellet was used for DNA and RNA extraction, respectively. There-

fore, gene expression levels of differentially methylated genes obtained from EPIC BeadChip analysis were assessed by qPCR in the corresponding RNA samples that were used for methylation profiling.

DNA isolation

Genomic DNA was isolated from cell lines using the QIAamp DNA Blood Mini Kit (Qiagen, Hilden, Germany) and quality controlled on the 2100 Bioanalyser (Agilent Technologies, Waldbronn, Germany) with DNA 7500 Kit according to the manufacturers' protocols.

Methylation profiling

The Illumina Infinium MethylationEPIC (850K) array was used to determine the DNA methylation status of 853,307 CpG sites (Illumina, San Diego, USA), according to the manufacturer's instructions at the Genomics and Proteomics Core Facility (GPCF) of the DKFZ applying 1000ng of total DNA with a concentration of 25 ng/µl. Raw data (IDATs) were normalized (control normalization) using the Methylation Module of GenomeStudio software (version 2011.1, Illumina) with the HumanMethylationEPIC manifest v1.0. For each CpG locus a methylation β-value was calculated by dividing the intensity of the methylated allele (C) by the sum of intensity of the methylated (M) and unmethylated (U) alleles [β=M/(M+U)]. CpG sites showing a β-value (Δβ) >|0.2| (p-value <0.05) compared to control cells were considered as differentially methylated.
For unsupervised hierarchical clustering, 1% of the probes with the highest variance across the beta values were selected. Samples were hierarchical clustered with Euclidean distance as the similarity measure using Cluster 3.0 [33] and Treeview software [34, 35]. The methylation levels were shown in a heat map from methylated and unmethylated status, encoded as 1 and -1, respectively.

RNA isolation, reverse transcription and quantitative real-time PCR

From the same samples that were used for methylation analysis, total RNA was isolated using the miRNeasy Mini Kit (Qiagen, Hilden, Germany). Total RNA was reverse transcribed using the RevertAid H Minus First Strand cDNA Synthesis Kit (Thermo Fisher Scientific). Relative mRNA levels were assessed by quantitative RT-PCR on the Lightcycler 480 (Roche Diagnostics, Mannheim, Germany) using Universal Probe Library (UPL) assays and primers listed in Supplementary Table S3.1. Linear expression levels were normalized to GAPDH using the $2^{(-\Delta\Delta Ct)}$ method [36].

Integrative analysis of methylation and gene expression data

DNA methylation data were integrated with the gene expression profiling data that had been obtained in chapter 2 [32]. Methylation and gene expression data were combined using the Methylation Module of GenomeStudio software (Illumina) with the HumanHT-

12 manifest v4.0. Methylation β and gene expression signal intensity values were sorted using Pearson's correlation coefficient (r) to identify inverse correlated genes (r=-1).

Pathway enrichment analysis

The Ingenuity Pathway Analysis (IPA) tool was used to identify pathways and biological processes that were over- or underrepresented. IPA uses the Ingenuity knowledge base, a database of protein and gene interactions integrated from published biomedical literature and 3rd party sources. Analysis using IPA (version 26127183) was performed between October 2016 and July 2017. Genes near differentially methylated CpG sites were used for this analysis.

Functional annotations

Gene expression changes were categorized into functional annotations of molecular and cellular mechanisms. The Ingenuity knowledge base provides a predicted direction of change for the biological function (downstream effect analysis), represented by an activation z-score, where z >2.0 or <-2.0 is predictive for activation or reduction of the process, respectively. A p-value <0.05 indicates a statistically significant association between a set of differentially expressed genes and a given process.

Pathway enrichment analysis

Ingenuity knowledge base provides an analysis of metabolic and cell signaling pathways that are significantly enriched in the gene expression signature. Pathway significance values were calculated based on Fisher's right tailed exact test and the –log(p-value) by IPA. Pathways meeting the threshold p-value <0.05 were considered as significant.
Using the 'Compare' tool, IPA identified the intersection and unique gene sets among T/E III and T/E VI versus empty vector datasets. Upstream regulator analysis can identify molecules upstream of the genes in the dataset that potentially explain the observed gene expression changes and molecular functions. It is based on prior knowledge of expected effects between transcriptional regulators and their target genes stored in the Ingenuity knowledge base.

Integration with TCGA prostate cancer patient data

Prostate cancer patient data from The Cancer Genome Atlas Prostate Cancer (TCGA PRAD) were retrieved using the UCSC Cancer Browser (https://genome-cancer.ucsc.edu/). For graphical view of genomic data, gene expression RNAseq (n = 550, version: 2016-08-16), exon expression RNAseq (n = 550, version: 2016-08-16), copy number (n = 495, version: 2016-11-16), and DNA methylation (Methylation450k) (n = 549, version: 2016-11-16) data were analysed using the Xena browser. A detailed description of data generation and instructions can be viewed on https://xenabrowser.net.

Luminex immunoassay for histone modification detection

The histone extraction kit (Active Motif) was used for acid extraction of histones from cell culture samples. The assay was performed according to the manufacturer's instructions. Cells were treated with Dox to induce ERG overexpression. After 72h of induction, cells were harvested using trypsin and washed twice with 1x ice-cold PBS. Ice-cold extraction buffer was added to cells, resuspended and incubated for 2h at 4°C. Cells were centrifuged at 20,000 x g for 10 minutes, the supernatant was transferred to a new pre-chilled microcentrifuge tube and snap-frozen in a dry-ice/methanol bath. Samples were neutralized by adding neutralization buffer with 0.1M DTT, deacetylase inhibitor, phosphatase inhibitor, protease inhibitor and vortexed. Protein concentrations were determined using Qubit fluorometric quantitation (Thermo Fisher Scientific).
The Histone H3 PTM Multiplex Assay (Active Motif) was used for detection of histone modifications and performed according to the manufacturer's instructions. Five hundred ng of acid histone extracted samples were used. A multiplexed bead master mix was prepared with antibodies against total histone H3, histone H3K9ac, histone H3K9me2, histone H3K9me3, and histone H3K4me2. Biotinylated histone H3 antibody was diluted 1:250 in Assay Buffer. The fluorescent reporter signals were analysed by a Bio-Plex 200 reader (Bio-Rad).

Statistical testing

Differences between the induced and uninduced cells were analysed using a paired t-test and between induced cells of T/E III and VI by an unpaired t-test. Statistical significance of t-test depicted as *p<0.05, **p<0.01, ***p<0.001.

RESULTS

T/E overexpression induces global epigenetic changes in PCa cell lines

The epigenetic changes induced by T/E overexpression compared to uninduced control cells were investigated by methylome analysis on >850,000 CpG sites. The 1% most variable differentially methylated CpG sites (n=8,668) were selected for further analysis. Comparison of the DNA methylation level of those CpG sites showed a global hypomethylation profile in T/E expressing cells (Figure 3.1). Of note, stratification by genetic and epigenetic location revealed that hypomethylated CpGs were enriched in promoter regions (transcription start sites -1500 to -200 bp, 5' UTR), gene bodies, intergenic and open sea regions, but underrepresented in first exons, 3'UTRs and exon/intron boundaries in T/E III (Figure 3.1A and B) as well as T/E VI expressing cells (Figure 3.1C and D).

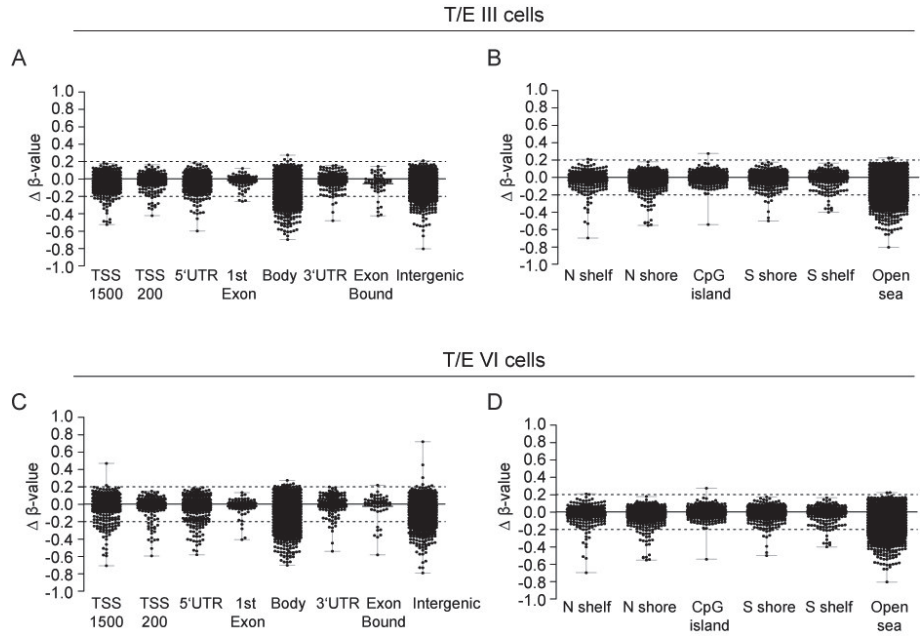

Figure 3.1: Global methylation profile of the top 1% most variable CpG sites in T/E expressing cells. Differentially methylated CpG sites in Dox-induced (A, B) LNCaP-T/E III and (C, D) LNCaP-T/E VI cells compared to uninduced control cells. For analysis, the 1% most variable CpG sites of a total of >850,000 CpG sites in the dataset were used. A and C show the differentially methylated CpGs assigned to different genetic features based on the annotations of Illumina Infinium Human MethylationEPIC (850K) Beadchip Array. B and D show the CpG methylation status per epigenetic region according to Illumina annotation. A global hypomethylation profile is observed in T/E-overexpressing cells. A large number of differentially methylated regions were observed in intergenic and open sea regions. TSS - transcription start site, UTR - untranslated region, shore - region immediately flanking the CpG island within 0-2kb, shelf - regions 2-4kb away from the CpG island, N – upstream (5') of CpG island, S = downstream (3') of CpG island, open sea – isolated CpG sites in the genome with no specific designation to a gene. Δβ-value – ratio of methylation intensity at a specific probe and the overall methylation intensity (sum of intensity of the methylated and unmethylated alleles). A Δβ-value of >|0.2| is considered as differential methylation.

To identify DNA methylation patterns that are shared between T/E III and T/E VI expressing cells, the overlap of the 1% CpG sites was calculated. For integrative analysis with expression profiling data, we focused on differentially methylated CpG sites with designation to a specific gene. Those CpG sites involved 3,422 genes in T/E III and 2,637 genes in T/E VI expressing cells, respectively (Figure 3.2). Of these, 1,255 differentially methylated CpG sites associated with coding genes overlapped between T/E III and T/E VI cells (Figure 3.3A).

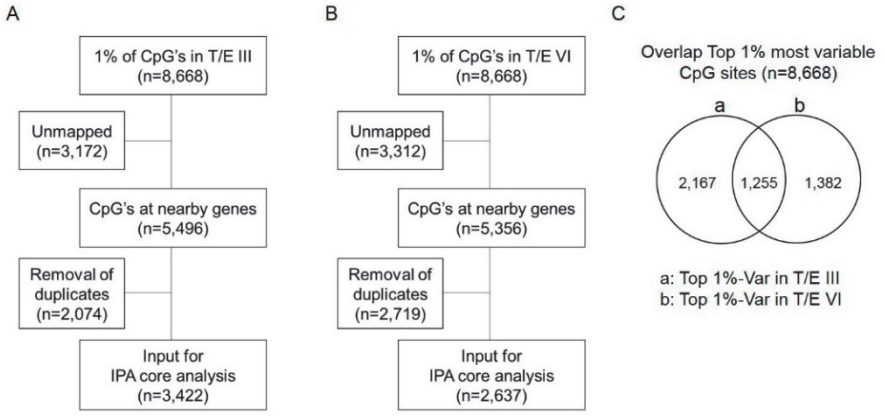

Figure 3.2: Strategy for CpG site selection with designation to a gene that were used as input for IPA analysis in (A) T/E III and (B) T/E VI cells. The 1% most variable CpG sites are used as initial input in IPA. In T/E III cells, 3,172 CpG sites do not map to a gene annotation using Illumina annotation. (C) Identification of differentially methylated CpG sites that are annotated to a gene according to Illumina annotation, and that are common to both T/E expressing cells or specific to TE III or T/E VI cells, respectively.

Unsupervised hierarchical clustering was performed on these differentially methylated CpG sites to identify differences of the DNA methylation profile between T/E expressing and control cells. This cluster analysis showed a separation of T/E III and T/E VI expressing cells from their corresponding uninduced control cells, respectively, indicating that T/E expressing cells have a distinct DNA methylation pattern (Figure 3.3B). A subset of hypomethylated CpG sites was common to both T/E expressing cells (Figure 3.3B, red box) proposing that this methylation profile could be used as a classifier of T/E-specific methylation. This set of differentially methylated CpG sites (n=355; Supplementary Table S3.2) was subsequently applied for pathway analysis using the gene designation as input for the IPA tool to characterize the biological processes and functions of the protein-coding genes, in which the differentially methylated CpG sites were found (Figure 3.3C). *ERG* and the histone deacetylase 2 (*HDAC2*) were found as upstream regulator indicating activation of the HDAC pathway as consequence of T/E overexpression in LNCaP cells. HDAC1 has been identified as an ERG-interacting protein and its upregulation accompanied by target gene silencing in association with ERG gene expression has previously been reported [24]. The biological processes affected by the T/E-induced methylation profile were related to 'Cytoskeleton organization', 'Cell migration' and 'Neuron differentiation' (Supplementary Table S3.3). The canonical pathways associated with these processes were 'Gastrin signaling' as well as 'cAMP signaling' (Supplementary Table S3.4).

A

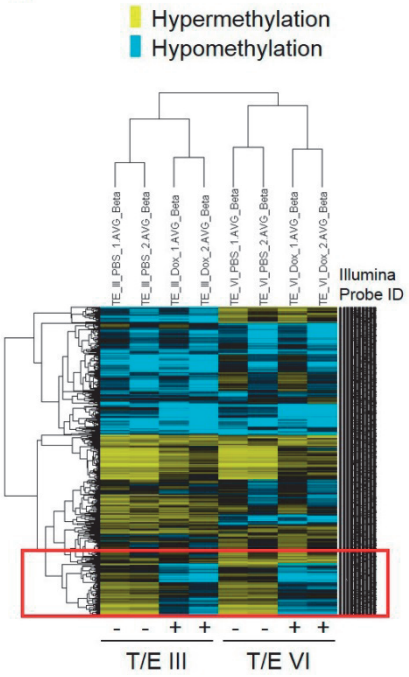

B

Upstream Regulator	p-value	# Genes
VEGF	8.38E-05	20
ERG	1.92E-04	11
TGFB1	1.46E-03	42
HDAC2	5.25E-02	5
PI3K complex	3.18E-02	9

Figure 3.3: Global methylation profile in T/E expressing cells. (A) Unsupervised hierarchical clustering of methylation patterns of the top 1% variable CpG sites in LNCaP-T/E expressing cells. Rows display the methylation levels by continuous β values of the top 1% CpG sites (n=1,255) with the largest intersample methylation variability. Samples are clustered in columns using Euclidean distance as similarity measure. A distinct cluster of hypomethylated CpG sites was observed in T/E expressing cells (red box). Blue – hypomethylation, yellow – hypermethylation. (B) An upstream regulator analysis was performed to study potential mechanisms regulating the methylation changes associated with T/E overexpression. This analysis revealed *ERG* as well as *HDAC2* as upstream regulator.

Correlation of methylation status and gene expression

We next aimed to link the DNA methylation patterns to transcriptional modulation. Differentially methylated CpG sites with a β-value of at least 0.2 were correlated to the mRNA expression level of associated genes using the microarray gene expression data that had been used in chapter 2 [32]. Out of these genes that were at least 1.5-fold differentially regulated upon T/E overexpression compared to uninduced control cells were selected (n=68; Supplementary Table S3.2). These genes were compared to data from the TCGA prostate cancer cohort (TCGA PRAD) that had been retrieved from the UCSC Cancer Browser (https://genome-cancer.ucsc.edu/). First, gene expression was integrated with the T/E fusion status (Figure 3.4). Of note, high expression of the WNT-receptor Frizzled-4 (*FZD4*) and human leukocyte antigen class II histocompatibility antigen, DM beta chain (*HLA-DMB*), correlated to the T/E fusion in the TCGA PRAD data

(Figure 3.4A and Figure 3.4B ii and iii). These candidates were therefore analysed in more detail. ERG expression was used as surrogate for the T/E fusion status as visualized in Figure 3.4A. Integration of the DNA methylation level and gene expression from the TCGA PRAD data showed increased expression of *FZD4* and *HLA-DMB* in T/E fusion-positive compared to fusion-negative and benign samples (Figure 3.4B ii and iii). This increase was accompanied by a lower DNA methylation level of *FZD4* as well as *HLA-DMB* (Figure 3.4B iv and v). T/E-induced upregulation of *FZD4* has been reported to promote Wnt signaling and EMT [37, 38]. Hypomethylation-induced upregulation of gene expression could be a regulatory mechanism for *FZD4* upregulation in T/E expressing cells. Further, ERG-associated upregulation of *HLA-DMB* is consistent with previous reports [24, 25, 39].

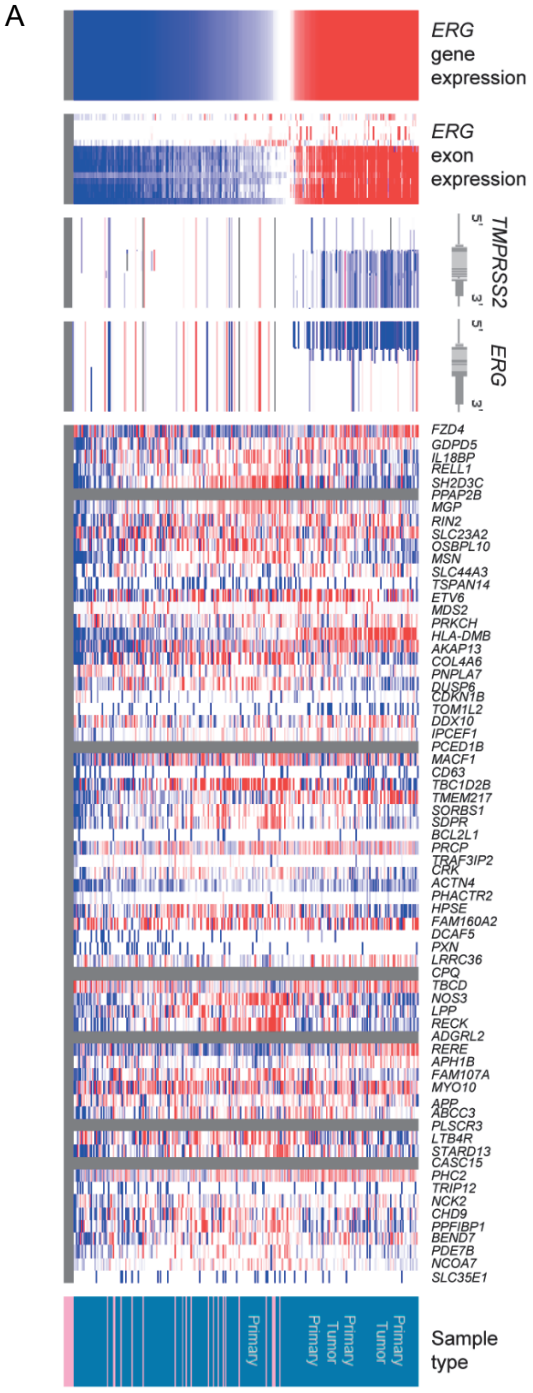

Figure 3.4: RNA transcript and DNA methylation level in TCGA PRAD data.

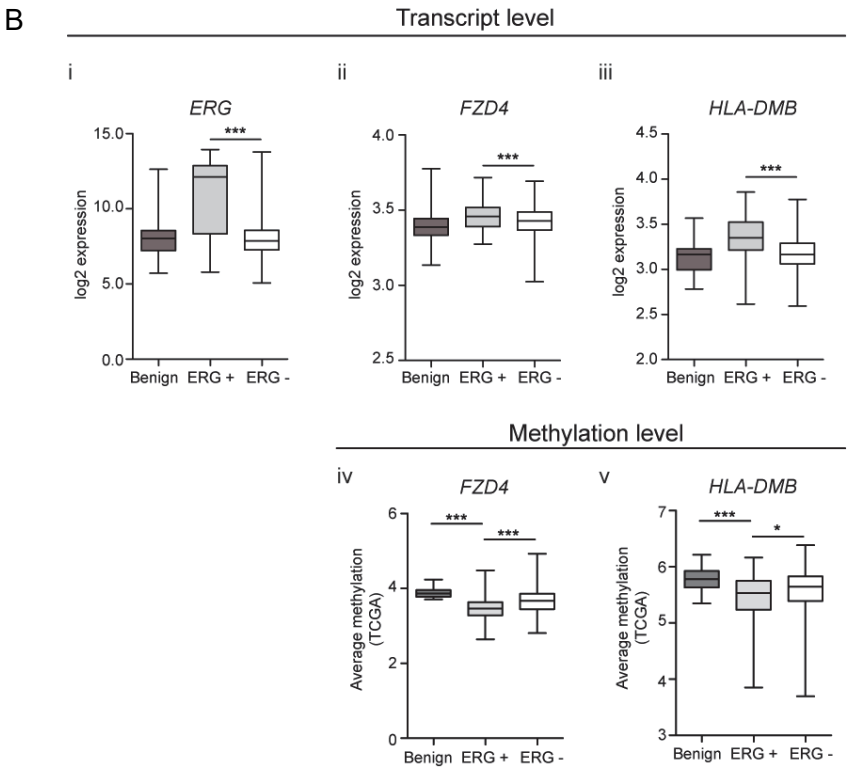

Figure 3.4 continued: (A) Graphical view of the TCGA data using the UCSC Xena browser (http://xena.ucsc.edu). Each row is a sample in the dataset, with different types of data mapped to that sample along the columns. In this view, data is sorted by RNAseq *ERG* gene expression (left column). Genes that were at least 1.5-fold differentially regulated and differentially methylated upon T/E overexpression in T/E III and VI expressing cells compared to uninduced control cells are depicted (n=68). Samples are mean normalized. Red – high expression, blue – low expression. Sample type: blue – primary tumor, pink – solid tissue normal. (B) Analysis of mRNA expression and DNA methylation according to the T/E fusion status in the TCGA PRAD cohort (n=568). (i) *ERG* expression. Expression of (ii) *FZD4* and (iii) *HLA-DMB* is significantly higher in T/E fusion-positive (ERG+) compared to fusion-negative (ERG-) and benign samples. DNA methylation of (iv) *FZD4* and (v) *HLA-DMB* is reduced in T/E fusion-positive samples. *ERG* expression was used as surrogate for the T/E fusion status. * p<0.05, ***p<0.001

Hypomethylation of a region of 2kb within the transcription start site of *FZD4* was found in T/E fusion-positive samples compared to fusion-negative and benign samples (p<0.01) by Börno et al. using MeDIP-Seq analysis [23] (data available under GEO accession number GSE35342.). No differential methylation for *HLA-DMB* was identified in their dataset. Analysis of the genomic context of the differentially methylated region associated with *FZD4* revealed that the CpG site was located within the gene body, a region showing enrichment for the histone H3 mark H3K4Me1, as determined within the ENCODE consortium [40] (Figure 3.5A). For *HLA-DMB*, the hypomethylated CpG sites was located within 1500 bp upstream of the transcription start site, a region that is

enriched for the histone H3 marks H3K4Me1 and H3K27ac [40] (Figure 3.5B), suggesting that, apart from differential DNA methylation, alterations in histone modifications might represent an additional level of regulation of gene expression in T/E expressing cells.

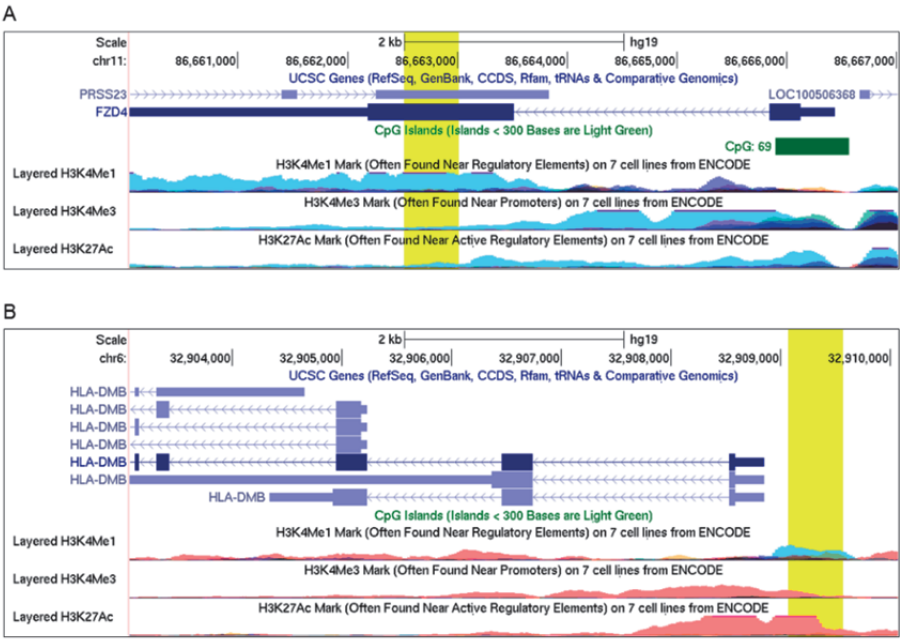

Figure 3.5: Graphical view showing the genomic and epigenetic context of *FZD4* and *HLA-DMB*. (A) *FZD4* gene region on chromosome 11 in hg19 assembly derived from the UCSC Genome Browser (http://genome.ucsc.edu/). A CpG island is found upstream of the transcription start site of *FZD4* at coordinate chr11:86665902-86666567. The chromosomal coordinate of the CpG site that is hypomethylated upon T/E overexpression is chr11: 86662968 (yellow box in A, depicted as 500 bp bin at chr11:86662515-86663014), which is in N-shelf position in relation to the CpG island, and located within a DNase hypersensitivity site at chr11:86662740-86663030. (B) *HLA-DMB* gene region on chromosome 6 in hg19. The chromosomal coordinate of the CpG site in the *HLA-DMB* gene that is hypomethylated upon T/E overexpression is chr6: 32909440 (yellow box in B, depicted as 500 bp bin at chr6:32909069-32909568), which is 1500 bp upstream of the TSS (TSS1500) in the regulatory feature at chr6:32908496-32909716 according to Illumina annotation. Half-height boxes – 5'UTR, fullheight boxes - coding regions, thin line with transcription-direction arrows – introns. Layered H3K - levels of enrichment of the H3K4Me1, H3K4Me3, and H3K27ac histone mark across the genome as determined by a ChIP-seq assay [40]. The H3K4Me1 mark is associated with enhancers and with DNA regions downstream of transcription starts. The H3K4Me3 histone mark is associated with promoters that are active or poised to be activated. The H3K27ac is thought to enhance transcription possibly by blocking the spread of the repressive histone mark H3K27Me3.

Microarray profiling indicates differentially expressed epigenetic regulators

To identify the regulatory mechanisms of T/E-induced epigenetic changes in LNCaP-T/E cells, microarray gene expression profiling data were analyzed [32]. Several genes encoding epigenetic regulators were differentially expressed in T/E expressing cells compared to control cells (Figure 3.6A). These included the histone demethylase *JMJD1C*,

chromodomain helicase DNA binding proteins (CHDs), CpG-binding proteins, histone demethylases, arginine methyltransferases (PRMTs), and histone methyltransferases (Figure 3.6A). Validation of the transcriptional modulation by qPCR confirmed the increased expression of *PRDM1*, *JMJD1C*, *CHD9*, *SIRT2*, *SETD1B*, and *CXXC1*, and reduced expression of *SUV39H1*, *PRMT1*, *PRMT5*, *PRMT6* (Figure 3.6B).

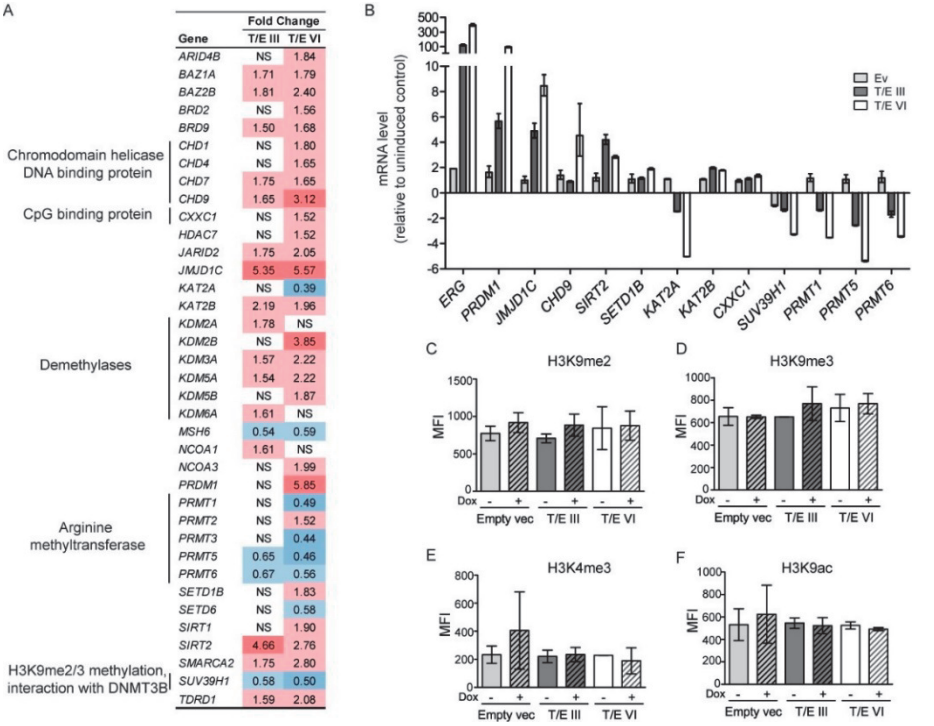

Figure 3.6: Transcriptional modulation of epigenetic regulators and posttranslational histone modifications in LNCaP-T/E cells. (A) Microarray gene expression data indicating differentially expressed epigenetic regulators. (B) qPCR validation of T/E-induced gene expression changes relative to uninduced controls. The mRNA expression profile after T/E overexpression is associated with an open chromatin state facilitating gene transcription characterized by increased H3K9 acetylation, as well as H3K9 and H3K4 methylation. For example, *JMJD1C*, a histone demethylase also known as *KDM3C*, is involved in maintaining low H3K9me2 levels that are associated with activated target gene expression. *JMJD1C* has been described as coactivator for several transcription factors including AR [41, 42]. A general interaction between Jmj-containing KDM proteins and ERG has been reported to lead to activation of the YAP1 proliferation pathway [43]. *JMJD1C* expression has further been implicated in the reactivation of silenced genes in diverse tissues and cancer [44]. *SIRT2*, a histone deacetylase, was implicated in tumor progression in hepatocellular cancer by promoting EMT and cell motility [45]. The histone methylation transferase *SUV39H1* is required to establish an H3K9me2/3 methylation pattern by interacting with *DNMT3B* [46, 47]. Since H3K9 methylation is associated with repressed gene expression, downregulation of *SUV39H1* could be associated with low H3K9me2/3 methylation and increased gene transcription that has been associated with cancer progression [48]. Data are shown as ΔCp values relative to *GAPDH* measured in the same samples, which had been used for the MethylationEPIC Beadchip array. (C-F) Luminex measurements of the histone H3 modification levels: (C) histone H3 lysine 9 di-methylation (H3K9me2), (D) histone H3 lysine 9 tri-methylation (H3K9me3), (E) histone H3 lysine 4 tri-methylation (H3K4me3) and (F) histone H3 lysine 9 acetylation (H3K9ac). MFI – mean fluorescent intensity. Ev - Empty vector; NS - not significant. Red - upregulated; blue – downregulated.

The expression analysis of genes encoding epigenetic regulators revealed differential regulation of histone modifiers. Histone modifications play an important role in chromatin organization and transcriptional modulation indicating a link between histone modification and differential DNA methylation, which is supported in many recent studies [49, 50]. This further suggested that dysregulation of histone modifying genes could lead to an altered DNA methylation in T/E expressing cells. The gene expression profile of those histone modifiers indicated a histone modification pattern characterized by increased H3K9 acetylation, as well as increased H3K9 and H3K4 methylation that could reflect the gene expression status. Lysine methylation can be recognized by epigenetic readers that regulate the recruitment of additional enzymatic activities affecting gene transcription [51]. We therefore analysed the global changes in posttranslational histone modification pattern upon T/E overexpression in LNCaP cells using a Luminex histone modification assay (Figure 3.6C-F). However, this analysis did not reveal a significant differential histone modification in T/E expressing cells compared to control cells suggesting that the differentially expressed histone modifying enzymes do not affect the global profile of histone modifications. Alternative techniques such as chromatin immunoprecipitation could provide more insights into the epigenetic changes induced by T/E overexpression.

DISCUSSION

Clear genomic driver events are lacking for many prostate tumors [6], while DNA methylation changes have been recurrently described [5]. Specific alterations of the DNA methylation profile are known to occur within specific molecular PCa subtypes implying DNA methylation as biomarker in PCa [7]. The functional consequences of those methylation changes remain unclear.

By inducing T/E overexpression in a LNCaP cell model, we found a global hypomethylation profile. However, the majority of these methylation differences showed only a moderate change. Gene ontology analysis revealed that the T/E-induced methylation changes correlated with cell migration and neuron differentiation. Neuronal transformation has been associated with an aggressive clinical phenotype in PCa as reviewed in chapter 1. Our integrative analysis on epigenetic regulation and gene expression in LNCaP-T/E cells demonstrated that T/E overexpression drives upregulation of *FZD4* and *HLA-DMB* that could be correlated with loss of DNA methylation and histone modification in PCa cells. This data corroborated previous findings of T/E-induced transcriptional modulation of *TDRD1* expression by loss of DNA methylation [52].

Most CpG sites showing a significant differential methylation, were located in gene bodies, which is of interest regarding the proposed role of gene body methylation in transcriptional regulation by impacting the efficiency of transcription elongation, regulation of alternative promoters and RNA splicing or repression of anti-sense transcripts [53, 54]. Gene body methylation has frequently been associated with increased mRNA

transcription [55]. DNA methylation was proposed to be mechanistically facilitated by open and actively transcribed chromatin [56]. In our study, gene body hypomethylation correlated with increased mRNA expression, supporting earlier findings that demonstrated low gene body methylation in highly expressed genes potentially due to interference of DNA accessibility to methylating enzymes by the transcriptional machinery [56]. *FZD4* mRNA was shown to be upregulated upon T/E overexpression thereby activating Wnt/β-catenin signaling in PCa (chapter 2, [32]). It is not clear from the present analysis whether T/E-induced *FZD4* body hypomethylation represents a potential regulatory mechanism of activated gene expression. However, the enriched pattern of histone H3K4me1 modification at the hypomethylated gene body CpG site, which is often associated with promoters and enhancers, supports a regulatory role of gene body hypomethylation [53]. Another interesting finding is that this hypomethylated CpG site is located within a DNAse hypersensitivity site generally characterized by an open chromatin structure and transcriptional activity [57].

HLA-DMB is a non-classical major histocompatibility complex (MHC) class II molecule acting as a peptide editor for classical MHCII proteins [58]. ERG-associated upregulation of *HLA-DMB* in PCa cells is consistent with previous reports and was shown as a target of HDAC1-mediated gene regulation [24, 39]. Treatment of VCaP cells with the HDAC inhibitor Trichostatin A (TSA) led to downregulation of *HLA-DMB* [25]. *HLA-DMB* expression has previously been correlated with increased cytotoxic T lymphocyte infiltration and improved prognosis in ovarian cancer [59]. The role within the pathogenesis of PCa or as marker of a T/E-induced transcriptional profile remains unknown.

In conclusion, we show that T/E overexpression affects the epigenetic and transcriptional profile in PCa cells that are correlated with aggressive cell behavior on the global level. Future research is necessary to reveal the mechanistic basis of those molecular changes and to analyse the role of differential CpG methylation in regulating transcriptional changes. We used a high-throughput methylation profiling approach to detect global variations in DNA methylation. Bisulfite sequencing is the gold standard for measuring DNA methylation by determining the fraction of bisulfite-converted and unconverted (methylated) cytosines and should be used for subsequent validation of pre-selected genomic regions with single-nucleotide resolution. Further analysis of the epigenomic and transcriptional mechanisms of ERG can be achieved by chromatin immunoprecipitation followed by high-throughput sequencing (ChIP-seq). ChIP-seq analysis using our Dox-inducible LNCaP-T/E cell model would be a valuable contribution to existing data to generate a broader view of the molecular and cellular consequences of T/E overexpression.

SUPPLEMENTARY INFORMATION

Content

1. Supplementary materials

Supplementary Table S3.1: List of primer sequences and probes used for qPCR

Name	#UPL probe	Sequence forward 5' - 3'	Sequence reverse 5' – 3'
CHD9	75	tcatcagcatttacatgacagaaa	ccagaaccatcgctcttctt
CXXC1	13	ctcagatgactgtggcatgaa	gtgctcttcagcaatgcaag
ERG_T/E	64	ggttaatgcatgctagaaacaca	agatggttgagcagctttcg
FZD4	19	aactttcacaccgctcatcc	tgcacattggcacataaaca
GADPH	60	agccacatcgctcagacac	gcccaatacgaccaaatcc
JMJD1C	18	gaagatttgaaacccaatggag	actgaacgaggaatgccagt
KAT2A	25	tcctcactcacttccccaaa	ttggagagtttgccccatag
KAT2B	83	ctgcgatctcccaatgatg	ctgtggcacgttgcagtaa
PRDM1	67	acgtgtgggtacgaccttg	ctgccaatccctgaaacct
PRMT1	10	ccccaaacagctggtcac	ggtcttccaccttgacggta
PRMT5	6	gactagtcatcccggagaagc	ggccgattcttagcaggtt
PRMT6	44	accgcctgggtatccttc	cccacgtccagtaccgtct
SETD1B	22	ctggcttaacgacacgctct	ccatcgtcccgtttcttct
SETDB1	10	aggcacgtggtggaagtc	ccactcacatcttttgtcatcc
SIRT2	52	gaaggtgcaggaggctca	caggaagtccatgtctgcttc
SUV39H1	13	gtcatggagtacgtgggagag	cctgacggtcgtagatctgg

2. Supplementary data

Supplementary Table S3.2: Functional annotation of genes differentially methylated upon T/E overexpression

Gene Symbol	TE III FC	TE III Δβ	TE VI FC	TE VI Δβ	Gene Region	CpG Location	Chr.	Illumina Probe ID
FZD4	22.707	-0.400	49.555	-0.415	Body	N_Shelf	11	cg06659209
GDPD5	22.227	-0.255	12.495	-0.190	5'UTR	0	11	cg22171321
IL18BP	12.989	-0.323	9.233	-0.407	TSS200	0	11	cg26149678
RELL1	12.107	-0.341	12.068	-0.488	Body	0	4	cg18672030
SH2D3C	10.850	-0.347	21.081	-0.595	TSS200	0	9	cg02356631

Supplementary Table S3.2: continued

PPAP2B	9.174	-0.166	9.486	-0.256	Body	0	1	cg01860101
MGP	7.846	-0.336	2.549	-0.334	TSS200	0	12	cg00431549
RIN2	7.195	-0.247	8.236	-0.387	1stExon	0	20	cg06856720
SLC23A2	6.663	-0.479	15.669	-0.572	Body	0	20	cg22147446
OSBPL10	6.524	-0.632	4.495	-0.598	Body	0	3	cg02311396
MSN	4.847	-0.147	8.723	-0.255	Body	0	X	cg26588779
SLC44A3	4.841	-0.295	6.315	-0.271	Body	0	1	cg01463768
TSPAN14	4.571	-0.216	7.382	-0.187	Body	0	10	cg08448786
ETV6	4.354	-0.222	7.012	-0.155	Body	0	12	cg06252636
MDS2	4.354	-0.164	7.012	-0.304	Body	0	1	cg10372630
PRKCH	4.008	-0.255	3.175	-0.250	Body	0	14	cg16918236
HLA-DMB	3.894	-0.263	4.169	-0.279	TSS1500	0	6	cg10518264
AKAP13	3.860	-0.117	3.363	-0.379	Body	0	15	cg05254518
COL4A6	3.836	-0.135	2.320	-0.227	Body	0	X	cg02033305
PNPLA7	3.548	-0.136	2.541	-0.230	Body	N_Shore	9	cg01701837
DUSP6	3.331	-0.331	4.156	-0.302	Body	N_Shore	12	cg10077746
CDKN1B	3.269	-0.169	4.968	-0.230	TSS1500	N_Shore	12	cg21142548
TOM1L2	3.179	-0.201	1.815	-0.272	Body	0	17	cg08151968
DDX10	3.032	-0.432	4.918	-0.547	Body	0	11	cg13225881
IPCEF1	2.990	-0.336	4.930	-0.299	ExonBnd	0	6	cg12263540
PCED1B	2.958	-0.229	6.040	-0.143	5'UTR	0	12	cg06869032
MACF1	2.947	-0.216	5.745	-0.199	Body	0	1	cg21122391
CD63	2.863	-0.215	3.415	-0.290	TSS1500	S_Shore	12	cg26418880
TBC1D2B	2.665	-0.274	2.251	-0.202	Body	0	15	cg12192261
TMEM217	2.623	-0.465	4.237	-0.563	TSS1500	S_Shore	6	cg00480799
SORBS1	2.580	-0.386	6.418	-0.424	5'UTR	0	10	cg11041353
SDPR	2.563	-0.188	6.100	-0.265	5'UTR	0	2	cg08390172
BCL2L1	2.542	-0.202	3.626	-0.195	Body	0	20	cg15488794
PRCP	2.491	-0.497	4.378	-0.565	Body	0	11	cg00808150
CAP2	2.376	-0.350	0.996	-0.263	Body	0	6	cg22753611
TRAF3IP2	2.347	-0.257	4.178	-0.269	Body	0	6	cg00590039
CRK	2.302	-0.438	4.621	-0.419	Body	0	17	cg06742476
ACTN4	2.283	-0.269	1.900	-0.318	Body	0	19	cg14891553

Supplementary Table S3.2: continued

PHACTR2	2.272	-0.133	2.707	-0.232	Body	0	6	cg24598922
HPSE	2.245	-0.138	13.495	-0.313	Body	0	4	cg13186580
FAM160A2	2.186	-0.332	2.280	-0.323	Body	0	11	cg13301956
DCAF5	2.145	-0.552	2.184	-0.539	Body	N_Shore	14	cg21250594
PXN	2.124	-0.232	2.101	-0.325	Body	0	12	cg25220336
FN1	2.095	-0.239	1.197	-0.191	Body	0	2	cg14222615
LRRC36	2.090	-0.271	2.887	-0.242	Body	0	16	cg09879805
CPQ	2.042	-0.444	2.660	-0.360	Body	0	8	cg23762726
TBCD	2.040	-0.177	6.227	-0.294	Body	S_Shore	17	cg18102305
NOS3	2.017	-0.519	2.012	-0.607	Body	N_Shore	7	cg07643980
LPP	1.968	-0.373	1.787	-0.317	5'UTR	0	3	cg23070717
RECK	1.954	-0.461	4.103	-0.434	Body	0	9	cg09959196
ADGRL2	1.951	0.069	4.118	-0.204	5'UTR	0	1	cg17083209
RERE	1.927	-0.240	1.894	-0.273	Body	0	1	cg07836226
SLC25A45	1.922	-0.545	1.304	-0.574	0	N_Shore	11	cg24215776
APH1B	1.921	-0.154	2.256	-0.305	Body	0	15	cg25074326
FAM107A	1.916	-0.300	5.671	-0.352	TSS1500	0	3	cg04232458
MYO10	1.903	-0.269	3.980	-0.433	Body	0	5	cg02288345
APP	1.897	-0.269	5.314	-0.244	Body	0	21	cg23877117
SAAL1	1.889	-0.413	1.420	-0.360	ExonBnd	0	11	cg14220104
ABCC3	1.856	-0.198	11.120	-0.209	Body	0	17	cg06926619
PLSCR3	1.841	-0.120	2.062	-0.330	Body	N_Shore	17	cg21368706
TXNRD2	1.825	-0.423	1.119	-0.451	Body	0	22	cg07073234
LTB4R	1.812	-0.144	4.980	-0.372	5'UTR	S_Shore	14	cg20542800
SH3YL1	1.806	-0.321	0.732	-0.224	Body	N_Shore	2	cg17500664
STARD13	1.784	-0.198	2.388	-0.267	Body	0	13	cg20497682
CASC15	1.780	-0.355	2.756	-0.401	Body	0	6	cg03680338
PHC2	1.777	-0.252	1.757	-0.288	Body	0	1	cg03944314
KDM2A	1.776	-0.347	1.481	-0.184	Body	0	11	cg16322424
TRIP12	1.752	-0.226	1.995	0.143	Body	0	2	cg11149952
NSMCE2	1.751	-0.585	1.448	-0.475	Body	0	8	cg23009206
NCK2	1.730	-0.525	1.681	-0.594	TSS1500	N_Shore	2	cg26032413
INTS3	1.679	-0.379	1.242	-0.583	ExonBnd	0	1	cg18006944

Supplementary Table S3.2: continued

CHD9	1.652	-0.202	3.120	-0.286	5'UTR	0	16	cg25775667
PKM	1.643	-0.272	1.314	-0.351	Body	0	15	cg09485853
PRKAB1	1.585	-0.579	0.896	-0.437	Body	0	12	cg14654609
EML6	1.578	-0.220	1.086	-0.064	Body	0	2	cg07450514
PPFIBP1	1.565	-0.241	1.703	-0.266	5'UTR	0	12	cg03114371
BEND7	1.561	-0.163	1.509	-0.281	TSS1500	0	10	cg02648003
PDE7B	1.561	-0.246	1.609	-0.242	Body	0	6	cg11285173
NCOA7	1.550	-0.271	2.657	-0.188	5'UTR	0	6	cg19684445
HSD17B2	1.544	-0.280	0.967	-0.406	Body	0	16	cg07307142
IST1	1.544	-0.205	1.483	-0.126	3'UTR	0	16	cg04266019
SLC10A7	1.543	-0.319	1.080	-0.276	Body	0	4	cg12484495
SCARB2	1.538	-0.532	0.704	-0.554	Body	N_Shelf	4	cg13870520
ATG7	1.527	-0.335	1.178	-0.402	Body	0	3	cg11507857
TSPAN15	1.515	-0.381	0.817	-0.434	Body	0	10	cg01632881
SLC35E1	1.505	-0.209	2.242	0.032	Body	0	19	cg26683792
PLEKHM1	1.493	-0.233	1.653	-0.368	Body	0	17	cg13030804
SEPT9	1.492	-0.656	1.007	-0.662	Body	0	17	cg07089333
TNS2	1.485	-0.184	1.794	-0.236	5'UTR	S_Shelf	12	cg12934686
PPP4R1	1.471	-0.148	1.711	-0.437	Body	0	18	cg18483766
CLHC1	1.458	-0.161	1.497	-0.221	5'UTR	0	2	cg22213014
CALD1	1.427	-0.295	1.115	-0.269	Body	0	7	cg20055548
NDRG2	1.391	-0.371	3.891	-0.553	Body	N_Shore	14	cg23288563
HDAC7	1.389	-0.224	1.518	-0.231	Body	0	12	cg04381888
GPCPD1	1.375	-0.350	2.205	-0.462	Body	0	20	cg05287483
STX17	1.374	-0.308	1.150	-0.270	Body	0	9	cg03807032
MBNL1	1.374	-0.270	1.219	-0.231	Body	0	3	cg12656221
BRD2	1.370	-0.205	1.558	-0.194	TSS1500	N_Shore	6	cg05111146
MGST3	1.366	-0.168	1.135	-0.252	5'UTR	0	1	cg21165486
MARK2	1.347	-0.249	1.118	-0.332	TSS1500	N_Shore	11	cg23999391
ERGIC1	1.347	-0.225	1.587	-0.169	Body	0	5	cg26899249
FNDC3B	1.340	-0.302	2.432	-0.299	Body	0	3	cg02889177
NRP1	1.323	-0.494	1.965	-0.508	Body	0	10	cg09030553
DDX17	1.320	-0.280	1.365	-0.249	Body	0	22	cg15906007

Supplementary Table S3.2: continued

VPS26B	1.315	-0.275	0.973	-0.264	3'UTR	0	11	cg24000223
CLSTN3	1.314	-0.217	1.268	-0.211	TSS1500	0	12	cg00489652
RAPGEF2	1.313	-0.226	1.280	-0.278	Body	0	4	cg16882824
FAM114A1	1.307	-0.222	1.306	-0.473	5'UTR	0	4	cg24576960
ITFG3	1.301	-0.599	1.618	-0.581	5'UTR	0	16	cg09335566
GNL1	1.300	-0.190	1.626	-0.252	3'UTR	0	6	cg01132522
BTNL8	1.287	-0.218	1.098	-0.179	Body	0	5	cg17826428
RNF130	1.286	-0.378	0.828	-0.298	Body	0	5	cg01402360
MIPOL1	1.278	-0.043	1.099	0.225	Body	0	14	cg27224192
INMT	1.277	-0.166	6.083	-0.251	TSS1500	0	7	cg07252961
PCMTD1	1.265	-0.049	1.241	-0.243	Body	0	8	cg01730030
MYL12A	1.256	-0.492	1.039	-0.707	TSS1500	N_Shore	18	cg08543623
FGGY	1.256	-0.343	1.207	-0.221	Body	0	1	cg06329202
MLLT10	1.253	-0.257	1.979	-0.367	Body	0	10	cg14673506
PRKCZ	1.252	-0.081	2.509	-0.262	Body	0	1	cg24475758
SKI	1.227	-0.517	1.835	-0.457	Body	0	1	cg11514097
SREK1	1.214	-0.443	1.307	-0.002	Body	0	5	cg11497377
EXD2	1.208	-0.481	1.193	-0.541	3'UTR	0	14	cg18836689
LXN	1.201	-0.212	1.360	-0.369	TSS1500	0	3	cg17977250
ZNF346	1.193	-0.609	1.157	-0.609	Body	0	5	cg22782782
CUBN	1.187	-0.132	1.556	-0.230	Body	0	10	cg07732336
MINK1	1.176	-0.217	1.112	-0.343	Body	0	17	cg01322380
FAM167B	1.175	-0.157	2.031	-0.318	TSS1500	N_Shore	1	cg20555536
SNX27	1.174	-0.362	0.999	-0.333	Body	0	1	cg08504644
CREM	1.170	-0.149	1.247	-0.296	Body	0	10	cg26273724
SGPL1	1.167	-0.465	0.719	-0.395	Body	0	10	cg19721326
BMP6	1.152	-0.318	1.228	-0.075	Body	S_Shelf	6	cg23623251
MGRN1	1.151	-0.270	0.916	-0.273	Body	0	16	cg03168818
SH3RF3	1.149	-0.196	1.291	-0.221	Body	0	2	cg03063658
ERC1	1.133	-0.125	1.091	-0.225	Body	0	12	cg03422015
C6orf10	1.132	-0.376	1.693	-0.414	Body	0	6	cg14704780
ANKH	1.131	-0.229	1.223	-0.330	Body	0	5	cg03315407
GHRLOS	1.130	-0.233	1.129	-0.289	Body	0	3	cg08489410

Supplementary Table S3.2: continued

LRP1B	1.123	-0.392	0.973	-0.285	Body	0	2	cg16711069
SHB	1.115	-0.233	0.960	-0.364	Body	0	9	cg14195115
KANSL1	1.113	-0.108	1.031	0.219	Body	0	17	cg18699337
PAICS	1.113	-0.381	1.026	-0.375	Body	0	4	cg18743463
DCLK2	1.113	-0.268	1.057	-0.270	Body	0	4	cg18426033
RASAL2	1.111	-0.142	1.346	-0.235	Body	0	1	cg15523606
RASGRP3	1.111	-0.092	1.137	-0.290	TSS200	0	2	cg24134261
STX11	1.110	-0.128	1.855	-0.215	3'UTR	S_Shelf	6	cg22164087
GNAT2	1.109	-0.223	1.062	-0.157	TSS1500	0	1	cg22941294
TRNT1	1.108	-0.360	1.176	-0.297	Body	S_Shelf	3	cg11485152
CLEC4E	1.106	0.029	0.998	-0.230	Body	0	12	cg00394101
ARMC2	1.104	-0.217	1.186	-0.334	Body	0	6	cg07963885
LIN28B	1.102	-0.203	1.091	-0.167	Body	0	6	cg23983043
TTC28	1.102	-0.479	1.091	-0.550	Body	0	22	cg26480862
PIEZO2	1.100	-0.098	0.945	-0.234	Body	0	18	cg11830692
SUSD4	1.096	-0,031	1.050	-0.047	Body	0	1	cg13791188
UCKL1	1.096	-0.336	1.771	-0.357	Body	N_Shore	20	cg07507493
LATS2	1.092	-0.404	0.971	-0.392	Body	0	13	cg04022586
CHRM5	1.084	-0.321	1.044	-0.310	TSS1500	0	15	cg11451033
REM2	1.082	-0.141	1.688	-0.281	TSS1500	0	14	cg04539476
MITF	1.082	-0.368	1.011	-0.233	Body	0	3	cg18618113
SDK1	1.080	-0.263	1.058	-0.284	Body	0	7	cg08102516
ACSL6	1.079	-0.153	1.049	-0.234	Body	0	5	cg14841483
ABLIM1	1.078	-0.390	0.997	-0.409	5'UTR	0	10	cg26051956
C2orf61	1.078	-0.386	1.041	-0.247	Body	0	2	cg11709788
ZMIZ1	1.077	-0.244	1.224	-0.427	Body	0	10	cg09819520
FMNL3	1.077	-0.295	1.412	-0.352	Body	0	12	cg20906710
PRR14L	1.076	-0.264	1.173	-0.304	Body	0	22	cg02483891
ENDOU	1.073	-0.203	1.091	-0.276	Body	0	12	cg06475653
SUFU	1.073	-0.406	1.119	-0.492	Body	0	10	cg24198237
FAM122C	1.072	-0.180	1.062	-0.448	3'UTR	0	X	cg22695906
TULP4	1.071	-0.286	0.906	-0.034	Body	0	6	cg24489868
DNM3	1.070	-0.349	1.258	-0.412	Body	0	1	cg23577610

Supplementary Table S3.2: continued

MICAL2	1.067	-0.155	0.970	-0.272	5'UTR	0	11	cg17871234
CXorf36	1.066	-0.158	1.371	-0.387	TSS200	0	X	cg15029285
FAM120A	1.066	-0.302	0.887	-0.371	Body	0	9	cg14730017
NRCAM	1.064	0.013	1.052	-0.248	5'UTR	0	7	cg00019997
M1AP	1.064	-0.224	1.021	-0.285	Body	0	2	cg04994425
CNR2	1.061	-0.236	1.007	-0.530	5'UTR	0	1	cg01586797
GRID1	1.060	0.224	1.035	-0.027	Body	0	10	cg03534166
GIMAP8	1.060	-0.151	3.935	-0.408	1stExon	0	7	cg18769241
MIR548N	1.059	0.072	1.095	0.210	Body	N_Shelf	2	cg19648023
MAP2K6	1.056	-0.284	1.090	-0.413	Body	0	17	cg18326562
GLIS3	1.054	-0.347	1.059	-0.378	Body	0	9	cg06241070
ASB4	1.052	-0.048	1.038	0,093	TSS200	0	7	cg14557807
C10orf76	1.050	-0.356	1.508	-0.408	Body	0	10	cg10228989
ARID1B	1.050	-0.331	1.079	-0.230	Body	0	6	cg14692468
FOXN3	1.050	-0.206	1.028	-0.195	Body	0	14	cg00616028
NINJ2	1.050	-0.155	1.053	-0.225	Body	0	12	cg09409035
IFT140	1.047	-0.200	1.062	-0.355	Body	0	16	cg07016549
WIPF1	1.047	-0.190	1.042	-0.318	5'UTR	0	2	cg22047295
FAM50A	1.046	-0.157	1.374	-0.345	Body	0	X	cg07910434
MIRLET7G	1.046	-0.183	1.042	-0.254	TSS200	0	3	cg09066298
CSTA	1.045	-0.260	1.025	-0.282	1stExon	0	3	cg21932814
TMEM131	1.045	-0.196	1.206	-0.214	Body	0	2	cg15177103
RXFP4	1.045	-0.341	1.008	-0.300	TSS1500	0	1	cg21284779
MCC	1.044	-0.274	1.058	-0.514	Body	0	5	cg02028114
RBM18	1.043	-0.146	0.819	-0.214	Body	0	9	cg09128612
SLC9A9	1.042	-0.499	1.036	-0.629	Body	0	3	cg27419508
KIAA1522	1.042	-0.210	0.528	-0.149	Body	S_Shelf	1	cg05710142
NEDD4	1.041	-0.377	1.049	-0.244	Body	0	15	cg09602650
FAM19A5	1.041	0.061	0.992	-0.203	Body	0	22	cg06409673
CHKA	1.040	-0.228	1.108	-0.276	Body	0	11	cg24397554
GRK5	1.039	-0.241	2.152	-0.270	Body	0	10	cg07835234
SLC5A9	1.038	-0.199	1.120	-0.290	Body	0	1	cg14705496
XRN2	1.037	-0.443	0.908	-0.401	Body	0	20	cg22265539

Supplementary Table S3.2: continued

ZNF366	1.037	-0.311	1.338	-0.409	TSS200	0	5	cg04710768
ZFPM2-AS1	1.035	-0.112	1.069	-0.221	Body	0	6	cg08140558
GSG1	1.034	-0.108	1.084	-0.226	Body	N_Shelf	12	cg20618695
TRAPPC8	1.034	-0.270	1.084	-0.270	Body	0	18	cg04605261
TACR1	1.027	-0.331	1.088	-0.222	Body	0	2	cg14632793
TTC7A	1.022	-0.211	1.026	-0.413	Body	0	2	cg20090162
KCNK12	1.017	-0.112	1.036	-0.221	Body	N_Shore	2	cg17885628
FLJ22447	1.015	-0.331	1.067	-0.324	0	0	14	cg18728780
SBF2	1.015	-0.386	0.986	-0.299	Body	0	11	cg16622342
PKDCC	1.015	-0.196	0.995	-0.221	Body	0	2	cg12066235
DENND3	1.013	-0.260	1.089	-0.326	Body	0	8	cg02574175
CHD3	1.011	-0.152	1.030	-0.354	ExonBnd	0	17	cg03096171
C11orf49	1.011	-0.305	1.002	-0.252	Body	0	11	cg16379731
NCOR2	1.011	-0.152	1.181	-0.204	Body	S_Shelf	12	cg12349623
AJUBA	1.009	-0.239	0.994	-0.240	Body	N_Shore	14	cg08188555
PDS5B	1.008	-0.004	1.149	0.205	Body	0	13	cg23199907
ATRX	1.005	-0.511	1.002	-0.262	Body	0	X	cg23266487
MYO1C	1.005	-0.154	2.141	-0.258	TSS200	S_Shore	17	cg09269848
BIN1	1.004	-0.178	0.995	-0.242	Body	S_Shore	2	cg17509462
GOT1	1.001	-0.266	1.807	-0.263	ExonBnd	0	10	cg13901620
GRK7	1.001	-0.109	1.017	-0.337	Body	N_Shelf	3	cg07768761
COA1	1.000	-0.286	1.202	-0.373	0	0	7	cg15148064
GATA3	1.000	-0.184	1.047	-0.384	Body	S_Shore	10	cg17489908
C1QL3	0.998	-0.502	1.074	-0.404	TSS1500	S_Shore	10	cg12875950
SMURF1	0.997	-0.261	1.001	-0.188	Body	0	7	cg17232924
RANBP17	0.995	-0.545	1.007	-0.501	Body	0	5	cg05617141
EEF1DP3	0.995	-0.159	0.920	-0.202	Body	N_Shelf	13	cg00648883
DYM	0.995	-0.598	0.744	-0.664	Body	0	18	cg24420086
TMEM204	0.995	-0.369	0.994	-0.389	Body	N_Shelf	16	cg07013955
DNAJC18	0.991	-0.161	0.957	-0.267	Body	0	5	cg09622871
PKD1L1	0.990	-0.102	1.270	-0.212	TSS1500	0	7	cg15302078
CNNM4	0.989	-0.246	0.952	-0.140	Body	0	2	cg17415382
MSH2	0.988	-0.230	0.969	0.183	Body	0	2	cg14051210

Supplementary Table S3.2: continued

NEK4	0.987	-0.171	0.947	-0.312	Body	0	3	cg12911970
RIOK2	0.981	-0.002	0.735	0.209	Body	0	5	cg09922808
ARHGEF28	0.980	-0.361	1.148	-0.586	Body	0	5	cg18159467
LGALS4	0.978	-0.330	1.009	-0.360	Body	0	19	cg27061207
CACNA2D3	0.978	-0.395	0.971	-0.369	Body	0	3	cg00846417
GCNT2	0.978	-0.488	1.060	-0.584	TSS1500	0	6	cg14112601
FBXO31	0.975	-0.151	1.101	-0.357	Body	0	16	cg21533743
CSRNP3	0.975	-0.306	1.882	-0.138	5'UTR	0	2	cg12084046
THSD7A	0.970	-0.253	0.917	0.043	Body	0	7	cg04688366
SCUBE1	0.967	-0.096	0.991	-0.233	Body	0	22	cg03879473
CLCN4	0.967	-0.171	0.958	-0.213	5'UTR	0	X	cg02383649
SLC16A1	0.967	-0.151	0.943	-0.221	Body	0	1	cg07572909
SLC2A13	0.966	-0.286	0.998	-0.234	Body	0	12	cg18568497
PTPRE	0.962	-0.232	1.156	-0.459	5'UTR	0	10	cg08048809
SLC39A11	0.959	-0.236	0.812	-0.339	Body	0	17	cg17303039
C3orf52	0.959	-0.275	1.003	-0.288	Body	S_Shelf	3	cg16217908
SMC4	0.959	-0.410	1.072	-0.283	Body	0	3	cg15729450
CDCP2	0.958	-0.303	1.180	-0.316	TSS200	0	1	cg01367140
WDR82	0.957	-0.186	0.910	-0.284	Body	0	3	cg25236791
CELSR1	0.957	-0.376	0.949	-0.278	Body	N_Shore	22	cg04332442
C6orf136	0.956	-0.211	0.800	-0.178	3'UTR	0	6	cg02434880
EXOC5	0.956	-0.697	0.945	-0.703	Body	N_Shelf	14	cg25653900
RBM47	0.955	-0.191	0.771	-0.252	TSS1500	0	4	cg09249657
GPR45	0.954	-0.230	0.937	-0.287	TSS1500	N_Shore	2	cg11223196
TPD52	0.948	-0.241	0.861	-0.381	Body	0	8	cg09597589
ACKR2	0.947	-0.146	1.080	-0.369	5'UTR	0	3	cg13702846
CCL17	0.944	-0.134	0.970	-0.253	5'UTR	0	16	cg02573340
TAOK3	0.944	-0.232	0.987	-0.220	5'UTR	0	12	cg01341698
CLRN3	0.942	-0.142	0.954	-0.249	Body	0	10	cg07269647
ARID1A	0.940	-0.423	0.959	-0.291	Body	0	1	cg09849688
PGAP2	0.938	-0.171	0.714	-0.429	5'UTR	0	11	cg11559794
PIP4K2A	0.936	-0.434	1.709	-0.550	Body	0	10	cg09273683
PITPNC1	0.935	-0.440	1.047	-0.436	Body	0	17	cg08708167

Supplementary Table S3.2: continued

SLC1A1	0.928	-0.309	0.842	-0.277	Body	0	9	cg14366878
EPB41L1	0.925	-0.261	0.986	-0.188	5'UTR	0	20	cg20296980
CMTM7	0.922	-0.249	1.685	-0.318	TSS1500	N_Shore	3	cg10101634
NPEPL1	0.913	-0.282	0.800	-0.303	TSS200	N_Shelf	20	cg00771376
YLPM1	0.908	-0.348	0.936	-0.411	Body	0	14	cg02536712
TANGO6	0.906	-0.238	0.922	-0.365	Body	0	16	cg22375758
DOCK9	0.903	-0.308	0.851	-0.249	Body	0	13	cg13570883
SPTLC2	0.901	-0.494	0.905	-0.539	Body	0	14	cg05690233
KIAA0391	0.900	-0.273	0.788	-0.387	Body	0	14	cg18680181
MAP2K4	0.895	-0.352	0.869	-0.184	Body	0	17	cg12046729
MOB1B	0.892	-0.249	0.865	-0.277	Body	0	4	cg04576707
PTPRG	0.884	-0.351	1.458	-0.290	Body	0	3	cg01071477
PBX4	0.879	-0.308	1.040	-0.291	Body	0	19	cg01153902
RALGDS	0.874	-0.161	0.990	-0.308	Body	N_Shore	9	cg07521475
FAM104B	0.857	-0.177	0.891	-0.309	Body	0	X	cg17243829
TRAPPC6A	0.846	-0.304	0.882	-0.122	Body	0	19	cg26097728
RALGPS1	0.845	-0.091	1.172	-0.238	Body	0	9	cg09874683
ADGRG1	0.841	-0.227	0.314	-0.424	5'UTR	0	16	cg26955845
KCNH4	0.841	-0.190	1.052	-0.338	Body	0	17	cg06685556
CA12	0.839	-0.313	0.776	-0.234	Body	N_Shelf	15	cg08947167
POC1B	0.839	-0.254	1.018	-0.477	Body	0	12	cg13598864
DIAPH3	0.836	0.170	0.813	-0.229	Body	0	13	cg24289237
AP2B1	0.820	-0.320	0.776	-0.304	Body	0	17	cg04170952
TBL1X	0.813	-0.186	0.966	-0.278	Body	0	X	cg13853116
C5orf63	0.809	-0.225	0.815	-0.540	5'UTR	N_Shore	5	cg00207226
DCPS	0.803	-0.283	0.572	-0.303	Body	0	11	cg05522498
DPP4	0.802	-0.513	3.137	-0.645	Body	N_Shelf	2	cg12649175
CRELD2	0.794	-0.203	0.675	-0.215	Body	S_Shore	22	cg20610988
POLR3A	0.770	-0.515	0.688	-0.544	Body	0	10	cg02586876
LARS2	0.745	-0.379	0.641	-0.311	Body	0	3	cg05380759
IARS2	0.733	-0.501	0.512	-0.595	Body	0	1	cg11170368
ARID5B	0.722	-0.453	0.544	-0.317	Body	0	10	cg13541977
RINL	0.704	-0.458	0.637	-0.232	5'UTR	0	19	cg09565670

Supplementary Table S3.2: continued

SUCLG2	0.695	-0.194	0.521	-0.287	Body	0	3	cg09067993
GMDS	0.689	-0.327	0.547	-0.359	Body	0	6	cg11058558
MRPL33	0.680	-0.377	0.359	-0.597	Body	S_Shelf	2	cg15947193
OVOL2	0.676	-0.129	0.549	-0.234	Body	N_Shore	20	cg05728394
TACC1	0.665	-0.361	0.530	-0.272	5'UTR	0	8	cg18316192
RNLS	0.634	-0.584	0.601	-0.667	Body	0	10	cg09721144
C12orf10	0.619	-0.286	0.519	-0.518	TSS1500	N_Shore	12	cg08525575
PCK2	0.611	-0.283	0.662	-0.463	TSS1500	N_Shore	14	cg10264529
SEC62	0.598	-0.360	0.619	-0.480	Body	0	3	cg04602039
GFM1	0.598	-0.424	0.575	-0.293	ExonBnd	0	3	cg22141067
SLC7A5	0.592	0.274	0.948	-0.004	Body	Island	16	cg08617020
ACLY	0.581	-0.201	0.654	-0.159	Body	N_Shelf	17	cg02486737
FAM198B	0.578	-0.138	0.769	-0.349	Body	0	4	cg01589294
IL1RAPL1	0.555	-0.064	0.626	0.210	Body	0	X	cg17531668
DHRS7	0.549	-0.329	0.488	-0.252	Body	0	14	cg15520210
RAP1GAP	0.548	-0.242	0.422	-0.241	Body	0	1	cg06165723
SLC35F2	0.543	-0.427	0.992	-0.324	Body	0	11	cg16408039
CDK19	0.382	-0.351	0.330	-0.251	Body	0	6	cg01725626
HSD17B12	0.358	0.013	0.477	-0.206	TSS1500	N_Shore	11	cg06112137
ECT2	0.354	-0.543	0.299	0.719	0	Island	3	cg12393503
SLC7A1	0.323	-0.391	0.313	-0.403	5'UTR	0	13	cg11069855
STK39	0.274	-0.597	0.193	-0.605	Body	0	2	cg10123669
RHOU	0.161	-0.155	0.337	-0.250	Body	S_Shelf	1	cg10922143
BBOX1-AS1	#NV	-0.432	#NV	-0.449	Body	0	11	cg19130723
DGUOK-AS1	#NV	-0.608	#NV	-0.556	Body	0	2	cg02418306
DLGAP1-AS2	#NV	-0.279	#NV	-0.280	TSS200	0	18	cg05757358
FAM53B-AS1	#NV	-0.422	#NV	-0.431	TSS200	0	10	cg11937172
GLIS2-AS1	#NV	-0.394	#NV	-0.268	TSS1500	S_Shore	16	cg26196104
ITPKB-IT1	#NV	-0.383	#NV	-0.455	Body	0	1	cg24113686
KCCAT211	#NV	-0.460	#NV	-0.502	Body	0	3	cg08046836
KIAA1211L	#NV	-0.292	#NV	-0.354	3'UTR	0	2	cg24047187
KIAA2012	#NV	-0.325	#NV	-0.379	ExonBnd	0	2	cg06203744
LINC00271	#NV	-0.217	#NV	-0.212	Body	0	6	cg05739816

Supplementary Table S3.2: continued

LINC00313	#NV	-0.229	#NV	-0.250	TSS1500	0	21	cg21655830
LINC00487	#NV	-0.206	#NV	-0.252	0	0	2	cg02738156
LINC00589	#NV	-0.328	#NV	-0.316	Body	0	8	cg17315703
LINC00920	#NV	-0.207	#NV	-0.198	0	S_Shore	16	cg27326306
LINC01119	#NV	-0.212	#NV	-0.443	Body	0	2	cg22661501
LINC01237	#NV	-0.183	#NV	-0.281	Body	0	2	cg07262940
LNX1-AS2	#NV	-0.285	#NV	-0.224	TSS1500	0	4	cg00729984
LOC100506368	#NV	-0.214	#NV	-0.304	Body	0	11	cg12452371
LOC101929450	#NV	-0.218	#NV	-0.177	Body	0	8	cg23363841
LOC101929596	#NV	-0.322	#NV	-0.519	Body	0	2	cg23813542
LOC102724050	#NV	-0.352	#NV	-0.318	Body	0	12	cg25516577
LOC102724312	#NV	-0.250	#NV	-0.382	Body	N_Shore	1	cg07898743
LOC286059	#NV	-0.202	#NV	-0.338	Body	0	8	cg15666431
LOC643542	#NV	-0.278	#NV	-0.111	Body	0	18	cg12294310
LOC729867	#NV	-0.400	#NV	-0.338	5'UTR	S_Shelf	1	cg13109911
MIR4290	#NV	-0.363	#NV	-0.221	TSS1500	0	9	cg09253224
MIR5009	#NV	-0.236	#NV	-0.261	Body	0	21	cg12975010
MIR99AHG	#NV	-0.217	#NV	-0.118	Body	0	21	cg02711653
ZFPM2-AS1	#NV	-0.270	#NV	0.039	Body	0	8	cg05718647

Supplementary Table S3.3: Functional annotation of genes differentially methylated upon T/E overexpression

Functional annotation	Genes	p-value	z-score*	# Genes†
Organization of cytoskeleton	*FN1, SEPT9, MARK2, WIPF1, MSN, NRP1, MYO10, CRK, NRCAM, NCK2*	7.27E-07	3.667	29
Cellular homeostasis	*ATG7, BCL2L1, GATA3, APP, CHRM5, CDKN1B, PRKCH, STK39, MIRLET7G, SLC16A1*	3.63E-03	4.012	25
Cell migration	*FN1, APP, CCL17, PXN, NOS3, NRP1, LTB4R, BMP6, CDKN1B, GATA3*	9.06E-06	3.609	45
Neuron differentiation	*APP, BCL2L1, IL1RAPL1, GDPD5, MIR-LET7G, ECT2, CHKA, FN1, BMP6*	9.22E-03	2.549	9

Top 10 differentially expressed genes in our dataset that were annotated to a function. A gene was selected when its annotation to the indicated function was based on at least two findings in the Ingenuity knowledge base. *Activation z-score is a measure of predicted change (increase or decrease) of the process. †Total number of genes supporting a specific functional annotation.

Supplementary Table S3.4: Canonical pathway analysis of genes differentially methylated upon T/E overexpression

Ingenuity Canonical Pathways	p-value	z-score*	# Genes†
Gastrin signaling	7.89E-04	2.646	7 (101)
Rho GTPase signaling	1.29E-03	1.667	11 (248)
Moleculer Mechanisms of Cancer	1.61E-03	NaN	14 (376)
cAMP signaling	6.40E-03	0.707	9 (223)
Ephrin signaling	1.56E-02	2.646	7 (174)

Significantly enriched canonical pathways across the dataset of commonly methylated genes between T/E III and VI are shown. *Activation z-score is a measure of predicted change (activated or reduced) of the process. NaN – not a number. †Number of genes in the dataset, which are represented in the pathway. Numbers in brackets depict the total number of genes in the pathway in the reference gene set.

REFERENCES

1. Kumar A, White TA, MacKenzie AP, Clegg N, Lee C, Dumpit RF, Coleman I, Ng SB, Salipante SJ, Rieder MJ, Nickerson DA, Corey E, Lange PH, Morrissey C, Vessella RL, Nelson PS, et al. Exome sequencing identifies a spectrum of mutation frequencies in advanced and lethal prostate cancers. Proc Natl Acad Sci U S A. 2011; 108(41):17087-17092.
2. Taylor BS, Schultz N, Hieronymus H, Gopalan A, Xiao Y, Carver BS, Arora VK, Kaushik P, Cerami E, Reva B, Antipin Y, Mitsiades N, Landers T, Dolgalev I, Major JE, Wilson M, et al. Integrative genomic profiling of human prostate cancer. Cancer Cell. 2010; 18(1):11-22.
3. Ross-Adams H, Lamb AD, Dunning MJ, Halim S, Lindberg J, Massie CM, Egevad LA, Russell R, Ramos-Montoya A, Vowler SL, Sharma NL, Kay J, Whitaker H, Clark J, Hurst R, Gnanapragasam VJ, et al. Integration of copy number and transcriptomics provides risk stratification in prostate cancer: A discovery and validation cohort study. EBioMedicine. 2015; 2(9):1133-1144.
4. Tomlins SA, Rhodes DR, Perner S, Dhanasekaran SM, Mehra R, Sun XW, Varambally S, Cao X, Tchinda J, Kuefer R, Lee C, Montie JE, Shah RB, Pienta KJ, Rubin MA and Chinnaiyan AM. Recurrent fusion of TMPRSS2 and ETS transcription factor genes in prostate cancer. Science. 2005; 310(5748):644-648.
5. Friedlander TW, Roy R, Tomlins SA, Ngo VT, Kobayashi Y, Azameera A, Rubin MA, Pienta KJ, Chinnaiyan A, Ittmann MM, Ryan CJ and Paris PL. Common structural and epigenetic changes in the genome of castration-resistant prostate cancer. Cancer Res. 2012; 72(3):616-625.
6. Barbieri CE, Baca SC, Lawrence MS, Demichelis F, Blattner M, Theurillat JP, White TA, Stojanov P, Van Allen E, Stransky N, Nickerson E, Chae SS, Boysen G, Auclair D, Onofrio RC, Park K, et al. Exome sequencing identifies recurrent SPOP, FOXA1 and MED12 mutations in prostate cancer. Nat Genet. 2012; 44(6):685-689.
7. Cancer Genome Atlas Research N. The Molecular Taxonomy of Primary Prostate Cancer. Cell. 2015; 163(4):1011-1025.
8. Aryee MJ, Liu W, Engelmann JC, Nuhn P, Gurel M, Haffner MC, Esopi D, Irizarry RA, Getzenberg RH, Nelson WG, Luo J, Xu J, Isaacs WB, Bova GS and Yegnasubramanian S. DNA methylation alterations exhibit intraindividual stability and interindividual heterogeneity in prostate cancer metastases. Sci Transl Med. 2013; 5(169):169ra110.
9. Mundbjerg K, Chopra S, Alemozaffar M, Duymich C, Lakshminarasimhan R, Nichols PW, Aron M, Siegmund KD, Ukimura O, Aron M, Stern M, Gill P, Carpten JD, Orntoft TF, Sorensen KD, Weisenberger DJ, et al. Identifying aggressive prostate cancer foci using a DNA methylation classifier. Genome Biol. 2017; 18(1):3.
10. Park JY, Zheng W, Kim D, Cheng JQ, Kumar N, Ahmad N and Pow-Sang J. Candidate tumor suppressor gene SLC5A8 is frequently down-regulated by promoter hypermethylation in prostate tumor. Cancer Detect Prev. 2007; 31(5):359-365.
11. Brocks D, Assenov Y, Minner S, Bogatyrova O, Simon R, Koop C, Oakes C, Zucknick M, Lipka DB, Weischenfeldt J, Feuerbach L, Cowper-Sal Lari R, Lupien M, Brors B, Korbel J, Schlomm T, et al. Intratumor DNA methylation heterogeneity reflects clonal evolution in aggressive prostate cancer. Cell Rep. 2014; 8(3):798-806.
12. Lee WH, Isaacs WB, Bova GS and Nelson WG. CG island methylation changes near the GSTP1 gene in prostatic carcinoma cells detected using the polymerase chain reaction: a new prostate cancer biomarker. Cancer Epidemiol Biomarkers Prev. 1997; 6(6):443-450.
13. Zelic R, Fiano V, Zugna D, Grasso C, Delsedime L, Daniele L, Galliano D, Pettersson A, Gillio-Tos A, Merletti F and Richiardi L. Global Hypomethylation (LINE-1) and Gene-Specific Hypermethylation (GSTP1) on Initial Negative Prostate Biopsy as Markers of Prostate Cancer on a Rebiopsy. Clin Cancer Res. 2016; 22(4):984-992.
14. Lee WH, Morton RA, Epstein JI, Brooks JD, Campbell PA, Bova GS, Hsieh WS, Isaacs WB and Nelson WG. Cytidine methylation of regulatory sequences near the pi-class glutathione S-transferase gene accompanies human prostatic carcinogenesis. Proc Natl Acad Sci U S A. 1994; 91(24):11733-11737.

15. Yegnasubramanian S, Kowalski J, Gonzalgo ML, Zahurak M, Piantadosi S, Walsh PC, Bova GS, De Marzo AM, Isaacs WB and Nelson WG. Hypermethylation of CpG islands in primary and metastatic human prostate cancer. Cancer Res. 2004; 64(6):1975-1986.
16. Fraser M, Sabelnykova VY, Yamaguchi TN, Heisler LE, Livingstone J, Huang V, Shiah YJ, Yousif F, Lin X, Masella AP, Fox NS, Xie M, Prokopec SD, Berlin A, Lalonde E, Ahmed M, et al. Genomic hallmarks of localized, non-indolent prostate cancer. Nature. 2017; 541(7637):359-364.
17. Lin PC, Giannopoulou EG, Park K, Mosquera JM, Sboner A, Tewari AK, Garraway LA, Beltran H, Rubin MA and Elemento O. Epigenomic alterations in localized and advanced prostate cancer. Neoplasia. 2013; 15(4):373-383.
18. Angulo JC, Andres G, Ashour N, Sanchez-Chapado M, Lopez JI and Ropero S. Development of Castration Resistant Prostate Cancer can be Predicted by a DNA Hypermethylation Profile. J Urol. 2016; 195(3):619-626.
19. Beltran H, Prandi D, Mosquera JM, Benelli M, Puca L, Cyrta J, Marotz C, Giannopoulou E, Chakravarthi BV, Varambally S, Tomlins SA, Nanus DM, Tagawa ST, Van Allen EM, Elemento O, Sboner A, et al. Divergent clonal evolution of castration-resistant neuroendocrine prostate cancer. Nat Med. 2016; 22(3):298-305.
20. Yegnasubramanian S, Haffner MC, Zhang Y, Gurel B, Cornish TC, Wu Z, Irizarry RA, Morgan J, Hicks J, DeWeese TL, Isaacs WB, Bova GS, De Marzo AM and Nelson WG. DNA hypomethylation arises later in prostate cancer progression than CpG island hypermethylation and contributes to metastatic tumor heterogeneity. Cancer Res. 2008; 68(21):8954-8967.
21. Schulz WA, Elo JP, Florl AR, Pennanen S, Santourlidis S, Engers R, Buchardt M, Seifert HH and Visakorpi T. Genomewide DNA hypomethylation is associated with alterations on chromosome 8 in prostate carcinoma. Genes Chromosomes Cancer. 2002; 35(1):58-65.
22. Kim JH, Dhanasekaran SM, Prensner JR, Cao X, Robinson D, Kalyana-Sundaram S, Huang C, Shankar S, Jing X, Iyer M, Hu M, Sam L, Grasso C, Maher CA, Palanisamy N, Mehra R, et al. Deep sequencing reveals distinct patterns of DNA methylation in prostate cancer. Genome Res. 2011; 21(7):1028-1041.
23. Borno ST, Fischer A, Kerick M, Falth M, Laible M, Brase JC, Kuner R, Dahl A, Grimm C, Sayanjali B, Isau M, Rohr C, Wunderlich A, Timmermann B, Claus R, Plass C, et al. Genome-wide DNA methylation events in TMPRSS2-ERG fusion-negative prostate cancers implicate an EZH2-dependent mechanism with miR-26a hypermethylation. Cancer Discov. 2012; 2(11):1024-1035.
24. Iljin K, Wolf M, Edgren H, Gupta S, Kilpinen S, Skotheim RI, Peltola M, Smit F, Verhaegh G, Schalken J, Nees M and Kallioniemi O. TMPRSS2 fusions with oncogenic ETS factors in prostate cancer involve unbalanced genomic rearrangements and are associated with HDAC1 and epigenetic reprogramming. Cancer Res. 2006; 66(21):10242-10246.
25. Bjorkman M, Iljin K, Halonen P, Sara H, Kaivanto E, Nees M and Kallioniemi OP. Defining the molecular action of HDAC inhibitors and synergism with androgen deprivation in ERG-positive prostate cancer. Int J Cancer. 2008; 123(12):2774-2781.
26. Yang L, Xia L, Wu DY, Wang H, Chansky HA, Schubach WH, Hickstein DD and Zhang Y. Molecular cloning of ESET, a novel histone H3-specific methyltransferase that interacts with ERG transcription factor. Oncogene. 2002; 21(1):148-152.
27. Yang L, Mei Q, Zielinska-Kwiatkowska A, Matsui Y, Blackburn ML, Benedetti D, Krumm AA, Taborsky GJ, Jr. and Chansky HA. An ERG (ets-related gene)-associated histone methyltransferase interacts with histone deacetylases 1/2 and transcription co-repressors mSin3A/B. Biochem J. 2003; 369(Pt 3):651-657.
28. Yu J, Yu J, Mani RS, Cao Q, Brenner CJ, Cao X, Wang X, Wu L, Li J, Hu M, Gong Y, Cheng H, Laxman B, Vellaichamy A, Shankar S, Li Y, et al. An integrated network of androgen receptor, polycomb, and TMPRSS2-ERG gene fusions in prostate cancer progression. Cancer Cell. 2010; 17(5):443-454.
29. M. Zoma LC, D. Shinde, A. Mitra, D. Albino, S. Rossi, G. Civenni, M. Losa, G. Thalmann, G. Chiorino, C.V. Catapano, G.M. Carbone. (2017). A novel epigenetic crosstalk between ERG and EZH2 leads to prostate cancer progression. 32nd Annual EAU Congress. (London, United Kingdom.
30. Castro F, Dirks WG, Fahnrich S, Hotz-Wagenblatt A, Pawlita M and Schmitt M. High-throughput SNP-based authentication of human cell lines. Int J Cancer. 2013; 132(2):308-314.

31. Schmitt M and Pawlita M. High-throughput detection and multiplex identification of cell contaminations. Nucleic Acids Res. 2009; 37(18):e119.
32. Ratz L, Laible M, Kacprzyk LA, Wittig-Blaich SM, Tolstov Y, Duensing S, Altevogt P, Klauck SM and Sultmann H. TMPRSS2:ERG gene fusion variants induce TGF-beta signaling and epithelial to mesenchymal transition in human prostate cancer cells. Oncotarget. 2017; 8(15):25115-25130.
33. de Hoon MJ, Imoto S, Nolan J and Miyano S. Open source clustering software. Bioinformatics. 2004; 20(9):1453-1454.
34. Saldanha AJ. Java Treeview--extensible visualization of microarray data. Bioinformatics. 2004; 20(17):3246-3248.
35. Eisen MB, Spellman PT, Brown PO and Botstein D. Cluster analysis and display of genome-wide expression patterns. Proc Natl Acad Sci U S A. 1998; 95(25):14863-14868.
36. Pfaffl MW. A new mathematical model for relative quantification in real-time RT-PCR. Nucleic Acids Res. 2001; 29(9):e45.
37. Gupta S, Iljin K, Sara H, Mpindi JP, Mirtti T, Vainio P, Rantala J, Alanen K, Nees M and Kallioniemi O. FZD4 as a mediator of ERG oncogene-induced WNT signaling and epithelial-to-mesenchymal transition in human prostate cancer cells. Cancer Res. 2010; 70(17):6735-6745.
38. Wu L, Zhao JC, Kim J, Jin HJ, Wang CY and Yu J. ERG is a critical regulator of Wnt/LEF1 signaling in prostate cancer. Cancer Res. 2013; 73(19):6068-6079.
39. Paulo P, Ribeiro FR, Santos J, Mesquita D, Almeida M, Barros-Silva JD, Itkonen H, Henrique R, Jeronimo C, Sveen A, Mills IG, Skotheim RI, Lothe RA and Teixeira MR. Molecular subtyping of primary prostate cancer reveals specific and shared target genes of different ETS rearrangements. Neoplasia. 2012; 14(7):600-611.
40. Consortium EP. An integrated encyclopedia of DNA elements in the human genome. Nature. 2012; 489(7414):57-74.
41. Kim SM, Kim JY, Choe NW, Cho IH, Kim JR, Kim DW, Seol JE, Lee SE, Kook H, Nam KI, Kook H, Bhak YY and Seo SB. Regulation of mouse steroidogenesis by WHISTLE and JMJD1C through histone methylation balance. Nucleic Acids Res. 2010; 38(19):6389-6403.
42. Wolf SS, Patchev VK and Obendorf M. A novel variant of the putative demethylase gene, s-JMJD1C, is a coactivator of the AR. Arch Biochem Biophys. 2007; 460(1):56-66.
43. Kim TD, Shin S and Janknecht R. ETS transcription factor ERG cooperates with histone demethylase KDM4A. Oncol Rep. 2016; 35(6):3679-3688.
44. Katoh M and Katoh M. Comparative integromics on JMJD1C gene encoding histone demethylase: conserved POU5F1 binding site elucidating mechanism of JMJD1C expression in undifferentiated ES cells and diffuse-type gastric cancer. Int J Oncol. 2007; 31(1):219-223.
45. Chen J, Chan AW, To KF, Chen W, Zhang Z, Ren J, Song C, Cheung YS, Lai PB, Cheng SH, Ng MH, Huang A and Ko BC. SIRT2 overexpression in hepatocellular carcinoma mediates epithelial to mesenchymal transition by protein kinase B/glycogen synthase kinase-3beta/beta-catenin signaling. Hepatology. 2013; 57(6):2287-2298.
46. Lehnertz B, Ueda Y, Derijck AA, Braunschweig U, Perez-Burgos L, Kubicek S, Chen T, Li E, Jenuwein T and Peters AH. Suv39h-mediated histone H3 lysine 9 methylation directs DNA methylation to major satellite repeats at pericentric heterochromatin. Curr Biol. 2003; 13(14):1192-1200.
47. Snowden AW, Gregory PD, Case CC and Pabo CO. Gene-specific targeting of H3K9 methylation is sufficient for initiating repression in vivo. Curr Biol. 2002; 12(24):2159-2166.
48. Braig M, Lee S, Loddenkemper C, Rudolph C, Peters AH, Schlegelberger B, Stein H, Dorken B, Jenuwein T and Schmitt CA. Oncogene-induced senescence as an initial barrier in lymphoma development. Nature. 2005; 436(7051):660-665.
49. Cedar H and Bergman Y. Linking DNA methylation and histone modification: patterns and paradigms. Nat Rev Genet. 2009; 10(5):295-304.
50. Rose NR and Klose RJ. Understanding the relationship between DNA methylation and histone lysine methylation. Biochim Biophys Acta. 2014; 1839(12):1362-1372.

51. Hojfeldt JW, Agger K and Helin K. Histone lysine demethylases as targets for anticancer therapy. Nat Rev Drug Discov. 2013; 12(12):917-930.
52. Kacprzyk LA, Laible M, Andrasiuk T, Brase JC, Borno ST, Falth M, Kuner R, Lehrach H, Schweiger MR and Sultmann H. ERG induces epigenetic activation of Tudor domain-containing protein 1 (TDRD1) in ERG rearrangement-positive prostate cancer. PLoS One. 2013; 8(3):e59976.
53. Mendizabal I, Zeng J, Keller TE and Yi SV. Body-hypomethylated human genes harbor extensive intragenic transcriptional activity and are prone to cancer-associated dysregulation. Nucleic Acids Res. 2017; 45(8):4390-4400.
54. Lou S, Lee HM, Qin H, Li JW, Gao Z, Liu X, Chan LL, Kl Lam V, So WY, Wang Y, Lok S, Wang J, Ma RC, Tsui SK, Chan JC, Chan TF, et al. Whole-genome bisulfite sequencing of multiple individuals reveals complementary roles of promoter and gene body methylation in transcriptional regulation. Genome Biol. 2014; 15(7):408.
55. Yang X, Han H, De Carvalho DD, Lay FD, Jones PA and Liang G. Gene body methylation can alter gene expression and is a therapeutic target in cancer. Cancer Cell. 2014; 26(4):577-590.
56. Jjingo D, Conley AB, Yi SV, Lunyak VV and Jordan IK. On the presence and role of human gene-body DNA methylation. Oncotarget. 2012; 3(4):462-474.
57. Thurman RE, Rynes E, Humbert R, Vierstra J, Maurano MT, Haugen E, Sheffield NC, Stergachis AB, Wang H, Vernot B, Garg K, John S, Sandstrom R, Bates D, Boatman L, Canfield TK, et al. The accessible chromatin landscape of the human genome. Nature. 2012; 489(7414):75-82.
58. Shiina T, Hosomichi K, Inoko H and Kulski JK. The HLA genomic loci map: expression, interaction, diversity and disease. J Hum Genet. 2009; 54(1):15-39.
59. Callahan MJ, Nagymanyoki Z, Bonome T, Johnson ME, Litkouhi B, Sullivan EH, Hirsch MS, Matulonis UA, Liu J, Birrer MJ, Berkowitz RS and Mok SC. Increased HLA-DMB expression in the tumor epithelium is associated with increased CTL infiltration and improved prognosis in advanced-stage serous ovarian cancer. Clin Cancer Res. 2008; 14(23):7667-7673.

Chapter 4

INSM1 induces a neuroendocrine phenotype in prostate cancer cells

Leonie Ratz, Peter Altevogt, Sabine M Klauck, Holger Sültmann

In preparation

ABSTRACT

Risk stratification and discrimination of indolent versus clinically significant potentially lethal prostate cancer (PCa) is challenged by its heterogeneous appearance. Neuroendocrine differentiation of ADT-treated PCa is considered a highly aggressive variant of the disease. Due to a lack of rebiopsy specimens and underestimation of this subtype, the molecular characteristics of neuroendocrine prostate cancer are poorly understood. A systematic selection of PCa-relevant candidate genes from expression profiling and RNA-sequencing data of PCa patient tumor samples revealed the neuronal transcription factor *INSM1* as a prominent regulator of a neuroendocrine network. Functional characterization of the role of *INSM1* in the PCa cell lines VCaP, NCI-H660, PC-3, and LNCaP showed regulation of NE marker expression (*ASCL1*, *CHGA*, *CHGB*, *SYP*, *TUBB3*) and increased oncogenic properties of the cells, such as migration and invasion, by *INSM1*. A strong correlation between *INSM1* expression and the transcription factor *ERG* was observed in clinical data and PCa cells. ERG overexpression was accompanied by high expression of NE markers (*TUBB3*, *SCG3*, *ASCL1*). *INSM1* overexpression led to reduced expression of the RE-1 silencing transcription factor (*REST*). *REST* was shown to mediate repression of neuronal genes (e.g. *SYP*, *CHGB*) as well as *MYCN*, *NCAM*, and *L1CAM* in PCa cells. This finding is consistent with earlier reports in different tumors. We showed that *REST* was also involved in the regulation of *INSM1* expression. Comparative microarray expression profiling analysis upon siRNA-mediated knockdown of *INSM1*, *REST*, and *L1CAM* identified the extracellular glycoprotein reelin (*RELN*), which is involved in neuronal migration, as a factor that could confer aggressive properties in PCa cells by activation of oncogenic signaling pathways. In conclusion, we identified *INSM1* as a promising determinant of a neuroendocrine transcriptional network in PCa cells. Since *INSM1* expression is usually restricted to neuronal and endocrine tissue, reactivation of *INSM1* in PCa could be of major interest for future studies and drug development. We provide a rationale for future examination of *INSM1* as marker in histological diagnosis of PCa and to address its role as specific therapeutic target for neuroendocrine prostate cancer.

INTRODUCTION

Prostate cancer (PCa) is a disease with complex histopathological and molecular features and divergent clinical outcome. Tumor heterogeneity and genomic complexity of PCa pose challenges of the determination of aggressive lethal disease, which is not recognized by histological grading alone, and for the optimal therapy decision. The identification of genes playing a critical role in the progression of PCa could provide markers of aggressive disease, improve existing diagnostic tests and risk stratification, and reveal novel drug targets.

Neuroendocrine prostate cancer (NEPC) is a highly aggressive manifestation of advanced PCa, as reviewed earlier in chapter 1. NEPC is predominantly detected in previously treated adenocarcinomas and may be linked to androgen-deprivation therapy (ADT) resistance. NEPC is considered as an adaptive clinical phenotype established under the treatment stress of prolonged ADT. This is corroborated by the detection of differential gene expression and copy number alterations between adenocarcinoma cells and NEPC [1-6]. Reduced expression of the androgen receptor (AR) is a hallmark of NEPC [7, 8]. As a consequence, the AR-regulated genes *PSA*, *TMPRSS2*, and *NKX3.1* are recurrently downregulated in NEPC [2, 7-9]. Histopathologically, NEPC is distinguished from prostatic adenocarcinoma by unique ultrastructural characteristics, such as neurosecretory granules, and immunohistochemical staining for various neuroendocrine elements and polypeptide hormones (e.g. synaptophysin (SYP), chromogranins A and B (CHGA, CHGB), neuron-specific enolase (NSE/ENO2), or neuronal cell adhesion molecule (NCAM1/CD56)) [10-12].

It was initially assumed that NEPC developed from outgrowth of normal prostatic NE cells, promoted by the selective pressure of androgen-independent growth [13]. Current evidence indicates that NEPC originates from prostate adenocarcinoma cells supported by concordant molecular alterations, involving *TMPRSS2:ERG* (T/E) gene fusion and *TP53* mutations [14-16]. This concept suggests that prostate adenocarcinoma cells transdifferentiate into cells with NE characteristics, underpinned by the detection of epithelial markers in NEPC cells such as expression of CK8, CK18, and AMACR [5, 17, 18], as wells as allelotyping studies showing a genetic link between PCa cells and NE differentiated tumor cells [14]. NEPC is currently diagnosed by means of clinical characteristics and is increasingly documented during the clinical course of PCa which is of significance regarding the advent of novel highly potent AR-targeted therapies. Since sampling of PCa metastases is rare in routine practice, the molecular mechanisms determining neuroendocrine transformation are poorly explored [7, 19].

MATERIAL AND METHODS

Strategy for target gene selection

A systematic selection of PCa-relevant genes of PCa patient tumor samples was performed using data from the expression profiling NGFN IG Prostate Cancer project (IGP) [20] and RNA-sequencing data from the International Cancer Genome Consortium-Early Onset Prostate Cancer project (ICGC-EOPC) [21]. A candidate gene approach was used to prioritize relevant genes. Genes showing a fold change of >|1.5|, an FPKM (fragments per kilobase of exon per million fragments mapped) >1, and a count (number of reads aligned to each transcript) >100 were selected for further analysis. Those candidates were further prioritized according to the 'guilt-by-association' concept, which identifies most promising candidates based on their similarity to genes already known to be linked to a biological process of interest, such as PTEN-PI3K/AKT and AR signaling including co-factors regulating AR activity [22, 23]. Next, by using disease-specific web tools for cancer transcriptomic data analysis (Oncomine, TCGA), genes were correlated to mutational and functional information, such as ERG overexpression. The online software tool Ingenuity Pathway Analysis (IPA) was used to predict cancer-relevant gene function, and to identify interaction networks and pathway involvement, thereby linking the selected candidates to PCa-relevant biological processes. Subsequently, the biological relevance of our candidate genes was experimentally validated using cell culture models.

Cell lines and culturing

RWPE-1, LNCaP, VCaP, DU-145, PC-3 and NCI-H660 cells were purchased from American Type Culture Collection (ATCC, Manassas, VA, USA) (Supplementary Table S4.1). LNCaP and DU-145 cells were cultured in RPMI1640 supplemented with 10% FBS. VCaP cells were maintained in DMEM medium supplemented with 10% FBS. PC-3 cells were cultured in F12-K medium supplemented with 10% FBS. NCI-H660 cells were maintained in HITES medium supplemented with 5% fetal bovine serum according to the provider's instructions. RWPE-1 cells were cultured in Keratinocyte Serum Free Medium (K-SFM, Invitrogen 17005) supplemented with bovine pituitary extract (BPE) and epidermal growth factor (EGF). All cell lines were authenticated using Multiplex Cell Authentication by Multiplexion (Heidelberg, Germany) as described recently [24]. The SNP profiles matched known profiles or were unique. The purity of cell lines was validated using the Multiplex cell Contamination Test by Multiplexion (Heidelberg, Germany) as described recently [25]. No Mycoplasma, SMRV or interspecies contamination was detected.
LNCaP cells stably expressing T/E variants (LNCaP-T/E) were described earlier [26] (see chapter 2). Transgene expression was induced with 50 ng/mL Dox (Sigma-Aldrich, Munich, Germany) in RPMI1640 containing 10% tet-FBS. Medium of the uninduced cells was supplemented with the respective volume of PBS only.

RNA isolation, reverse transcription and quantitative real-time PCR

Total RNA was isolated from cell lines using the miRNeasy Mini Kit (Qiagen, Hilden, Germany) and quality controlled on the 2100 Bioanalyser (Agilent Technologies, Waldbronn, Germany) with RNA 6000 Nano Kit according to manufacturer's protocols. Total RNA was reverse transcribed using the RevertAid H Minus First Strand cDNA Synthesis Kit (Thermo Fisher Scientific). HotStarTaqDNA polymerase (Qiagen) was used for RT-PCR with 50ng of cDNA template. Relative mRNA levels were assessed by quantitative RT-PCR on the Lightcycler 480 (Roche Diagnostics, Mannheim, Germany) using Universal Probe Library (UPL) assays and primers listed in Supplementary Table S4.2. Linear expression levels were normalized to *GAPDH* using the $2^{(-\Delta\Delta Ct)}$ method [27].

Microarray gene expression profiling

RNA was isolated with the RNase-Free DNase Set (Qiagen) according to the manufacturer's protocol. After quality control, 500ng of total RNA with a concentration of 50 ng/µl were submitted to the DKFZ Genomics and Proteomics Core Facility (GPCF) for Illumina Whole-Genome Expression Beadchip Analysis (Human HT-12 Chip). The raw data were quantile-normalized using the Bioconductor package preprocessCore in R. Genes showing expression fold change >|1.3| (p-value <0.05) were considered as differentially expressed and were analysed with Ingenuity Pathway Analysis (IPA) (see below). Genes involved in relevant biological processes obtained from microarray analysis were validated by qPCR in the same samples that were used for microarray profiling.

siRNA-mediated gene knock-down

Cells were transfected with siRNA (Qiagen, Supplementary Table S4.3) using Lipofectamine RNAiMAX (Thermo Fisher Scientific) and OptiMEM® I (Thermo Fisher Scientific) according to the manufacturer's protocol. VCaP and NCI-H660 cells were transfected with 50nM siRNA against *INSM1* or *ERG* (Qiagen), LNCaP cells were treated with 20nM siRNA against *REST* (Qiagen), and PC-3 cells were transfected with 10nM siRNA against *L1CAM* and *RELN*, respectively. Cells transfected with nonsilencing AllStars Negative Control siRNA (Qiagen) were used as controls. All cells were incubated for 72h in 5% CO2 at 37°C and processed for further analysis.

Chemical transformation of bacteria

Chemically competent TOP10 E. coli cells (Invitrogen) were transformed with recombinant plasmids (Supplementary Table S4.4) using the heat shock method. Fifty µL of competent cells were thawed on ice. Two µl of plasmid DNA was added to 10µl of competent cells and incubated on ice for 30 min. Then the cells were subjected to a heat shock at 42°C for 30 sec in a water bath and directly placed on ice for 2 min thereafter. 200µL of pre-warmed SOC medium (Invitrogen) was added to the bacteria for recovery from the heat shock. The bacteria were then incubated for 1h at 37°C horizontally sha-

king at 220 rpm. 100µL of the bacteria solution was plated on LB agar plates containing the appropriate antibiotic and incubated over night at 37°C.

Colony PCR

Colony PCR was used to screen for successfully recombined plasmids from bacterial transformation reactions. Single bacterial colonies were picked up from the agar plates with a sterile pipet tip and transferred to PCR tubes containing 25µl of PCR master mix while cooled on ice. DreamTaq DNA polymerase (Thermo Scientific) was used for colony PCR (1.25 U/reaction). The following reagents are contained in the PCR master mix: 2x DreamTaq Green PCR Master Mix (12.5µL) containing 0.4mM dNTPs, 20µM primer mix (0.75µL), and water (ad 25µL). The following temperature cycling was performed in a thermal cycler: initial denaturation (1 min at 95°C), denaturation (30 sec at 95°C), annealing (30 sec at 50°C), extension (1 min/kb expected PCR product size at 72°C). Steps from denaturation to extension were repeated 35 times followed by a final extension step for 10min at 72°C and cooling to 10°C. PCR products were analysed by agarose gel electrophoresis.

Cryopreservation of bacterial stocks

Glycerol stocks for long term storage of the bacteria clones and re-inoculation of growth medium were prepared from over-night cultures. Bacteria culture (800µl) was mixed with 200µl of 87% sterile glycerol, transferred to a 1.8mL CryoTube (Nunc) and frozen at -80°C.

Sanger sequencing

Sanger sequencing was used to verify sequences of cloned DNA fragments. DNA and primers were submitted to GATC Biotech (Konstanz, Germany) where the sequencing reactions were performed.

Agarose gel electrophoresis

DNA fragments or PCR products were separated by agarose gel electrophoresis. Agarose was added to 1xTAE buffer to the desired concentration (2% for standard use) and boiled until the agarose was completely dissolved. Liquid agarose was cooled down to ~50°C before casting the gels. Gels were run in 1xTAE buffer containing 0.5 mg/L ethidium bromide solution at 80V until the loading dye had migrated for the desired distance. Bands were visualized using a UV transilluminator.

Plasmid DNA preparation

For plasmid preparation, LB medium containing the correct antibiotic was inoculated from a single bacterial colony and incubated over night at 37°C while horizontally shaking at 220 rpm. For cloning, plasmids were prepared with the Plasmid Mini Kit (Qia-

gen). The Plasmid Midi Kit (Qiagen) were used to prepare plasmid DNA for transfection of cell lines. All kits were used according to the manufacturer's instructions.

Plasmid transfection

DNA transfection of cell lines was performed using the jetPEI DNA transfection reagent (VWR International). Cells (LNCaP and PC-3 at 1.5 x 10^5 cells, VCaP at 3 x 10^5 cells) were seeded 24-48h in 6-well plates prior to transfection. One µg of DNA was diluted in 100µl of 150mM NaCl. Four µl jetPEI transfection reagent (VWR International) was diluted in 100µl of 150mM NaCl. The jetPEI solution was added to the DNA solution, vortexed and incubated for 30 min at RT. Meanwhile, the culture medium of the cells was aspirated and refreshed by 1800µl of growth medium. 200µl of the jetPEI/DNA mixture was added drop-wise onto the culture medium in each well, homogenized by gently swirling the plate and incubated at 37° C for 72h.

Cell proliferation assay

Cells were transfected with siRNA or overexpression plasmid for 48h and subsequently seeded into 96-well plates at 5000 cells/well in 90µl 10% FBS-containing medium in triplicate and again incubated for 24h. Ten µl of the colorimetric WST-1 reagent (Roche Diagnostics) was added to the medium and incubated at 37°C. Absorbance was measured 2h after addition of WST-1 reagent using a Tecan Infinite® M200 microplate reader (Tecan Group Ltd., Männedorf, Switzerland).

Colony formation assay

Cells were transfected with siRNA or overexpression plasmid for 48h and subsequently seeded into 6-well plates at 700 cells/well in 2000µl 10% FBS-containing medium in duplicate and incubated for 20 days in 5% CO2 at 37°C. Colonies of >50 cells were fixed with 100% methanol on ice and stained with 0.1% Crystal Violet (Sigma- Aldrich). Colonies were counted using the Clono-Counter software [28].

Migration and invasion assays

In vitro cell migration assays were performed in duplicate using 24-well transwell chambers with 8µm pore size (Merck Millipore). Cells were transfected with siRNA or overexpression plasmid for 48h and subsequently seeded at 5x10^5 cells/mL into the upper chamber in 200µl serum-free medium. Seven hundred µl of medium supplemented with 10% FBS as chemoattractant was filled into the bottom well. After 48h of cultivation in 5% CO2 at 37°C, migrated cells attached to the lower surface of the insert were fixed with 100% methanol on ice and stained with 0.1% crystal violet (Sigma- Aldrich). Migrated cells were counted in four random fields under a light microscope (10x magnification).

Invasion assays were performed analogously after coating the transwell chambers with 100µl Matrigel (BD Biosciences, Heidelberg, Germany) per filter.

Cell lysis and Western blot analysis

Whole-cell lysates were prepared in RIPA lysis buffer (50mM Tris-HCl pH 8.0, 150mM NaCl, 1% NP-40, 0.5% sodium deoxycholate, 0.1% SDS), supplemented with 1x cOmplete Mini Protease Inhibitor Cocktail (Roche Diagnostics) and 1x PhosSTOP Phosphatase Inhibitor Cocktail (Roche Diagnostics). Lysates were boiled 5 min at 95°C with 4x reducing Roti-Load protein loading buffer (Roth, Karlsruhe, Germany). Samples were separated on a mini polyacrylamide gel (Bio-Rad, Munich, Germany) and transferred to PVDF membranes using the Trans-Blot Turbo semi-dry blotting system (Bio-Rad) at 1.3A, 25V for 7-10 min. After blocking with 5% BSA in Tween-20/PBS, membranes were probed with primary antibodies prepared in blocking solution overnight at 4°C on a roller, followed by incubation with horseradish peroxidase-conjugated secondary antibody in blocking solution for 1h at room temperature and ECL detection (Thermo Fisher Scientific) by the ChemiDoc XRS+ system (Bio-Rad). Western blotting was performed using primary antibodies against INSM1 (Sigma-Aldrich, Munich, Germany), REST (EMD Millipore, Darmstadt, Germany), L1CAM (clone L1-11A, by Peter Altevogt), and GAPDH (Cell Signaling Technology, Danvers, MA, USA) at 1:1000 dilution. Secondary antibodies used were anti-rabbit-HRP (at 1:25000 dilution; Dianova, Hamburg, Germany) and anti-mouse-HRP (at 1:10000 dilution; Cell Signaling). Quantitative analysis of protein expression relative to GAPDH was done using Image Lab software (Bio-Rad).

Ingenuity Pathway Analysis

Functional annotation and pathway enrichment of differentially regulated genes were identified using Ingenuity Pathway Analysis (IPA) software (Qiagen). IPA uses the Ingenuity knowledge base, a database of protein and gene interactions integrated from published biomedical literature and third party sources. Analysis using IPA was performed between September 2015 and February 2016 (Ingenuity version 26127183).

Functional annotations

Gene expression changes were categorized into functional annotations of molecular and cellular mechanisms. The Ingenuity knowledge base provides a predicted direction of change for the biological function (downstream effect analysis), represented by an activation z-score, where $z > 2.0$ or < -2.0 is predictive for activation or reduction of the process, respectively. A p-value < 0.05 indicates a statistically significant association between a set of differentially expressed genes and a given process.

Pathway enrichment analysis

Ingenuity knowledge base provides an analysis of metabolic and cell signaling pathways that are significantly enriched in the gene expression signature. Pathway significance values were calculated based on Fisher's right tailed exact test and the –log(p-value) by IPA. Pathways meeting the threshold p-value <0.05 were considered as significant.

Statistical testing

Expression differences between the induced and uninduced cells were analysed using a paired t-test and between induced cells of T/E III and VI by an unpaired t-test. Statistical significance of t-test depicted as *p<0.05, **p<0.01, ***p<0.001.

RESULTS

INSM1 is highly expressed in ERG fusion-positive PCa samples and cell lines

A systematic candidate gene selection was performed to prioritize PCa-relevant genes using data from the expression profiling NGFN IG Prostate Cancer project (IGP) [20] and RNA-sequencing data from the International Cancer Genome Consortium-Early Onset Prostate Cancer project (ICGC-EOPC) [21]. The gene insulinoma-associated-1 (*INSM1*) was strongly upregulated in tumor samples (21-fold, count: 1259, FPKM: 1.537) compared to normal tissue of the ICGC-EOPCA RNA-seq data set. INSM1 plays a role in pancreatic and neuronal development and is usually expressed during the embryonic development of NE tissue [29, 30]. In adult tissue, *INSM1* expression levels are low or absent. In NE tumors of different origin, *INSM1* shows aberrant high expression [31]. Differential gene expression analysis for *ERG* fusion-positive versus *ERG* fusion-negative tumor samples using the ICGC RNA-seq data (unpublished) further revealed increased expression of *INSM1* (1.4-log fold, p-value<0.005) in *ERG* fusion-positive samples (Figure 4.1A). The association of *INSM1* with *ERG* was evaluated using the TCGA PRAD RNA-seq (IlluminaHiSeq) (n=550) dataset confirming an increased expression of *INSM1* in *ERG* fusion-positive tumor samples (p-value<0.0001; Figure 4.1B). Together, these data indicated that the expression of *INSM1* was upregulated in PCa tumor samples and correlated with the T/E fusion status.

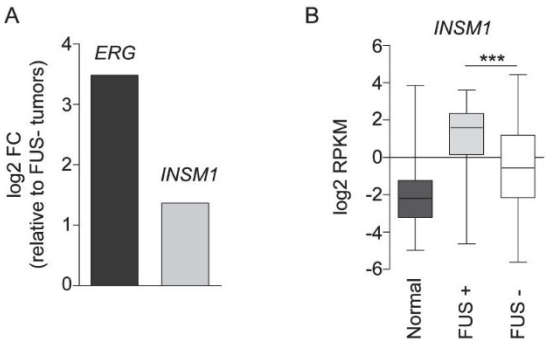

Figure 4.1: Gene expression levels of *INSM1* in prostate tissue. (A) Differential gene expression of *INSM1* in PCa tumor samples using ICGC RNA-seq data (n=90). Expression values are shown as log2FC in T/E fusion-positive samples relative to fusion-negative samples. (B) *INSM1* expression using the TCGA PRAD RNA-seq (IlluminaHiSeq) (n=550) dataset. Values are given as log2 RPKM. FUS – *TMPRSS2:ERG* fusion.

To assess the expression pattern of *INSM1* in PCa cells, qPCR analysis was performed across cell lines representing different characteristics of PCa. *INSM1* mRNA levels were high in VCaP (~30,000-fold) and NCI-H660 (~97,000-fold) cells, both positive for the T/E gene fusion [32], compared to the non-neoplastic human epithelial prostate cells RWPE-1 [33] (Figure 4.2A), indicating that the expression of *INSM1* also correlated with the presence of the T/E gene fusion in PCa cell lines. The high expression of *INSM1* in the NE-like NCI-H660 cell line, which was originally derived from a prostatic small cell carcinoma, suggested that *INSM1* is associated with the neuroendocrine phenotype [32]. The classical fusion-negative cell lines LNCaP, DU-145, and PC-3 cells, showed low or absent *INSM1* expression (Figure 4.2A).

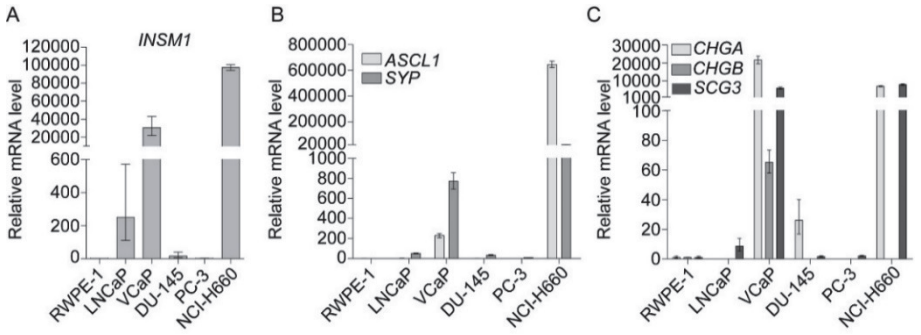

Figure 4.2: T/E-positive PCa cell lines express *INSM1* and NE markers. (A) qPCR analysis across different PCa cell lines shows upregulation of *INSM1* mRNA in the T/E-positive cells VCaP and NCI-H660 compared to RWPE-1 cells. (B-C) mRNA expression of the NE markers (B) *SYP*, *ASCL1*, and (C) *CHGA*, *CHGB*, and *SCG3* is high in VCaP and NCI-H660 cells. ΔCp values from three independent experiments are shown relative to *GAPDH*.

INSM1 induces a NE molecular signature in PCa cells

The linkage of *INSM1* to neuronal processes stimulated us to analyse its function in the development of NEPC. First, basic expression levels of the pro-neural transcription factor achaete-scute homolog 1 (*ASCL1*), the membrane glycoprotein synaptophysin (*SYP*), chromogranin A and B (*CHGA*, *CHGB*), and secretogranin 3 (*SCG3*), markers of neuroendocrine neoplasms [34], could be detected in VCaP and NCI-H660 cells, but not in LNCaP, DU-145, PC-3, and RWPE-1 cells (Figure 4.2B and C). The high expression of NE markers in NCI-H660 cells is in accordance with the neuroendocrine origin of this cell line [32]. Further, expression levels of NE markers in VCaP and NCI-H660 cells correlated with the high expression of *INSM1* in these cells.

The role of *INSM1* in controlling neuroendocrine differentiation (NED) in PCa cells was analysed using siRNA-mediated knockdown and plasmid overexpression. Knockdown of *INSM1* in VCaP cells resulted in 50% reduced expression of *CHGA* and revealed increased mRNA expression (1.5-fold) of the RE-1 silencing transcription factor (*REST*/*NRSF*), a transcriptional repressor of neuronal genes [35] (Figure 4.3A), indicating that *INSM1* functions as negative regulator of REST in NED. Knockdown of *INSM1* in NCI-H660 cells reduced the expression of *CHGA* (60-75% reduction) and *SYP* (60% reduction) (Figure 4.3B). Upon *INSM1* overexpression in LNCaP cells, the NE markers *SYP* and *ASCL1* were increased (3.5-fold and 7-fold, respectively) (Figure 4.3C). Western blot analysis showed that overexpression of INSM1 reduced REST protein levels in LNCaP cells (Figure 4.3D). Likewise, INSM1 overexpression in PC-3 cells induced upregulation of SYP (3-fold, Figure 4.3E), the neuron-associated tubulin beta 3 (*TUBB3*) [36] (1.3-fold) (Figure 4.3F) and *L1CAM* mRNA (4-fold, Figure 4.3F) as well as L1CAM protein (Figure 4.3G-H). The neuronal L1 cell adhesion molecule (L1CAM), a member of the neuronal immunoglobulin (Ig) super-family is involved in neurite outgrowth and migration [37]. It has been associated with poor prognosis and tumor progression [38, 39]. Taken together, these results indicate that *INSM1* induces NE marker expression, which are not normally expressed in PCa cells and present *INSM1* as negative regulator of *REST* expression. However, evidence for a direct regulation of *REST* by *INSM1* needs further experimental validation.

To identify the transcriptional modulation and regulatory function induced by *INSM1*, Illumina microarray expression profiling after siRNA-knockdown was performed. Microarray services were provided by the Genomics and Proteomics Core Facility at the DKFZ. Normalized data were analysed for differential expression. Genes showing >|1.3| fold change compared to control were considered as significantly differentially regulated and used for further analysis using the Ingenuity Pathway analysis (IPA) tool (Supplementary Table S4.5). Comparison of differential mRNA expression between the *INSM1* knockdown expression signature obtained by microarray profiling in VCaP cells

(Supplementary Table S4.5) and RNA-seq data in NEPC [2] revealed consistent differential expression, including the genes *STEAP1*, *ALDH1A3*, *HEPACAM2*, and *E2F2*. For example, *ALDH1A3*, an AR-regulated gene [40-42], and *STEAP1*, suggested as a marker of prostate adenocarcinoma [43, 44], were higher expressed in prostate adenocarcinoma samples compared to NEPC tissue [2] and were upregulated upon *INSM1* knockdown.

Gene ontology terms were determined to reveal the functional context upon *INSM1* knockdown. 'Neuritogenesis' was among the most significant biological processes (Supplementary Table S4.6A), which was consistent with the involvement of *INSM1* and its regulated genes in neuronal functions. Pathway analysis (Supplementary Table S4.6B) revealed the 'Protein Ubiquitination Pathway', suggesting a role in protein processing and degradation that could be involved in a cellular phenotype change. Further, 'Gap Junction Signaling', 'EIF2 Signaling', and 'Melatonin Signaling' were identified, implying the involvement of *INSM1* in intercellular communication and cAMP signaling that could be associated with neuronal signaling mechanisms [45-47].

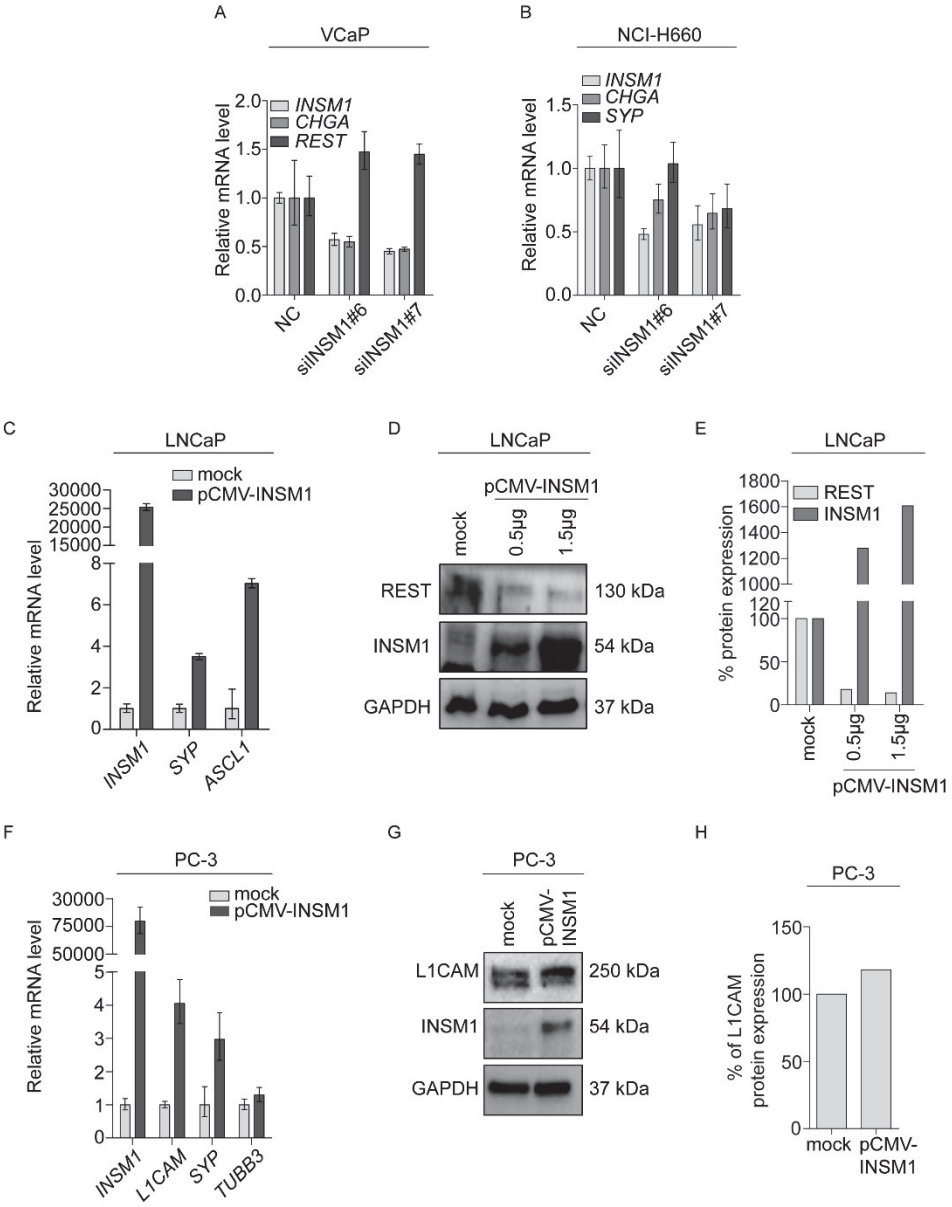

Figure 4.3: *INSM1* is involved in the expression of a NE transcriptional network. SiRNA-mediated knockdown of *INSM1* in (A) VCaP and (B) NCI-H660 cells using 50nM siRNA shows downregulation of NE markers. *REST* is upregulated in VCaP cells. (C-E) *INSM1* overexpression in LNCaP cells shows upregulation of *SYP* and *ASCL1*, and reduced expression of REST protein. (E) Densitometric analysis of Western blot bands shown in (D). (F-H) *INSM1* overexpression in PC-3 cells induced upregulation of L1CAM mRNA and protein, and increased *SYP* and *TUBB3* mRNA levels. (H) Densitometric analysis of L1CAM Western blot bands shown in (G). NC – non-target control.

INSM1 plays a role in migration and invasion in prostate cancer cells

Overexpression of *INSM1* was performed to determine its role on cellular functions. In PC-3 cells, overexpression of *INSM1* increased cell viability (Figure 4.4A). *INSM1*-overexpressing PC-3 cells further showed significantly faster migration and invasion after 24h of observation (Figure 4.4B). Assessment of viability in LNCaP cells revealed a slight reduction (Figure 4.4C) and reduced clonogenic potential as demonstrated by decreased colony formation upon *INSM1* overexpression (Figure 4.4D). *INSM1* overexpression further led to a strong enhancement of the migratory potential (Figure 4.4E) of LNCaP cells. Together, these data provide evidence that *INSM1* is involved in the regulation of an oncogenic cellular phenotype, but with distinct outcomes depending on the individual genetic tumor background. The observed discrepancy in viability outcome is most likely due to the distinct genetic backgrounds of the cell lines, but also reflects the diverse reports regarding the dynamics of NEPC cells, which will be discussed in more detail later.

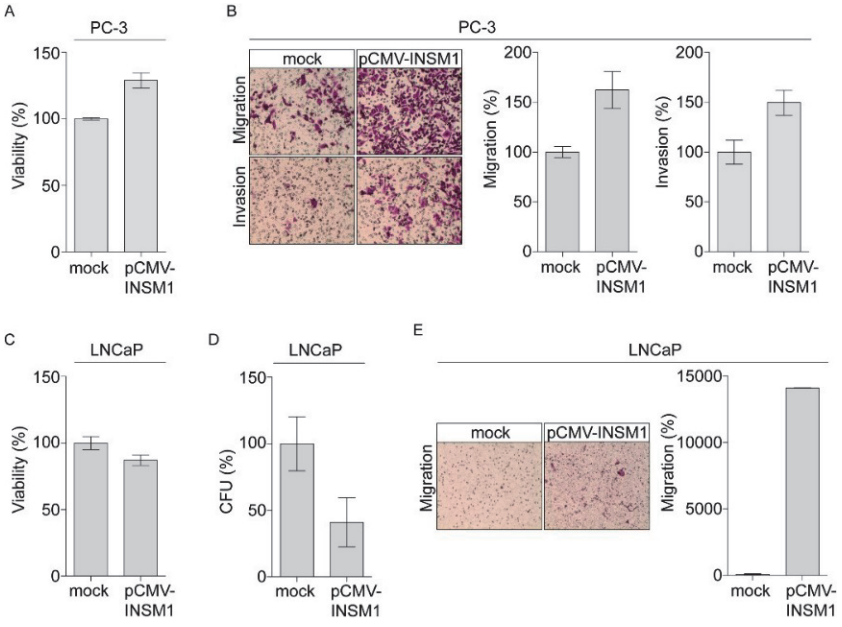

Figure 4.4: Functional characterization of *INSM1* by its overexpression in PC-3 and LNCaP cells. (A) Increased viability was determined by using the WST-1 assay in PC-3 cells. (B) In the transwell migration and invasion assay PC-3 cells show significantly faster migration and invasion after 24h of observation. (C) Slightly reduced viability of LNCaP cells using the WST-1 assay is noted. (D) Colony formation in LNCaP cells reveals reduced clonogenic potential in LNCaP cells. CFU: colony forming units. (E) *INSM1* overexpression leads to strong enhancement of the migratory potential in LNCaP cells.

ERG promotes a NE-like gene expression signature

Since a correlation between the expression of *INSM1* and *ERG* was observed in PCa samples and the T/E-positive cell lines VCaP and NCI-H660, we evaluated this link in more detail by knocking down and overexpressing *ERG* in different cell models. SiRNA-mediated *ERG* knockdown in VCaP (Figure 4.5A) and NCI-H660 (Figure 4.5B) cells led to reduced expression of *INSM1* and was accompanied by reduced mRNA levels of the neuroblastoma Myc oncogene (*MYCN*), which has previously been characterized as a driver of NEPC [48, 49]. In contrast, *REST* expression in VCaP cells was increased after siRNA knockdown of *ERG* (Figure 4.5A). *MYCN* was also reduced upon *ERG* knockdown in NCI-H660 cells, accompanied by reduced *CHGA* and *SYP* expression (Figure 4.5B). However, we did not observe a reduction in *REST* mRNA upon *ERG* knockdown in NCI-H660 cellS (data not shown).

The correlation between *INSM1* and *ERG* overexpression was further examined using the previously described LNCaP-T/E expressing cell model [26]. This revealed increased *INSM1* mRNA levels in T/E expressing cells, respectively, compared to uninduced cells (Figure 4.5C) corroborating ERG-dependent regulation of *INSM1* expression. In this cell model, induction of T/E expression further revealed increased levels of *L1CAM*, *ASCL1*, *TUBB3*, and *SCG3* (Figure 4.5C). In summary, our data provide a profound rationale for the role of *INSM1* and *ERG* in the development of a NE signature.

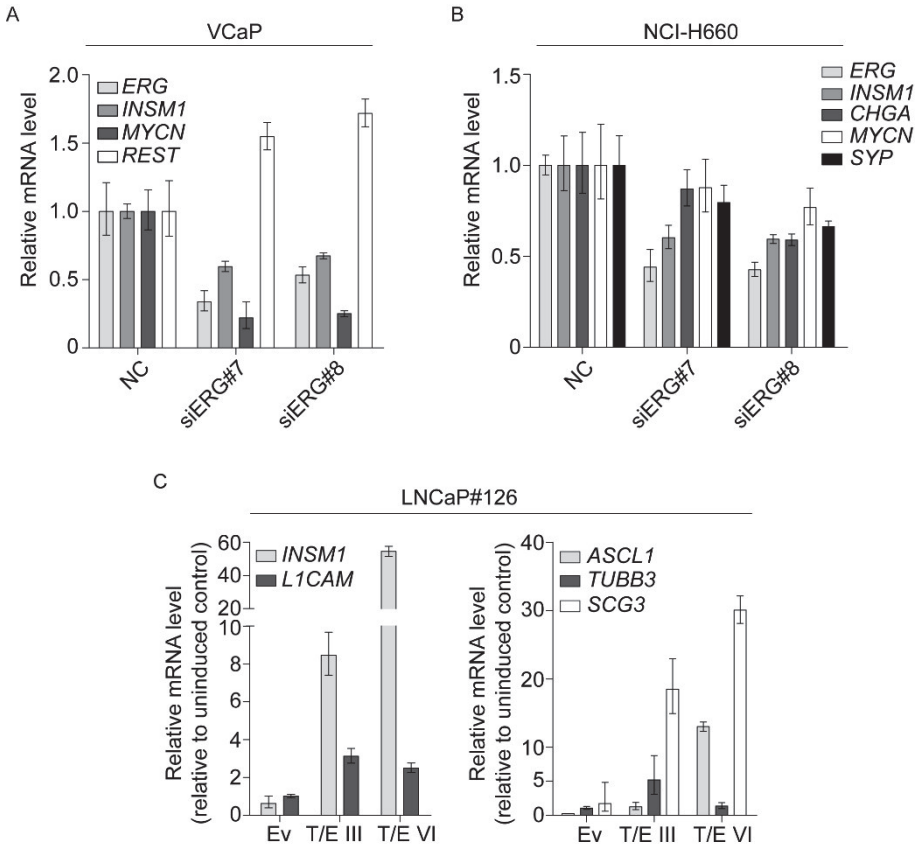

Figure 4.5: *ERG* regulates *INSM1* and NE markers. (A-B) qPCR analysis upon siRNA-mediated *ERG* knockdown using 50nM siRNA in (A) VCaP cells and (B) NCI-H660 cells. (C) qPCR analysis of NE markers in ERG-overexpressing LNCaP cells (parental clone #126). NC: non-target control; Ev - empty vector. T/E III and T/E VI - *TMPRSS2:ERG* gene fusion variants III and VI, respectively.

The neuronal gene silencer REST represses NE markers in PCa cells

REST is known to mediate the restriction of neuronal gene expression in neuronal progenitors and non-neuronal tissue [50, 51]. REST expression decreases with terminal differentiation into mature neurons and has been shown to be lost in NEPC [2, 35]. Assessment of *REST* mRNA expression levels in PCa cells using qPCR revealed reduced levels in VCaP and NCI-H660 cells, as well as in PC-3 cells compared to RWPE-1 cells (Figure 4.6A). *REST* levels were highest in LNCaP and DU-145 cells (Figure 4.6A). Correlation analysis using the ExonArray IGP [20] dataset showed an inverse correlation between *REST* and *INSM1* expression (Figure 4.6B). This analysis further identified an inverse correlation of *REST* with the expression of *CHGA*, *SYP*, and *L1CAM* (Figure 4.6B).

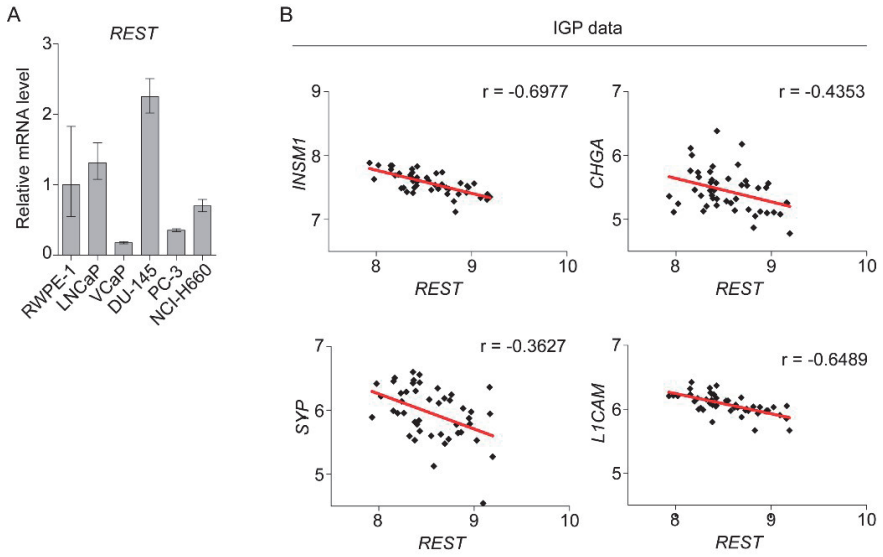

Figure 4.6: *REST* expression in PCa cells. (A) LNCaP and DU-145 cells show increased *REST* mRNA levels, while *REST* expression is low in VCaP, NCI-H660 and PC-3 cells compared to RWPE-1 cells. (B) Correlation of gene expression in the ExonArray IGP dataset, showing negative correlation between *REST* and *INSM1*, *CHGA*, *SYP*, and *L1CAM*, respectively. IGP data - ExonArray expression profiling from the NGFN IG Prostate Cancer (IGP) project.

Microarray gene expression profiling was performed upon siRNA-mediated *REST* knockdown in LNCaP cells. Genes showing >|1.5| fold change compared to control were considered as significantly differentially regulated and used for further analysis using the Ingenuity Pathway analysis (IPA) tool (Supplementary Table S4.7). Gene ontology analysis revealed activation of genes involved in biological mechanisms that are associated with neuronal function, such as 'Neurite growth', 'Neuronal migration' and 'Molecule transport' (Supplementary Table S4.8A) supporting the repressive role of *REST* on these processes. Interestingly, 'Glioma signaling' and 'Reelin signaling in neurons' were among the top regulated canonical pathways upon *REST* knockdown (Supplementary Table S4.8B). The transcriptional profile induced by *REST* knockdown thus indicated that LNCaP cells acquire a gene expression signature and cellular processes that are characteristic for neuronal and NE tumor cells, when the repressive effect of *REST* is lost. Comparison of differential mRNA expression between *REST* knockdown in LNCaP cells (Supplementary Tables S4.7) and RNA-seq data in NEPC [2] revealed opposed differential expression, including the genes *BEX1*, *VGF*, *SYP*, *DDC*, *CHGA*, *CHGB*, *ONECUT2*, *ADCY1*, that have been associated with NE transdifferentiation. The effect of *REST* on *INSM1* expression and the NE signature was analysed in more detail using overexpression and knockdown of *REST*. In VCaP cells, *REST* overexpression reduced *INSM1* and *L1CAM* expression levels, as well as expression of *SYP*, *CHGB*, *MYCN* and

NCAM (Figure 4.7A). When knocking down *REST* using siRNAs, the levels of *CHGA*, and *SYP*, as well as of *L1CAM* increased in PC-3 and LNCaP cells (Figures 4.7B and C), which was consistent with previous findings [51]. *REST* knockdown further stimulated *L1CAM* protein expression in PC-3 and DU-145 cells, which corroborated the *REST*-mediated repression of neuronal genes in PCa cells (Figure 4.7D and E). Cell migration and invasion were reduced upon *REST* overexpression in VCaP cells (Figure 4.8A), whereas in LNCaP cells, *REST* knockdown led to enhanced cell migration (Figure 4.8B) indicating that loss of *REST* facilitates an aggressive phenotype in PCa cells.

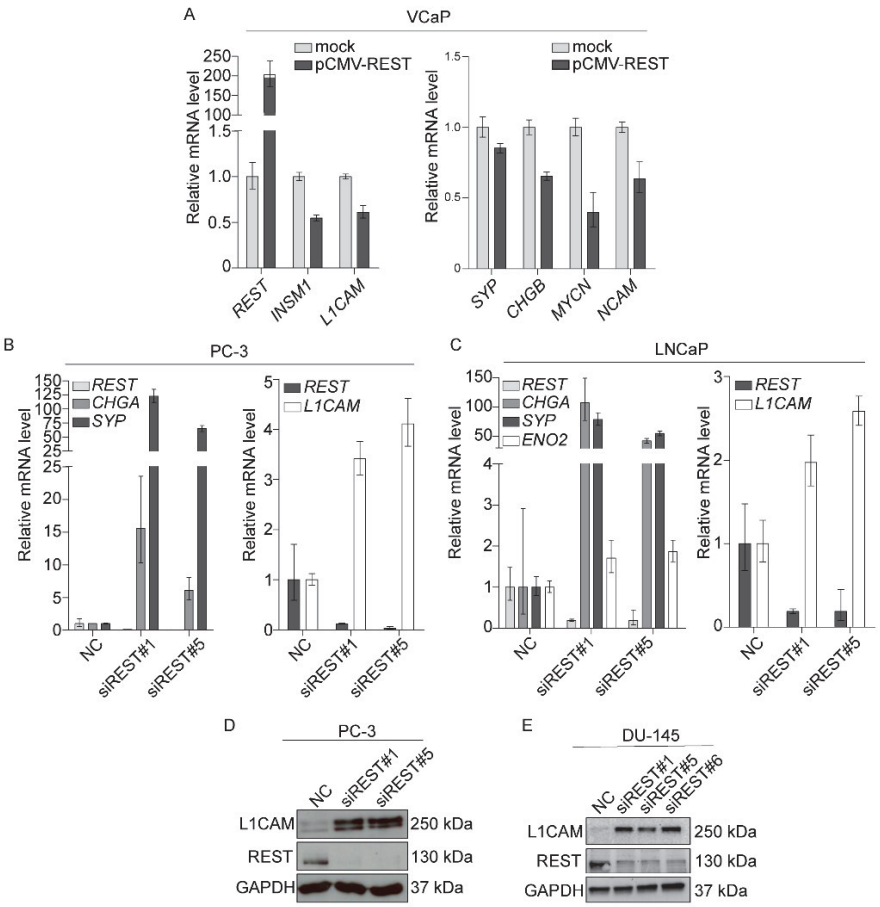

Figure 4.7: *REST* regulates NE markers in PCa cells. Upon *REST* overexpression VCaP cells show reduced levels of (A) *INSM1* and *L1CAM* as well as the neuronal genes *SYP*, *CHGB*, *MYCN*, and *NCAM*. (B-C) *REST* knockdown in (B) PC-3 and (C) LNCaP cells leads to increased NE-marker expression, determined by qPCR. Protein and mRNA levels of the neuronal cell adhesion molecule L1CAM were increased upon *REST* knockdown in (B, D) PC-3, (C) LNCaP, and (E) DU-145 cells. NC - non-target control.

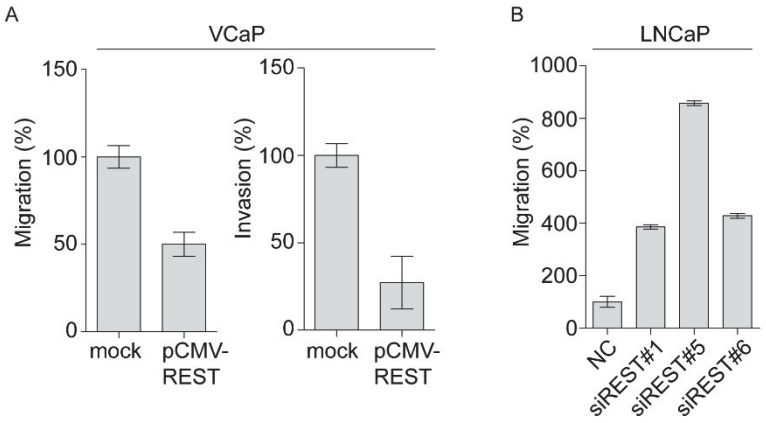

Figure 4.8: Functional consequences of *REST* overexpression or knockdown. (A) *REST* overexpression in VCaP cells led to significantly reduced migration and invasion of the cells compared to mock control. (B) SiRNA-mediated knockdown of *REST* in LNCaP cells (20nM of siRNA) induced significantly faster migration of the cells compared to NC-treated control cells. NC - non-target control.

L1CAM is a marker of NE differentiation in PCa cells

The neuronal cell adhesion molecule *L1CAM* is an established target of REST [52] and plays an important role in the developing nervous system and neuronal migration. In several human tumors, its expression was correlated to poor clinical outcome and therapy resistance [38, 39, 53]. Recently, L1CAM was implicated in metastasis formation in PCa [54]. We showed that *L1CAM* was regulated by *INSM1* together with NE markers (Figure 4.3F). Among the analysed PCa cell lines, the *L1CAM* mRNA level was highest in the neuroendocrine NCI-H660 cells (Figure 4.9A). In human PCa samples of the ExonArray IGP cohort, *L1CAM* was negatively correlated to *AR* expression (Figure 4.9B), which is consistent with earlier reports [55]. In contrast, *L1CAM* further showed positive correlation with *CHGA* and *SYP* (Figure 4.9B) suggesting that it is upregulated when PCa cells lose their epithelial properties.

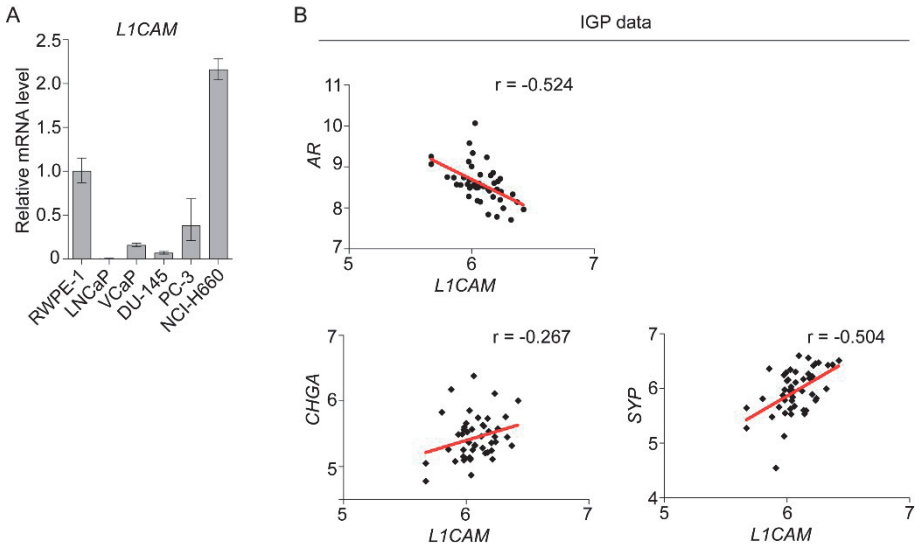

Figure 4.9: *L1CAM* expression in PCa cells and PCa tumor samples. (A) NCI-H660 cells show increased *L1CAM* mRNA levels compared to RWPE-1 cells. (B) Correlation of gene expression in the IGP dataset, showing negative correlation between *L1CAM* and *AR*, but positive correlation of *L1CAM* with *CHGA*, and *SYP*, respectively.

Reelin is a central signaling hub in neuroendocrine differentiation in PCa cell lines

To this point, we identified *INSM1* as a gene involved in NE differentiation in prostate cancer cells, and *REST* as a negative regulator of this process. To obtain insights into the downstream mechanisms that guide PCa cells into NED, we performed a comparative analysis of the *INSM1* and the *REST* knockdown signatures using our expression profiling data. We also performed gene expression profiling upon *L1CAM* knockdown in PC-3 cells (Supplementary Table S4.9) to further elucidate the cellular mechanisms involved in L1CAM-associated migration and metastasis formation in PCa (Supplementary Table S4.10A and B). Of note, the extracellular glycoprotein Reelin (*RELN*) emerged as a common signaling pathway downstream of *INSM1*, *L1CAM* and *REST* (Figure 4.10B). Reelin controls essential steps of neuronal migration and positioning during nervous system development and synaptic plasticity [56, 57]. On the surface of neurons, Reelin binds to its receptors (VLDLR, APOER2, and α3β1 integrin) relaying signaling intracellularly via the DAB1 adaptor protein (Figure 4.11C). DAB1 is a tyrosine-phosphorylated protein promoting interaction with the nonreceptor tyrosine kinases Src, Fyn, Abl, and connecting Reelin to molecular mechanisms of migration such as PI3K/AKT signaling [58]. DAB1 also recruits Crk adaptor proteins (CRK, CRKL) to activate integrin α5β1 signaling [59].

A literature-based survey of gene expression that defines Reelin signaling identified an altered gene expression profile of major Reelin signaling components [60]. Upon *REST*

knockdown in LNCaP cells, upregulation of the signaling components *CDK5R1*, *MAPK8IP2*, *MAPT*, *MAP1B*, *PIK3CB*, and *PIK3R1* was detected. Reelin and its downstream signaling molecules (*MAP2K4*, *PAFAH1B3*) were reduced upon *INSM1* knockdown in VCaP cells as well as upon *L1CAM* knockdown in PC-3 cells. However, *APOE*, which antagonizes Reelin signaling through the *APOER2* receptor [61], was upregulated upon *L1CAM* knockdown, indicating reduced activity of Reelin signaling when *L1CAM* levels are reduced.

A NE marker expression

Gene Symbol	Fold Change siREST	siINSM1	siL1CAM
TUBB3	2.60	0.88	0.57
SYP	4.80	NS	NS
STX1A	1.90	1.12	NS
KCNQ2	1.60	NS	NS
CHGB	1.60	NS	NS
CHGA	1.35	0.95	NS
SCG3	8.70	0.96	NS
SYT4	1.80	0.84	NS
SYT7	1.70	NS	NS
STMN3	11.00	NS	NS
BEX1	11.20	NS	0.55
CELSR3	5.40	NS	NS
VGF	5.30	1.28	1.69
MDK	NS	NS	0.39
CD24	1.12	NS	0.58
ENO2	1.13	NS	2.98

B Reelin signaling

Gene Symbol	Fold Change siREST	siINSM1	siL1CAM
RELN	1.38	0.73	0.64
CDK5	1.13	NS	NS
CDK5R1	1.76	0.88	NS
CRK	0.70	1.19	0.62
CRKL	NS	0.85	NS
BDNF	NS	0.81	0.54
APOE	NS	NS	2.63
NDEL1	0.71	NS	NS
LYN	0.73	1.16	NS
MAPK8IP2	2.28	NS	NS
MAPT	1.43	NS	NS
PAFAH1B3	1.30	0.73	NS
PIK3CB	1.45	1.15	NS
PIK3R1	1.47	NS	NS
MAP1B	1.80	NS	NS
VLDLR	1.16	0.88	3.27
MAP2K4	NS	0.76	NS

Figure 4.10: Transcriptional modulation of a neuroendocrine network in PCa cells. (A-B) Microarray gene expression after knockdown of *REST*, *INSM1*, and *L1CAM* indicating (A) NE marker expression and (B) deregulated Reelin signaling. Red - upregulated; Blue - downregulated; NS - not significant.

Genes involved in Reelin signaling obtained from the microarray analysis were validated by qPCR in the same samples that had been used for microarray analysis (Figure 4.11). As expected, *INSM1* knockdown was accompanied by a 50% reduction of Reelin mRNA level (Figure 4.11A). To validate the role of *INSM1*, its overexpression in PC-3 and LNCaP cells led to increased Reelin expression (~2-fold) (Figure 4.11B). We subsequently analysed the transcriptional changes of signaling molecules downstream of Reelin (Figure 4.11C). *INSM1* overexpression had a stimulating effect on the mRNA expression of Reelin-associated signaling molecules (Figure 11.D). Validation of Reelin mRNA levels in *REST* knockdown samples revealed up to 6-fold elevated expression (Figure 4.11E) and Reelin mRNA responded to forced *REST* expression by a 3-fold decrease in the expression level (Figure 4.11F). Expression of Reelin and its signaling components also responded to *L1CAM* knockdown (Figure 4.11G and H) corresponding to siRNA-mediated Reelin knockdown (Figure 4.11I).

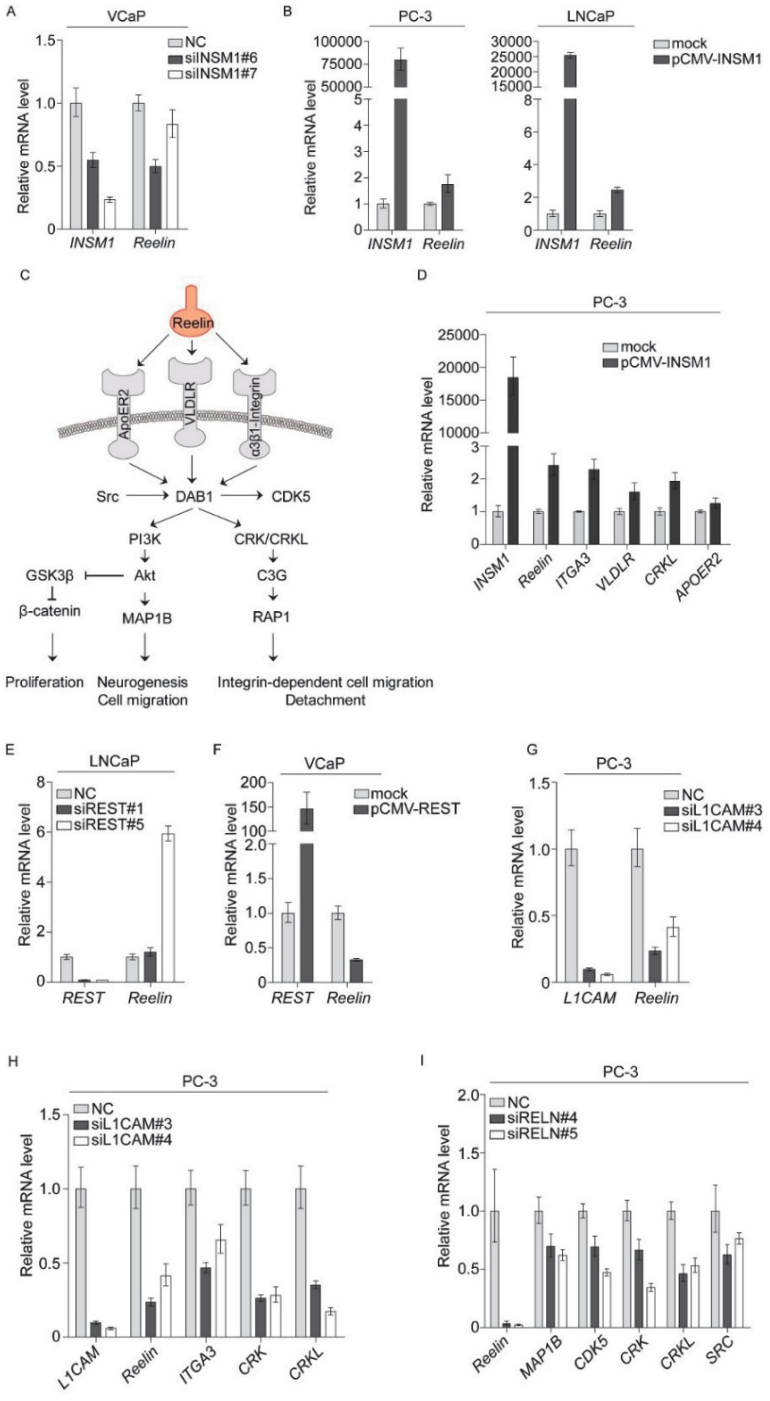

Figure 4.11: Reelin guidance is a common signaling pathway in PCa cells that acquired a NE profile.

Figure 4.11: continued
(A) SiRNA-mediated *INSM1* knockdown leads to reduced Reelin levels in VCaP cells. (B) Reelin increases upon *INSM1* overexpression in PC-3 and LNCaP cells. (C) Schematic model of Reelin and downstream signaling mechanisms. (D) Expression levels of the Reelin signaling components *ITGA3*, *VLDLR*, *CRKL*, and *APOER2* are increased by *INSM1* overexpression in PC-3 cells. (E) Upon *REST* knockdown, Reelin is increased in LNCaP cells. (F) Overexpression of *REST* represses Reelin mRNA levels in VCaP cells. (G) SiRNA-mediated *L1CAM* knockdown reveals a reducing effect on Reelin expression and (H) downstream signaling molecules (*ITGA3*, *CRK*, *CRKL*) in PC-3 cells. (I) Using siRNA-knockdown of Reelin, downstream molecules (*MAP1B*, *CDK5*, *CRK*, *CRKL*, *SRC*) are also reduced, indicating their regulation by Reelin expression. NC – non-target control.

DISCUSSION

Neuroendocrine differentiation in the context of metastatic PCa is of clinical concern due to its unresponsiveness to hormone therapy, aggressive clinical course and poor prognosis [7]. Defining the molecular characteristics of NEPC is necessary to understand the mechanisms of therapy-resistance and disease progression of aggressive PCa. By using a candidate gene approach, we identified *INSM1* as regulator of a NE transcriptional program that stimulates PCa cells to express NE markers. The transcription factor *INSM1* (IA-1), originally cloned from a human insulinoma subtraction library [31], is involved in pancreatic and neuronal development controlling the early stages of NE differentiation. The *INSM1* promoter confers tissue-restricted expression pattern throughout the nervous system during normal embryonic development with an expression peak during the onset of neurogenesis [29, 30]. In adult tissue, *INSM1* expression levels are normally low or absent, but are maintained in the lateral ventricle wall, a site of adult neurogenesis [62]. However, *INSM1* has been found to be aberrantly expressed in NE tumors of different origin including insulinoma, pituitary tumor, pheochromocytoma, medullary thyroid carcinoma, medulloblastoma, neuroblastoma, retinoblastoma, and small cell lung carcinoma [31]. It has recently been shown that *INSM1* is a sensitive marker of human gastrointestinal NED and small cell lung cancer [63-65]. In PCa, adenocarcinomas with a NED component exhibited high expression of *INSM1*, while tumors without NED were negative for *INSM1* [63].

Our results demonstrate that *INSM1* regulates expression of *CHGA*, *ASCL1*, and *SYP* in PCa cell lines, NE markers that were recently detected as differentially expressed in NEPC compared to prostatic adenocarcinomas [9]. Increased CHGA expression has been associated with progression to CRPC and negatively correlated to overall survival [66]. High *ASCL1* mRNA expression was present in tissue specimens of patients that had been treated with ADT and showed NED features [67]. Recently, INSM1-induced expression of ASCL1, CHGA, NCAM1, SYP, and BRN2 was demonstrated in PCa and lung adenocarcinoma cells. A ChIP-assay revealed *ASCL1* promoter binding by INSM1 suggesting INSM1 as direct regulator of a NE program in lung cancer [68, 69]. INSM1 recruits cyclin D1 and histone deacetylase 3 (HDAC3) leading to altered histone H3/4 acetylation and reduced promoter activity of target genes [70]. Further, concordant mechanisms in the

endocrine differentiation of β-cells and NED in PCa have been suggested [71-73]. INSM1 was shown to co-occupy regulatory sequences that maintain the gene expression program in endocrine β-cells together with the bHLH protein NEUROD1 and FoxA2. INSM1 binds the *HES1* promoter in neuroendocrine lung cells thereby repressing Notch signaling, which is required for adequate development of neuroendocrine cells in the lung, and has been implicated in small cell lung cancer [74, 75]. RNA-seq data of NEPC revealed differential expression of neuroendocrine-associated genes compared to PCa that were also differentially regulated upon *INSM1* knockdown in VCaP cells [9]. Intriguingly, *INSM1* expression was shown to be induced by N-myc in neuroblastoma cells resulting in increased N-myc stabilization and tumor aggressiveness. This effect was mediated by extra-nuclear activity of INSM1 that stimulated PI3K/AKT signaling, leading to reduced GSK3β kinase activity and failure to phosphorylate and subsequently degrade NMYC [76]. In neuroblastoma, medulloblastoma and small cell lung cancer, *INSM1* expression was suggested as a downstream target of sonic hedgehog signaling activity [76-79].

The cell type of origin of NEPC is controversially discussed. However mounting evidence points towards a lineage crisis or transdifferentiation mechanism from initial AR-positive adeno-PCa in favor of AR-independent survival [5, 80]. The T/E gene fusion is detected in primary adenocarcinoma as well as in NEPC suggesting a common origin of these disease manifestations [15]. In our study, different cell models were used to analyse the role of ERG in NEPC. In VCaP and NCI-H660 cells, we demonstrated ERG-dependent regulation of *INSM1* expression upon siRNA-mediated *ERG* knockdown. Using transgene T/E expressing LNCaP clones, we showed that T/E gene fusion variants induce molecular changes and cellular phenotypes related to a NE phenotype, suggesting that the detection of T/E rearrangements could implicate a causal mechanism for the development of NEPC, although controversial data exist [9, 81].

In the transformation process towards a NEPC phenotype, two consecutive stages are assumed: First, NED as an adaptive response to survive androgen deprivation, and second, the induction of cell proliferation [82]. Upon *INSM1* overexpression, we observed increased migration but different effects on the proliferation of PC-3 and LNCaP cells, suggesting that additional factors are involved in the regulation of proliferation during NED. This is also reflected by contradicting reports concerning the proliferative activity of NE cells: In the pancreatic cancer cell Panc-1, cell cycle arrest was observed upon *INSM1* overexpression, mediated by competitive binding of *INSM1* to Cyclin D1, thereby interrupting cyclin D1 binding to CDK4 rendering Rb in a hypophosphorylated state and failure of cell cycle progression. INSM1-mediated cell cycle arrest was suggested to facilitate entry into a NE differentiation route [83, 84]. NE cancer cells have been considered as non-proliferative, postmitotic cells located adjacent to proliferative Bcl-2-positive cells [13, 85]. NED areas exhibited the highest proliferation index across tumor tissue and the extent of NED correlated with a higher proliferation index of the whole tumor [86, 87]. It was further shown that NE cancer cells secrete growth stimulating peptides (e.g. bombesin) inducing increased proliferation of adjacent PCa cells [86, 88-93]. However, in small cell PCa cells, upregulation of mitotic genes (*UBE2C*, *AURKA*) and

the proliferation-associated polo-like kinase 1 (*PLK1*) co-expressed with NE markers was identified [86] [94, 95]. It therefore remains a matter of discussion and further research to elucidate the dynamics of NE tumor cells in PCa. Interestingly, *UBE2C* was shown to be under positive regulation of the *AR* splice variant *AR-V7* in PCa that promoted proliferation of VCaP cells and has emerged as clinically relevant resistance mechanism under enzalutamide treatment [96, 97]. The fact that resistance subtypes to enzalutamide has also been proposed as precursor for NEPC differentiation (as described in chapter 1) further highlights the complexity of resistance mechanisms leading to mCRPC [98].

Our results suggest that upon *INSM1* overexpression PCa cells adapt a neuronal expression programme accompanied by NE marker upregulation, enhanced cell migration and invasion. Our concept implicates that compromised REST activity facilitates the conversion into NED demonstrated by reduced *REST* expression upon *INSM1* overexpression (Figure 4.12). Putative INSM1 binding sites were identified in the *REST* promoter region using the JASPAR database [72]. REST regulates neuronal gene transcription in stem cells and non-neuronal tissue through recognition of neuron restrictive silencing elements (NRSE/RE-1 binding sites) and subsequent recruitment of histone modifiers and chromatin-binding proteins (referred to as REST cofactors), thereby blocking target gene expression [50, 51, 99]. REST has been described as regulator of NED in PCa [100]. Upon *REST* knockdown in LNCaP cells, GO terms indicated enrichment in neuronal functions. Differential gene expression of associated genes underlying NED processes (*STMN3*, *VGF*, *BSN*, *ONECUT2*, *AURKA*, *LMNB1*) in our dataset was consistent with RNA-seq data from NEPC tissue [9]. Of note, REST was reported to repress a genetic program required for pancreatic β-cells development, corroborating our proposed model of opposing functions of INSM1 and REST in NED [101, 102]. Since *REST* overexpression resulted in reduced INSM1 expression, a reciprocal regulatory mechanism is suggested, but it remains open for further research whether this is a direct consequence.

In small cell lung cancer cell lines, redued *REST* transcript levels resulted in increased expression of *L1CAM* and *NCAM* [103]. L1CAM has been identified as a neuronal cell adhesion molecule that plays an important role in the nervous system development by regulating neuronal migration and adhesion, and guidance of neurite outgrowth [104]. It has been correlated to a poor prognosis in many human tumors, in which it promoted cell motility, invasion, metastasis formation and chemoresistance [38, 39]. Recently, L1CAM was shown to promote PCa metastases and was expressed by androgen receptor-negative PCa cell lines [54]. However, its precise role in PCa is poorly investigated, inciting our study to analyse the involvement of *L1CAM* within the regulatory circuit of *INSM1* and *REST* as potential marker of NEPC. We showed positive regulation of *L1CAM* by *INSM1* along with NE markers, but negative regulation by *REST*. RE-1 binding sites within the promoter of *L1CAM* are recognized by REST conferring restriction of *L1CAM* expression to neuronal tissue and inhibiting its expression in non-neuronal tissue [52]. The regulatory mechanisms between *INSM1* and *L1CAM* have not been described before and needs to be further evaluated in future studies.

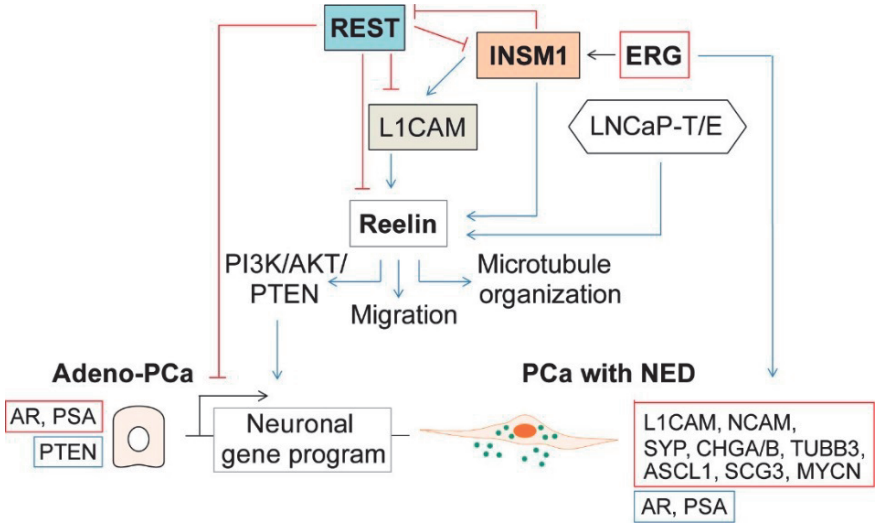

Figure 4.12: Schematic model of the INSM1-REST-L1CAM network. A network involving the neuronal transcription factor INSM1, neuronal cell adhesion molecule L1CAM, and the negative regulator of neuronal gene transcription REST playing a role in NE differentiation in PCa was identified. Blue arrows indicate activating, red arrows indicate inhibitory (indirect) interaction.

It is interesting to note that the extracellular glycoprotein and neuronal guidance molecule Reelin emerged as a central molecule in the regulatory network involving *INSM1*, L1CAM and *REST*. Reelin, commonly secreted by Cajal-Retzius cells in the developing nervous system, is increased in small cell lung cancer, retinoblastoma, esophageal cancer and multiple myeloma [105-108]. In PCa, a correlation between Reelin expression and Gleason score has been described [109]. However, the molecular mechanisms of Reelin signaling in the aggressiveness of PCa is yet unknown. Downstream signaling events of Reelin involve recruitment of CRK and CRKL [110], and Src family tyrosine kinases, mediating subsequent activation of the PI3K/AKT pathway and inhibition of GSK3β [111, 112]. Recently, the Src, STAT3 and AKT pathways, hyperactivated in NEPC, were shown to be stimulated by Reelin signaling in multiple myeloma corroborating the importance of Reelin signaling in NEPC [108, 113]. Notably, Reelin induced upregulation of HIF1α in multiple myeloma, which has also been implicated in NEPC [108, 114]. Upregulation of Reelin signaling components (*MAP1B*, *MAPK8IP1*, *NDEL1*) in NEPC tissue has been identified by RNA-seq [9]. Positive regulation of Reelin and downstream signaling components by *INSM1* could implicate utilization of Reelin signaling in NEPC suggesting Reelin pathway activation as marker of NEPC. Our results further show that *REST* restricts the expression of Reelin and downstream molecules suggesting that loss of *REST* facilitates Reelin signaling in NEPC. These findings encourage future studies to investigate the value of Reelin as biomarker in NEPC and target for therapies.

The connection between *L1CAM* and Reelin signaling has not been described earlier. Both signals have been reported to use integrins as adaptor molecules that can synergize with diverse cell surface receptor systems for signaling modulation. Reelin/α3β1-integrin interactions could contribute to appropriate neuronal positioning [115]. In neuroblastoma cells, L1CAM binding to β1-integrins promotes cell migration and neurite outgrowth through the signaling intermediates c-Src and PI3K [116].

In conclusion, we identified *INSM1* as a promising factor of a neuroendocrine transcriptional network in PCa cells (Figure 4.12). Since *INSM1* is not expressed in adult non-neuronal tissues and considering its established role in neuronal and endocrine tissues, reactivation of *INSM1* in PCa could be of major interest for future studies and drug development. We provide a rationale for future examination of INSM1 as a marker in histological diagnosis of PCa and to address its role as specific therapeutic target for NEPC.

SUPPLEMENTARY INFORMATION

1. Supplementary materials
2. Supplementary data

1. Supplementary materials

Supplementary Table S4.1: Cell lines

Cell lines	Supplier	Catalog Number	Origin
DU145	ATCC	HTB-81	prostate carcinoma, brain metastasis
LNCaP (clone FGC)	ATCC	CRL-1740	prostate carcinoma, lymph node metastasis
NCI-H660	ATCC	CRL-5813	prostate small cell carcinoma, lymph node metastasis
PC-3	ATCC	CRL-1435	prostate adenocarcinoma, bone metastasis
RWPE1	ATCC	CRL-11609	normal prostatic epithelium immortalized with a single copy of HPV-18
VCaP	ATCC	CRL-2876	prostate carcinoma, vertebral metastasis

Supplementary Table S4.2: List of primer sequences and probes used for qPCR

Name	#UPL probe	Sequence forward 5' - 3'	Sequence reverse 5' – 3'
APOER2	27	ctcccgaagaaccctctttc	gcttaatgccactcgcttg
ASCL1	38	cgacttcaccaactggttctg	atgcaggttgtgcgatca
CDK5	3	cgatgaccagttgaagaggat	tctggcagcttggtcataga
CHGA	17	caaaccgcagaccagagg	tccagctctgcttcaatgg
CHGB	75	agccgccatcttcctttc	Cactggcatggaattgacag
CRK	16	ccagtcccttacgtcgagaa	tttaccagctcaccgacctc
CRKL	77	tggagttttacaagatccactacct	attggtgggcttggatacc
ENO2	27	actttgtcagggactatcctgtg	tccctacattggctgtgaact
ERG_T/E	64	ggttaatgcatgctagaaacaca	agatggttgagcagctttcg
GAPDH	60	agccacatcgctcagacac	gcccaatacgaccaaatcc
INSM1	54	cgctgtgttcatggtctagaaa	catagagagcagagattggtaggc
ITGA3	13	gaggacatgtggcttggagt	gtagcggtgggcacagac
L1CAM	18	caaatggctgtgaagaccaa	cacaaagccgatgaaccag
MAP1B	43	gacgctttgttggaaggaaa	ctgagtcatgagttgggatcag
NCAM	20	ttaccgcggcaagaacat	ccacctgcagagaaactgc
NTS	35	tgctactcctggctttcagc	gcatattggtcaagaaatctgct
RELN	24	tgagagccagcctacagga	tcgttccacattctgtaccaa
REST	2	tggaaaatgcaactatttttcaga	gaacttgagtaaggacaaagttcaca
SCG3	79	aagcttgaaggattccacaaaa	ctgatggcttccaaataggc

Supplementary Table S4.2: continued

SRC	61	ccatgttcactccggttttac	ttcaaatcctggctctgtctc
SYP	83	acatggacgtggtgaatcag	cattgcagcaccttcacaa
TUBB3	12	gcctgacaatttcatctttggt	gcaggcagtcgcagtttt
VLDLR	80	ggagaagatgaagaaaactgtgg	catcctggccattgcatac

Supplementary Table S4.3: List of siRNAs

Name	Catalog number	Supplier
Allstar Negative Control	SI03650318	Qiagen
siERG#7	SI03064726	Qiagen
siERG#8	SI03089443	Qiagen
siINSM1#6	SI03204901	Qiagen
siINSM1#7	SI04179392	Qiagen
siRELN#4	SI00071806	Qiagen
siRELN#5	SI03051818	Qiagen
siREST#1	SI00701407	Qiagen
siREST#5	SI04153765	Qiagen
siREST#6	SI04179434	Qiagen
siL1CAM#3	SI00009289	Qiagen
siL1CAM#4	SI00009296	Qiagen
siL1CAM#6	SI04179434	Qiagen

Supplementary Table S4.4: Plasmid vectors

Vector	Catalog number	Source
pCMV6-AC with ACVRL1 cDNA (NM_000020)	SC321860	Origene
pCMV6-XL5 with INSM1 cDNA (NM_002196	SC303146-OR	Origene
pCMV6-XL4 with L1CAM cDNA (NM_000425.2)	SC109376-OR	Origene
pCMV6-XL5 with REST cDNA (NM_005612)	SC318496-OR	Origene
TCF REPORTER PLASMID KIT	17-285	Merck
TOPflash TCF Reporter Plasmid (NM_000545.4)		
FOPflash TCF Reporter Plasmid Negative Control		

2. Supplementary data

Supplementary Table S4.5: Genes with FC >|1.3| upon *INSM1* knockdown in VCaP cells

Gene ID	Fold change	p-value
DDC	1.8969	5.187E-14
PPPDE1	1.8492	6.154E-18
CCNC	1.7735	1.653E-15
STEAP1	1.6628	6.374E-08
REG4	1.6189	2.272E-14
MAP2K2	1.6176	4.508E-06
ALDH1A3	1.5743	1.012E-13
TMTC1	1.5575	7.183E-14
RPL6	1.5332	1.599E-13
NPDC1	1.5128	6.208E-10
BTBD1	1.5098	2.128E-10
PMEPA1	1.5064	5.315E-09
MAL2	1.4960	2.603E-17
NOV	1.4951	4.324E-16
HOXA10	1.4893	5.903E-13
FASTK	1.4844	1.691E-08
TROVE2	1.4839	2.997E-11
OCRL	1.4752	2.955E-10
AKIRIN1	1.4748	5.555E-13
RPL29	1.4746	1.024E-12
RPL7L1	1.4743	1.692E-08
UCHL1	1.4639	1.234E-11
TSC22D1	1.4614	2.794E-13
CLEC2D	1.4513	4.220E-08
MCCC2	1.4487	1.903E-06
HIST1H2AC	1.4424	3.772E-10
AP1S1	1.4403	7.640E-10
STUB1	1.4371	2.688E-07
THOC3	1.4367	3.050E-09
GNAQ	1.4337	3.466E-08
DYRK1A	1.4336	1.288E-07
RAB28	1.4329	8.095E-10
NAAA	1.4320	3.740E-08
PECI	1.4291	4.239E-09
PFN1	1.4288	2.046E-07
TSPAN3	1.4257	4.563E-08
RAB4A	1.4243	8.670E-11
FLJ21511	1.4243	1.437E-07
CROT	1.4209	3.262E-10
LY6E	1.4208	1.471E-08
TOP1MT	1.4206	5.883E-08
HNRPK	1.4191	9.068E-08
CDC42EP3	1.4179	1.452E-08
STAG3L1	1.4169	2.326E-08
AMD1	1.4125	1.176E-07
RYK	1.4122	2.250E-09
CD151	1.4114	3.986E-09
PLEK2	1.4107	1.050E-08
RPL29	1.4100	1.576E-10
NAAA	1.4080	2.232E-12
C17orf95	1.4078	3.894E-09
STEAP1	1.4059	1.445E-12
MGC35361	1.4034	3.977E-10
ACTB	1.4022	1.038E-09
EIF4G2	1.3987	9.545E-11
DPAGT1	1.3913	1.780E-07
UBB	1.3895	3.810E-06
STXBP1	1.3880	1.019E-07
C4orf18	1.3845	1.789E-08
M6PR	1.3842	1.315E-10
C20orf177	1.3835	1.706E-10
AP1S1	1.3829	3.840E-06
CAMK2B	1.3824	4.830E-08
MED27	1.3814	1.240E-09
PPM1A	1.3810	3.490E-08
SNCA	1.3802	4.920E-14
MORF4L2	1.3793	8.836E-09
ACTG1	1.3785	4.300E-07
NAAA	1.3766	2.425E-13
C1orf109	1.3761	1.734E-10
SLC31A1	1.3759	6.766E-06
DDX47	1.3753	1.810E-07
RPS26	1.3750	9.204E-07
PRDX2	1.3743	1.304E-08
PIAS1	1.3742	2.788E-07
STEAP1	1.3737	6.582E-11
TSPO	1.3727	1.645E-10
C12orf11	1.3727	5.844E-08
SIPA1	1.3716	2.530E-07
CASC4	1.3713	3.494E-08
MGAT2	1.3708	2.332E-06
PRDX3	1.3695	3.038E-09
KRT19	1.3693	1.035E-08
UBE1	1.3681	9.135E-07
C21orf59	1.3668	3.736E-06
ABHD11	1.3658	2.043E-08
INPP5A	1.3655	3.420E-10
PCBD1	1.3644	3.552E-07
LYRM2	1.3635	7.227E-10
NAMPT	1.3616	9.487E-08
PSMC1	1.3597	3.406E-12
ROPN1B	1.3592	3.810E-09
GUF1	1.3587	6.853E-08
TADA3	1.3579	1.259E-07
SC4MOL	1.3572	2.261E-06
ADD3	1.3541	1.399E-09
PSPH	1.3525	1.677E-07

Supplementary Table S4.5: continued

RRM2B	1.3525	3.514E-08
TRAPPC6B	1.3512	6.985E-10
YWHAE	1.3492	6.769E-07
RPS24	1.3485	4.122E-11
FAM135A	1.3481	1.271E-06
CAPNS1	1.3480	1.056E-08
FAM127C	1.3479	2.283E-10
AFF4	1.3456	8.351E-09
ARPC1B	1.3444	2.287E-08
MFF	1.3440	9.348E-08
FZD4	1.3436	3.921E-06
DNAJB6	1.3434	5.556E-09
CKMT1B	1.3428	4.774E-11
FAM135A	1.3424	2.492E-09
C1orf63	1.3421	5.862E-07
TMPO	1.3402	1.909E-08
PCSK1N	1.3401	5.943E-07
DHCR24	1.3396	6.400E-09
PIPSL	1.3395	1.135E-09
CCT7	1.3392	3.972E-08
PSMC4	1.3390	3.765E-08
CKMT1A	1.3389	1.429E-09
NBPF10	1.3385	6.916E-09
RPL8	1.3384	5.305E-07
C20orf191	1.3381	2.739E-06
GALK2	1.3370	4.113E-07
PRDX2	1.3356	6.199E-07
TBL1XR1	1.3345	1.018E-06
HPN	1.3334	6.930E-07
LAMP2	1.3330	9.877E-08
NBPF11	1.3330	1.578E-09
CTBP1	1.3327	1.460E-05
IKBIP	1.3318	3.248E-07
CICE	1.3315	8.650E-09
TUBG1	1.3311	1.381E-05
NAB2	1.3305	3.923E-07
ATP6V0C	1.3298	8.743E-08
HSPBP1	1.3290	1.297E-06
XPOT	1.3284	2.374E-06
POLR1D	1.3282	1.896E-06
MAPKAP1	1.3272	4.298E-08
RFC3	1.3265	9.516E-07
PRKAR1B	1.3264	1.957E-07
KCTD3	1.3260	3.541E-06
THAP1	1.3254	6.845E-06
SSR2	1.3249	4.797E-07
NDRG3	1.3248	1.331E-03
MRPL18	1.3240	1.489E-09
RAB3B	1.3238	1.710E-07
OPA3	1.3233	3.096E-05
MST4	1.3231	4.466E-09
DYRK1A	1.3231	4.366E-06
UBE2E1	1.3230	1.842E-07
DPP7	1.3227	3.443E-06
PRMT1	1.3218	7.197E-07
RBBP5	1.3185	1.883E-05
AASDHPPT	1.3179	9.916E-06
UBE2G2	1.3173	6.799E-11
C5orf44	1.3163	1.124E-06
RPL32	1.3153	2.637E-06
BLOC1S1	1.3150	4.056E-03
MAZ	1.3149	2.889E-08
TMEM38B	1.3146	1.272E-05
KRT18	1.3135	1.493E-07
RFC2	1.3128	1.056E-05
C1orf59	1.3128	1.344E-06
SLC25A1	1.3122	1.405E-07
IRS2	1.3115	7.618E-07
C11orf48	1.3109	1.739E-13
LSM12	1.3103	5.807E-05
HPN	1.3102	8.572E-06
HMBS	1.3100	2.684E-06
PGAM4	1.3094	1.310E-06
LIMS1	1.3090	3.324E-05
SBDSP	1.3086	1.456E-07
TCEA1	1.3081	3.847E-04
TAF9L	1.3077	6.788E-07
TJP1	1.3071	3.500E-05
NT5C3	1.3070	7.491E-06
C12orf5	1.3069	6.120E-05
C10orf32	1.3065	4.165E-06
SLC39A3	1.3064	4.327E-05
PBRM1	1.3051	3.130E-05
OCRL	1.3047	3.561E-12
TPM1	1.3042	1.220E-04
TRIM37	1.3038	2.571E-06
PIR	1.3030	5.255E-06
NEDD8	1.3029	1.055E-05
STARD10	1.3028	3.892E-06
GAR1	1.3026	2.909E-06
PFKFB2	1.3025	4.056E-04
QKI	1.3021	1.261E-02
SNORD31	1.3014	2.044E-06
ASS1	1.3001	5.375E-06
ZDHHC5	0.7698	1.258E-04
SNORA64	0.7697	2.623E-10
RAPGEF1	0.7693	9.952E-08
SLC30A4	0.7691	4.205E-05
KIAA1875	0.7689	3.103E-03
ZNF544	0.7689	3.181E-08
MGC15634	0.7689	1.390E-02
HEPACAM2	0.7682	5.236E-09
DPY19L4	0.7679	2.406E-07
IQGAP2	0.7677	1.436E-04
PPP1R14A	0.7672	9.162E-05
C15orf42	0.7670	2.798E-08
ZNF157	0.7666	2.760E-03
SERPING1	0.7665	7.713E-04

Supplementary Table S4.5: continued

TMEM141	0.7663	3.171E-08
FOLR1	0.7656	1.592E-03
ISG20	0.7653	1.284E-09
ANKRD22	0.7651	5.802E-04
METTL7A	0.7647	1.221E-06
ZNF586	0.7646	5.447E-06
SLC12A2	0.7645	8.631E-04
CXXC1	0.7643	1.170E-05
DUS2L	0.7640	7.654E-08
JAG1	0.7640	1.367E-08
DSTN	0.7635	8.463E-06
MYO10	0.7634	3.613E-05
KIAA1731	0.7630	2.351E-05
IP6K1	0.7629	3.669E-06
APOBEC3D	0.7623	6.540E-05
ZNF583	0.7620	1.136E-08
GRPEL2	0.7617	9.283E-08
DCUN1D4	0.7614	1.240E-04
H2BFWT	0.7605	8.353E-04
SLC26A11	0.7600	5.404E-08
KIAA0090	0.7598	5.352E-07
PCDHB9	0.7596	3.547E-05
HIPK2	0.7596	3.912E-07
CAPRIN1	0.7595	1.025E-07
EIF2C2	0.7594	1.443E-06
HNMT	0.7594	4.347E-07
SIL1	0.7592	2.179E-09
MAP2K4	0.7586	2.604E-07
RAP2C	0.7581	5.506E-07
TFPI	0.7578	1.015E-04
USP48	0.7575	1.045E-06
SLC25A22	0.7573	4.876E-10
PCGF6	0.7573	4.043E-05
CDC25A	0.7571	2.556E-11
C10orf57	0.7564	3.312E-06
IRAK2	0.7561	7.381E-08
DNAJB9	0.7560	3.049E-04
RBM12	0.7559	1.428E-07
ZNF302	0.7544	1.263E-06
CYP1B1	0.7536	1.918E-05
PKD2	0.7533	1.580E-06
NCAPG	0.7533	6.417E-09
HSPA5	0.7532	1.733E-09
SPC24	0.7530	8.045E-06
ACOT7	0.7524	5.448E-10
MAP3K2	0.7523	2.439E-05
RPS27L	0.7518	1.595E-04
PELI2	0.7514	5.621E-09
RAPGEF2	0.7504	7.505E-06
POLR3B	0.7503	3.084E-09
UBE3A	0.7502	3.901E-08
C2orf42	0.7501	8.173E-06
PCM1	0.7499	1.077E-06
SERF2	0.7496	4.985E-10
SEC63	0.7493	7.851E-05
CBFB	0.7485	9.301E-08
TP53INP1	0.7484	1.618E-08
MARCKS	0.7477	3.191E-14
NR1H3	0.7475	4.555E-07
S100A11	0.7470	9.099E-10
DSCC1	0.7466	2.327E-05
RBMS1	0.7465	6.551E-11
DSEL	0.7454	3.787E-06
ATPBD1B	0.7451	2.150E-07
MCM10	0.7450	7.767E-08
PTAR1	0.7450	1.222E-07
LYPLA2	0.7431	8.215E-05
NFX1	0.7430	8.495E-06
DCP2	0.7428	3.584E-08
HIST1H2BH	0.7427	8.451E-07
RPL9	0.7425	3.604E-06
E2F2	0.7425	1.595E-05
ARL5B	0.7410	1.888E-05
KLHDC2	0.7405	5.256E-08
POLR1E	0.7392	1.577E-08
SPC25	0.7390	1.009E-07
SESN3	0.7373	2.460E-08
HIC2	0.7365	3.626E-11
ZFYVE21	0.7362	4.163E-07
SNORA22	0.7358	1.341E-09
SNORA23	0.7356	8.451E-12
PAFAH1B3	0.7341	6.688E-10
IFT122	0.7338	2.557E-06
TPRG1L	0.7337	3.432E-10
DENND4C	0.7329	1.614E-09
FAM111A	0.7327	1.091E-13
ASB1	0.7326	2.272E-08
HMGB1	0.7317	9.999E-08
CDC23	0.7316	9.146E-10
C5orf28	0.7297	3.166E-02
MOBKL2A	0.7294	1.852E-06
RELN	0.7293	5.965E-10
POLQ	0.7280	1.345E-05
FAM160B1	0.7279	6.709E-07
CHRFAM7A	0.7276	1.322E-03
MIR1264	0.7271	8.485E-03
TSEN15	0.7261	2.035E-07
DICER1	0.7256	4.968E-06
PAPSS1	0.7254	5.135E-06
TSPAN8	0.7254	1.659E-13
POU2F1	0.7254	2.052E-07
MNS1	0.7191	1.485E-09
PRKD1	0.7184	4.109E-06
LPP	0.7179	5.473E-10
FRG1	0.7168	1.921E-08

Supplementary Table S4.5: continued

TFAP2C	0.7167	5.729E-10
RBL2	0.7135	1.644E-10
SHISA2	0.7087	2.480E-07
CDT1	0.7073	5.248E-10
BOLA2	0.7068	1.058E-05
FDPS	0.7063	3.654E-07
PPIL3	0.7060	5.135E-12
SCARNA22	0.7052	1.337E-05
SLC41A3	0.7042	3.846E-10
ULK1	0.7029	5.903E-17
RAB11FIP5	0.7005	3.047E-13
C1orf218	0.6994	6.919E-07
ATG5	0.6992	7.897E-09
KATNAL1	0.6985	3.059E-07
TELO2	0.6979	3.293E-02

ULK1	0.6958	4.020E-18
PKIA	0.6957	1.073E-13
C9orf5	0.6943	3.081E-11
CAMSAP1	0.6916	6.955E-12
DCBLD2	0.6889	2.496E-10
TMEM54	0.6843	4.084E-13
LAMP2	0.6803	8.163E-08
SNORA38B	0.6799	1.136E-12
CST2	0.6757	1.346E-05
SUGT1	0.6723	3.590E-08
TM4SF1	0.6692	1.698E-07
LYSMD2	0.6625	4.964E-11
SCARNA11	0.6574	1.598E-14
P15RS	0.6573	1.197E-12
WWP1	0.6569	1.952E-10

FSTL1	0.6469	9.232E-12
TNFRSF19	0.6421	8.346E-13
HIST2H2AA3	0.6378	2.465E-05
IFI6	0.6368	6.239E-05
SLC44A2	0.6311	4.312E-15
SNORA63	0.6188	1.381E-21
SSBP4	0.6101	4.348E-14
ATPAF1	0.5942	1.425E-20
BAMBI	0.5907	1.513E-16
DEPDC1B	0.5264	2.469E-11
INSM1	0.3894	7.752E-38

Supplementary Table S4.6A: Functional annotation of genes differentially regulated upon *INSM1* knockdown in VCaP cells

Functional annotation	Genes	p-value	z-score*	# Genes†
Cell death	*STUB1, GNAQ, STXBP1, SNCA, PRDX2, NAMPT, CAPNS1, KRT18, JAG1, HIPK2*	2.91E-06	-0.60	94
Neuritogenesis	*PFN1, RYK, SNCA, CAPNS1, RAPGEF2, UBE3A, RELN, DICER1, ULK1, CAMSAP1*	1.32E-03	1.049	20
Metabolism of DNA	*SNCA, ISG20, PCM1, E2F2, HMGB1, CDT1, PFN1, CDC25A, S100A11*	1.53E-04	0.259	18
Proliferation of tumor cell lines	*PMEPA1, NOV, UCHL1, HNRPK, CD151, PRDX2, KRT19, TADA3, HSPA5, RBL2,*	1.74E-02	-0.189	38
Formation of cellular inclusion bodies	*ATG5, DNAJB6, KRT18, PSMC4, SNCA, STUB1, UBE3A, UCHL1*	2.48E-05	0.28	8

Top 10 differentially expressed genes in our dataset that were annotated to a function. A gene was selected when its annotation to the indicated function was based on at least two findings in the Ingenuity knowledge base. *Activation z-score is a measure of predicted change (increase or decrease) of the process. †Total number of genes supporting a specific functional annotation.

Supplementary Table S4.6B: Canonical pathway analysis of genes differentially regulated upon *INSM1* knockdown in VCaP cells

Ingenuity Canonical Pathways	p-value	z-score*	# Genes†
EIF2 Signaling	7.90E-07	2.33	15(221)
Protein Ubiquitination Pathway	7.43E-06	NaN	15(265)
Gap Junction Signaling	3.88E-05	NaN	11(171)
Melatonin Signaling	5.91E-04	1.63	6(72)
Integrin Signaling	3.46E-04	3.16	11(219)

Significantly enriched canonical pathways across the dataset of commonly regulated genes between T/E III and VI are shown. *Activation z-score is a measure of predicted change (activated or reduced) of the process. NaN – not a number. †Number of genes in the dataset, which are represented in the pathway. Numbers in brackets depict the total number of genes in the pathway in the reference gene set.

Supplementary Table S4.7: Genes with FC >|1.5| upon *REST* knockdown in LNCaP cells

Gene ID	Fold change	p-value
BEX1	11.269	2.760E-36
STMN3	10.979	4.284E-40
SCG3	10.136	3.621E-33
TMEM145	5.434	8.235E-39
CELSR3	5.404	7.054E-49
VGF	5.279	1.911E-45
SYP	4.762	2.193E-49
CPLX1	3.573	1.605E-30
BSN	2.859	5.147E-37
DPYSL4	2.701	6.654E-36
TUBB3	2.645	2.400E-29
MANEAL	2.467	2.476E-22
MIR1282	2.448	5.355E-01
DISP2	2.417	4.768E-31
KIAA1324	2.340	5.396E-34
ASPHD1	2.331	3.928E-36
CAMKV	2.294	6.221E-35
MAPK8IP2	2.290	2.149E-30
CECR6	2.130	9.683E-24
KCNMA1	2.101	1.272E-29
DDC	2.091	1.478E-40
STX1A	1.980	9.228E-19
RELL2	1.952	2.218E-35
BEX2	1.947	2.274E-27
GDAP1	1.929	2.978E-16
TMEM180	1.911	2.764E-23
KREMEN2	1.905	9.072E-26
CKMT1B	1.884	2.510E-27
FAM134B	1.883	1.193E-20
OGDHL	1.879	1.948E-16
CKMT1A	1.864	6.557E-24
C7orf63	1.841	1.446E-19
UGT2B28	1.829	1.433E-13
BCHE	1.822	3.356E-32
HBQ1	1.816	6.402E-29
SYT4	1.799	2.880E-28
GRB10	1.786	1.351E-26
SLC4A4	1.775	1.070E-26
CDK5R1	1.763	1.282E-12
MAP1B	1.757	8.981E-26
TMEM198	1.753	3.102E-22
HEPACAM	1.753	3.351E-18
UGT2B11	1.752	3.597E-12
SYT7	1.733	1.013E-24
SEZ6L2	1.723	1.977E-18
ABCB11	1.720	3.030E-19
C19orf4	1.715	5.297E-06
PAQR4	1.710	2.249E-23
APLP1	1.710	2.572E-24
NFASC	1.697	1.718E-21
HIST1H2BK	1.685	6.687E-20
MAST4	1.681	1.910E-28
CAMK2N2	1.651	9.938E-18
WASF3	1.646	1.849E-16
ACPP	1.640	9.448E-19
MFSD6	1.635	9.146E-16
EPPB9	1.635	8.849E-20
OCRL	1.634	7.084E-22
GNG4	1.630	1.260E-17
CHPF	1.626	4.097E-17
HIST1H2BD	1.621	2.669E-17
MYT1	1.609	2.137E-16
NMNAT2	1.605	3.805E-13
TMEFF2	1.600	5.001E-32
SBK1	1.599	3.548E-31
VWF	1.598	6.187E-12
TELO2	1.594	4.016E-02
CBLN2	1.593	6.550E-11
PPM1E	1.583	2.447E-10
BCYRN1	1.583	4.678E-16
RTN1	1.581	7.167E-18
SPIRE2	1.580	7.911E-23
ANG	1.579	4.697E-23
C5orf53	1.579	3.418E-17
DSC2	1.574	6.376E-13
ABHD2	1.572	6.321E-15
VSTM2L	1.567	9.164E-21
ATP6V0A1	1.563	1.201E-26
CHGB	1.561	4.940E-17
LRP11	1.561	4.349E-14
CHPT1	1.560	9.778E-21
PBX3	1.559	1.997E-16
SLC10A7	1.559	1.334E-19
ONECUT2	1.554	4.232E-16
TMEM43	1.552	9.942E-20
KCNQ2	1.550	1.370E-09
S100P	1.546	7.245E-14
CFDP1	1.546	3.179E-20
RAP1GAP	1.544	3.934E-21
B9D1	1.544	2.097E-18
SLC22A17	1.544	8.463E-27
SRGAP3	1.543	3.841E-20
PKNOX2	1.542	7.930E-14
SCAMP5	1.541	2.429E-16
B3GNT1	1.537	2.069E-10
MYNN	1.536	1.916E-17
LUZP2	1.536	3.191E-10
PLAGL2	1.536	5.661E-16
FERMT2	1.529	3.200E-12
SLC22A3	1.525	3.162E-16

Supplementary Table S4.7: continued

MCCC2	1.522	6.871E-09
PLA2G2A	1.522	1.590E-11
BRWD1	1.520	3.313E-13
TSC22D3	1.519	2.052E-15
ABCG1	1.517	2.146E-18
KIAA1618	1.513	3.056E-16
CRIP2	1.511	9.875E-16
HIST1H2BC	1.507	4.059E-10
MBOAT7	1.506	5.394E-10
HIST1H2AC	1.505	5.090E-14
FBXO2	1.504	7.607E-11
HIST1H2BJ	1.502	7.418E-09
RILPL2	1.501	3.082E-11
CROT	1.501	1.211E-12
COQ4	1.500	3.571E-03

ARPP19	0.664	2.437E-15
MTHFD2	0.662	2.639E-15
PDHX	0.662	9.988E-14
EML4	0.657	3.500E-18
PQLC1	0.653	6.306E-20
SESN3	0.651	1.192E-10
KIF20A	0.650	3.460E-16
FOXK1	0.649	1.641E-10
VPS26A	0.644	2.807E-21
ODAM	0.643	1.435E-16
COMMD8	0.643	2.257E-12
PRPF4	0.639	8.476E-21
LIPA	0.635	9.630E-16
CLIC4	0.624	2.361E-11
SCOC	0.624	2.116E-17

PIB5PA	0.619	4.410E-24
THOC7	0.608	5.935E-16
RELL1	0.601	1.355E-12
SPRYD5	0.592	3.034E-27
YRDC	0.587	4.106E-26
BAMBI	0.587	1.777E-17
TRIM48	0.570	1.976E-24
C18orf56	0.568	1.310E-26
HMGB2	0.551	1.089E-17
COMMD6	0.546	3.079E-30
HGD	0.542	8.798E-17
C9orf123	0.528	3.024E-27
NT5DC3	0.522	5.835E-29
HSPE1	0.505	6.318E-04

Supplementary Table S4.8A: Functional annotation of genes differentially regulated upon *REST* knockdown in LNCaP cells

Functional annotation	Genes	p-value	z-score*	# Genes†
Formation of cellular protrusions	*MAPT, MAP1B, RELN, CRK, VGF, BSN, CELSR3, ONECUT2, MAPK8IP2, CDK5R1*	5.97E-05	2.297	21
Growth of neurites	*VGF, HBA2, GPRIN1, SLC12A2, EXOC5, CDK5R1, CDC2, MAP1B, DCX, RAP1GAP*	2.62E-03	2.318	20
Migration of neurons	*CELSR3, MAP1B, CDK5R1, DCX, SLC12A2, LAMA1, AURKA, LMNB1, CNTNAP2, SEMA6A*	2.77E-03	1.255	12
Microtubule dynamics	*MAPT, MAP1B, MAPRE1, RELN, PALM, PACSIN1, NCAM2, LYN, BBS4, STMN3*	9.65E-06	2.475	30
Transport of molecule	*LYN, CROT, ABCG1, TTR, SLC6A9, ATP13A2, CNKSR3, SLC7A2, SLC16A10, SLC46A1*	5.11E-03	3.757	20

Top 10 differentially expressed genes in our dataset that were annotated to a function. A gene was selected when its annotation to the indicated function was based on at least two findings in the Ingenuity knowledge base. *Activation z-score is a measure of predicted change (increase or decrease) of the process. †Total number of genes supporting a specific functional annotation.

Supplementary Table S4.8B: Canonical pathway analysis of genes differentially regulated upon *REST* knockdown in LNCaP cells

Ingenuity Canonical Pathways	p-value	z-score*	# Genes†
CDK5 Signaling	5.12E-03	1.63	6(99)
Reelin Signaling in Neurons	1.07E-03	0	8(92)
Neuregulin Signaling	1.34E-02	1.34	5(88)
Glioma Signaling	1.30E-02	1.34	7(112)
cAMP-mediated Signaling	1.21E-02	-0.63	11(223)

Significantly enriched canonical pathways across the dataset of commonly regulated genes between T/E III and VI are shown. *Activation z-score is a measure of predicted change (activated or reduced) of the process. †Number of genes in the dataset, which are represented in the pathway. Numbers in brackets depict the total number of genes in the pathway in the reference gene set.

Supplementary Table S4.9: Genes with FC >|1.5| upon *L1CAM* knockdown in PC-3 cells

Gene ID	Fold change	p-value
ANGPTL4	17,907	1,324E-53
S100P	10,371	9,887E-54
GDF15	9,283	1,394E-41
MUC5AC	9,017	1,403E-33
RASD1	8,354	4,638E-51
RBP4	6,570	2,339E-28
TFF3	6,503	1,084E-46
SUSD2	6,247	1,628E-30
COL2A1	6,117	1,898E-35
FABP4	6,081	8,445E-36
IGFBP5	5,992	2,533E-35
SYT11	5,750	1,457E-22
C15orf48	5,743	5,416E-29
IGFBP3	5,376	2,710E-28
ITGA1	5,364	6,535E-39
KIF5C	4,759	6,272E-33
LFNG	4,355	3,286E-36
KRT4	4,306	2,882E-38
SLC22A18	4,051	1,661E-45
CDKN1C	4,047	1,990E-37
ERO1L	4,040	6,760E-37
MAL	4,038	2,815E-30
C6orf85	4,001	1,415E-36
TNFRSF6B	3,933	2,879E-38
TMPRSS2	3,932	1,124E-28
SERPINE2	3,896	2,279E-32
MSLN	3,732	8,626E-29
MGC16121	3,694	4,845E-34
COL5A1	3,679	5,785E-32
TFF1	3,653	9,670E-23
NT5E	3,645	4,501E-30
HOXA11AS	3,610	2,149E-31
ADM	3,587	1,242E-38
SEMA3B	3,536	7,330E-26
MEGF6	3,506	1,099E-31
FERMT2	3,424	3,759E-26
OLFML3	3,389	5,148E-23
WIPI1	3,359	2,857E-40
HIST2H2AC	3,347	1,419E-51
CFD	3,337	1,485E-43
RGS11	3,336	4,639E-29
GPX2	3,331	2,926E-29
HIST2H2AA3	3,328	9,359E-31
FSTL1	3,317	1,869E-49
HIST2H2AA4	3,311	1,941E-31
MUC16	3,285	1,347E-26
FER1L4	3,281	1,419E-20
VLDLR	3,270	6,030E-22
TTC19	3,267	9,883E-34
RDH10	3,260	1,283E-33
TMEM45B	3,250	1,637E-34
WNK4	3,232	4,500E-47
PGM2L1	3,198	1,466E-34
ASS1	3,197	2,034E-38
KIAA1199	3,183	4,318E-49
LGALS3	3,172	4,221E-28
FBN2	3,160	4,898E-38
MMP23B	3,136	2,090E-36
B4GALT4	3,111	7,724E-31
ERMP1	3,105	1,396E-24
MB	3,045	1,525E-43
NIPA1	3,032	6,112E-26
INHBB	3,013	3,566E-30
ITGB4	3,012	2,657E-29
C21orf58	3,000	8,874E-27
CYR61	2,990	1,184E-29
ENO2	2,979	3,323E-31
DDIT4	2,952	5,617E-31
HTRA1	2,949	5,161E-35
SPTLC3	2,945	5,805E-34
ITGB2	2,927	7,214E-45
GLS	2,918	1,112E-26
GAS6	2,893	2,762E-31
SELM	2,881	9,053E-40
IGSF3	2,863	1,725E-20
SPDEF	2,853	4,483E-48
CRIP1	2,847	4,702E-28
INSIG1	2,846	6,858E-33
SERPIND1	2,842	2,127E-28
C10orf41	2,831	2,762E-27
CPZ	2,831	1,066E-30
ADSSL1	2,802	4,733E-38
KLK5	2,787	2,003E-34
UPK2	2,784	6,642E-32
ZNF467	2,783	1,245E-46
HIST1H4H	2,779	4,569E-34
SDCBP2	2,774	5,973E-45
SMARCD3	2,767	6,353E-31
ALPP	2,766	5,772E-41
HOXA10	2,762	2,575E-30
MMP23A	2,758	7,102E-36
TGFBR3	2,751	4,268E-31
TNPO1	2,746	3,148E-20
EPAS1	2,744	5,861E-28
IL1R2	2,726	1,027E-25
P4HA2	2,722	1,259E-26
MATN2	2,720	5,998E-30
ABCC3	2,708	1,840E-37
PLAT	2,706	7,735E-38
NOXA1	2,693	2,330E-18
FTHL11	2,685	1,497E-20
TMCO3	2,680	2,298E-43
COL7A1	2,677	1,920E-20
DRAM1	2,674	1,009E-27
ACHE	2,660	5,253E-30
FGB	2,649	1,832E-32
TUBB2B	2,639	3,774E-70
SLC4A7	2,636	8,496E-28
TNNC1	2,635	2,843E-25
KIFC2	2,634	2,499E-15
NDRG4	2,633	1,151E-29
APOE	2,630	2,690E-27
PLOD2	2,627	5,755E-27
KLK6	2,626	3,912E-33
PIM1	2,626	1,225E-32
CNTNAP1	2,623	3,097E-36
RBM24	2,622	4,253E-24
CPT1C	2,612	1,326E-37
JAG2	2,611	2,002E-21
ABCB6	2,610	8,170E-37
GPRC5A	2,600	1,722E-31
NOTCH3	2,599	1,629E-35
IL6	2,594	5,071E-34
SELENBP1	2,593	1,013E-19
BGN	2,591	8,050E-35
CCL26	2,590	1,754E-27
NGF	2,588	4,803E-32
HIST1H1C	2,587	5,852E-24
EFEMP2	2,571	4,396E-27
MICAL1	2,568	3,376E-24
SCARA5	2,562	4,188E-40
TAGLN3	2,561	2,851E-35
TLE6	2,552	4,008E-26
DSC2	2,549	1,162E-36

Supplementary Table S4.9: continued

GPR177	2,547	2,715E-23	*PDGFRL*	2,409	6,024E-23	*MT1A*	2,318	1,703E-30	*PLXNA3*	2,241	1,228E-31
LIMCH1	2,540	1,967E-24	*PNPLA7*	2,408	3,590E-19	*DENND3*	2,315	1,587E-26	*LIPG*	2,239	1,125E-23
LAMC2	2,539	6,283E-22	*CTGF*	2,408	3,183E-27	*SLC22A17*	2,309	8,107E-37	*ZFHX3*	2,236	2,325E-23
FAM188A	2,533	2,523E-37	*FBXO2*	2,406	1,053E-30	*DCP2*	2,307	1,082E-27	*SLPI*	2,226	4,458E-34
LAMC1	2,529	1,566E-32	*HIST2H2BE*	2,398	3,667E-29	*WNT7B*	2,307	8,606E-23	*APLP2*	2,219	6,268E-24
SLC22A23	2,528	3,286E-25	*H2AFJ*	2,395	6,769E-26	*ASAP3*	2,305	4,903E-22	*TSC22D3*	2,217	9,326E-33
ADAMTS1	2,524	2,784E-29	*CSPG5*	2,394	5,638E-18	*CCNA1*	2,302	1,567E-27	*DENND5B*	2,217	2,055E-29
FLJ20920	2,518	3,120E-36	*GABBR2*	2,393	6,775E-32	*MUM1*	2,297	8,598E-33	*FAT1*	2,213	1,239E-25
DUSP1	2,515	4,950E-28	*NOV*	2,390	6,465E-27	*TCEA3*	2,295	9,859E-44	*C10orf140*	2,211	4,480E-32
SLC29A4	2,505	1,762E-37	*HPGD*	2,389	5,509E-32	*ALDOC*	2,294	1,872E-33	*LYPD3*	2,208	4,549E-35
C20orf46	2,502	9,788E-29	*IGFBP6*	2,389	1,480E-36	*ACSF2*	2,293	4,073E-27	*DHX40*	2,207	8,834E-24
HOXA5	2,494	7,039E-33	*PTPRM*	2,384	1,671E-32	*LAMB3*	2,290	2,383E-22	*BAMBI*	2,207	2,490E-35
GDPD3	2,493	6,541E-30	*CST1*	2,379	3,809E-41	*CDH2*	2,289	3,726E-32	*EPS8L1*	2,207	3,177E-20
HOXA13	2,484	5,562E-32	*HHIP*	2,378	3,017E-29	*INPPL1*	2,289	5,334E-29	*LGMN*	2,203	2,190E-32
IL8	2,473	6,684E-15	*LHFPL2*	2,377	9,296E-27	*ANG*	2,288	2,527E-30	*TRIM6*	2,198	1,957E-25
HMGCS1	2,473	1,765E-32	*AIG1*	2,376	3,262E-38	*C10orf116*	2,280	7,680E-36	*SLC4A11*	2,194	1,421E-26
LEPREL1	2,467	4,690E-27	*KIAA1881*	2,376	6,174E-30	*CKB*	2,273	3,513E-40	*C7orf41*	2,194	5,641E-20
ENC1	2,464	4,589E-27	*KRT7*	2,373	2,571E-47	*GABARAPL1*	2,273	2,504E-27	*ITGA5*	2,191	5,022E-27
APPL2	2,461	1,465E-24	*TBX3*	2,369	2,318E-21	*THBS1*	2,272	2,893E-18	*PDGFB*	2,190	1,306E-25
GBX2	2,459	5,852E-36	*LAMA3*	2,367	1,451E-24	*SESN1*	2,269	1,217E-23	*KRT15*	2,190	5,094E-24
FSD1	2,455	3,681E-31	*BRSK1*	2,362	1,833E-39	*BRWD1*	2,269	5,227E-29	*PLCH2*	2,188	7,851E-30
EPB41L4B	2,451	1,811E-20	*NDRG1*	2,359	1,131E-26	*PHLDA3*	2,268	1,397E-30	*SVIL*	2,188	1,254E-24
ATRN	2,450	3,816E-23	*OSTalpha*	2,357	7,523E-26	*GDPD5*	2,267	1,475E-40	*PCSK1N*	2,188	8,508E-29
CDH15	2,447	5,560E-47	*GATA2*	2,353	3,545E-29	*CHN2*	2,265	8,473E-34	*RGL1*	2,187	5,570E-27
ZDHHC11	2,444	1,268E-36	*CFDP1*	2,342	9,511E-39	*PIR*	2,260	1,564E-41	*AHNAK2*	2,184	2,040E-21
OSR1	2,438	9,639E-37	*RAB15*	2,338	7,077E-33	*RNF24*	2,260	2,232E-27	*CACNA1H*	2,181	3,605E-33
C1S	2,426	1,701E-18	*RNF165*	2,337	3,378E-27	*CTSB*	2,259	4,742E-34	*FLJ36131*	2,180	1,135E-31
MT2A	2,423	6,067E-30	*ZNF682*	2,335	1,434E-23	*CAPN12*	2,255	1,019E-29	*MST1*	2,176	5,973E-17
PRRT3	2,420	4,206E-25	*SLC44A4*	2,333	8,753E-24	*C20orf56*	2,254	3,693E-31	*ANKZF1*	2,173	2,056E-24
TSPAN8	2,420	4,234E-32	*FTHL2*	2,327	3,100E-25	*FLJ33996*	2,252	2,003E-32	*DOCK6*	2,172	1,160E-32
LAMB2	2,414	6,501E-34	*DLK2*	2,322	1,142E-45	*KRT8*	2,247	1,447E-26	*SCPEP1*	2,172	9,609E-36
RABAC1	2,413	2,242E-34	*NLRP3*	2,321	1,731E-20	*LRCH4*	2,247	2,524E-30	*FTHL3*	2,170	2,875E-35
RHPN1	2,410	3,058E-28	*REG4*	2,321	1,586E-21	*MIR1282*	2,246	9,691E-02	*SC5DL*	2,169	2,520E-35

Supplementary Table S4.9: continued

SCNN1D	2,167	5,568E-23	*TMTC1*	2,106	1,733E-23	*TUBG2*	2,046	1,065E-32	*RNASE4*	2,014	1,476E-22
PLXNB2	2,165	2,288E-35	*MIA3*	2,103	5,163E-21	*NCCRP1*	2,045	3,779E-31	*PDZK1*	2,013	1,367E-21
LRP8	2,161	2,000E-26	*ARID5B*	2,102	5,963E-22	*ITPR1*	2,044	2,108E-22	*LTBP2*	2,011	1,485E-22
VEGFA	2,160	4,000E-14	*SPIRE2*	2,102	9,762E-29	*SOX8*	2,042	4,519E-20	*TMEM64*	2,011	1,437E-24
DPYSL2	2,159	5,383E-25	*FBXO32*	2,096	9,664E-25	*TNFAIP2*	2,041	3,231E-22	*FSTL3*	2,011	2,042E-25
CCBE1	2,157	1,831E-27	*CD63*	2,096	1,224E-19	*FAM43A*	2,041	3,067E-32	*TIMP2*	2,008	9,732E-31
BNIP3	2,156	7,725E-34	*PLTP*	2,095	6,698E-32	*CDKN1B*	2,040	8,797E-32	*ARHGAP28*	2,007	2,700E-19
EID2B	2,153	7,789E-30	*CYP1B1*	2,092	5,465E-23	*TXNRD1*	2,040	1,337E-31	*CDC14B*	2,006	3,790E-24
TP53INP1	2,149	8,626E-18	*G0S2*	2,090	3,597E-23	*TSPAN3*	2,039	3,107E-29	*GPT2*	2,006	1,037E-24
PANX2	2,147	4,187E-43	*FAM175A*	2,084	6,971E-24	*HIATL2*	2,039	1,393E-27	*ST6GAL1*	2,002	1,123E-19
C5orf39	2,144	3,689E-21	*RNASET2*	2,084	1,369E-38	*SPTBN1*	2,037	1,068E-20	*UNC93B1*	2,002	7,810E-28
C8orf45	2,141	5,039E-19	*TGFB3*	2,083	1,581E-28	*SLC16A2*	2,037	2,751E-26	*KIAA1751*	2,002	2,228E-24
HAGHL	2,140	1,413E-22	*TNFSF4*	2,082	6,625E-33	*MTMR11*	2,034	6,629E-19	*SYT7*	1,996	5,250E-33
ROR1	2,140	1,407E-24	*SC4MOL*	2,081	1,334E-22	*BCYRN1*	2,034	1,790E-20	*PTX3*	1,995	6,591E-20
AGRN	2,135	1,073E-33	*HK2*	2,080	2,681E-19	*SLIT2*	2,032	9,764E-34	*ARFGAP3*	1,992	1,971E-23
APLP1	2,132	5,724E-23	*GPR64*	2,080	5,947E-17	*HIST1H2BG*	2,032	2,926E-27	*C2CD2*	1,991	9,560E-32
PMS2L5	2,129	1,977E-17	*ATP2C2*	2,078	2,070E-15	*TTC3*	2,031	1,321E-21	*CAP2*	1,990	2,360E-15
MYOF	2,128	5,120E-26	*HIST1H2BC*	2,077	3,656E-20	*RHOQ*	2,030	1,963E-23	*DYSF*	1,990	3,571E-24
KIAA1324	2,127	1,174E-21	*WNT4*	2,076	1,354E-29	*PRSS35*	2,030	1,585E-20	*SLC9A1*	1,989	6,433E-28
SRGN	2,122	6,607E-29	*MAP3K12*	2,072	1,688E-23	*C10orf10*	2,028	7,705E-29	*KIAA0513*	1,989	9,054E-20
KIF1B	2,122	8,006E-24	*FAM73A*	2,072	6,148E-19	*C11orf70*	2,027	2,629E-27	*P2RY2*	1,989	1,768E-29
NOX5	2,120	2,626E-31	*OSBPL10*	2,069	8,725E-33	*ITGB5*	2,026	1,334E-38	*CLIC3*	1,988	1,414E-25
NTN4	2,118	3,279E-16	*CCNYL1*	2,066	1,398E-22	*ABCC5*	2,024	8,469E-27	*SPAG4*	1,987	1,939E-26
GPC2	2,118	2,200E-18	*FLNC*	2,062	2,139E-34	*LMCD1*	2,024	9,898E-30	*PPL*	1,984	3,007E-19
ATP8B2	2,116	2,243E-33	*EFNA1*	2,061	1,656E-29	*RAB40B*	2,024	4,642E-29	*SEMA3E*	1,984	2,855E-26
PLA2G4B	2,115	4,450E-23	*FTHL16*	2,057	2,102E-25	*GDI1*	2,023	1,024E-36	*NME3*	1,983	6,188E-31
ITM2C	2,115	2,929E-34	*CYFIP2*	2,057	1,254E-24	*PLEKHH3*	2,023	6,039E-33	*HOMER3*	1,983	3,474E-15
CGNL1	2,114	6,300E-27	*UNKL*	2,056	1,116E-25	*C4orf34*	2,022	7,482E-25	*ACAA1*	1,981	6,930E-27
GLCE	2,113	2,901E-25	*FRMD6*	2,054	1,144E-23	*RND3*	2,020	2,129E-28	*C1orf116*	1,979	4,351E-23
FER1L3	2,109	1,918E-27	*WSB1*	2,054	1,689E-20	*LPIN1*	2,016	2,391E-28	*STC1*	1,979	2,582E-25
CATSPER2	2,109	9,299E-25	*MAN2B2*	2,053	2,998E-28	*SORL1*	2,016	7,002E-21	*TFF2*	1,976	5,457E-14
TSC22D1	2,109	1,224E-26	*TGFB2*	2,052	5,045E-17	*HLA-F*	2,015	7,413E-29	*HBEGF*	1,974	1,589E-29
SOD3	2,107	1,611E-30	*UBL3*	2,048	7,796E-21	*FBLN1*	2,015	6,369E-25	*NELF*	1,974	9,971E-31

Supplementary Table S4.9: continued

CHRNA5	1,974	2,113E-27
TBXAS1	1,973	9,804E-24
SLC38A10	1,972	2,752E-28
TDP1	1,971	6,633E-20
WDR54	1,969	9,599E-38
PXDN	1,968	1,890E-18
CAMK2N1	1,968	3,960E-31
ITGA3	1,967	4,276E-27
LIF	1,965	2,667E-23
EVPL	1,965	3,851E-26
UBFD1	1,964	5,365E-24
PTPRF	1,963	4,520E-26
COL16A1	1,961	5,602E-19
HLA-B	1,961	1,016E-22
GPRC5C	1,960	1,102E-32
FAM26A	1,956	1,215E-23
OBFC2A	1,955	7,894E-24
BIN1	1,953	1,653E-26
MCOLN1	1,953	1,000E-26
C1orf106	1,952	2,253E-29
B4GALNT1	1,951	3,143E-26
CHSY3	1,948	2,600E-21
SLC27A3	1,943	4,853E-33
HIST2H4A	1,942	5,133E-20
DOCK11	1,940	1,940E-13
HLA-H	1,940	8,545E-26
PPPDE1	1,939	5,070E-23
HLA-E	1,938	7,273E-30
SLC2A8	1,937	3,209E-24
GADD45B	1,937	3,650E-30
TTLL3	1,936	4,297E-18
IL1RL1	1,933	1,191E-17
MARCH4	1,932	6,151E-27
ZNF669	1,932	6,560E-27
RAB24	1,930	1,706E-16
UST	1,930	1,849E-20
ATHL1	1,929	8,866E-25
CITED2	1,929	9,576E-23
GGA2	1,922	1,009E-30
CHPF2	1,922	8,976E-23
ATP2B4	1,922	1,676E-36
MFSD6	1,920	7,036E-18
YIPF1	1,918	1,948E-19
TPM2	1,918	3,236E-24
EPHX1	1,917	6,812E-24
CLDND1	1,915	6,047E-22
LIPA	1,913	8,708E-38
FAM46C	1,912	5,403E-21
GAA	1,912	5,147E-26
MAP1B	1,911	8,963E-21
RHBDF1	1,909	7,498E-28
ZNF14	1,908	2,484E-29
EDN1	1,906	1,284E-24
LAMA5	1,906	1,328E-14
CERK	1,906	1,117E-25
COL1A1	1,905	8,772E-24
GAPDH	1,905	9,381E-33
PNMA2	1,904	2,069E-18
LAMB1	1,903	8,323E-16
PTHLH	1,903	3,738E-16
C14orf149	1,902	6,336E-28
DGKQ	1,901	1,476E-27
EHBP1L1	1,899	1,342E-21
RCOR2	1,898	9,490E-21
C17orf58	1,897	2,832E-25
CTH	1,897	4,923E-16
GAPDHL6	1,896	4,570E-22
SH3GL3	1,896	1,850E-26
SRPX2	1,895	1,601E-19
CORO2A	1,894	2,515E-21
C16orf7	1,893	3,409E-29
RHBDL2	1,892	5,808E-24
CBS	1,891	2,939E-32
FAM116B	1,891	1,084E-25
FAM83H	1,890	2,390E-30
NFIB	1,890	1,209E-28
FTH1	1,890	3,268E-20
STAG3L2	1,888	6,351E-17
ADAM8	1,888	1,294E-30
PTGER1	1,888	2,137E-22
SATB2	1,886	1,872E-24
RPS-1022P6.2	1,886	3,619E-25
SPRY4	1,886	1,310E-31
QRFPR	1,885	1,671E-23
OPLAH	1,885	1,386E-23
ARL16	1,884	2,468E-19
C20orf111	1,884	2,405E-19
IL23A	1,881	9,668E-20
CD276	1,879	3,390E-19
PAM	1,879	3,163E-26
C14orf78	1,879	6,356E-21
PLCD4	1,878	2,130E-35
PYGB	1,877	2,464E-31
SEMA5A	1,875	2,560E-26
TCIRG1	1,874	3,467E-23
TGM1	1,874	4,056E-15
ALCAM	1,873	2,289E-19
ARID3A	1,873	3,159E-16
ABCA7	1,872	1,094E-25
CORO1B	1,872	6,076E-33
CSAD	1,872	7,874E-20
PGCP	1,872	3,110E-19
STAG3L1	1,871	7,509E-19
OLFML2A	1,869	1,281E-24
AKIRIN1	1,869	5,586E-28
NR2F1	1,869	7,293E-32
FLJ14213	1,869	7,346E-20
PDLIM7	1,868	7,745E-34
ELF3	1,867	1,342E-29
SLC12A2	1,866	5,652E-15
MGC42105	1,865	3,905E-18
RAXL1	1,865	1,156E-16
IL10RB	1,865	2,404E-35
DDX41	1,862	3,230E-23
SERINC3	1,859	4,804E-24
PLXNB1	1,859	9,615E-21
GSN	1,859	1,203E-18
CDKN2AIPNL	1,857	6,953E-30
FLJ40722	1,857	2,473E-23
MAN1B1	1,856	1,639E-25
MIR1978	1,856	1,381E-37
SDC2	1,856	1,492E-14
CALHM3	1,855	3,763E-25
MTE	1,853	1,323E-22
MYL5	1,853	3,591E-14
MOCS1	1,852	8,345E-22
TNK2	1,851	1,065E-20
FZD4	1,851	3,077E-38
ITGB1	1,847	1,233E-17
TFAP2C	1,846	6,451E-27
HBP1	1,845	1,307E-26
CXXC5	1,843	2,548E-14

Supplementary Table S4.9: continued

CROT	1,842	2,486E-22
DRAP1	1,841	7,498E-37
NMNAT2	1,836	6,649E-19
SLC44A3	1,836	2,884E-23
AHNAK	1,835	1,864E-13
EPDR1	1,835	2,987E-21
CHST15	1,834	6,063E-20
FLJ37644	1,833	2,497E-20
MVD	1,831	1,814E-20
SEZ6L2	1,831	5,197E-23
CDH1	1,831	2,104E-24
GRIPAP1	1,830	5,440E-19
SLC16A3	1,829	1,239E-44
GLB1	1,828	1,322E-21
OXTR	1,828	1,026E-19
KREMEN2	1,827	1,270E-14
CRIM1	1,824	2,777E-16
METRNL	1,824	8,752E-18
BID	1,823	*2,540E-25*
CA9	1,820	*7,172E-25*
STOM	1,820	*3,591E-21*
TBX2	1,820	*1,099E-29*
DTWD2	1,820	*1,467E-23*
N4BP2L2	1,819	*5,223E-28*
CGN	1,819	*1,019E-18*
TMC4	1,819	*2,988E-20*
PODXL	1,819	2,535E-25
TIMP1	1,819	*2,706E-21*
CCDC151	1,818	*1,388E-24*
CAMK1D	1,816	*2,869E-19*
HIST1H2BE	1,816	*2,857E-14*
PLAUR	1,815	7,774E-33
HEG1	1,815	*8,703E-21*
BAT5	1,815	*2,719E-26*
ASGR1	1,814	*6,884E-32*
C5orf53	1,814	*4,554E-22*
ST3GAL4	1,814	*3,097E-20*
LEP	1,814	*8,779E-18*
KIAA0922	1,814	*1,023E-20*
TGIF1	1,813	4,846E-25
TJP3	1,810	1,502E-17
ARHGEF10	1,810	1,161E-17
GRB2	1,809	1,239E-11
LOXL4	1,809	1,061E-22
HSPA5	1,808	2,252E-31
CSF2RA	1,808	1,296E-17
KIAA1147	1,807	1,521E-23
GALNTL4	1,806	3,794E-19
SOX15	1,806	9,165E-24
FIS1	1,804	5,896E-23
SQSTM1	1,804	1,931E-31
HIST1H4E	1,803	1,818E-14
KLHL17	1,803	5,398E-13
CD164	1,802	7,200E-17
AFAP1L1	1,802	7,149E-18
LAMP2	1,800	2,080E-16
HCG2P7	1,800	3,747E-30
FLNB	1,799	3,764E-26
PTGER2	1,797	3,480E-21
APH1B	1,795	5,481E-26
ANKRD37	1,793	3,239E-31
CCDC125	1,792	1,143E-23
NPAL3	1,792	6,393E-28
FLJ35390	1,790	1,143E-27
HHIPL2	1,789	7,882E-18
FAM39DP	1,788	5,126E-18
MGC102966	1,788	2,185E-25
FAM62B	1,787	2,641E-27
FHL1	1,787	2,134E-28
RELL2	1,787	3,710E-24
C3orf57	1,786	1,213E-15
PHKG2	1,785	7,065E-25
NEDD4	1,784	3,373E-22
PC	1,784	1,791E-18
ACSL3	1,784	2,289E-33
TMPRSS3	1,783	3,558E-23
KRT86	1,783	4,086E-26
TMEM17	1,783	6,896E-19
RAB6B	1,783	1,554E-25
NMD3	1,782	1,264E-16
KLF13	1,782	5,416E-22
C19orf4	1,782	7,347E-11
TNNT1	1,781	3,078E-23
ZNF702P	1,781	3,775E-23
IL1B	1,780	6,233E-31
ZNF394	1,780	1,347E-24
EPHB6	1,780	5,771E-23
VPS4B	1,780	2,359E-16
ELAVL1	1,779	3,370E-24
DUSP16	1,779	5,259E-25
IL17RD	1,779	1,801E-26
SDF4	1,777	1,705E-32
MAPK8IP3	1,776	2,035E-21
SPINT1	1,776	1,239E-19
C3orf34	1,775	1,835E-19
ACLY	1,774	1,316E-23
TPBG	1,774	5,189E-21
AR	1,774	1,133E-22
SLC35F3	1,774	1,286E-14
TALDO1	1,774	1,447E-23
PHF21A	1,774	4,498E-24
WNT7A	1,773	1,059E-23
NLRP8	1,773	1,337E-29
GOLGA8B	1,773	5,712E-20
PIP5K2B	1,772	3,518E-16
BMS1P5	1,772	2,029E-26
MVP	1,770	2,016E-22
FUCA1	1,769	1,565E-26
DMC1	1,768	8,912E-29
SOX18	1,768	9,587E-28
SMOX	1,766	4,950E-21
PPP2R2C	1,766	4,771E-28
SLC2A10	1,765	1,157E-20
C10orf54	1,765	1,673E-18
UAP1L1	1,764	2,585E-19
MAP6	1,764	2,589E-18
SEL1L3	1,764	2,268E-23
C14orf85	1,764	4,658E-27
PLEK2	1,763	2,603E-17
SERPINB7	1,762	1,059E-30
P4HA1	1,762	2,140E-31
FLVCR2	1,761	2,657E-25
RPS6KA2	1,761	6,653E-30
OSBP2	1,760	1,438E-20
SYT17	1,760	7,479E-23
SH3D19	1,759	1,186E-16
DPY19L1	1,759	6,575E-24
MAN2B1	1,759	1,188E-17
CATSPER1	1,758	4,045E-22
METRN	1,757	9,596E-19
ALDH3A1	1,756	1,343E-22
IGFBP4	1,756	2,938E-29

Supplementary Table S4.9: continued

DFNB59	1,756	1,691E-18
S100A13	1,755	2,948E-29
RNF144B	1,755	3,772E-22
ZMAT3	1,754	2,249E-23
LRRC37B2	1,754	2,964E-18
DDX51	1,754	1,130E-26
PILRB	1,753	9,252E-25
OSBPL1A	1,752	3,927E-22
ODZ4	1,751	1,723E-19
LSS	1,750	8,308E-29
HSPC268	1,750	4,896E-23
HTATIP2	1,749	4,139E-25
C11orf63	1,748	4,010E-19
TMEM2	1,747	1,461E-17
ATF3	1,747	9,748E-21
CHSY1	1,745	1,867E-23
SSH3	1,745	7,682E-17
PTPLAD2	1,744	8,542E-23
RBM6	1,741	1,020E-11
FKBP1A	1,741	1,390E-15
CTSL1	1,740	6,866E-17
FERMT1	1,740	3,247E-25
SAMD14	1,739	5,326E-25
SLC6A6	1,736	2,556E-13
SH3PXD2A	1,736	3,523E-24
SMCR5	1,736	4,512E-21
MCART1	1,736	1,400E-20
LRAP	1,736	8,794E-24
HSD17B7	1,735	7,345E-22
C5orf41	1,735	5,478E-17
GALIG	1,734	5,635E-14
ZNF486	1,734	6,964E-15
PTGR2	1,733	1,324E-15
NET1	1,732	3,708E-20
SNX8	1,731	1,729E-17
OSBPL2	1,731	3,373E-29
TMEM49	1,731	2,973E-26
ANXA2P1	1,731	4,160E-16
NEBL	1,731	1,822E-25
SERPINA3	1,730	5,618E-21
AGR2	1,729	1,769E-20
ZFAND2A	1,729	1,008E-26
TFAP2A	1,729	1,169E-29
HIST1H2BD	1,728	4,394E-20
ITFG1	1,728	2,905E-23
ITPKA	1,727	3,779E-32
JMJD1A	1,727	5,424E-16
N4BP2	1,727	1,428E-14
C16orf74	1,725	3,982E-12
LDHD	1,725	9,449E-16
LRP1	1,725	6,244E-16
BNIP3L	1,724	1,149E-17
ARMC7	1,724	9,653E-28
COL18A1	1,724	1,978E-19
SERPINB1	1,724	5,895E-15
SMAD6	1,724	9,687E-30
FLJ44124	1,724	7,309E-24
CSF2	1,724	5,184E-20
FAM119A	1,723	2,628E-21
UBR4	1,723	6,391E-23
FYN	1,722	1,591E-12
TNRC6A	1,722	3,985E-15
RNF149	1,722	4,238E-23
UPK1A	1,721	3,661E-20
LDHA	1,721	4,944E-19
SIPA1L2	1,720	1,152E-24
C20orf177	1,719	6,202E-18
DEM1	1,719	3,035E-24
PPA2	1,718	8,452E-27
PNCK	1,717	9,116E-21
ERBB2	1,717	2,916E-23
BLVRB	1,715	2,127E-30
PADI3	1,714	6,010E-22
AMHR2	1,714	3,088E-19
GNG5	1,713	9,051E-23
AXIN2	1,713	2,892E-23
CTPS2	1,712	7,029E-29
RUNDC3A	1,712	8,628E-23
ESM1	1,711	3,548E-13
RHOU	1,711	2,152E-16
MBD4	1,711	1,925E-19
HMHA1	1,711	3,667E-19
FAM173A	1,711	5,238E-26
C2orf69	1,711	5,734E-21
C14orf173	1,710	2,757E-30
UCA1	1,710	5,514E-20
ZC3H12A	1,710	7,391E-13
PHTF1	1,709	1,235E-16
YRDC	1,708	2,324E-22
HS6ST2	1,708	1,260E-20
KIAA0363	1,708	6,056E-18
C15orf52	1,708	2,574E-20
SFTA1P	1,708	2,763E-16
ERBB3	1,707	3,446E-19
SLC4A3	1,707	1,121E-19
CYCSL1	1,707	6,203E-15
ABCC4	1,706	4,345E-23
HEATR1	1,706	4,312E-22
FIBCD1	1,705	4,507E-15
POFUT1	1,705	2,899E-25
THBS3	1,705	2,486E-21
NAGK	1,704	7,499E-33
PON2	1,704	6,479E-24
PKD2	1,704	9,538E-24
ETS2	1,704	3,498E-23
TMEM106A	1,704	7,812E-22
SGSM2	1,703	1,613E-17
ZSWIM6	1,702	3,073E-15
PRODH	1,702	1,980E-15
LMOD3	1,702	1,070E-18
STUB1	1,700	1,618E-15
CD9	1,700	1,014E-20
WDR22	1,700	1,931E-18
FAM63A	1,700	3,191E-21
SLC20A1	1,698	4,462E-29
HLA-A	1,698	1,009E-19
VGF	1,697	3,675E-18
SLC2A12	1,697	2,509E-16
GALNT1	1,697	3,573E-16
TUBB4	1,697	8,311E-21
ZNF738	1,697	2,351E-18
ANTXR2	1,696	3,012E-24
CMTM8	1,696	2,706E-21
GCNT2	1,696	1,659E-22
FXYD3	1,696	4,464E-24
PNPT1	1,696	7,109E-24
STARD13	1,695	4,299E-13
C1orf115	1,695	2,803E-14
CDK5RAP3	1,695	3,938E-26
DPP9	1,695	3,333E-16
CAMSAP1L1	1,694	2,061E-19
UCKL1	1,694	6,871E-20

Supplementary Table S4.9: continued

ELOVL4	1,693	2,349E-13
RASSF7	1,693	1,553E-21
SEPT5	1,692	2,022E-20
CCDC146	1,692	8,296E-16
BLZF1	1,691	1,483E-15
JAG1	1,691	1,456E-15
SECISBP2	1,691	1,531E-23
ADARB1	1,690	5,996E-25
C14orf153	1,689	4,357E-18
ADCK5	1,689	1,189E-26
UBE2L6	1,688	8,489E-30
IL13RA1	1,688	3,064E-30
AGAP8	1,688	1,675E-18
PAOX	1,687	6,047E-22
EIF4G3	1,687	2,420E-14
CAPN5	1,687	1,056E-21
TNNI3	1,687	2,673E-23
GOLM1	1,687	2,582E-14
SLC26A11	1,685	1,190E-22
ATP1B1	1,684	6,865E-17
ZNF483	1,683	6,550E-15
KISS1R	1,683	1,286E-18
CDS2	1,683	7,069E-29
MAGED2	1,682	7,978E-18
NRBP2	1,680	3,226E-23
GRN	1,680	9,216E-23
XRCC2	1,680	3,324E-14
ATP6V0B	1,680	5,388E-12
HES2	1,678	6,132E-21
HYOU1	1,676	3,034E-17
MYADM	1,676	1,864E-17
RRBP1	1,676	3,245E-16
DUSP19	1,673	1,544E-24
CCNG2	1,672	7,359E-17
ZNF462	1,672	1,705E-20
PITPNM1	1,671	1,370E-23
NXF1	1,671	7,410E-23
B4GALNT4	1,671	1,926E-16
MT1G	1,671	4,214E-13
PAPSS1	1,670	2,179E-15
CEBPB	1,670	2,301E-31
CADM4	1,670	1,480E-23
CKMT1A	1,670	5,364E-21
MCCC1	1,670	5,409E-19
WDR68	1,670	6,509E-22
KLHL3	1,669	5,298E-20
YPEL5	1,668	3,055E-19
RGS10	1,668	2,477E-23
PLDN	1,667	1,325E-18
FAM20C	1,667	2,350E-14
ERRFI1	1,666	6,873E-22
DAPP1	1,663	3,067E-20
LMTK3	1,663	2,148E-24
FCAR	1,662	9,019E-22
SCNN1G	1,661	1,285E-11
C19orf10	1,661	3,803E-13
CD99L2	1,660	3,600E-26
PNPLA2	1,660	3,364E-23
DUXAP3	1,659	2,248E-18
ARHGAP23	1,658	3,282E-18
MPPE1	1,658	2,231E-11
KCNMB2	1,657	3,420E-16
SYTL2	1,657	2,295E-17
IGDCC4	1,657	1,130E-20
MFSD11	1,655	2,313E-19
ZNF69	1,655	4,357E-21
PRKAA1	1,655	8,182E-18
PTGFRN	1,654	1,027E-16
HLA-C	1,654	1,347E-13
EPB41L1	1,653	8,094E-15
FJX1	1,653	1,622E-21
RAB26	1,653	3,274E-24
PURB	1,653	2,701E-21
HLA-DRA	1,652	7,135E-21
SLC1A3	1,652	4,162E-22
AACS	1,652	8,911E-17
CRCP	1,652	5,523E-09
CLK2	1,651	3,679E-19
ADAM17	1,651	1,764E-21
PIP4K2A	1,651	3,945E-18
ANXA11	1,651	5,189E-16
KAT2B	1,651	4,935E-15
ICA1	1,650	2,558E-11
FLJ20489	1,650	5,201E-22
SH3GL2	1,649	6,725E-18
ENDOD1	1,648	1,061E-13
SLC2A6	1,647	1,119E-28
PLLP	1,647	9,889E-15
VIPR1	1,646	2,848E-16
PDGFA	1,646	8,547E-18
PPFIA4	1,645	9,935E-16
RNU1G2	1,644	7,417E-28
C14orf37	1,644	3,124E-16
INF2	1,644	2,051E-23
NES	1,644	1,585E-17
TUSC3	1,643	1,683E-20
CYP26B1	1,643	6,666E-13
P2RY5	1,642	1,060E-17
C1orf24	1,642	4,862E-17
CDKL3	1,642	6,921E-22
SULT1A1	1,641	9,479E-19
TBCB	1,641	5,514E-18
ARTN	1,641	6,410E-19
LAMA4	1,641	3,300E-17
CEACAM6	1,640	5,663E-14
KIAA0913	1,640	9,921E-24
RNF215	1,640	4,736E-15
MIB2	1,640	1,929E-19
RALGDS	1,639	2,058E-25
FKBP14	1,639	2,369E-19
ZNF185	1,639	5,803E-21
KCNK6	1,639	9,465E-20
ITGAV	1,639	2,542E-18
BCOR	1,639	2,256E-15
OCRL	1,638	1,327E-27
DYNC1H1	1,638	6,126E-22
SGK1	1,638	3,248E-18
CKMT1B	1,638	3,057E-20
FLJ25363	1,638	5,831E-15
VPS28	1,636	2,538E-28
SLC15A4	1,636	1,076E-16
SULF2	1,636	3,096E-17
MAP4K2	1,636	2,603E-26
SEC14L1	1,636	2,409E-18
TMEM163	1,635	1,193E-16
PPM1H	1,634	9,857E-18
ATP6AP1	1,634	1,869E-27
PCYT2	1,634	4,545E-19
SLC38A2	1,634	1,071E-19
C5orf13	1,633	3,164E-15
TRIM13	1,633	5,877E-19
PTPN13	1,632	4,854E-18
MCM8	1,632	9,935E-19
SRGAP3	1,632	1,413E-18
SLC2A1	1,632	5,506E-16
SEC61A2	1,632	1,058E-23

Supplementary Table S4.9: continued

SLC25A29	1,631	1,171E-14
ZNF652	1,631	4,487E-20
STXBP2	1,631	1,925E-18
ST6GALNAC 2	1,631	4,545E-13
GRAMD1B	1,629	2,528E-21
NIN	1,628	1,165E-21
PRO1853	1,628	5,287E-12
CD24	1,628	1,516E-24
CREB1	1,628	9,789E-20
HNRNPU	1,627	7,692E-12
LCOR	1,627	1,277E-23
TMEM156	1,627	7,265E-27
FLJ46309	1,626	1,096E-17
NFE2L1	1,626	2,999E-23
CA12	1,625	8,889E-19
TSPAN5	1,624	2,609E-18
DACT3	1,624	1,510E-20
FLJ38717	1,624	4,113E-18
DMKN	1,624	1,477E-21
RGS2	1,623	2,243E-16
SPTLC1	1,623	2,592E-19
GPR56	1,623	3,761E-22
LCN2	1,621	1,461E-15
C16orf13	1,621	2,384E-32
MYH9	1,621	7,819E-20
SIGIRR	1,620	7,590E-19
NT5C2	1,619	1,809E-23
HLTF	1,618	2,265E-12
ABTB1	1,617	3,938E-18
FAM193B	1,617	6,729E-20
TRIM3	1,615	6,447E-18
ARFGEF1	1,614	1,040E-16
CLDN1	1,614	2,164E-12
CLCN6	1,614	1,963E-14
HLCS	1,614	3,840E-16
UBE2O	1,612	7,459E-16
BCAP31	1,612	3,974E-20
PMP22	1,612	1,910E-21
ZNF160	1,612	1,778E-17
PRKAB2	1,611	7,954E-14
C19orf12	1,611	6,968E-18
PFKP	1,610	2,307E-30
RIMKLA	1,610	2,223E-21
KLHDC8B	1,610	1,734E-23
DGAT1	1,609	7,577E-21
PRR4	1,609	6,389E-20
HOMER2	1,609	5,335E-17
APP	1,609	6,847E-20
ANKRD13D	1,608	1,930E-14
RHPN2	1,608	2,727E-11
ODC1	1,607	5,087E-20
ZNF786	1,607	4,319E-18
FAM69B	1,606	2,074E-26
FTHL12	1,606	8,755E-26
TNFRSF1A	1,606	4,847E-21
ACP2	1,606	5,471E-13
DSTYK	1,605	1,525E-16
BMP1	1,605	3,680E-12
MYST4	1,605	1,330E-16
RASSF5	1,605	1,445E-25
LRIG1	1,603	4,950E-15
NUDT16L1	1,602	2,105E-15
EFCAB4A	1,602	1,188E-11
SHROOM4	1,602	1,176E-22
NICN1	1,601	6,179E-20
ABHD12	1,601	1,032E-20
ZNF223	1,601	5,360E-22
GMPR	1,601	7,081E-11
ADI1	1,599	2,679E-16
TBC1D9B	1,599	6,787E-19
TLE2	1,599	7,944E-25
PTBP2	1,599	3,418E-17
QSOX1	1,598	3,013E-16
PPP1R10	1,598	5,121E-11
PSMD1	1,598	1,471E-22
CAMK2B	1,597	2,212E-17
GPX4	1,597	7,872E-24
ROBLD3	1,597	1,971E-20
RRAS	1,596	2,807E-20
CALM1	1,596	8,561E-26
EDEM1	1,596	1,826E-17
ZNF91	1,595	6,040E-10
FOXO3	1,595	3,910E-24
PRKCD	1,595	3,579E-23
HRK	1,594	1,586E-18
C6orf170	1,593	3,018E-17
RAB3B	1,593	2,746E-18
ADCY6	1,593	2,700E-10
ATP9A	1,592	2,808E-23
MBOAT2	1,592	5,246E-14
COTL1	1,592	1,146E-05
SFXN5	1,592	5,564E-20
HINT3	1,591	3,453E-09
RAPGEFL1	1,590	5,137E-17
PYCRL	1,590	1,178E-14
CACNB3	1,590	1,270E-19
DDR1	1,590	2,935E-21
MAPT	1,590	1,520E-16
LRRFIP1	1,589	6,989E-11
C3orf58	1,589	2,014E-20
FBXO15	1,589	1,202E-17
ZNF577	1,588	4,527E-20
SSU72	1,588	2,342E-18
MOXD1	1,588	9,560E-18
COL6A3	1,588	1,189E-17
WFDC3	1,587	1,986E-14
ERGIC3	1,587	4,111E-25
dj341D10.1	1,586	2,997E-11
STAG3L3	1,586	1,684E-19
HMGA2	1,586	1,960E-17
ZNF365	1,586	8,567E-29
BIRC3	1,586	1,960E-22
STX6	1,585	8,250E-15
MED24	1,585	1,483E-23
USMG5	1,585	7,996E-21
ACAD8	1,585	1,947E-09
KCNK1	1,583	2,640E-14
ARL4A	1,583	9,295E-22
RAC3	1,583	5,106E-19
HCST	1,583	7,938E-14
C1orf51	1,583	3,049E-17
TGM2	1,583	5,039E-15
ANO6	1,583	8,941E-12
CPA4	1,582	2,683E-15
TMEM63B	1,582	3,112E-17
HK1	1,582	1,082E-19
CEP27	1,582	2,744E-16
CCDC136	1,582	5,145E-16
MAGT1	1,582	2,338E-17
ASB1	1,581	1,167E-17
MAPBPIP	1,581	3,426E-28
BCKDHA	1,581	4,430E-23

Supplementary Table S4.9: continued

IFFO2	1,580	2,053E-14
TNRC6B	1,580	6,776E-15
ZMYM3	1,580	5,488E-16
HSD11B1L	1,580	1,882E-14
SAT1	1,580	3,523E-16
CXorf38	1,580	2,815E-15
CRY2	1,580	1,208E-17
STK38	1,579	1,564E-22
FAM120B	1,579	4,129E-24
PPP2R5B	1,578	2,760E-21
GUCA1B	1,578	2,941E-23
MGLL	1,578	3,587E-18
EPOR	1,577	6,959E-16
C19orf6	1,577	1,855E-11
TANC1	1,577	1,580E-15
ULBP1	1,577	6,639E-18
SCYL1	1,576	1,142E-25
FZD2	1,576	9,209E-30
GCLM	1,575	2,042E-15
C2orf82	1,575	1,431E-15
NEDD4L	1,575	1,604E-20
CAPS	1,574	1,417E-20
PAG1	1,574	1,662E-15
BCL6	1,574	1,070E-19
SLC9A6	1,574	2,063E-18
C7orf68	1,573	2,120E-14
C10orf33	1,572	1,244E-18
TSPYL2	1,572	1,129E-10
BMI1	1,572	2,397E-17
SLC22A4	1,571	1,220E-14
RPS6KA1	1,570	2,631E-17
POLD4	1,570	7,977E-16
FAM40B	1,570	3,490E-14
ARRDC2	1,570	8,122E-24
PLXNB3	1,569	6,299E-15
PCOLCE2	1,568	6,669E-17
KIAA1875	1,568	4,284E-12
EIF5A2	1,568	1,693E-22
PHKA2	1,568	1,550E-19
USP49	1,567	6,282E-17
GJB2	1,567	2,993E-18
RAC2	1,567	5,258E-22
UGDH	1,567	2,833E-17
SDHALP1	1,567	1,005E-14
GRINA	1,566	1,870E-19
HSPA1A	1,565	3,485E-16
SH3TC1	1,565	1,744E-16
VCP	1,564	1,057E-25
TOB1	1,564	1,484E-14
FCGRT	1,564	5,963E-21
ANXA2P3	1,564	1,551E-10
SNTB1	1,563	2,810E-19
LIMS2	1,563	1,075E-24
ULK1	1,563	2,623E-18
CCNDBP1	1,563	5,400E-23
PROS1	1,563	1,001E-15
VGLL1	1,563	1,374E-17
FLJ20021	1,563	9,735E-16
DENND1A	1,562	3,145E-19
EFNB1	1,562	2,122E-18
NUMA1	1,562	6,670E-14
FGFR4	1,562	6,955E-20
MAP6D1	1,562	1,776E-16
MZF1	1,562	9,120E-21
DYRK2	1,561	8,825E-19
KLHL28	1,561	5,517E-12
BTBD3	1,561	1,611E-13
SAPS2	1,561	3,676E-19
ZNF211	1,560	1,201E-15
NAPB	1,559	2,805E-18
STAMBP	1,559	9,919E-13
RBM33	1,559	4,066E-14
FHOD1	1,556	2,554E-20
TSPAN31	1,556	4,330E-17
OCIAD1	1,556	5,118E-25
TMEM120A	1,555	7,823E-19
GATS	1,554	4,170E-15
KIAA1598	1,554	2,726E-18
TMC6	1,553	1,946E-18
KCNMA1	1,553	1,354E-22
HES1	1,553	3,583E-18
AKR1C3	1,552	2,070E-19
PGK1	1,552	8,745E-24
RHBDD2	1,552	2,447E-17
PPIC	1,552	1,924E-24
PMS2L3	1,551	4,849E-18
LILRB1	1,551	1,375E-23
ICAM5	1,551	9,005E-16
SS18L1	1,551	2,206E-25
DFNA5	1,551	5,192E-12
SCHIP1	1,550	6,371E-12
RNU1-5	1,549	1,558E-17
CDA	1,549	6,256E-17
SAMD4A	1,548	8,742E-18
VPS41	1,548	1,319E-14
PRR15L	1,548	1,183E-19
NNMT	1,548	2,365E-17
C22orf36	1,547	2,231E-18
PCNX	1,546	1,128E-18
TDRD1	1,546	6,045E-20
SNAPC1	1,546	5,741E-17
ELOVL1	1,546	5,855E-15
C17orf28	1,546	9,301E-19
KRT19	1,546	1,338E-22
CRTAP	1,545	6,031E-16
TRPM4	1,544	1,661E-21
SLC4A5	1,544	2,632E-13
NCRNA00161	1,543	8,509E-17
ZBED5	1,543	6,016E-08
MAPRE3	1,543	3,071E-18
APBA2BP	1,543	2,498E-18
FKBP9L	1,543	4,891E-18
MXRA7	1,543	1,015E-11
TNFSF14	1,543	8,301E-20
C20orf194	1,542	9,917E-16
MSRB3	1,542	1,026E-16
SURF1	1,541	3,603E-13
PCYOX1L	1,541	2,603E-14
LRP11	1,541	4,626E-14
ANO1	1,540	1,447E-20
DDIT3	1,540	1,407E-11
GSTM2	1,540	1,226E-15
MACROD1	1,540	4,076E-15
TPM1	1,539	1,558E-14
PPAP2A	1,538	4,175E-18
C7orf20	1,538	3,932E-13
AIRE	1,538	3,992E-21
TMEM16A	1,537	7,633E-19
CSNK1D	1,537	3,315E-17
UBE2G2	1,537	6,001E-24
ATP7B	1,537	1,194E-14
HSPA1B	1,537	8,818E-17

Supplementary Table S4.9: continued

POFUT2	1,537	5,739E-22
TNFRSF18	1,536	1,686E-17
IGFBP2	1,536	3,750E-11
SGK	1,536	2,479E-20
PRRT2	1,536	2,113E-10
GPD1L	1,535	9,869E-18
DKFZp434K191	1,535	3,824E-14
ACSL1	1,534	2,650E-12
MIR21	1,534	8,860E-14
RPS15A	1,534	8,797E-24
SIDT2	1,534	4,186E-22
RIN1	1,533	4,093E-15
ALDH2	1,533	1,196E-11
GOLGA3	1,533	2,280E-18
CSRNP3	1,532	3,286E-19
HELZ	1,532	4,986E-14
C8orf37	1,532	3,126E-16
TRAPPC6B	1,532	3,748E-23
CRABP1	1,531	1,271E-12
GCAT	1,531	8,273E-15
DLG4	1,531	3,653E-15
SCARNA13	1,531	1,009E-16
CCDC84	1,530	8,882E-19
RAD51C	1,530	5,928E-17
PDIA3P	1,530	1,208E-11
COL17A1	1,529	5,820E-14
NUDT1	1,529	4,192E-16
RCAN1	1,528	7,631E-19
COL9A2	1,528	8,728E-14
ZNF860	1,527	5,579E-12
DHRS13	1,527	9,251E-13
MT3	1,526	8,366E-15
TYRO3	1,525	1,221E-16
RAB11FIP2	1,525	9,735E-15
DNAJB2	1,525	6,183E-18
CD3EAP	1,524	1,698E-27
CTGLF3	1,524	1,209E-15
PGM3	1,524	1,482E-10
BAX	1,524	4,753E-16
C21orf57	1,523	1,484E-12
CPT2	1,523	3,376E-20
S1PR3	1,523	1,659E-15
RBCK1	1,523	2,189E-16
MBTD1	1,523	1,397E-09
CCDC92	1,522	1,976E-28
SLC30A7	1,522	2,064E-14
SIPA1	1,522	9,412E-28
MTX3	1,522	6,876E-13
ACY1	1,522	3,954E-12
NCRNA00085	1,521	1,202E-16
SKIV2L	1,521	4,719E-17
MAP1LC3B	1,520	1,582E-15
CCNE1	1,520	9,661E-17
RASSF2	1,520	8,215E-12
SLC22A5	1,519	2,786E-13
PTPLA	1,519	2,602E-11
TGFBR2	1,519	7,025E-15
GPR37	1,518	8,869E-09
WDR74	1,518	5,220E-10
PSMC4	1,518	4,249E-18
C11orf35	1,517	1,473E-14
EXT1	1,517	1,922E-16
SH3BGRL3	1,516	1,653E-22
PSMD7	1,516	5,058E-23
MMP1	1,516	5,395E-12
ESYT1	1,516	1,197E-24
AIM1L	1,516	4,057E-15
PTK6	1,515	3,060E-18
HIST2H2AB	1,515	1,105E-12
C9orf130	1,515	3,516E-17
NQO2	1,514	1,089E-16
SLC25A18	1,514	4,277E-07
FLJ32252	1,514	2,930E-11
TOM1	1,513	1,019E-18
ANKRD30B	1,513	7,370E-19
MIR185	1,512	9,308E-10
ATXN1	1,512	1,401E-13
PNMA1	1,512	1,180E-17
C17orf101	1,511	2,517E-13
UNC84A	1,511	6,631E-13
ISYNA1	1,511	4,388E-17
ENO3	1,511	8,437E-15
CENTG3	1,511	2,646E-14
YEATS2	1,511	7,683E-21
ISG20	1,511	7,607E-16
CXCL1	1,511	2,394E-06
PHLDA1	1,511	6,575E-18
PHACTR3	1,510	4,242E-20
ZCWPW1	1,510	5,339E-20
CYTH3	1,510	1,548E-13
KDM5B	1,509	1,490E-12
ACADVL	1,509	3,285E-15
TTLL11	1,509	2,069E-17
PPP1R1B	1,508	2,719E-20
LRPAP1	1,508	3,049E-20
PARVA	1,508	3,425E-17
PACSIN1	1,508	8,168E-15
TNFRSF14	1,508	1,363E-15
PCYOX1	1,507	2,915E-16
CNO	1,507	6,142E-12
TERC	1,507	1,282E-16
FLJ44342	1,507	2,218E-11
SPHK1	1,507	2,002E-13
ZNF251	1,506	9,175E-09
DGKA	1,506	5,429E-16
MCAM	1,506	8,525E-13
MAST1	1,506	1,071E-10
UBXN6	1,505	1,611E-15
C6orf70	1,505	1,282E-11
DOCK10	1,505	2,562E-13
ANKRD23	1,505	4,286E-12
SLC35E1	1,504	1,056E-07
RN7SK	1,504	1,331E-18
OSTM1	1,503	1,676E-14
DENR	1,503	3,173E-16
BHLHB2	1,503	9,986E-19
GMIP	1,502	1,141E-13
TECPR1	1,501	5,208E-15
ACADM	1,501	1,304E-18
SSTR2	1,500	3,261E-13
COMMD3	1,500	1,079E-17
NEU1	1,500	6,344E-15
KLF4	1,500	1,588E-14
GPR126	1,500	2,377E-12
TMEM127	0,668	2,671E-15
G3BP2	0,668	5,150E-11
PPA1	0,668	1,728E-21
DUSP4	0,668	5,322E-14
LY6G5C	0,668	1,602E-10
FAM110A	0,667	1,893E-17
WDFY1	0,667	1,205E-20
RAB25	0,667	1,962E-15

Supplementary Table S4.9: continued

FLJ20444	0,667	3,672E-19	*DDX21*	0,664	1,755E-14	*THAP10*	0,658	1,168E-14	*SAPS1*	0,654	8,471E-14
RP11-529I10.4	0,667	6,214E-16	*HEATR7A*	0,664	3,251E-12	*PKIB*	0,658	5,969E-14	*CDCA2*	0,654	1,434E-17
STX5	0,667	1,465E-20	*TRO*	0,664	1,543E-12	*XYLB*	0,658	2,356E-16	*OSTC*	0,653	2,626E-17
LSM3	0,667	6,318E-18	*C9orf69*	0,664	1,061E-18	*TEAD4*	0,658	7,761E-22	*C12orf49*	0,653	1,519E-11
ITGA10	0,667	4,147E-12	*C6orf108*	0,663	1,040E-23	*NANP*	0,658	4,951E-13	*NCAPD3*	0,653	1,996E-15
FAM131A	0,667	1,337E-13	*KCNF1*	0,663	3,285E-13	*MSH6*	0,658	9,682E-22	*CDK2*	0,653	4,367E-19
WDR43	0,667	4,567E-14	*SF3A3*	0,663	4,206E-23	*MRE11A*	0,658	4,447E-16	*IFI44L*	0,653	3,370E-14
PRMT3	0,667	1,237E-15	*POLR3F*	0,663	9,013E-18	*EXOSC8*	0,658	5,706E-08	*C11orf48*	0,652	4,230E-18
C1orf57	0,666	3,224E-17	*ARV1*	0,663	3,701E-15	*DERA*	0,658	1,316E-14	*SPRYD4*	0,652	5,662E-18
LAS1L	0,666	6,814E-17	*UBE2E1*	0,663	9,402E-14	*C1orf43*	0,657	2,097E-10	*CBWD3*	0,652	3,660E-15
C7orf49	0,666	3,704E-13	*CENPO*	0,662	1,188E-13	*UNC84B*	0,657	1,158E-11	*CSRP2*	0,652	9,150E-12
PLAGL2	0,666	1,577E-17	*STAT1*	0,662	4,774E-15	*NAP1L1*	0,657	1,836E-14	*STOML2*	0,652	1,440E-27
LDOC1	0,666	8,935E-17	*OAS1*	0,662	2,389E-09	*PHB2*	0,657	8,125E-17	*RFC2*	0,652	2,472E-14
PPP4R1	0,666	1,315E-16	*COPZ1*	0,662	2,002E-14	*C11orf60*	0,657	3,579E-18	*ABI3BP*	0,651	5,361E-20
PIGQ	0,665	4,158E-19	*GPBP1*	0,662	2,231E-14	*TRIM68*	0,657	2,238E-20	*LPXN*	0,651	4,204E-19
C14orf126	0,665	5,142E-12	*ADRBK1*	0,662	1,089E-22	*AP2B1*	0,657	1,723E-19	*SDC1*	0,650	1,313E-13
TDG	0,665	4,475E-14	*NT5DC3*	0,661	3,781E-21	*MPRIP*	0,657	1,571E-11	*GMPS*	0,650	9,782E-20
GRPR	0,665	1,017E-12	*ERCC6L*	0,661	2,343E-10	*MMS19*	0,656	2,052E-12	*EIF2C1*	0,650	8,400E-14
BLM	0,665	1,247E-16	*CS*	0,661	7,246E-23	*CEPT1*	0,656	6,661E-17	*MKRN2*	0,650	2,556E-14
NUP88	0,665	3,774E-18	*FCGR2A*	0,661	1,583E-11	*MED20*	0,656	5,711E-23	*XPO6*	0,650	1,676E-13
PNKD	0,665	1,353E-16	*HAUS8*	0,661	1,779E-07	*SLC25A28*	0,656	4,205E-22	*MLST8*	0,650	1,170E-14
RPL34	0,665	1,918E-14	*TNFAIP1*	0,661	1,526E-14	*CTSA*	0,656	2,532E-15	*DDX39*	0,650	4,625E-16
FUCA2	0,665	2,236E-15	*PRDX2*	0,660	1,428E-15	*DUS2L*	0,656	1,774E-19	*RPL21*	0,650	1,179E-20
AGK	0,665	3,007E-11	*TAF12*	0,660	2,043E-10	*SPATA2L*	0,656	8,415E-15	*DNASE1L1*	0,650	8,255E-16
RPS7	0,665	1,107E-18	*KIAA0020*	0,660	1,111E-14	*GCSH*	0,656	9,754E-17	*FBXW4*	0,649	5,140E-13
EPM2AIP1	0,665	7,543E-17	*JOSD1*	0,660	4,227E-15	*CYB561D1*	0,655	1,193E-19	*WDR18*	0,649	9,095E-16
MED4	0,665	1,263E-12	*IP6K1*	0,660	1,782E-12	*WDR12*	0,655	3,100E-10	*MET*	0,649	2,859E-21
DPP4	0,664	9,339E-15	*CACYBP*	0,660	4,243E-10	*UCK2*	0,655	2,342E-08	*ASB9*	0,648	4,490E-21
C13orf3	0,664	4,776E-19	*TBL1X*	0,660	4,882E-23	*TIMM8A*	0,655	1,570E-14	*UBE2F*	0,648	7,622E-22
CLTA	0,664	2,045E-14	*STX8*	0,660	1,034E-22	*NOP56*	0,655	1,485E-17	*KIAA0494*	0,648	1,570E-16
C1orf85	0,664	3,235E-25	*C10orf76*	0,659	6,087E-16	*GCA*	0,655	1,050E-14	*SFRS6*	0,648	2,715E-21
FASTK	0,664	5,512E-11	*PGAM1*	0,659	6,759E-11	*MTCP1*	0,655	3,288E-19	*XBP1*	0,648	1,557E-11
SRF	0,664	9,039E-17	*HSPD1*	0,659	2,413E-29	*IPO5*	0,654	2,891E-18	*UBE2N*	0,648	4,017E-13

Supplementary Table S4.9: continued

MRPS6	0,648	9,276E-18	*CGI-96*	0,643	9,044E-19	*RNF220*	0,638	2,372E-18	*FAM171A1*	0,633	7,728E-24
XRCC3	0,648	1,269E-12	*E2F7*	0,643	2,320E-17	*E2F5*	0,637	1,837E-14	*TOMM34*	0,633	7,442E-19
RUVBL1	0,648	6,690E-17	*SDHC*	0,642	1,091E-27	*FAM120A*	0,637	7,623E-23	*SH2B3*	0,633	4,531E-09
UBL7	0,648	2,062E-18	*SLFN11*	0,642	1,131E-09	*NRBF2*	0,637	1,013E-18	*BZW2*	0,633	6,903E-24
GLIPR1	0,648	2,832E-14	*ATG5*	0,642	2,248E-19	*SLC41A3*	0,637	1,739E-21	*GLTP*	0,632	6,453E-16
MLF1IP	0,648	3,373E-22	*C14orf124*	0,642	7,095E-15	*XRCC6BP1*	0,637	2,210E-16	*NOC3L*	0,632	1,659E-18
TMEM48	0,648	1,481E-15	*IFI6*	0,642	5,145E-06	*POP5*	0,637	7,630E-19	*WASF2*	0,631	6,097E-17
TULP4	0,648	4,357E-14	*AMMECR1L*	0,641	1,287E-15	*CRYL1*	0,637	8,346E-19	*IPO9*	0,631	3,622E-15
NEIL3	0,647	6,343E-10	*GPR89B*	0,641	1,675E-10	*WDR75*	0,637	4,637E-20	*SLC35A5*	0,631	3,516E-12
KIF18A	0,647	3,326E-12	*C6orf136*	0,641	5,869E-20	*CCT6P1*	0,637	1,788E-23	*DKC1*	0,631	5,105E-19
MEIS2	0,647	1,598E-15	*GPN3*	0,641	6,462E-11	*GEMIN6*	0,636	1,709E-18	*PCGF2*	0,631	3,569E-17
PAK1IP1	0,647	4,513E-17	*RNPS1*	0,641	9,029E-19	*GINS4*	0,636	5,499E-15	*ATP5L*	0,630	1,077E-13
NMB	0,646	1,475E-14	*ARHGAP11B*	0,641	4,675E-19	*COMMD2*	0,636	7,092E-21	*TEAD2*	0,630	2,639E-23
DHRS11	0,646	5,150E-13	*UBE4B*	0,641	1,460E-18	*REXO1*	0,636	4,195E-25	*C22orf13*	0,630	3,970E-25
SLC25A11	0,646	4,999E-13	*TM4SF19*	0,641	3,562E-23	*RNASEH2A*	0,635	8,657E-22	*PRPF4*	0,630	1,978E-26
CDCP1	0,646	2,253E-21	*IRS1*	0,641	4,325E-18	*RIPK2*	0,635	1,164E-21	*SPC25*	0,630	3,426E-15
CHORDC1	0,646	1,985E-11	*HSPC111*	0,640	3,363E-22	*C10orf26*	0,635	3,419E-14	*NAV2*	0,630	2,765E-10
ZNF519	0,646	1,299E-18	*GNG11*	0,640	1,692E-18	*RAP2C*	0,635	1,231E-13	*ASH2L*	0,630	1,770E-16
LRFN3	0,645	6,215E-18	*SLC45A3*	0,640	4,186E-20	*MRPL30*	0,635	9,972E-12	*PATE3*	0,630	3,455E-17
HPRT1	0,645	1,073E-11	*IMPA2*	0,640	1,857E-19	*SLC7A5*	0,635	6,916E-23	*MRTO4*	0,629	6,905E-17
TUBA1B	0,645	2,899E-13	*VPS24*	0,640	8,125E-15	*SRPK1*	0,634	1,283E-13	*ARMC6*	0,629	4,189E-24
MYLIP	0,645	2,377E-17	*CHMP4C*	0,639	9,371E-12	*ZNF668*	0,634	3,464E-18	*CLCC1*	0,629	1,324E-14
CCDC56	0,645	1,983E-22	*ZNF469*	0,639	2,305E-17	*KLF11*	0,634	9,526E-18	*CITED4*	0,629	3,521E-17
EFHD2	0,645	3,168E-19	*C17orf63*	0,639	5,095E-14	*ALDH7A1*	0,634	3,517E-18	*CSNK2A2*	0,628	5,219E-18
PLXNA1	0,644	1,409E-14	*CCDC99*	0,639	2,984E-16	*PELP1*	0,634	1,276E-13	*CARM1*	0,628	1,515E-22
RANGAP1	0,644	2,368E-31	*CTSL2*	0,639	1,010E-23	*NCAPG2*	0,634	4,144E-21	*CDC34*	0,628	1,848E-19
BCL2L13	0,644	8,735E-20	*ZNF695*	0,639	4,506E-17	*MAD2L1BP*	0,633	2,986E-14	*MCAT*	0,628	8,103E-14
C2orf47	0,644	5,176E-08	*TXNDC15*	0,638	1,340E-14	*SHARPIN*	0,633	1,326E-10	*C11orf24*	0,628	4,253E-15
SEH1L	0,644	1,011E-11	*TBC1D13*	0,638	5,007E-24	*CCNE2*	0,633	4,611E-16	*FAM117B*	0,628	8,378E-18
POLE	0,644	2,411E-15	*FRAG1*	0,638	1,049E-16	*NUP37*	0,633	4,092E-23	*TTL*	0,627	9,258E-16
MGC4294	0,644	9,262E-18	*MTA1*	0,638	1,416E-16	*GBP2*	0,633	4,518E-13	*CLASP2*	0,627	3,274E-23
LZIC	0,644	5,309E-17	*UBE2L3*	0,638	3,988E-21	*TEX261*	0,633	3,277E-18	*MGC70857*	0,627	8,679E-15
RPA3	0,643	5,404E-15	*RSL1D1*	0,638	1,065E-20	*RBM15B*	0,633	2,427E-18	*SNORA76*	0,627	3,750E-12

Supplementary Table S4.9: continued

FAM32A	0,626	1,126E-16	*BTG3*	0,619	1,755E-16	*LGTN*	0,613	1,975E-22	*SF3B4*	0,605	2,895E-25
BTBD10	0,626	3,861E-15	*SCAMP3*	0,619	5,489E-20	*RPLP1*	0,612	6,097E-26	*CD320*	0,604	5,569E-27
MRPL37	0,626	2,576E-23	*ITGB1BP1*	0,619	9,093E-17	*ACN9*	0,612	4,140E-22	*EIF5A*	0,604	5,005E-33
HCLS1	0,625	1,897E-23	*AKR1B10*	0,619	1,049E-20	*CDC42*	0,611	5,584E-18	*SPC24*	0,604	4,242E-26
ORC6L	0,625	1,182E-14	*THUMPD2*	0,619	6,360E-20	*GLA*	0,611	6,689E-24	*DYM*	0,604	2,377E-16
CGGBP1	0,625	1,749E-17	*CSE1L*	0,619	4,909E-13	*C8orf30B*	0,611	9,919E-19	*TGFB1I1*	0,604	4,458E-26
GABPB2	0,625	8,120E-09	*SAE1*	0,618	1,159E-30	*LMAN2*	0,611	4,364E-12	*HNRNPC*	0,604	7,010E-20
TNFSF12	0,625	4,854E-17	*MCM7*	0,618	1,055E-23	*ITCH*	0,611	1,063E-19	*GTF3C6*	0,604	3,733E-16
RRP15	0,625	2,115E-21	*CDK6*	0,618	1,128E-22	*YWHAQ*	0,611	5,849E-24	*C16orf59*	0,603	4,403E-18
CBFB	0,625	1,863E-18	*ISG15*	0,618	5,295E-12	*ITPRIP*	0,611	7,787E-19	*PPP1R11*	0,603	1,541E-15
RPS23	0,624	1,954E-15	*THOC4*	0,617	1,467E-11	*C20orf27*	0,610	1,051E-29	*LPPR2*	0,603	8,730E-17
CHAF1A	0,624	6,205E-17	*CORO1C*	0,617	1,005E-19	*DPM3*	0,610	3,428E-18	*KIAA1712*	0,603	5,954E-17
RSRC1	0,624	8,846E-19	*IFITM3*	0,616	5,422E-14	*TTC27*	0,610	7,413E-24	*MRPS16*	0,602	3,432E-23
NUP205	0,624	7,604E-24	*SSSCA1*	0,616	3,782E-17	*PRSS3*	0,610	4,609E-19	*MED22*	0,602	2,101E-23
SLC25A22	0,624	2,451E-25	*GLTPD1*	0,616	5,709E-18	*ILF3*	0,610	7,062E-20	*PLK1*	0,602	6,625E-12
KIAA1524	0,623	1,953E-22	*ATL3*	0,616	2,887E-21	*POPDC3*	0,610	3,254E-13	*ABHD8*	0,602	2,208E-20
OAS3	0,623	2,110E-11	*NDC80*	0,616	8,759E-26	*CENPK*	0,610	2,831E-19	*CD151*	0,602	9,244E-28
C1orf112	0,623	3,223E-16	*MYC*	0,616	5,726E-19	*FIGNL1*	0,609	1,347E-18	*NR2C2AP*	0,602	7,251E-21
STK40	0,623	3,488E-23	*F8A1*	0,616	1,203E-18	*DPAGT1*	0,609	2,535E-13	*SNRPF*	0,601	1,689E-27
C16orf75	0,623	1,355E-17	*CXCL16*	0,616	1,162E-21	*SNHG6*	0,608	3,188E-17	*FCRLB*	0,601	7,475E-22
MPST	0,622	3,345E-15	*H1F0*	0,616	4,359E-19	*NCLN*	0,608	2,744E-19	*FARS2*	0,601	3,998E-19
SLC25A13	0,622	1,095E-16	*DCPS*	0,615	8,299E-20	*PERP*	0,608	2,709E-13	*ECE2*	0,601	6,333E-23
RALY	0,622	8,275E-21	*CHES1*	0,615	2,385E-22	*RPIA*	0,608	1,262E-19	*ZNF395*	0,600	3,106E-22
RAVER1	0,621	4,671E-16	*DHRS1*	0,615	2,763E-20	*BANF1*	0,607	1,120E-26	*FAM111A*	0,600	8,057E-19
PARP1	0,621	1,005E-20	*MRPS27*	0,615	4,595E-13	*KIF15*	0,607	1,544E-22	*VRK1*	0,600	1,347E-20
PKIA	0,621	4,166E-24	*ANKRD50*	0,615	1,735E-20	*WDR77*	0,606	9,638E-15	*THOP1*	0,600	2,530E-23
POLR3G	0,621	1,325E-14	*BYSL*	0,615	2,127E-26	*DEPDC1B*	0,606	1,246E-16	*SNORA12*	0,599	4,213E-17
YEATS4	0,620	5,542E-12	*HSPE1*	0,614	1,998E-03	*NDUFAB1*	0,606	2,334E-24	*MRPS26*	0,599	4,201E-30
CASP6	0,620	4,678E-10	*PHC2*	0,614	3,071E-17	*TMEM97*	0,605	1,113E-20	*RPS6KB2*	0,599	3,190E-18
NASP	0,620	4,968E-18	*WDHD1*	0,614	1,908E-17	*NOB1*	0,605	7,664E-14	*UCHL5IP*	0,599	4,784E-28
C20orf72	0,620	9,007E-22	*EIF3M*	0,614	2,926E-18	*MCM4*	0,605	2,080E-16	*IRF1*	0,599	2,198E-22
THOC6	0,620	6,119E-23	*UTP18*	0,614	1,139E-08	*SMUG1*	0,605	1,282E-22	*DCAF7*	0,599	1,073E-25
ZNF787	0,619	3,775E-26	*HPS1*	0,613	6,116E-22	*GULP1*	0,605	3,404E-13	*KIF22*	0,598	2,093E-16

Supplementary Table S4.9: continued

GPX1	0,598	8,766E-19
POM121C	0,598	1,080E-25
MUL1	0,597	2,095E-22
ZMAT2	0,597	3,840E-29
TMBIM4	0,596	2,150E-31
C3orf10	0,596	2,436E-21
MRPL1	0,596	1,012E-17
NUP62	0,596	6,858E-24
TFDP1	0,596	4,000E-15
TYW3	0,596	1,175E-18
COPS7A	0,595	4,743E-17
GNA11	0,594	3,842E-21
MCM6	0,594	8,048E-26
NUP35	0,593	1,586E-20
BARD1	0,593	1,071E-25
PFAS	0,592	9,434E-24
RRS1	0,592	6,695E-22
ID2	0,592	1,801E-22
MGST2	0,592	4,971E-28
PTMS	0,592	3,747E-25
RNF144A	0,591	8,342E-17
MED25	0,591	3,611E-35
DHX37	0,591	4,645E-22
ATP5G1	0,590	1,601E-22
MRPL48	0,590	1,609E-24
GPR81	0,589	2,110E-18
HJURP	0,589	3,122E-21
C17orf93	0,589	2,658E-17
SLC5A6	0,589	1,591E-23
DTL	0,588	8,442E-16
ADCY3	0,588	3,550E-21
TMEM123	0,588	5,163E-21
HSPBAP1	0,588	1,436E-21
MRPS35	0,587	9,596E-19
SH3GL1	0,586	3,709E-20
HMBS	0,586	1,033E-19
POLR3C	0,586	4,842E-24
COX10	0,586	1,356E-23
C8orf55	0,586	3,037E-30
B3GALT6	0,585	1,421E-24
TUBA1A	0,585	2,759E-20
GMNN	0,584	6,585E-16
PAXIP1	0,584	6,558E-25
RPL28	0,584	1,644E-15
GPR110	0,583	7,234E-25
PRNP	0,583	2,143E-25
GPSM2	0,583	4,294E-28
NRM	0,582	5,939E-17
TOMM40L	0,582	9,128E-24
TMEM216	0,582	8,502E-21
BUB1B	0,582	5,588E-17
PSMG4	0,581	2,024E-24
ATP6V0D1	0,581	7,178E-22
PECR	0,581	7,197E-31
CENPM	0,580	3,665E-25
CDC20	0,580	5,396E-25
CWF19L1	0,579	9,587E-22
ZDHHC5	0,579	2,972E-21
ABHD14A	0,579	1,367E-28
SNORD31	0,578	7,036E-17
AP3M2	0,578	6,300E-27
CDK5	0,578	1,026E-13
CENPL	0,578	1,551E-17
ZDHHC8	0,577	3,776E-18
KIAA1522	0,577	1,908E-18
BRIX1	0,577	9,967E-18
CDKN2B	0,577	1,432E-23
SLC25A3	0,577	2,684E-21
KNTC1	0,576	3,412E-21
TUBB	0,576	2,830E-29
HMMR	0,576	9,758E-17
STMN3	0,576	2,027E-31
PAQR4	0,575	9,892E-22
CCDC28A	0,575	8,369E-21
CCDC5	0,574	2,017E-15
CENPF	0,574	1,516E-23
C8orf33	0,574	4,557E-27
COQ3	0,573	2,452E-22
CDIPT	0,573	2,099E-18
DSN1	0,572	1,001E-12
TRIM4	0,572	1,097E-24
WDR4	0,572	4,740E-23
TXNIP	0,571	5,238E-28
RFC5	0,571	3,182E-19
CDC7	0,571	1,350E-17
ADNP2	0,571	2,518E-18
KIF4A	0,570	2,303E-21
SFXN4	0,570	2,879E-25
WDR67	0,568	2,698E-33
NOP16	0,568	8,397E-25
MED16	0,568	2,028E-15
METAP1	0,567	3,889E-23
ALDH1B1	0,567	1,272E-11
ARL6IP1	0,567	4,504E-23
PIGC	0,567	1,413E-19
TTK	0,567	3,407E-16
C11orf83	0,566	2,420E-24
TUBB3	0,566	3,323E-24
C1orf135	0,565	2,190E-31
RHOG	0,565	7,785E-29
FOXM1	0,565	3,944E-23
UBQLN4	0,565	2,331E-17
MAPK13	0,565	9,565E-23
LYAR	0,565	7,137E-23
RRAGB	0,564	3,483E-25
TMEM145	0,564	1,160E-21
RFWD3	0,564	1,980E-29
PHB	0,563	4,031E-31
MED30	0,563	1,782E-19
LRRC47	0,563	3,523E-27
CTDSP2	0,562	5,088E-28
TRIP6	0,562	2,451E-15
MTHFD1	0,561	2,748E-25
ACTL6A	0,561	1,250E-16
RAD54L	0,561	8,287E-27
SURF4	0,561	9,759E-26
BACE2	0,560	5,516E-34
GTSE1	0,558	3,072E-26
C11orf67	0,558	7,133E-27
BCL7C	0,558	3,895E-24
RASL11A	0,558	5,759E-16
HMGB1L1	0,558	3,645E-10
HSBP1	0,557	3,929E-28
ANLN	0,557	5,203E-26
CKAP5	0,557	1,089E-22
DEK	0,556	9,878E-27
PXN	0,555	6,586E-28
ETV4	0,555	1,513E-19
UBN1	0,555	1,184E-15
DNAJC9	0,554	2,067E-26
ZNHIT2	0,553	3,201E-19
DCK	0,553	6,797E-16

Supplementary Table S4.9: continued

EXTL3	0,553	7,530E-21	*DUT*	0,540	2,390E-29	*BUB1*	0,524	7,920E-23	*FAM64A*	0,505	2,638E-27
C14orf106	0,552	4,804E-24	*KATNB1*	0,539	1,494E-26	*PSMG1*	0,524	2,360E-26	*HNRNPA0*	0,505	4,346E-22
TMEM19	0,552	1,444E-19	*APOBEC3B*	0,538	7,132E-21	*HNRPA1P4*	0,523	1,542E-21	*ZNF362*	0,505	9,126E-25
ARHGAP1	0,551	3,711E-23	*UBA52*	0,538	6,081E-27	*HEATR2*	0,522	8,741E-23	*POLA1*	0,504	9,147E-33
WDR51A	0,551	1,138E-31	*TMEM126A*	0,538	1,330E-24	*SAAL1*	0,522	4,576E-36	*ZNF689*	0,504	1,354E-34
SNORD96A	0,550	5,448E-19	*VEGFC*	0,538	3,645E-21	*HAUS4*	0,521	1,930E-25	*FBXO5*	0,502	3,975E-21
SAC3D1	0,550	5,727E-25	*SLC25A6*	0,537	6,796E-23	*PITPNC1*	0,521	5,554E-23	*RFC4*	0,501	6,749E-29
KIAA0114	0,550	2,015E-26	*BDNF*	0,537	2,386E-24	*CHEK1*	0,521	8,774E-26	*SNX3*	0,500	1,429E-38
IMPDH2	0,550	4,786E-18	*MLLT11*	0,535	2,436E-24	*ARL6IP6*	0,520	1,451E-19	*ERAL1*	0,499	3,785E-32
C1orf86	0,549	2,131E-28	*C13orf34*	0,535	2,508E-16	*TMEM109*	0,519	3,636E-34	*B4GALT3*	0,499	3,950E-17
BEX1	0,549	5,436E-21	*UBIAD1*	0,535	2,779E-28	*PLK4*	0,519	5,407E-19	*RNF144*	0,498	1,630E-35
CDCA4	0,549	4,479E-27	*HN1*	0,535	2,570E-13	*C19orf48*	0,518	1,980E-29	*E2F2*	0,498	5,575E-24
TSGA14	0,548	1,057E-21	*ALS2CR4*	0,534	5,981E-25	*CLPTM1*	0,518	5,942E-24	*PPM1G*	0,498	7,370E-39
LMNB2	0,548	1,335E-28	*GART*	0,534	4,732E-33	*PFKL*	0,517	2,098E-20	*PTPMT1*	0,498	8,062E-25
SLMAP	0,548	4,516E-24	*C15orf23*	0,533	4,262E-28	*PHF19*	0,517	2,081E-32	*POLQ*	0,498	8,090E-27
CKAP2L	0,547	4,575E-29	*NEDD8*	0,532	1,226E-10	*LRRC20*	0,517	2,529E-23	*NDUFA3*	0,496	1,254E-34
TFCP2	0,547	1,179E-22	*CHAF1B*	0,531	3,373E-26	*CDCA3*	0,516	6,917E-34	*CDC25A*	0,496	4,144E-33
HAS3	0,546	6,291E-18	*ECT2*	0,530	5,781E-18	*ALG3*	0,516	1,955E-31	*EIF4EBP2*	0,495	2,891E-25
LMNB1	0,546	4,229E-18	*BOLA3*	0,530	7,106E-24	*CENPE*	0,515	2,530E-23	*PDLIM1*	0,495	1,304E-44
FSCN1	0,545	1,203E-28	*MCM2*	0,530	3,091E-24	*GGCT*	0,515	8,358E-27	*TOMM40*	0,494	9,590E-39
EMG1	0,545	1,914E-26	*TWIST1*	0,529	1,905E-24	*C13orf37*	0,515	6,712E-30	*RRM1*	0,494	1,249E-33
ASPM	0,544	1,451E-24	*STEAP1*	0,528	1,431E-25	*DPH2*	0,513	8,925E-30	*SNHG1*	0,494	5,857E-24
MAP4K4	0,544	6,161E-20	*POLR1D*	0,528	7,356E-29	*PTGES2*	0,512	1,153E-30	*XRCC5*	0,494	5,266E-26
SRM	0,544	2,864E-17	*IRAK1*	0,528	8,637E-23	*NETO2*	0,511	1,607E-21	*RBM9*	0,493	6,310E-29
POLD1	0,544	1,048E-23	*PRR11*	0,527	1,270E-19	*CENPB*	0,511	8,130E-30	*RRM2*	0,493	2,243E-25
COX7A2L	0,543	5,226E-25	*APEX1*	0,526	4,919E-34	*UNG*	0,508	6,003E-22	*CKS1B*	0,493	1,300E-26
BFAR	0,542	1,014E-21	*INCENP*	0,526	2,577E-36	*KIF11*	0,508	1,324E-20	*NUP107*	0,493	4,807E-33
MAF1	0,542	3,808E-26	*CCT6A*	0,525	3,035E-20	*HMGB2*	0,508	3,151E-26	*C16orf35*	0,492	1,297E-28
EXOSC9	0,541	7,738E-33	*KCTD10*	0,525	2,642E-20	*POLA2*	0,507	2,206E-23	*MMACHC*	0,492	1,406E-24
RACGAP1	0,541	5,622E-24	*PITX1*	0,525	1,301E-28	*NXT1*	0,507	4,039E-31	*BTBD2*	0,492	9,017E-39
EEF1E1	0,541	5,536E-29	*C16orf52*	0,524	1,142E-20	*CXCL6*	0,506	7,709E-21	*ARHGAP24*	0,491	4,203E-26
NRGN	0,541	7,212E-18	*NDE1*	0,524	1,539E-18	*FANCG*	0,506	1,894E-36	*RTN4*	0,491	9,892E-19
AQP11	0,540	2,812E-19	*TIMM9*	0,524	3,017E-21	*HRASLS3*	0,505	5,477E-23	*TMEM27*	0,490	3,313E-30

Supplementary Table S4.9: continued

CDS1	0,490	6,823E-27	*QTRT1*	0,471	2,291E-13	*TOP2A*	0,448	1,845E-34	*REPIN1*	0,414	5,385E-39
MELK	0,490	1,983E-28	*MRPL36*	0,470	2,261E-40	*CDKN2C*	0,447	8,658E-31	*SLC35A4*	0,414	2,146E-27
LXN	0,489	8,188E-25	*KIFC1*	0,470	3,458E-31	*H2AFX*	0,446	2,155E-28	*IFRD2*	0,413	1,356E-28
BCL2L12	0,489	3,699E-29	*BAG3*	0,470	3,100E-32	*TRAPPC1*	0,445	2,603E-37	*ZWILCH*	0,412	5,696E-21
MICB	0,487	4,452E-33	*KIF23*	0,469	1,773E-21	*TTF2*	0,445	2,233E-23	*MAD2L1*	0,412	7,439E-29
NFIX	0,486	7,476E-42	*CEP55*	0,469	1,207E-28	*NHP2*	0,443	1,161E-37	*KIF20A*	0,408	2,080E-40
CKS2	0,486	6,455E-22	*ATP6V0C*	0,469	1,307E-31	*RBBP8*	0,443	2,177E-37	*C12orf48*	0,407	7,638E-43
KIF14	0,486	7,008E-24	*MNS1*	0,468	8,125E-20	*TYMS*	0,440	5,352E-31	*CDCA7*	0,406	7,914E-43
TPX2	0,485	3,927E-33	*SUPT4H1*	0,468	1,438E-34	*SUV39H1*	0,440	5,239E-36	*DAP*	0,404	6,056E-44
UBE2I	0,484	3,438E-29	*RGS7*	0,467	7,271E-26	*PBK*	0,439	2,424E-34	*UHRF1*	0,404	3,891E-39
CCNG1	0,484	4,566E-25	*C2orf7*	0,466	4,139E-26	*PGD*	0,437	1,297E-36	*PPIL1*	0,403	5,025E-32
C3orf14	0,483	9,121E-28	*RFC3*	0,465	3,426E-25	*GLOD4*	0,436	6,203E-29	*CABLES1*	0,403	1,713E-31
NR1H2	0,483	6,843E-23	*FAM36A*	0,463	7,203E-19	*TIMELESS*	0,435	3,922E-41	*PRC1*	0,403	1,335E-32
DSCC1	0,483	1,721E-18	*OIP5*	0,463	7,069E-43	*SMARCD1*	0,433	1,585E-32	*JMJD8*	0,398	5,442E-30
PIGN	0,482	1,613E-28	*FEN1*	0,461	7,602E-24	*NUP85*	0,433	5,026E-27	*CDC2*	0,398	1,450E-26
G6PC3	0,482	7,892E-25	*RADS4B*	0,461	4,492E-25	*EHD1*	0,433	6,715E-30	*TROAP*	0,398	1,509E-35
CLEC2D	0,482	1,451E-14	*FANCI*	0,460	7,419E-27	*DDX54*	0,432	9,889E-29	*SHISA2*	0,397	8,118E-29
DIMT1L	0,482	3,999E-36	*ATAD2*	0,460	1,361E-15	*NGRN*	0,431	3,341E-32	*MDK*	0,395	8,950E-41
PLSCR1	0,482	2,787E-22	*C16orf33*	0,459	6,052E-28	*CDH11*	0,431	4,352E-33	*CLCN7*	0,394	3,268E-41
PIGT	0,482	1,960E-37	*PRIM1*	0,459	3,689E-22	*TMEM54*	0,430	1,746E-31	*SEPN1*	0,391	3,638E-44
SLC25A19	0,481	1,964E-39	*CENPA*	0,458	1,660E-30	*NCAPG*	0,428	1,083E-29	*FAM83D*	0,389	6,301E-35
NUSAP1	0,480	1,632E-18	*VARS*	0,458	1,522E-35	*EMP1*	0,428	2,063E-28	*POLE2*	0,388	3,287E-23
C9orf30	0,479	3,601E-19	*PLCXD3*	0,458	1,613E-27	*TMEM189*	0,427	1,306E-21	*AURKA*	0,388	1,687E-25
KATNAL1	0,479	4,218E-29	*CCNB1*	0,457	9,141E-19	*PAK4*	0,427	2,481E-20	*KIF2C*	0,387	8,351E-37
CCNA2	0,476	1,751E-21	*CCDC86*	0,456	8,547E-20	*CDK4*	0,426	3,404E-40	*NTSR1*	0,386	1,959E-34
MESP1	0,475	4,508E-31	*UBE2T*	0,456	2,281E-36	*GINS3*	0,425	1,479E-28	*TRIP13*	0,386	1,013E-30
RPL13A	0,474	1,937E-28	*CDCA8*	0,454	2,012E-36	*CENPN*	0,424	1,992E-19	*CCNB2*	0,385	8,758E-34
RHBDF2	0,474	2,943E-28	*KIF20B*	0,454	7,287E-29	*CDT1*	0,423	9,144E-40	*C11orf82*	0,385	4,625E-34
CBX6	0,473	8,475E-38	*C17orf53*	0,452	5,671E-34	*CDKN3*	0,423	3,720E-41	*HMGA1*	0,384	1,568E-41
SDHAF2	0,473	1,507E-32	*TTYH3*	0,452	3,358E-30	*LCP1*	0,420	8,422E-33	*EPN1*	0,380	1,228E-45
MRPS30	0,472	6,717E-27	*ANKRD22*	0,452	1,746E-27	*HAS2*	0,420	1,009E-31	*RRP7A*	0,379	4,868E-37
EXOSC6	0,472	2,131E-21	*ZNF358*	0,451	6,022E-28	*CLDN11*	0,417	3,104E-29	*RAD51AP1*	0,374	6,956E-24
ATP6V0E2	0,471	1,206E-35	*ANPEP*	0,448	1,969E-26	*ATP5SL*	0,415	2,198E-33	*CDC45L*	0,372	1,402E-34

Supplementary Table S4.9: continued

CYB5R3	0,372	7,446E-29
TMEM158	0,371	1,107E-28
HIST1H4C	0,370	4,163E-45
FOXQ1	0,368	3,404E-38
ENOPH1	0,365	8,211E-23
ZWINT	0,361	1,864E-30
SLC2A4RG	0,358	1,410E-30
CIRBP	0,358	2,520E-36
C6orf173	0,356	1,941E-29

PDCD6	0,354	1,527E-28
ASF1B	0,350	4,948E-33
POLE3	0,350	1,692E-31
SLC35F2	0,349	1,572E-30
FZD8	0,348	1,683E-38
HADH2	0,347	1,318E-29
C5orf46	0,344	9,388E-47
HEBP1	0,341	2,759E-36
DLGAP5	0,332	2,964E-29

MGC87042	0,328	1,107E-26
AURKB	0,327	1,454E-24
CALB2	0,322	2,929E-29
TPP1	0,318	3,612E-40
PTTG1	0,318	1,056E-28
CDCA5	0,316	2,138E-54
COMMD4	0,314	1,665E-28
NPM3	0,310	4,553E-35
HSD17B10	0,303	4,055E-41

GINS2	0,300	4,185E-42
TK1	0,293	3,815E-32
SET	0,280	4,783E-39
PTTG3P	0,263	1,726E-37
LGALS3BP	0,261	2,709E-27
DYNLRB1	0,248	2,020E-35
AHCY	0,222	8,607E-54

Supplementary Table S4.10A: Functional annotation of genes differentially regulated upon *L1CAM* knockdown in PC-3 cells

Functional annotation	Genes	p-value	z-score*	# Genes†
Differentiation of cells	*TGFBR2, IL1B, IL6, EPOR, LIF, HBEGF, RTN4, NGF, IL23A, GRB2*	2.47E-09	3.188	136
Interphase	*TGFBR2, ID2, CDKN1C, CDk2, RBBP8, AR, BIRC5, CDk4, TCF3, CDC2, E2F5*	1.01E-07	-2.396	33
Colony formation of tumor cell lines	*KPNA2, IFITM3, CYR61, KRT19, SEMA3B, HPGD, MDK, RASD1, E2F5, GRB2*	3.72E-06	-2.247	24
Invasion of cancer cells	*S100P, AHCY, IL6, KLK6, ITGB4, CTSL, ITGA1, PLAUR, FERMT2, GDF15*	1.58E-05	2.354	13
Cell death	*ADM, TOP2A, IL1B, AR, PTHLH, TGM2, DUSP1, DDIT4, TNFRSR6B, PDGFB*	1.63E-05	-2.082	43

Top 10 differentially expressed genes in our dataset that were annotated to a function. A gene was selected when its annotation to the indicated function was based on at least two findings in the Ingenuity knowledge base. *Activation z-score is a measure of predicted change (increase or decrease) of the process. †Total number of genes supporting a specific functional annotation.

Supplementary Table S4.10B: Canonical pathway analysis of genes differentially regulated upon *L1CAM* knockdown in PC-3 cells

Ingenuity Canonical Pathways	p-value	z-score*	# Genes†
ATM Signaling	5.21E-07	1.633	33(80)
Interferon Signaling	1.75E-06	3.317	11(36)
PPAR Signaling	4.25E-05	-3.357	16(95)
Pancreatic Adenocarcinoma Signaling	5.66E-04	2.53	16(118)
VDR/RXR Activation	9.53E-04	2	8(789)

Significantly enriched canonical pathways across the dataset of commonly regulated genes between T/E III and VI are shown. *Activation z-score is a measure of predicted change (activated or reduced) of the process. †Number of genes in the dataset, which are represented in the pathway. Numbers in brackets depict the total number of genes in the pathway in the reference gene set.

REFERENCES

1. Guate JL, Escaf S, Menendez CL, del Valle M and Vega JA. Neuroendocrine cells in benign prostatic hyperplasia and prostatic carcinoma: effect of hormonal treatment. Urol Int. 1997; 59(3):149-153.
2. Lapuk AV, Wu C, Wyatt AW, McPherson A, McConeghy BJ, Brahmbhatt S, Mo F, Zoubeidi A, Anderson S, Bell RH, Haegert A, Shukin R, Wang Y, Fazli L, Hurtado-Coll A, Jones EC, et al. From sequence to molecular pathology, and a mechanism driving the neuroendocrine phenotype in prostate cancer. J Pathol. 2012; 227(3):286-297.
3. Miyoshi Y, Uemura H, Kitami K, Satomi Y, Kubota Y and Hosaka M. Neuroendocrine differentiated small cell carcinoma presenting as recurrent prostate cancer after androgen deprivation therapy. BJU Int. 2001; 88(9):982-983.
4. Burchardt T, Burchardt M, Chen MW, Cao Y, de la Taille A, Shabsigh A, Hayek O, Dorai T and Buttyan R. Transdifferentiation of prostate cancer cells to a neuroendocrine cell phenotype in vitro and in vivo. J Urol. 1999; 162(5):1800-1805.
5. Germann M, Wetterwald A, Guzman-Ramirez N, van der Pluijm G, Culig Z, Cecchini MG, Williams ED and Thalmann GN. Stem-like cells with luminal progenitor phenotype survive castration in human prostate cancer. Stem Cells. 2012; 30(6):1076-1086.
6. Stratton M, Evans DJ and Lampert IA. Prostatic adenocarcinoma evolving into carcinoid: selective effect of hormonal treatment? J Clin Pathol. 1986; 39(7):750-756.
7. Wang HT, Yao YH, Li BG, Tang Y, Chang JW and Zhang J. Neuroendocrine Prostate Cancer (NEPC) progressing from conventional prostatic adenocarcinoma: factors associated with time to development of NEPC and survival from NEPC diagnosis-a systematic review and pooled analysis. J Clin Oncol. 2014; 32(30):3383-3390.
8. Gillessen S, Omlin A, Attard G, de Bono JS, Efstathiou E, Fizazi K, Halabi S, Nelson PS, Sartor O, Smith MR, Soule HR, Akaza H, Beer TM, Beltran H, Chinnaiyan AM, Daugaard G, et al. Management of patients with advanced prostate cancer: recommendations of the St Gallen Advanced Prostate Cancer Consensus Conference (APCCC) 2015. Ann Oncol. 2015; 26(8):1589-1604.
9. Beltran H, Rickman DS, Park K, Chae SS, Sboner A, MacDonald TY, Wang Y, Sheikh KL, Terry S, Tagawa ST, Dhir R, Nelson JB, de la Taille A, Allory Y, Gerstein MB, Perner S, et al. Molecular characterization of neuroendocrine prostate cancer and identification of new drug targets. Cancer Discov. 2011; 1(6):487-495.
10. Epstein JI, Amin MB, Beltran H, Lotan TL, Mosquera JM, Reuter VE, Robinson BD, Troncoso P and Rubin MA. Proposed morphologic classification of prostate cancer with neuroendocrine differentiation. Am J Surg Pathol. 2014; 38(6):756-767.
11. Qi J, Pellecchia M and Ronai ZA. The Siah2-HIF-FoxA2 axis in prostate cancer - new markers and therapeutic opportunities. Oncotarget. 2010; 1(5):379-385.
12. Hirano D, Jike T, Okada Y, Minei S, Sugimoto S, Yamaguchi K, Yoshikawa T, Hachiya T, Yoshida T and Takimoto Y. Immunohistochemical and ultrastructural features of neuroendocrine differentiated carcinomas of the prostate: an immunoelectron microscopic study. Ultrastruct Pathol. 2005; 29(5):367-375.
13. Bonkhoff H, Stein U and Remberger K. Endocrine-paracrine cell types in the prostate and prostatic adenocarcinoma are postmitotic cells. Hum Pathol. 1995; 26(2):167-170.
14. Sauer CG, Roemer A and Grobholz R. Genetic analysis of neuroendocrine tumor cells in prostatic carcinoma. Prostate. 2006; 66(3):227-234.
15. Lotan TL, Gupta NS, Wang W, Toubaji A, Haffner MC, Chaux A, Hicks JL, Meeker AK, Bieberich CJ, De Marzo AM, Epstein JI and Netto GJ. ERG gene rearrangements are common in prostatic small cell carcinomas. Mod Pathol. 2011; 24(6):820-828.
16. Hansel DE, Nakayama M, Luo J, Abukhdeir AM, Park BH, Bieberich CJ, Hicks JL, Eisenberger M, Nelson WG, Mostwin JL and De Marzo AM. Shared TP53 gene mutation in morphologically and phenotypically distinct concurrent primary small cell neuroendocrine carcinoma and adenocarcinoma of the prostate. Prostate. 2009; 69(6):603-609.

17. Huang J, Yao JL, di Sant'Agnese PA, Yang Q, Bourne PA and Na Y. Immunohistochemical characterization of neuroendocrine cells in prostate cancer. Prostate. 2006; 66(13):1399-1406.
18. Bonkhoff H, Stein U and Remberger K. Multidirectional differentiation in the normal, hyperplastic, and neoplastic human prostate: simultaneous demonstration of cell-specific epithelial markers. Hum Pathol. 1994; 25(1):42-46.
19. Wyatt AW, Mo F, Wang K, McConeghy B, Brahmbhatt S, Jong L, Mitchell DM, Johnston RL, Haegert A, Li E, Liew J, Yeung J, Shrestha R, Lapuk AV, McPherson A, Shukin R, et al. Heterogeneity in the inter-tumor transcriptome of high risk prostate cancer. Genome Biol. 2014; 15(8):426.
20. Brase JC, Johannes M, Mannsperger H, Falth M, Metzger J, Kacprzyk LA, Andrasiuk T, Gade S, Meister M, Sirma H, Sauter G, Simon R, Schlomm T, Beissbarth T, Korf U, Kuner R, et al. TMPRSS2-ERG -specific transcriptional modulation is associated with prostate cancer biomarkers and TGF-beta signaling. BMC cancer. 2011; 11:507.
21. Weischenfeldt J, Simon R, Feuerbach L, Schlangen K, Weichenhan D, Minner S, Wuttig D, Warnatz HJ, Stehr H, Rausch T, Jager N, Gu L, Bogatyrova O, Stutz AM, Claus R, Eils J, et al. Integrative genomic analyses reveal an androgen-driven somatic alteration landscape in early-onset prostate cancer. Cancer Cell. 2013; 23(2):159-170.
22. Tranchevent LC, Capdevila FB, Nitsch D, De Moor B, De Causmaecker P and Moreau Y. A guide to web tools to prioritize candidate genes. Brief Bioinform. 2011; 12(1):22-32.
23. Taylor BS, Schultz N, Hieronymus H, Gopalan A, Xiao Y, Carver BS, Arora VK, Kaushik P, Cerami E, Reva B, Antipin Y, Mitsiades N, Landers T, Dolgalev I, Major JE, Wilson M, et al. Integrative genomic profiling of human prostate cancer. Cancer Cell. 2010; 18(1):11-22.
24. Castro F, Dirks WG, Fahnrich S, Hotz-Wagenblatt A, Pawlita M and Schmitt M. High-throughput SNP-based authentication of human cell lines. Int J Cancer. 2013; 132(2):308-314.
25. Schmitt M and Pawlita M. High-throughput detection and multiplex identification of cell contaminations. Nucleic Acids Res. 2009; 37(18):e119.
26. Ratz L, Laible M, Kacprzyk LA, Wittig-Blaich SM, Tolstov Y, Duensing S, Altevogt P, Klauck SM and Sultmann H. TMPRSS2:ERG gene fusion variants induce TGF-beta signaling and epithelial to mesenchymal transition in human prostate cancer cells. Oncotarget. 2017; 8(15):25115-25130.
27. Pfaffl MW. A new mathematical model for relative quantification in real-time RT-PCR. Nucleic Acids Res. 2001; 29(9):e45.
28. Tsai H, Morais CL, Alshalalfa M, Tan HL, Haddad Z, Hicks J, Gupta N, Epstein JI, Netto GJ, Isaacs WB, Luo J, Mehra R, Vessella RL, Karnes RJ, Schaeffer EM, Davicioni E, et al. Cyclin D1 Loss Distinguishes Prostatic Small-Cell Carcinoma from Most Prostatic Adenocarcinomas. Clin Cancer Res. 2015; 21(24):5619-5629.
29. Duggan A, Madathany T, de Castro SC, Gerrelli D, Guddati K and Garcia-Anoveros J. Transient expression of the conserved zinc finger gene INSM1 in progenitors and nascent neurons throughout embryonic and adult neurogenesis. J Comp Neurol. 2008; 507(4):1497-1520.
30. Mellitzer G, Bonne S, Luco RF, Van De Casteele M, Lenne-Samuel N, Collombat P, Mansouri A, Lee J, Lan M, Pipeleers D, Nielsen FC, Ferrer J, Gradwohl G and Heimberg H. IA1 is NGN3-dependent and essential for differentiation of the endocrine pancreas. EMBO J. 2006; 25(6):1344-1352.
31. Goto Y, De Silva MG, Toscani A, Prabhakar BS, Notkins AL and Lan MS. A novel human insulinoma-associated cDNA, IA-1, encodes a protein with "zinc-finger" DNA-binding motifs. J Biol Chem. 1992; 267(21):15252-15257.
32. Mertz KD, Setlur SR, Dhanasekaran SM, Demichelis F, Perner S, Tomlins S, Tchinda J, Laxman B, Vessella RL, Beroukhim R, Lee C, Chinnaiyan AM and Rubin MA. Molecular characterization of TMPRSS2-ERG gene fusion in the NCI-H660 prostate cancer cell line: a new perspective for an old model. Neoplasia. 2007; 9(3):200-206.
33. Bello D, Webber MM, Kleinman HK, Wartinger DD and Rhim JS. Androgen responsive adult human prostatic epithelial cell lines immortalized by human papillomavirus 18. Carcinogenesis. 1997; 18(6):1215-1223.
34. Wiedenmann B, Franke WW, Kuhn C, Moll R and Gould VE. Synaptophysin: a marker protein for neuroendocrine cells and neoplasms. Proc Natl Acad Sci U S A. 1986; 83(10):3500-3504.

35. Ballas N, Grunseich C, Lu DD, Speh JC and Mandel G. REST and its corepressors mediate plasticity of neuronal gene chromatin throughout neurogenesis. Cell. 2005; 121(4):645-657.
36. Katsetos CD, Legido A, Perentes E and Mork SJ. Class III beta-tubulin isotype: a key cytoskeletal protein at the crossroads of developmental neurobiology and tumor neuropathology. J Child Neurol. 2003; 18(12):851-866; discussion 867.
37. Maness PF and Schachner M. Neural recognition molecules of the immunoglobulin superfamily: signaling transducers of axon guidance and neuronal migration. Nat Neurosci. 2007; 10(1):19-26.
38. Huszar M, Pfeifer M, Schirmer U, Kiefel H, Konecny GE, Ben-Arie A, Edler L, Munch M, Muller-Holzner E, Jerabek-Klestil S, Abdel-Azim S, Marth C, Zeimet AG, Altevogt P and Fogel M. Up-regulation of L1CAM is linked to loss of hormone receptors and E-cadherin in aggressive subtypes of endometrial carcinomas. J Pathol. 2010; 220(5):551-561.
39. Held-Feindt J, Schmelz S, Hattermann K, Mentlein R, Mehdorn HM and Sebens S. The neural adhesion molecule L1CAM confers chemoresistance in human glioblastomas. Neurochem Int. 2012; 61(7):1183-1191.
40. Trasino SE, Harrison EH and Wang TT. Androgen regulation of aldehyde dehydrogenase 1A3 (ALDH1A3) in the androgen-responsive human prostate cancer cell line LNCaP. Exp Biol Med (Maywood). 2007; 232(6):762-771.
41. Le Magnen C, Bubendorf L, Rentsch CA, Mengus C, Gsponer J, Zellweger T, Rieken M, Thalmann GN, Cecchini MG, Germann M, Bachmann A, Wyler S, Heberer M and Spagnoli GC. Characterization and clinical relevance of ALDHbright populations in prostate cancer. Clin Cancer Res. 2013; 19(19):5361-5371.
42. Casanova-Salas I, Masia E, Arminan A, Calatrava A, Mancarella C, Rubio-Briones J, Scotlandi K, Vicent MJ and Lopez-Guerrero JA. MiR-187 Targets the Androgen-Regulated Gene ALDH1A3 in Prostate Cancer. PLoS One. 2015; 10(5):e0125576.
43. Gomes IM, Arinto P, Lopes C, Santos CR and Maia CJ. STEAP1 is overexpressed in prostate cancer and prostatic intraepithelial neoplasia lesions, and it is positively associated with Gleason score. Urol Oncol. 2014; 32(1):53 e23-59.
44. Ihlaseh-Catalano SM, Drigo SA, de Jesus CM, Domingues MA, Trindade Filho JC, de Camargo JL and Rogatto SR. STEAP1 protein overexpression is an independent marker for biochemical recurrence in prostate carcinoma. Histopathology. 2013; 63(5):678-685.
45. Cox ME, Deeble PD, Lakhani S and Parsons SJ. Acquisition of neuroendocrine characteristics by prostate tumor cells is reversible: implications for prostate cancer progression. Cancer Res. 1999; 59(15):3821-3830.
46. Deeble PD, Murphy DJ, Parsons SJ and Cox ME. Interleukin-6- and cyclic AMP-mediated signaling potentiates neuroendocrine differentiation of LNCaP prostate tumor cells. Mol Cell Biol. 2001; 21(24):8471-8482.
47. Cox ME, Deeble PD, Bissonette EA and Parsons SJ. Activated 3',5'-cyclic AMP-dependent protein kinase is sufficient to induce neuroendocrine-like differentiation of the LNCaP prostate tumor cell line. J Biol Chem. 2000; 275(18):13812-13818.
48. Mosquera JM, Beltran H, Park K, MacDonald TY, Robinson BD, Tagawa ST, Perner S, Bismar TA, Erbersdobler A, Dhir R, Nelson JB, Nanus DM and Rubin MA. Concurrent AURKA and MYCN gene amplifications are harbingers of lethal treatment-related neuroendocrine prostate cancer. Neoplasia. 2013; 15(1):1-10.
49. Lee JK, Phillips JW, Smith BA, Park JW, Stoyanova T, McCaffrey EF, Baertsch R, Sokolov A, Meyerowitz JG, Mathis C, Cheng D, Stuart JM, Shokat KM, Gustafson WC, Huang J and Witte ON. N-Myc Drives Neuroendocrine Prostate Cancer Initiated from Human Prostate Epithelial Cells. Cancer Cell. 2016; 29(4):536-547.
50. Otto SJ, McCorkle SR, Hover J, Conaco C, Han JJ, Impey S, Yochum GS, Dunn JJ, Goodman RH and Mandel G. A new binding motif for the transcriptional repressor REST uncovers large gene networks devoted to neuronal functions. J Neurosci. 2007; 27(25):6729-6739.
51. Bruce AW, Donaldson IJ, Wood IC, Yerbury SA, Sadowski MI, Chapman M, Gottgens B and Buckley NJ. Genome-wide analysis of repressor element 1 silencing transcription factor/neuron-restrictive silencing factor (REST/NRSF) target genes. Proc Natl Acad Sci U S A. 2004; 101(28):10458-10463.

52. Kallunki P, Edelman GM and Jones FS. Tissue-specific expression of the L1 cell adhesion molecule is modulated by the neural restrictive silencer element. J Cell Biol. 1997; 138(6):1343-1354.
53. Altevogt P, Doberstein K and Fogel M. L1CAM in human cancer. Int J Cancer. 2016; 138(7):1565-1576.
54. Sung SY, Wu IH, Chuang PH, Petros JA, Wu HC, Zeng HJ, Huang WC, Chung LW and Hsieh CL. Targeting L1 cell adhesion molecule expression using liposome-encapsulated siRNA suppresses prostate cancer bone metastasis and growth. Oncotarget. 2014; 5(20):9911-9929.
55. Doberstein K, Milde-Langosch K, Bretz NP, Schirmer U, Harari A, Witzel I, Ben-Arie A, Hubalek M, Muller-Holzner E, Reinold S, Zeimet AG, Altevogt P and Fogel M. L1CAM is expressed in triple-negative breast cancers and is inversely correlated with androgen receptor. BMC cancer. 2014; 14:958.
56. Ayala R, Shu T and Tsai LH. Trekking across the brain: the journey of neuronal migration. Cell. 2007; 128(1):29-43.
57. Zhao S and Frotscher M. Go or stop? Divergent roles of Reelin in radial neuronal migration. Neuroscientist. 2010; 16(4):421-434.
58. Kawabe H and Brose N. The role of ubiquitylation in nerve cell development. Nat Rev Neurosci. 2011; 12(5):251-268.
59. Sekine K, Kawauchi T, Kubo K, Honda T, Herz J, Hattori M, Kinashi T and Nakajima K. Reelin controls neuronal positioning by promoting cell-matrix adhesion via inside-out activation of integrin alpha5beta1. Neuron. 2012; 76(2):353-369.
60. Lee GH and D'Arcangelo G. New Insights into Reelin-Mediated Signaling Pathways. Front Cell Neurosci. 2016; 10:122.
61. D'Arcangelo G, Homayouni R, Keshvara L, Rice DS, Sheldon M and Curran T. Reelin is a ligand for lipoprotein receptors. Neuron. 1999; 24(2):471-479.
62. Farkas LM, Haffner C, Giger T, Khaitovich P, Nowick K, Birchmeier C, Paabo S and Huttner WB. Insulinoma-associated 1 has a panneurogenic role and promotes the generation and expansion of basal progenitors in the developing mouse neocortex. Neuron. 2008; 60(1):40-55.
63. Rosenbaum JN, Guo Z, Baus RM, Werner H, Rehrauer WM and Lloyd RV. INSM1: A Novel Immunohistochemical and Molecular Marker for Neuroendocrine and Neuroepithelial Neoplasms. Am J Clin Pathol. 2015; 144(4):579-591.
64. Lan MS, Russell EK, Lu J, Johnson BE and Notkins AL. IA-1, a new marker for neuroendocrine differentiation in human lung cancer cell lines. Cancer Res. 1993; 53(18):4169-4171.
65. Chen C, Breslin MB and Lan MS. Ectopic expression of a small cell lung cancer transcription factor, INSM1 impairs alveologenesis in lung development. BMC Pulm Med. 2016; 16:49.
66. Berruti A, Mosca A, Porpiglia F, Bollito E, Tucci M, Vana F, Cracco C, Torta M, Russo L, Cappia S, Saini A, Angeli A, Papotti M, Scarpa RM and Dogliotti L. Chromogranin A expression in patients with hormone naive prostate cancer predicts the development of hormone refractory disease. J Urol. 2007; 178(3 Pt 1):838-843; quiz 1129.
67. Rapa I, Ceppi P, Bollito E, Rosas R, Cappia S, Bacillo E, Porpiglia F, Berruti A, Papotti M and Volante M. Human ASH1 expression in prostate cancer with neuroendocrine differentiation. Mod Pathol. 2008; 21(6):700-707.
68. Fujino K, Motooka Y, Hassan WA, Ali Abdalla MO, Sato Y, Kudoh S, Hasegawa K, Niimori-Kita K, Kobayashi H, Kubota I, Wakimoto J, Suzuki M and Ito T. Insulinoma-Associated Protein 1 Is a Crucial Regulator of Neuroendocrine Differentiation in Lung Cancer. Am J Pathol. 2015; 185(12):3164-3177.
69. Bishop JL, Thaper D, Vahid S, Davies A, Ketola K, Kuruma H, Jama R, Nip KM, Angeles A, Johnson F, Wyatt AW, Fazli L, Gleave ME, Lin D, Rubin MA, Collins CC, et al. The Master Neural Transcription Factor BRN2 Is an Androgen Receptor-Suppressed Driver of Neuroendocrine Differentiation in Prostate Cancer. Cancer Discov. 2017; 7(1):54-71.
70. Liu WD, Wang HW, Muguira M, Breslin MB and Lan MS. INSM1 functions as a transcriptional repressor of the neuroD/beta2 gene through the recruitment of cyclin D1 and histone deacetylases. Biochem J. 2006; 397(1):169-177.

71. Jia S, Ivanov A, Blasevic D, Muller T, Purfurst B, Sun W, Chen W, Poy MN, Rajewsky N and Birchmeier C. Insm1 cooperates with Neurod1 and Foxa2 to maintain mature pancreatic beta-cell function. EMBO J. 2015; 34(10):1417-1433.
72. Osipovich AB, Long Q, Manduchi E, Gangula R, Hipkens SB, Schneider J, Okubo T, Stoeckert CJ, Jr., Takada S and Magnuson MA. Insm1 promotes endocrine cell differentiation by modulating the expression of a network of genes that includes Neurog3 and Ripply3. Development. 2014; 141(15):2939-2949.
73. Gupta A, Wang Y, Browne C, Kim S, Case T, Paul M, Wills ML and Matusik RJ. Neuroendocrine differentiation in the 12T-10 transgenic prostate mouse model mimics endocrine differentiation of pancreatic beta cells. Prostate. 2008; 68(1):50-60.
74. Jia S, Wildner H and Birchmeier C. Insm1 controls the differentiation of pulmonary neuroendocrine cells by repressing Hes1. Dev Biol. 2015; 408(1):90-98.
75. George J, Lim JS, Jang SJ, Cun Y, Ozretic L, Kong G, Leenders F, Lu X, Fernandez-Cuesta L, Bosco G, Muller C, Dahmen I, Jahchan NS, Park KS, Yang D, Karnezis AN, et al. Comprehensive genomic profiles of small cell lung cancer. Nature. 2015; 524(7563):47-53.
76. Chen C, Breslin MB and Lan MS. INSM1 increases N-myc stability and oncogenesis via a positive-feedback loop in neuroblastoma. Oncotarget. 2015; 6(34):36700-36712.
77. De Smaele E, Fragomeli C, Ferretti E, Pelloni M, Po A, Canettieri G, Coni S, Di Marcotullio L, Greco A, Moretti M, Di Rocco C, Pazzaglia S, Maroder M, Screpanti I, Giannini G and Gulino A. An integrated approach identifies Nhlh1 and Insm1 as Sonic Hedgehog-regulated genes in developing cerebellum and medulloblastoma. Neoplasia. 2008; 10(1):89-98.
78. diIorio PJ, Moss JB, Sbrogna JL, Karlstrom RO and Moss LG. Sonic hedgehog is required early in pancreatic islet development. Dev Biol. 2002; 244(1):75-84.
79. Watkins DN, Berman DM, Burkholder SG, Wang B, Beachy PA and Baylin SB. Hedgehog signalling within airway epithelial progenitors and in small-cell lung cancer. Nature. 2003; 422(6929):313-317.
80. Roubaud G, Liaw BC, Oh WK and Mulholland DJ. Strategies to avoid treatment-induced lineage crisis in advanced prostate cancer. Nat Rev Clin Oncol. 2017; 14(5):269-283.
81. Mounir Z, Lin F, Lin VG, Korn JM, Yu Y, Valdez R, Aina OH, Buchwalter G, Jaffe AB, Korpal M, Zhu P, Brown M, Cardiff RD, Rocnik JL, Yang Y and Pagliarini R. TMPRSS2:ERG blocks neuroendocrine and luminal cell differentiation to maintain prostate cancer proliferation. Oncogene. 2015; 34(29):3815-3825.
82. Akamatsu S, Wyatt AW, Lin D, Lysakowski S, Zhang F, Kim S, Tse C, Wang K, Mo F, Haegert A, Brahmbhatt S, Bell R, Adomat H, Kawai Y, Xue H, Dong X, et al. The Placental Gene PEG10 Promotes Progression of Neuroendocrine Prostate Cancer. Cell Rep. 2015; 12(6):922-936.
83. Zhang T, Liu WD, Saunee NA, Breslin MB and Lan MS. Zinc finger transcription factor INSM1 interrupts cyclin D1 and CDK4 binding and induces cell cycle arrest. J Biol Chem. 2009; 284(9):5574-5581.
84. Lukaszewicz AI and Anderson DJ. Cyclin D1 promotes neurogenesis in the developing spinal cord in a cell cycle-independent manner. Proc Natl Acad Sci U S A. 2011; 108(28):11632-11637.
85. Jongsma J, Oomen MH, Noordzij MA, Van Weerden WM, Martens GJ, van der Kwast TH, Schroder FH and van Steenbrugge GJ. Kinetics of neuroendocrine differentiation in an androgen-dependent human prostate xenograft model. Am J Pathol. 1999; 154(2):543-551.
86. Grobholz R, Griebe M, Sauer CG, Michel MS, Trojan L and Bleyl U. Influence of neuroendocrine tumor cells on proliferation in prostatic carcinoma. Hum Pathol. 2005; 36(5):562-570.
87. Grigore AD, Ben-Jacob E and Farach-Carson MC. Prostate cancer and neuroendocrine differentiation: more neuronal, less endocrine? Front Oncol. 2015; 5:37.
88. DaSilva JO, Amorino GP, Casarez EV, Pemberton B and Parsons SJ. Neuroendocrine-derived peptides promote prostate cancer cell survival through activation of IGF-1R signaling. Prostate. 2013; 73(8):801-812.
89. Yuan TC, Veeramani S, Lin FF, Kondrikou D, Zelivianski S, Igawa T, Karan D, Batra SK and Lin MF. Androgen deprivation induces human prostate epithelial neuroendocrine differentiation of androgen-sensitive LNCaP cells. Endocr Relat Cancer. 2006; 13(1):151-167.

90. Deeble PD, Cox ME, Frierson HF, Jr., Sikes RA, Palmer JB, Davidson RJ, Casarez EV, Amorino GP and Parsons SJ. Androgen-independent growth and tumorigenesis of prostate cancer cells are enhanced by the presence of PKA-differentiated neuroendocrine cells. Cancer Res. 2007; 67(8):3663-3672.
91. Bonkhoff H, Wernert N, Dhom G and Remberger K. Relation of endocrine-paracrine cells to cell proliferation in normal, hyperplastic, and neoplastic human prostate. Prostate. 1991; 19(2):91-98.
92. Yang JC, Ok JH, Busby JE, Borowsky AD, Kung HJ and Evans CP. Aberrant activation of androgen receptor in a new neuropeptide-autocrine model of androgen-insensitive prostate cancer. Cancer Res. 2009; 69(1):151-160.
93. Tsapakidis K, Vlachostergios PJ, Voutsadakis IA, Befani CD, Patrikidou A, Hatzidaki E, Daliani DD, Moutzouris G, Liakos P and Papandreou CN. Bortezomib reverses the proliferative and antiapoptotic effect of neuropeptides on prostate cancer cells. Int J Urol. 2012; 19(6):565-574.
94. Tzelepi V, Zhang J, Lu JF, Kleb B, Wu G, Wan X, Hoang A, Efstathiou E, Sircar K, Navone NM, Troncoso P, Liang S, Logothetis CJ, Maity SN and Aparicio AM. Modeling a lethal prostate cancer variant with small-cell carcinoma features. Clin Cancer Res. 2012; 18(3):666-677.
95. Wang Q, Li W, Zhang Y, Yuan X, Xu K, Yu J, Chen Z, Beroukhim R, Wang H, Lupien M, Wu T, Regan MM, Meyer CA, Carroll JS, Manrai AK, Janne OA, et al. Androgen receptor regulates a distinct transcription program in androgen-independent prostate cancer. Cell. 2009; 138(2):245-256.
96. Liu LL, Xie N, Sun S, Plymate S, Mostaghel E and Dong X. Mechanisms of the androgen receptor splicing in prostate cancer cells. Oncogene. 2014; 33(24):3140-3150.
97. Hornberg E, Ylitalo EB, Crnalic S, Antti H, Stattin P, Widmark A, Bergh A and Wikstrom P. Expression of androgen receptor splice variants in prostate cancer bone metastases is associated with castration-resistance and short survival. PLoS One. 2011; 6(4):e19059.
98. Hu R, Lu C, Mostaghel EA, Yegnasubramanian S, Gurel M, Tannahill C, Edwards J, Isaacs WB, Nelson PS, Bluemn E, Plymate SR and Luo J. Distinct transcriptional programs mediated by the ligand-dependent full-length androgen receptor and its splice variants in castration-resistant prostate cancer. Cancer Res. 2012; 72(14):3457-3462.
99. Bruce AW, Lopez-Contreras AJ, Flicek P, Down TA, Dhami P, Dillon SC, Koch CM, Langford CF, Dunham I, Andrews RM and Vetrie D. Functional diversity for REST (NRSF) is defined by in vivo binding affinity hierarchies at the DNA sequence level. Genome Res. 2009; 19(6):994-1005.
100. Svensson C, Ceder J, Iglesias-Gato D, Chuan YC, Pang ST, Bjartell A, Martinez RM, Bott L, Helczynski L, Ulmert D, Wang Y, Niu Y, Collins C and Flores-Morales A. REST mediates androgen receptor actions on gene repression and predicts early recurrence of prostate cancer. Nucleic Acids Res. 2014; 42(2):999-1015.
101. Martin D, Kim YH, Sever D, Mao CA, Haefliger JA and Grapin-Botton A. REST represses a subset of the pancreatic endocrine differentiation program. Dev Biol. 2015; 405(2):316-327.
102. Martin D and Grapin-Botton A. The Importance of REST for Development and Function of Beta Cells. Front Cell Dev Biol. 2017; 5:12.
103. Kreisler A, Strissel PL, Strick R, Neumann SB, Schumacher U and Becker CM. Regulation of the NRSF/REST gene by methylation and CREB affects the cellular phenotype of small-cell lung cancer. Oncogene. 2010; 29(43):5828-5838.
104. Schafer MK and Altevogt P. L1CAM malfunction in the nervous system and human carcinomas. Cell Mol Life Sci. 2010; 67(14):2425-2437.
105. Virtanen C, Ishikawa Y, Honjoh D, Kimura M, Shimane M, Miyoshi T, Nomura H and Jones MH. Integrated classification of lung tumors and cell lines by expression profiling. Proc Natl Acad Sci U S A. 2002; 99(19):12357-12362.
106. Seigel GM, Hackam AS, Ganguly A, Mandell LM and Gonzalez-Fernandez F. Human embryonic and neuronal stem cell markers in retinoblastoma. Mol Vis. 2007; 13:823-832.
107. Wang Q, Lu J, Yang C, Wang X, Cheng L, Hu G, Sun Y, Zhang X, Wu M and Liu Z. CASK and its target gene Reelin were co-upregulated in human esophageal carcinoma. Cancer Lett. 2002; 179(1):71-77.

108. Qin X, Lin L, Cao L, Zhang X, Song X, Hao J, Zhang Y, Wei R, Huang X, Lu J and Ge Q. Extracellular matrix protein Reelin promotes myeloma progression by facilitating tumor cell proliferation and glycolysis. Sci Rep. 2017; 7:45305.
109. Perrone G, Vincenzi B, Zagami M, Santini D, Panteri R, Flammia G, Verzi A, Lepanto D, Morini S, Russo A, Bazan V, Tomasino RM, Morello V, Tonini G and Rabitti C. Reelin expression in human prostate cancer: a marker of tumor aggressiveness based on correlation with grade. Mod Pathol. 2007; 20(3):344-351.
110. Park TJ and Curran T. Crk and Crk-like play essential overlapping roles downstream of disabled-1 in the Reelin pathway. J Neurosci. 2008; 28(50):13551-13562.
111. Leemhuis J and Bock HH. Reelin modulates cytoskeletal organization by regulating Rho GTPases. Commun Integr Biol. 2011; 4(3):254-257.
112. Ballif BA, Arnaud L and Cooper JA. Tyrosine phosphorylation of Disabled-1 is essential for Reelin-stimulated activation of Akt and Src family kinases. Brain Res Mol Brain Res. 2003; 117(2):152-159.
113. Caplin NJ, O'Leary P, Bulsara M, Davis EA and Jones TW. Subcutaneous glucose sensor values closely parallel blood glucose during insulin-induced hypoglycaemia. Diabet Med. 2003; 20(3):238-241.
114. Qi J, Nakayama K, Cardiff RD, Borowsky AD, Kaul K, Williams R, Krajewski S, Mercola D, Carpenter PM, Bowtell D and Ronai ZA. Siah2-dependent concerted activity of HIF and FoxA2 regulates formation of neuroendocrine phenotype and neuroendocrine prostate tumors. Cancer Cell. 2010; 18(1):23-38.
115. D'Arcangelo G, Miao GG, Chen SC, Soares HD, Morgan JI and Curran T. A protein related to extracellular matrix proteins deleted in the mouse mutant reeler. Nature. 1995; 374(6524):719-723.
116. Kiefel H, Pfeifer M, Bondong S, Hazin J and Altevogt P. Linking L1CAM-mediated signaling to NF-kappaB activation. Trends Mol Med. 2011; 17(4):178-187.

Chapter 5

General discussion

At the time of diagnosis, PCa will frequently present as organ-confined disease or with locoregional spread and most tumors will persist as indolent clinical condition [1, 2]. The individual risk to develop clinically significant and potentially lethal disease is not recognized by histological grading alone. The heterogeneous clinical course that is observed among PCa cases is determined by complex and dynamic genomic aberrations. The biological and clinical significance of those molecular aberrations is not well understood limiting the availability of prognostic markers for risk stratification in current clinical practice. Simultaneously, a broader spectrum of therapeutic targets in addition to ADT is required to improve the clinical management of metastatic PCa [3]. An ideal situation would be if the molecular subtypes of PCa that are characterized by distinct genomic alterations, could be treated differently and specifically. Far away from personalized treatment, all PCa patients are treated rather by the same therapeutics. The only FDA-approved targeted therapy in PCa is currently sipuleucel-T, an autologous cellular immunotherapy containing PAP-activated peripheral blood mononuclear cells indicated for the treatment of asymptomatic or minimally symptomatic mCRPC [4]. A better understanding of the contribution of molecular alterations to the biological characteristics of PCa is essential to identify novel markers for risk assessment and targets for improved therapeutic management.

The aim of the studies compiled in this thesis was to identify candidate driver genes of aggressive PCa and to provide a functional and mechanistic evaluation of these candidates in prostate cancer cell lines. The role of the *TMPRSS2:ERG* gene fusion, the most frequent genomic aberration in PCa, was studied in detail. Detection of the *TMPRSS2:ERG* gene fusion has currently no prognostic or therapeutic implications in routine clinical management. Several clinical trials are currently evaluating the predictive value of the *TMPRSS2:ERG* gene fusion alone (NCT02588404) or in combination with the PTEN deletion (NCT02573636) for failure of hormonal therapy, and for response to enzalutamide (NCT02288936). The analysis of T/E-induced molecular mechanisms identified resistance mechanisms with potential implications for existing treatment regimens. ERG was shown to bind to cytoplasmatic β-tubulin thereby reducing the availability of microtubules for taxane binding [5]. In DU145-ERG overexpressing xenografts, reduced taxane-induced apoptosis was observed compared to the DU145-GFP expressing control mice [5]. T/E fusion-positive CRPC patients showed reduced sensitivity to taxane-based chemotherapy suggesting a role for the TMPRSS2:ERG fusion as potential predictive marker [5].

When identifying driver alterations in cancer, the ‘druggability’, i.e. the ability to identify a druglike ligand that can modulate the activity of the target with a therapeutic benefit to the patient [6], is of major interest. Transcription factors are generally considered as difficult to target [7]. The evaluation of the druggability of ERG is limited to the *in vitro* and preclinical setting. The small molecule YK-4-279 (an ETS-family inhibitor) was shown

to inhibit VCaP and LNCaP prostate cancer cell motility and invasion *in vitro* [8] and *in vivo* [9]. In a murine model of Ewing sarcoma, a disease characterized by high occurrence of chromosomal translocations between the EWSR1 gene and various members of the ETS-family, YK-4-279 was able to inhibit transcriptional activity of the EWS–FLI1 fusion protein [10]. In neuroblastoma cells, YK-4-279 induced apoptosis by inhibition of mitosis [11]. However, no clear genotype underlying the YK-4-279 sensitivity could be identified, suggesting that YK-4-279 interrupts key protein interactions required for controlled mitosis and proliferation of cancers cells [11]. The di-(thiophene-phenylamidine) compound DB1255 was identified as an ERG/DNA binding inhibitor by interacting with part of the ERG-binding site thereby modulating ERG-regulated genes [12]. Recently, liposomal nanoparticles packaged with squalene-conjugated siRNA against *TMPRSS2:ERG* (siRNA-SQ NPs) conferred strong antitumoral activity and were suggested as alternative treatment approach to antiandrogen therapy with flutamide in VCaP cells [13].

An alternative approach under evaluation is to target ERG interacting proteins, such as PARP1, DNA protein kinases (DNA-PK), and HDAC1. In T/E overexpressing cells PARP1 inhibition induced increased vulnerability of prostate cancer cells to low-dose radiation [14, 15]. In the preclinical setting, T/E overexpressing xenografts were sensitized to growth arrest by inhibiting PARP1 suggesting that tumors respond to treatment with PARP1-inhibitors [14]. Recent studies showed that PCa patients with inherited mutations in BRCA1/2 and ataxia-telangiectasia mutated (ATM, a DNA-PK), who generally have a shorter survival, clinically responded to the PARP1 inhibitor olaparib [16, 17]. Inhibition of DNA-PK was able to reduce ERG transcriptional activity [14] and a phase I trial currently investigates the dual inhibition of DNA-PK and mTOR, an effector of PI3K signaling, in mCRPC patients using PSA response as secondary objective (clinicaltrials.gov: NCT02833883). HDAC1 inhibition reduced the expression of ERG-associated genes in VCaP cells [18] and diverse HDAC inhibitors are currently tested in clinical trials (NCT00878436, NCT01075308, and NCT01174199).

Taylor et al. previously showed that four key cancer pathways are affected in PCa and suggested those signaling pathways as basis for drug development [19]. In this thesis, we present the identification of novel driver mechanism that could be used for drug development in PCa extending the list of key cancer pathways in *TMPRSS2:ERG* fusion-positive PCa subtypes. First, the TGF-β/BMP and WNT/β-catenin signaling pathways as molecular determinants underlying T/E-mediated EMT in PCa cells were identified. Of note, the type I TGF-β receptor *ALK1* as well as the WNT receptor *FZD4* were identified as the mediators of transcriptional changes leading to EMT in T/E overexpressing cells. Activation of TGF-β-ALK1-p38 signaling promoting EMT in T/E expressing cells provides a rational basis for ALK1-blocking agents (which are currently already tested in clinical studies in various malignancies [20, 21]) to inhibit progression of T/E-positive PCa. The

soluble recombinant ALK1-Fc fusion protein dalantercept is currently evaluated as inhibitor of angiogenesis by binding of BMP9 and -10, and was shown to have antitumor activity in diverse refractory solid tumors in phase 1 studies (NCT00996957, NCT02024087) or phase 2 trials (NCT01642082, NCT01727336, NCT01720173).

This work further confirmed the previously reported finding that loss of cell adhesion and EMT in T/E overexpressing cells are associated with FZD4-induced activation of WNT signaling [22]. The druggability of the WNT-signaling pathway has for long been topic of discussion due to its complexity regarding ligand binding, downstream responses and signaling crosstalk, as well as its role in homeostasis and stem cell mechanisms raising substantial concerns. Among the targeted therapies, the selective Frizzled signaling pathway inhibitors (vantictumab against FZD7, ipafricept against FZD8) are currently tested in combination with taxane-based chemotherapies in HER2-negative breast cancer (NCT01973309), pancreatic cancer (NCT02005315, NCT02050178), NSCLC (NCT01957007), and ovarian cancer (NCT02092363). Although FZD4 is currently not addressed in clinical trials, these results support the feasibility of FZD4-targeted therapy in the future. The correlation between FZD4 hypomethylation and mRNA upregulation, although preliminary, represents another level of druggability in T/E fusion-positive tumors by methylation-modifying agents.

Second, we identified *INSM1* as transcriptional regulator of a neuroendocrine network in prostate cancer cell lines and further highlighted the integration of Reelin signaling in this regulatory network involving *INSM1*, *L1CAM* and *REST*. Taking advantage of its tissue-restricted expression pattern and re-activation in NE tumors, *INSM1* has gained attention regarding its role in suicide gene therapy approaches for tumor-specific systemic treatment in small cell lung cancer and neuroblastoma [23, 24]. Linking the *INSM1* promoter to a toxic transgene, such as herpes simplex virus thymidine kinase (HSV-TK), ganciclovir treatment resulted in increased cell death *in vitro* [23, 25] and tumor regression *in vivo* [24, 25]. Since shared gene signatures have previously been identified between different NE tumors, application of this method to diverse tumors with NE features has been suggested [24, 26]. These findings, though preliminary, present a potential strategy for targeted systemic therapy in NE tumors that could be implicated in NEPC as well. *INSM1* promoter constructs have further been proposed as diagnostic and disease monitoring tool to identify NE tumors by using a luciferase reporter vector that can detect the presence of NE tumors *in vivo* [24, 27]. These findings could have future implications for the management of NEPC. For example, the eligibility of *INSM1* for the identification of patients that are more likely to develop NEPC could be analysed in future studies. Selecting those patients is of importance for the consideration whether they could benefit from a chemotherapy-based treatment regimen rather than ADT.

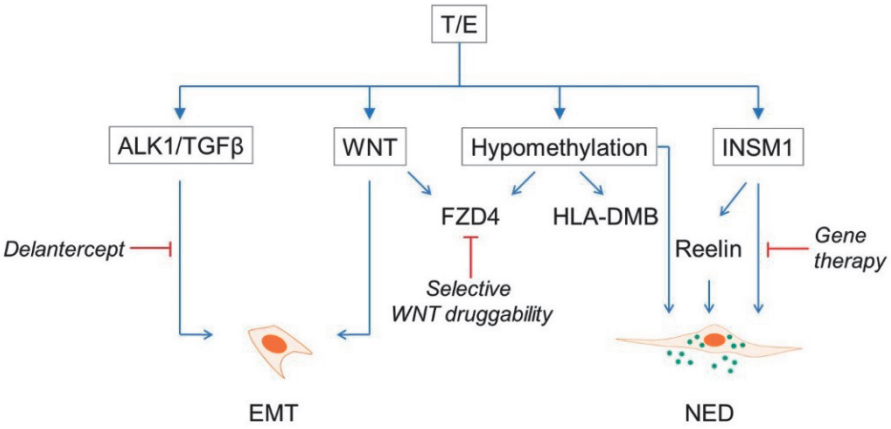

Figure 5.1: Summarizing model of the T/E-induced molecular mechanisms. This figure highlights the factors and mechanisms that are induced by T/E overexpression in prostate cancer cells. Further, potential implementations for treatment strategies are depicted (red arrow).

The molecular characterization of *INSM1* in prostate cancer cell lines presented in this work provided a molecular basis for further analysis of the clinical relevance of INSM1 as target in NEPC. This is supported by the progress regarding *INSM1* in gene therapy. We highlighted remarkable similarities in signaling pathways between NEPC and well-known models of NE tumors, such as small cell lung cancer, suggesting that insights into the mechanisms of NEPC might be derived from the molecular pathology of those NE cancers. Of note, the current National Comprehensive Cancer Network (NCCN) guidelines on PCa recommend the consultation of the specific guidelines for small cell lung cancer for management of small cell carcinoma of the prostate [28]. This knowledge could guide the emphasis of future research.

In conclusion, the work in this thesis accomplished the identification of novel drivers in the development of aggressive PCa at the molecular level of the tumor cells that point towards future strategies for clinical diagnosis and treatment.

REFERENCES

1. Penney KL, Stampfer MJ, Jahn JL, Sinnott JA, Flavin R, Rider JR, Finn S, Giovannucci E, Sesso HD, Loda M, Mucci LA and Fiorentino M. Gleason grade progression is uncommon. Cancer Res. 2013; 73(16):5163-5168.
2. Miller DC, Hafez KS, Stewart A, Montie JE and Wei JT. Prostate carcinoma presentation, diagnosis, and staging: an update form the National Cancer Data Base. Cancer. 2003; 98(6):1169-1178.
3. Georgi B, Korzeniewski N, Hadaschik B, Grullich C, Roth W, Sultmann H, Pahernik S, Hohenfellner M and Duensing S. Evolving therapeutic concepts in prostate cancer based on genome-wide analyses (review). Int J Oncol. 2014; 45(4):1337-1344.
4. Institute NC. FDA Approval for Sipuleucel-T.
5. Galletti G, Matov A, Beltran H, Fontugne J, Miguel Mosquera J, Cheung C, MacDonald TY, Sung M, O'Toole S, Kench JG, Suk Chae S, Kimovski D, Tagawa ST, Nanus DM, Rubin MA, Horvath LG, et al. ERG induces taxane resistance in castration-resistant prostate cancer. Nat Commun. 2014; 5:5548.
6. Verdine GL and Walensky LD. The challenge of drugging undruggable targets in cancer: lessons learned from targeting BCL-2 family members. Clin Cancer Res. 2007; 13(24):7264-7270.
7. Fontaine F, Overman J and Francois M. Pharmacological manipulation of transcription factor protein-protein interactions: opportunities and obstacles. Cell Regen (Lond). 2015; 4(1):2.
8. Rahim S, Beauchamp EM, Kong Y, Brown ML, Toretsky JA and Uren A. YK-4-279 inhibits ERG and ETV1 mediated prostate cancer cell invasion. PLoS One. 2011; 6(4):e19343.
9. Rahim S, Minas T, Hong SH, Justvig S, Celik H, Kont YS, Han J, Kallarakal AT, Kong Y, Rudek MA, Brown ML, Kallakury B, Toretsky JA and Uren A. A small molecule inhibitor of ETV1, YK-4-279, prevents prostate cancer growth and metastasis in a mouse xenograft model. PLoS One. 2014; 9(12):e114260.
10. Lamhamedi-Cherradi SE, Menegaz BA, Ramamoorthy V, Aiyer RA, Maywald RL, Buford AS, Doolittle DK, Culotta KS, O'Dorisio JE and Ludwig JA. An Oral Formulation of YK-4-279: Preclinical Efficacy and Acquired Resistance Patterns in Ewing Sarcoma. Mol Cancer Ther. 2015; 14(7):1591-1604.
11. Kollareddy M, Sherrard A, Park JH, Szemes M, Gallacher K, Melegh Z, Oltean S, Michaelis M, Cinatl J, Jr., Kaidi A and Malik K. The small molecule inhibitor YK-4-279 disrupts mitotic progression of neuroblastoma cells, overcomes drug resistance and synergizes with inhibitors of mitosis. Cancer Lett. 2017; 403:74-85.
12. Nhili R, Peixoto P, Depauw S, Flajollet S, Dezitter X, Munde MM, Ismail MA, Kumar A, Farahat AA, Stephens CE, Duterque-Coquillaud M, David Wilson W, Boykin DW and David-Cordonnier MH. Targeting the DNA-binding activity of the human ERG transcription factor using new heterocyclic dithiophene diamidines. Nucleic Acids Res. 2013; 41(1):125-138.
13. Urbinati G, de Waziers I, Slamic M, Foussigniere T, Ali HM, Desmaele D, Couvreur P and Massaad-Massade L. Knocking Down TMPRSS2-ERG Fusion Oncogene by siRNA Could be an Alternative Treatment to Flutamide. Mol Ther Nucleic Acids. 2016; 5:e301.
14. Brenner JC, Ateeq B, Li Y, Yocum AK, Cao Q, Asangani IA, Patel S, Wang X, Liang H, Yu J, Palanisamy N, Siddiqui J, Yan W, Cao X, Mehra R, Sabolch A, et al. Mechanistic rationale for inhibition of poly(ADP-ribose) polymerase in ETS gene fusion-positive prostate cancer. Cancer Cell. 2011; 19(5):664-678.
15. Chatterjee P, Choudhary GS, Sharma A, Singh K, Heston WD, Ciezki J, Klein EA and Almasan A. PARP inhibition sensitizes to low dose-rate radiation TMPRSS2-ERG fusion gene-expressing and PTEN-deficient prostate cancer cells. PLoS One. 2013; 8(4):e60408.
16. Na R, Zheng SL, Han M, Yu H, Jiang D, Shah S, Ewing CM, Zhang L, Novakovic K, Petkewicz J, Gulukota K, Helseth DL, Jr., Quinn M, Humphries E, Wiley KE, Isaacs SD, et al. Germline Mutations in ATM and BRCA1/2 Distinguish Risk for Lethal and Indolent Prostate Cancer and are Associated with Early Age at Death. Eur Urol. 2017; 71(5):740-747.
17. Fong PC, Boss DS, Yap TA, Tutt A, Wu P, Mergui-Roelvink M, Mortimer P, Swaisland H, Lau A, O'Connor MJ, Ashworth A, Carmichael J, Kaye SB, Schellens JH and de Bono JS. Inhibition of poly(ADP-ribose) polymerase in tumors from BRCA mutation carriers. N Engl J Med. 2009; 361(2):123-134.

18. Bjorkman M, Iljin K, Halonen P, Sara H, Kaivanto E, Nees M and Kallioniemi OP. Defining the molecular action of HDAC inhibitors and synergism with androgen deprivation in ERG-positive prostate cancer. Int J Cancer. 2008; 123(12):2774-2781.
19. Taylor BS, Schultz N, Hieronymus H, Gopalan A, Xiao Y, Carver BS, Arora VK, Kaushik P, Cerami E, Reva B, Antipin Y, Mitsiades N, Landers T, Dolgalev I, Major JE, Wilson M, et al. Integrative genomic profiling of human prostate cancer. Cancer Cell. 2010; 18(1):11-22.
20. Vecchia L, Olivieri C and Scotti C. Activin Receptor-like kinase 1: a novel anti-angiogenesis target from TGF-beta family. Mini Rev Med Chem. 2013; 13(10):1398-1406.
21. Bendell JC, Gordon MS, Hurwitz HI, Jones SF, Mendelson DS, Blobe GC, Agarwal N, Condon CH, Wilson D, Pearsall AE, Yang Y, McClure T, Attie KM, Sherman ML and Sharma S. Safety, pharmacokinetics, pharmacodynamics, and antitumor activity of dalantercept, an activin receptor-like kinase-1 ligand trap, in patients with advanced cancer. Clin Cancer Res. 2014; 20(2):480-489.
22. Gupta S, Iljin K, Sara H, Mpindi JP, Mirtti T, Vainio P, Rantala J, Alanen K, Nees M and Kallioniemi O. FZD4 as a mediator of ERG oncogene-induced WNT signaling and epithelial-to-mesenchymal transition in human prostate cancer cells. Cancer Res. 2010; 70(17):6735-6745.
23. Pedersen N, Pedersen MW, Lan MS, Breslin MB and Poulsen HS. The insulinoma-associated 1: a novel promoter for targeted cancer gene therapy for small-cell lung cancer. Cancer Gene Ther. 2006; 13(4):375-384.
24. Akerstrom V, Chen C, Lan MS and Breslin MB. Modifications to the INSM1 promoter to preserve specificity and activity for use in adenoviral gene therapy of neuroendocrine carcinomas. Cancer Gene Ther. 2012; 19(12):828-838.
25. Tseng AW, Chen C, Breslin MB and Lan MS. Tumor-specific promoter-driven adenoviral therapy for insulinoma. Cell Oncol (Dordr). 2016; 39(3):279-286.
26. Akerstrom V, Chen C, Lan MS and Breslin MB. Adenoviral insulinoma-associated protein 1 promoter-driven suicide gene therapy with enhanced selectivity for treatment of neuroendocrine cancers. Ochsner J. 2013; 13(1):91-99.
27. Breslin MB LM. (2012). Modified INSM1-promoter for neuroendocrine tumor therapy and diagnostics. In: College BOSOLSUAAAM, ed. (Louisiana United States
28. Network NCC. (05/26/16). Prostate Cancer (Version 3.2016).

Valorisation

Valorisation in its original sense means the creation of economic value. In biomedical research, valorisation aims to assess the contribution of scientific knowledge to industrial activities and its application as potential products or services with societal benefit. This chapter is meant to position the scientific results from the preceding chapters in the context of social utilisation and to generate potential health care returns in appreciation of public investments.

Social relevance

Getting the diagnosis of 'cancer' is a significant and dramatic incident for patients and their relatives. Prostate cancer (PCa) frequently shows an indolent clinical course with a 2.5-3% lifetime risk of dying from progressive disease [1]. However, risk stratification remains a major clinical question. Since clinicopathologic criteria are insufficient to efficiently distinguish between indolent and aggressive tumors, patients experience uncertainty about the risk of disease progression, which means an additional burden to them. Knowledge about the molecular profiles of an individual tumor and its potential to progress could provide clinicians with valuable information about the clinical course and support treatment recommendations. Proper counseling and involvement in therapy planning, especially of patients that could be considered for conservative management, positively affects patient's satisfaction after treatment [2]. Reducing overtreatment of patients with insignificant disease on the one hand would decrease comorbidity as a consequence of the PCa treatment, such as a surgical procedure, with benefit for the quality of life and reduction of health care costs. The accurate selection of patients that need aggressive treatment on the other hand would improve prognosis by avoding a delay until initiation of a potentially effective treatment.

Scientific and clinical relevance

PCa is the most prevalent non-cutaneous malignancy accounting for 15% of the cancers diagnosed in men [3]. Depending on risk estimation, different treatment options are possible. During the decision-making process towards radical treatment versus conservative management, clinicians use various prediction tools to determine patients that are at increased risk for disease progression. Those tools are based on clinicopathologic variables. However, PCa is a genomically complex disease. The molecular mechanisms and implications for clinical outcome of distinct genomic aberrations are yet poorly understood. Identification of the molecular profiles that promote aggressive tumor biology is therefore essential to support the prediction of progressive disease, and to recommend aggressive treatment to patients that will most likely benefit from it.

In the studies compiled in this doctoral thesis, novel targets have been identified that provide insights into the molecular mechanisms of *TMPRSS2:ERG* fusion-positive PCa. Defining tumors by their individual genetic constitution, rather than histopathological patterns could lead to more accurate risk stratification.

Detection of the *TMPRSS2:ERG* gene fusion has currently no prognostic or therapeutic implications in routine clinical management. Determination of the gene fusion status could direct the selection of patients for clinical trials that are most likely to benefit from a molecularly targeted therapy reducing the number of required patients to randomize and potentially increasing the chance of success of drug effectiveness testing (*targeted design*). This could further create an economically valuable strategy to control public investments into scientific research.

We suggest that the TGF-β-ALK1 receptor-mediated signaling pathway in *TMPRSS2:ERG* positive tumors could be a promising candidate for future evaluation as therapy target in PCa. However, targeted therapy approaches are vulnerable to intrinsic resistance due to redundancy in signaling pathways in cancer cells [4]. Since ERG-mediated signaling deployed a second route, the FZD4-WNT signaling pathway, inhibition of both pathways could be considered as a combined concept to inhibit tumor activity. The identification of the two molecular determinants of epithelial-to-mesenchymal transition (EMT) in *TMPRSS2:ERG* positive tumors is therefore promising basis for future therapeutic approaches.

Recognition of therapy resistance is important to avoid disease progression. Functional characterization of biological processes involved in therapy resistance could identify novel targets to improve clinical management. *INSM1* was identified as promising regulator of a neuroendocrine (NE) phenotype in PCa cells. The power of *INSM1* lies in its specific overexpression in NE tumors. Since prostate cancers with NE characteristics are less likely to respond to hormonal agents, detection of *INSM1* overexpression could be valuable in counseling patients towards a chemotherapeutic treatment or enrolment in a clinical trial [5].

REFERENCES

1. Howlader N NA, Krapcho M, Miller D, Bishop K, Kosary CL, Yu M, Ruhl J, Tatalovich Z, Mariotto A, Lewis DR, Chen HS, Feuer EJ, Cronin KA (eds). (2017). SEER Cancer Statistics Review, 1975-2014. National Cancer Institute. Bethesda, MD, USA).
2. Shariat SF, Kattan MW, Vickers AJ, Karakiewicz PI and Scardino PT. Critical review of prostate cancer predictive tools. Future Oncol. 2009; 5(10):1555-1584.
3. Ferlay J, Steliarova-Foucher E, Lortet-Tieulent J, Rosso S, Coebergh JW, Comber H, Forman D and Bray F. Cancer incidence and mortality patterns in Europe: estimates for 40 countries in 2012. Eur J Cancer. 2013; 49(6):1374-1403.
4. Stenvang J, Kumler I, Nygard SB, Smith DH, Nielsen D, Brunner N and Moreira JM. Biomarker-guided repurposing of chemotherapeutic drugs for cancer therapy: a novel strategy in drug development. Front Oncol. 2013; 3:313.
5. Mosquera JM, Beltran H, Park K, MacDonald TY, Robinson BD, Tagawa ST, Perner S, Bismar TA, Erbersdobler A, Dhir R, Nelson JB, Nanus DM and Rubin MA. Concurrent AURKA and MYCN gene amplifications are harbingers of lethal treatment-related neuroendocrine prostate cancer. Neoplasia. 2013; 15(1):1-10.

Summary

SUMMARY

The **general introduction** illustrates the challenges of prostate cancer (PCa) research and states the aims of my doctoral thesis. PCa is the most prevalent non-cutaneous malignancy accounting for 15% of the cancers diagnosed in men. It is the second leading cause of cancer-related death in men in Western countries. Family history and increasing age are the most important risk factors, with a 10-years risk of 5.50% to develop PCa for men aged 70 years. PCa frequently shows an indolent clinical course with a 2.5-3% lifetime risk of dying from PCa. Since clinicopathologic criteria are insufficient to efficiently distinguish between slow growing and progressive tumors, there is uncertainty about the individual risk of aggressive disease. Identifying biomarkers that predict clinically aggressive disease is a current challenge for PCa research. Those markers could be valuable to reduce overtreatment of insignificant disease on the one hand and select patients that are at risk of progressive disease and need aggressive treatment on the other hand. PCa is usually suspected based on elevated PSA value and abnormal result from digital rectal examination (DRE), but PSA level is not a direct surrogate for tumor stage. Definitive diagnosis requires histopathological evaluation of prostate biopsy cores that are classified according to the Gleason grading system. The dilemma with the Gleason score is that it does not reflect the diversity of genetic aberrations. Therefore, patients with with the same histological pattern can develop heterogeneous clinical outcomes.

My work aimed to identify novel molecular mechanisms of aggressive PCa. The focus was on the molecular and cellular consequences of ERG overexpression upon *TMPRSS2:ERG* (T/E) variant expression.

Chapter 1 provides a detailed overview about the distinct genetic and molecular aberrations that impacts the heterogeneity of PCa. The majority of prostate cancers are adenocarcinomas arising from multifocal hyperplasia of luminal secretory cells. These cells display continuous histomorphological aberrations ranging from low-grade dysplasia to 'carcinoma in situ', collectively described as prostatic intraepithelial neoplasia (PIN). PCa is characterized by a complex pathology with multiple histological foci that can harbor diverse genetic and molecular alterations. The spectrum of genomic aberrations, including point mutations, copy number alterations, structural rearrangements and DNA methylation changes, reflect distinct molecular subtypes. Major signaling pathways that are most commonly altered in PCa, including androgen receptor (AR), PTEN-PI3K/AKT, Ras/Raf/MEK/ERK and the retinoblastoma protein (pRB) signaling, are increasingly affected in metastatic tumors. Further in metastatic PCa, a large portion of the genome can be affected by deletions suggesting increased genomic instability with disease progression.

Androgens play a central role in PCa development and progression to metastatic disease. Blocking of the AR signaling pathway by androgen deprivation therapy (ADT) belongs to the initial treatment options of advanced-stage PCa. However, most cancers will relapse and progress to castration-resistant prostate cancer (CRPC). Neuroendo-

crine (NE) differentiation is a highly aggressive disease manifestation distinguished from adenocarcinoma by NE marker expression and unresponsiveness to hormone therapy.

Long-term androgen receptor signaling can induce DNA double-strand breaks driving the generation of chromosomal rearrangements. In PCa, gene fusions involving the ETS-transcription factors have been described. The *TMPRSS2:ERG* (T/E) gene fusion is the most prevalent genomic alteration in PCa present in approximately 50% of all PCa cases. This gene fusion, resulting from the fusion of the transcription factor ERG to the androgen responsive gene *TMPRSS2*, leads to upregulation of ERG protein and activation of downstream target genes. The expression of fusion mRNAs from distinct T/E variants is associated with clinicopathological parameters. However, the underlying molecular processes resulting from expression of T/E gene fusion variants remain unclear.

In **chapter 2**, the molecular alterations and functional implications caused by the T/E gene fusion were analysed. Using a doxycycline (Dox)-inducible overexpression LNCaP cell model (LNCaP-T/E), we showed that the TGF-β/BMP as well as the WNT/β-catenin signaling pathways are important regulators of T/E-mediated epithelial-to-mesenchymal transition (EMT) in PCa cells. Induction of T/E expression resulted in augmented secretion of TGF-β1 and -β2, and increased expression of *ALK1*, a member of the TGF-β receptor family. ALK1 inhibition in T/E expressing cells blocked p38 phosphorylation and reduced the expression of the TGF-β target genes *VIM*, *MMP1*, *CDH2*, and *SNAI2*. Induction of T/E expression further resulted in increased cellular migratory and invasive potential. We suggest that ALK1-mediated TGF-β signaling is a novel oncogenic mechanism in T/E positive PCa and provide a rational basis for ALK1-blocking agents in T/E positive PCa. The soluble recombinant ALK1-Fc fusion protein dalantercept is currently evaluated in various malignancies. It was shown to have antitumor activity in diverse refractory solid tumors in phase 1 (NCT00996957, NCT02024087) or phase 2 trials (NCT01642082, NCT01727336, NCT01720173) as discussed in **chapter 5**.

Further in **chapter 2**, we confirmed that WNT/β-catenin signaling and EMT in T/E expressing cells is mediated by the Frizzled receptor FZD4. Inhibition of FZD4 led to reduced phosphorylation of p38. Strikingly, we observed upregulation of *miR-503* exclusively in T/E variant VI overexpressing cells. Overexpression of *miR-503* was able to repress *SMAD7*, a known negative regulator of TGF-β and WNT/β-catenin signaling. *MiR-503*-mediated repression of *SMAD7* therefore appears to be a way to escape the inhibitory effect of SMAD7 on TGF-β and WNT/β-catenin signaling. Inhibition of FZD4-mediated signaling is currently not addressed in clinical trials. However, support for the feasibility of FZD4-targeted therapy is provided from the testing of selective Frizzled signaling pathway inhibitors against FZD7 (vantictumab) and FZD8 (ipafricept) in ongoing clinical trials in HER2-negative breast cancer (NCT01973309), pancreatic cancer (NCT02005315), non-small cell lung cancer (NCT01957007), and ovarian cancer (NCT02092363).

We explored the epigenetic alterations induced by the T/E gene fusion in **chapter 3**. Upon T/E overexpression, we found a global hypomethylation profile. Those differen-

tially methylated CpG sites were mostly located in gene bodies. An integrative analysis on epigenetic and gene expression changes in LNCaP-T/E cells demonstrated that T/E overexpression drives upregulation of *FZD4* and *HLA-DMB* that could be correlated with loss of DNA methylation. However, the relation of DNA hypomethylation and mRNA upregulation, as well as the mechanistic exploration of the T/E-induced epigenetic changes remain unclear from the present analysis. In addition to the discussion in chapter 2, the correlation between *FZD4* hypomethylation and mRNA upregulation, although preliminary, represents a basis for future research on the 'druggability' in T/E fusion-positive tumors.

In chapter 4, we identified the transcription factor *INSM1* as a regulator of neuroendocrine (NE) differentiation in prostate cancer cell lines. Neuroendocrine prostate cancer (NEPC) is a highly aggressive variant of advanced PCa, often occurring with conventional adenocarcinoma. A correlation between *INSM1* and the T/E gene fusion was observed in patient samples and cell lines. In cell culture experiments, ERG induced the expression of *INSM1* and the NE markers *TUBB3*, *SCG3*, *ASCL1*. These data indicate that the T/E gene fusion could be associated with NEPC. The tissue-restricted expression pattern and established role in neuronal and endocrine tissues of *INSM1* could be of advantage in the histological detection of NE differentiation in PCa and targeted therapy of NEPC. Re-expression of *INSM1* in NE tumors gained attention regarding its role in suicide gene therapy as tumor-specific treatment in small cell lung cancer and neuroblastoma. *INSM1* promoter constructs have further been proposed as diagnostic and disease monitoring tool for NE tumors *in vivo*. In addition to previous studies showing shared gene signatures between different NE tumors, the present study highlighted remarkable similarities in genetic and molecular aberrations between NEPC and well-known models of NE tumors, such as the Reelin signaling pathway, in chapter 4. This suggests that insights into the mechanisms of NEPC can be derived from the molecular mechanisms of known NE cancers and the suicide gene therapy could find application as targeted strategy for NEPC.

In conclusion, novel markers for refined risk stratification of progressive disease outcome and prediction of treatment response are needed. Several tissue-based multigene expression assays for the prediction of aggressive PCa are available for clinical application. Their routine implementation is currently hampered by intrinsic challenges of PCa research, such as heterogeneity, multifocality, and a small sample volume in prostate biopsy. Genetic instability increases the complexity of somatic genomic alterations leading to a specific combination of driver mutations in a tumor. However, molecular pathology is an emerging field in PCa as a growing number of targets with known correlation to tumor biology are recognized, such as *AR* splice variants. Further, differentiation markers of neuroendocrine manifestation, such as *INSM1* or *L1CAM,* may predict poor responsiveness to ADT. Current studies on novel molecular targets are discussed in chapter 5. Individual genetic aberrations could be interrogated by next generation sequencing and may find application for a personalized approach in clinical practice. Molecular and genetic analysis of biopsy cores is currently not included in the PCa guidelines. In future, it may complement the diagnosis of PCa as it has already been im-

plemented in other tumor entities, such as breast cancer, melanoma and, most recently, lung cancer. Simultaneously, a broader spectrum of therapeutic targets in addition to ADT is required to improve the clinical management of metastatic PCa. The functional and mechanistic evaluation of genetic markers, as presented in this doctoral thesis, is the basis for the development of novel drug targets and treatment strategies, and could guide the emphasis of future research.

Nederlandse samenvatting

NEDERLANDSE SAMENVATTING

De algemene introductie schetst de uitdagingen van prostaatkankeronderzoek en licht de doelen van mijn proefschrift toe. Prostaatkanker is de meest voorkomende niet-cutane maligniteit en maakt 15% van alle kankervormen in mannen uit. Het is tevens de één na belangrijkste doodsoorzaak door kanker in mannen in de Westerse wereld. Een positieve familiegeschiedenis en toenemende leeftijd zijn de belangrijkste risicofactoren, het 10-jaarsrisico voor mannen van 70 jaar om prostaatkanker te ontwikkelen is 5.50%. Prostaatkanker vertoont vaak een langzaam groeiend beloop met een 2.5-3% leeftijdsrisico om eraan te overlijden. De klinisch-pathologische criteria volstaan echter niet om tussen langzaam groeiende en progressief verlopende tumoren te onderscheiden, zodat er onzekerheid bestaat ten opzichte van het individuele risico op een agressief groeiende tumor. Eén van de uitdagingen voor het prostaatkankeronderzoek is de identificatie van biomarkers die een agressief ziekteverloop kunnen voorspellen. Met behulp van deze markers zou enerzijds overbehandeling van klinisch niet-relevante tumoren voorkomen worden. Anderzijds zouden patiënten geselecteerd kunnen worden die een verhoogd risico op ziekteprogressie hebben en een agressieve behandeling nodig hebben. De verdenking op prostaatkanker ontstaat op basis van een verhoogde PSA waarde en een afwijkend resultaat tijdens digitaal rectaal onderzoek. De hoogte van de PSA waarde is echter geen directe marker voor het tumorstadium. De definitieve diagnose vereist histopathologisch onderzoek van biopsiecoupes van de prostaat die volgens het Gleason score-systeem geclassificeerd worden. De heterogeniteit van de genetische en moleculaire afwijkingen bij prostaatkanker heeft tot gevolg dat patiënten met dezelfde Gleason score een zeer uiteenlopend klinisch beloop kunnen ontwikkelen.

Het doel van dit proefschrift was het identificeren van nieuwe moleculaire mechanismen van het agressieve prostaatcarcinoom. De focus werd gelegd op de moleculaire en cellulaire gevolgen van de ERG overexpressie in *TMPRSS2:ERG* (T/E) varianten.

Hoofdstuk 1 geeft een gedetailleerd overzicht over de diverse genetische en moleculaire afwijkingen die van invloed zijn op de heterogeniteit van prostaatkanker. De meeste prostaatkankers zijn adenocarcinomen, die door multifocale hyperplasie van luminale secretoire cellen ontstaan. Deze cellen vertonen continue histomorfologische veranderingen, die van laaggradige dysplasie tot 'carcinoma in situ' rijken, samengevat als prostaat intra-epitheliale neoplasie (PIN). Prostaatkanker wordt gekenmerkt door een complexe pathologie met multipele histologische foci, die uiting zijn van een combinatie van diverse genetische en moleculaire afwijkingen. Het spectrum van genomische afwijkingen, zoals puntmutaties, copynumbervariatie, structurele rearrangements en DNA methyleringsveranderingen, spiegelt verschillende moleculaire subtypen weer. Signaalroutes die het vaakst afwijken, zijn de androgen receptor, PTEN-PI3K/Akt, Ras/Raf/MEK/ERK en het retinoblastoom protein (pRB). Deze routes zijn tevens vaker aangedaan in gemetastaseerde prostaatkanker. Verder zijn in het gemetastaseerde prostaatcarcinoom grote genomische gebieden gedeleteerd, wat op een verhoogde genetische instabiliteit in gevorderde prostaatkanker duidt.

Androgenen spelen een centrale rol bij de ontwikkeling van prostaatkanker en progressie tot gemetastaseerde ziekte. Androgeen-deprivatie therapie (ADT) is de primaire behandeling van gevorderde prostaatkanker. Vaak treedt er onder deze behandeling echter een ziekterecidief en progressief beloop op. Neuroendocriene (NE) differentiatie is een zeer agressieve vorm van prostaatkanker, die onderscheiden wordt door expressie van NE markers en ongevoeligheid voor ADT. Langdurige blootstelling aan geactiveerde androgeen signaaltransductie kan leiden tot DNA dubbelstrengsbreuken, waardoor chromosomale rearrangements kunnen ontstaan. In prostaatkanker zijn genfusies van de ETS-transcriptiefactoren beschreven. De *TMPRSS2:ERG* (T/E) genfusie is de meest voorkomende genomische afwijking in prostaatkanker, aanwezig in rond 50% van alle prostaattumoren. Deze genfusie ontstaat door fusie van het transcriptiefactor *ERG* met het androgeen-sensitieve gen *TMPRSS2* en leidt tot opregulatie van het ERG proteïne gevolgd door activatie van target genen. De expressie van fusie mRNAs van verschillende T/E varianten is geassocieerd met klinisch-pathologische parameters. De moleculaire veranderingen ten gevolge van expressie van T/E genfusie-varianten zijn echter nog onvoldoende bekend.

In **hoofdstuk 2** werden de moleculaire veranderingen en functionele gevolgen door expressie van de T/E genfusie onderzocht. Gebruikmakend van een doxycycline (Dox)-induceerbaar overexpressie LNCaP cel model (LNCaP-T/E) werd aangetoond dat de TGF-β/BMP en de WNT/β-catenin signaleringsroutes belangrijke regulatoren van de T/E-gemedieerde epitheliale-tot-mesenchymale transitie (EMT) in prostaatkankercellen zijn. Inductie van T/E expressie resulteerde in een versterkte secretie van TGF-β1 en -β2, als een verhoogde expressie van *ALK1*, een receptor uit de TGF-β familie. Inhibitie van ALK1 in T/E expresserende cellen leidde tot verminderde p38 fosforylering en verminderde expressie van de TGF-β target genen *VIM*, *MMP1*, *CDH2* en *SNAI2*. T/E expressie leidde ook tot een versterkte migratie en invasie van de cellen. ALK1-gemedieerde TGF-β signalering is een nieuw oncogeen mechanisme in T/E positieve prostaatkanker en kan een basis zijn voor het testen van ALK1-blokkerende middelen in T/E positieve tumoren. Het oplosbare recombinante ALK1-Fc fusie eiwit dalantercept wordt momenteel onderzocht in diverse kankersoorten. In fase 1 (NCT00996957, NCT02024087) en fase 2 studies (NCT01642082, NCT01727336, NCT01720173) werd aangetoond dat dit middel anti-tumor activiteit in moeilijk behandelbare solide tumoren heeft, zoals besproken in **hoofdstuk 5**.

We laten verder in **hoofdstuk 2** zien dat de WNT/β-catenin signalering in T/E expresserende cellen gemedieerd wordt door de Frizzled receptor FZD4. Remming van FZD4 leidde eveneens tot verminderder fosforylering van p38. Opvallend was verder dat het microRNA *miR-503* enkel in T/E variant VI expresserende cellen verhoogd was. Overexpressie van *miR-503* verminderde de expressie van *SMAD7*, een negatieve regulator van TGF-β en WNT/β-catenin signalering. *MiR-503*-gemedieerde repressie van *SMAD7* kan een 'escape' route zijn om aan de remmende effecten van SMAD7 op TGF-β en WNT/β-catenin te ontsnappen. Therapeutische inhibitie van FZD4-gemedieerde signalering wordt momenteel niet getest in klinische studies. Aanleiding voor de haalbaarheid van een FZD4-gerichte therapie geven lopende studies die de selectieve Frizzled inhibitoren

tegen FZD7 (vantictumab) en FZD8 (ipafricept) aan in HER2-negatieve borstkanker (NCT01973309), pancreaskanker (NCT02005315), niet-kleincellig longkanker (NCT01957007), en eierstokkanker (NCT02092363) onderzoeken.

In hoofdstuk 3 werden de epigenetische veranderingen ten gevolge van de T/E genfusie onderzocht. Door T/E overexpressie werd er een globale hypomethylering geobserveerd. De differentieel gemethyleerde CpG sites werden meestal in genlichamen gevonden. Een integratieve analyse van de epigenetische en genexpressie veranderingen in LNCaP-T/E cellen liet zien dat T/E overexpressie tot opregulatie van *FZD4* en *HLA-DMB* leidde, die zou kunnen samenhangen met een verlies van DNA methylering. Er werd niet onderzocht of er een directe relatie tussen DNA methylering en mRNA opregulatie bestaat en wat de onderliggende mechanismen van de T/E-geïnduceerde epigenetische veranderingen zijn. Dit geeft aanleiding voor toekomstig onderzoek en zou kunnen bijdragen aan de behandelingsopties in T/E positieve tumoren.

In hoofdstuk 4 werd het transcriptiefactor *INSM1* gevonden als regulator van een neuro-endocrine (NE) differentiatie in prostaatkanker cellijnen. Neuro-endocrine prostaatkanker (NEPC) is een zeer agressieve vorm van gevorderde prostaatkanker, die vaak met gewone adenocarcinomen optreedt. Zowel in patiënten monsters als in cellijnen werd er een correlatie tussen *INSM1* en *ERG* expressie gezien. In cellcultuur experimenten leidde de overexpressie van *ERG* tot een verhoogde expressie van *INSM1* en van de NE markers *TUBB3*, *SCG3* en *ASCL1*. Deze resultaten laten vermoeden dat de T/E genfusie geassocieerd is met NEPC. De weefselspecifieke expressie van *INSM1* in neuronaal en endocrien weefsel zou van voordeel kunnen zijn bij de histologische detectie van NE differentiatie in prostaatkanker en gerichte behandeling van NEPC. Her-expressie van *INSM1* in NE tumoren heeft aandacht gekregen voor zijn functie bij de 'suicide' gentherapie als tumor-specifieke behandeling in kleincellig longkanker en neuroblastoom. *INSM1* promotor constructen werden voorgesteld als diagnostisch en ziektemonitoring tool voor NE tumoren in vivo. In de literatuur staat omschreven dat verschillende NE tumoren gelijkenissen in gensignaturen vertonen. De analyse in hoofdstuk 4 benadrukt eveneens opvallende overeenkomsten in de genetische en moleculaire afwijkingen van NEPC met bekende NE tumormodellen, zoals de Reelin signaleringsroute. Inzichten in de mechanismen van NEPC kunnen derhalve mogelijk afgeleid worden van de moleculaire mechanismen in andere NE tumoren. Verder geeft dit aanleiding voor de 'suicide' gentherapie als een potentiële strategie voor een gerichte therapie in NEPC.

Afsluitend geldt voor prostaatkanker dat nieuwe markers nodig zijn voor een verbeterde risicobeoordeling van een progressief ziekteverloop en predictie van de behandelingsrespons. Diverse weefsel-gebaseerde multigen expressie assays voor de predictie van agressieve prostaatkanker zijn beschikbaar voor de klinische toepassing. Echter wordt de implementatie ervan bemoeilijkt door de intrinsieke uitdagingen van prostaatkankeronderzoek, zoals heterogeniteit, multifocaliteit en beperkt monstervolume uit de prostaatbiopsie. Genetische instabiliteit verhoogt de complexiteit van somatische genomische afwijkingen die een specifieke combinatie van 'driver' mutaties in een tu-

mor veroorzaken. De moleculaire pathologie is echter een snelgroeiend onderzoeksgebied en een toenemend aantal aan 'targets' wordt bekend die samenhangen met de tumorbiologie, zoals bijvoorbeeld *AR* splice varianten. Bovendien zouden differentiatiemarkers die duiden op een NE manifestatie, zoals *INSM1* of *L1CAM*, een ongevoeligheid op ADT kunnen voorspellen. Recente studies naar nieuwe moleculaire 'targets' worden besproken in hoofdstuk 5.

De individuele genetische afwijkingen van een tumor kunnen geïdentificeerd worden door 'next generation sequencing' dat toegepast zou kunnen worden in een gepersonaliseerd aanpak in de kliniek. Een moleculaire en genetische analyse van biopsiemonsters is tegenwoordig niet opgenomen in de richtlijnen voor prostaatkanker. In toekomst zouden deze analyses echter een aanvulling bieden op de standaardbehandeling van prostaatkanker, zoals het reeds toegepast wordt in andere tumorvormen, namelijk borstkanker, melanoom en laatstelijk longkanker. Ook is er een breder spectrum van therapeutische 'targets' nodig als aanvulling op ADT om het klinische beleid van gemetastaseerde prostaatkanker te verbeteren. De functionele en mechanistische analyse van genetische markers, zoals het in dit proefschrift uitgewerkt werd, stelt de basis voor de ontwikkeling van nieuwe drug targets en behandelmogelijkheden en opent de deur voor toekomstig onderzoek.

Deutsche Zusammenfassung

DEUTSCHE ZUSAMMENFASSUNG

Die **allgemeine Einführung** schildert die Schwierigkeiten der Prostatakrebsforschung und erläutert die Zielsetzungen meiner Doktorarbeit. Prostatakrebs ist die häufigste nicht-kutane Krebserkrankung, die 15% aller Krebsdiagnosen des Mannes ausmacht. Er ist außerdem die zweithäufigste krebsbedingte Todesursache unter Männern in westlichen Ländern. Eine familiäre Vorbelastung, sowie zunehmendes Alter sind die wichtigsten Risikofaktoren. Das 10-Jahres-Risiko für 70-jährige Männer an Prostatakrebs zu erkranken liegt bei 5,50%. Die meisten Prostatakrebserkrankungen zeigen keine Tendenz zu einem aggressiven Verlauf und es besteht ein 2,5-3% Lebenszeitrisiko an Prostatakrebs zu versterben. Allerdings sind die klinisch-pathologischen Kriterien unzureichend für eine genaue Differenzierung zwischen langsam wachsenden und progredient verlaufenden Tumoren. Daher besteht eine Unsicherheit bezüglich des individuellen Risikos für eine aggressiv wachsende Krebsform. Eine der Herausforderungen in der aktuellen Prostatakrebsforschung liegt in der Identifizierung von Markern, die einen aggressiven Krankheitsverlauf prognostizieren können. Mithilfe dieser Marker könnten einerseits Übertherapie der klinisch nicht-relevanten Formen reduziert und andererseits Patienten mit einem erhöhten Risiko für einen trotz lokaler Therapie progredienten Krankheitsverlauf identifiziert und behandelt werden. Der Verdacht auf Prostatakrebs entsteht aufgrund eines erhöhten PSA Wertes sowie eines auffälligen digital-rektalen Untersuchungsergebnisses. Die Höhe des PSA Wertes korreliert jedoch nicht direkt mit dem Tumorstadium. Zur Diagnosesicherung ist eine feingewebliche Untersuchung der Drüsenmorphologie an Stanzbiopsien erforderlich. Diese werden nach dem Gleason Scoring-System eingeteilt. Die Heterogenität der molekularbiologischen Veränderungen im Prostatakrebs führt jedoch dazu, dass Patienten mit der gleichen Gleason-Score einen sehr variablen klinischen Verlauf entwickeln können.

Das Ziel meiner Arbeit war es, neue Erkenntnisse zu gewinnen über die molekularen Mechanismen, die zu aggressiven Prostatakrebserkrankungen führen. Der Schwerpunkt meiner Arbeit lag dabei auf der Untersuchung der molekularen und zellulären Veränderungen, die aus der Überexpression von ERG in *TMPRSS2:ERG* (T/E) Varianten resultieren.

Kapitel 1 liefert eine detaillierte Übersicht über die verschiedenen genetischen und molekularbiologischen Veränderungen, die zur Heterogenität des Prostatakrebses beitragen. Die überwiegende Mehrheit aller Prostatakrebserkankungen sind Adenokarzinome, die durch multifokales Wachstum luminaler sekretorischer Zellen entstehen. Diese Zellen weisen kontinuierliche histomorphologische Veränderungen auf, die von niedriggradiger Dysplasie bis hin zu einem 'carcinoma in situ' reichen und zusammenfassend als intraepitheliale Prostataneoplasie (PIN) bezeichnet werden. Prostatakrebs ist gekennzeichnet von einer komplexen Pathologie mit mehreren histologische Fokussen, die Ausdruck einer Mischung von mehreren genetischen und molekularbiologischen Veränderungen sind. Das Spektrum der genomischen Aberrationen, wie z.B. Punktmutationen, Kopienzahlvariationen, strukturelles Rearrangement und DNA Methylierungsveränderungen, spiegelt unterschiedliche molekulare Subtypen wider. Die am

häufigsten veränderten Signalwege sind die Signaltransduktion über Androgene, PTEN-PI3K/Akt, Ras/Raf/MEK/ERK und das Retinoblastom Protein (pRB). Diese sind vertärkt betroffen in metastasiertem Prostatakrebs. Auch sind im metastasierten Prostatakrebs große Genomabschnitte von Deletionen betroffen, was eine erhöhte genetische Instabilität in fortgeschrittenem Prostatakrebs vermuten lässt.

Androgene nehmen eine zentrale Rolle in der Entstehung und dem Fortschreiten von Prostatakrebs ein. Die hormonablative Behandlung gehört daher zu den primären Therapieoptionen des fortgeschrittenen Prostatakarzinom. Häufig tritt darunter jedoch ein Krankheitsrückfall und progressiver Verlauf hin zum kastrationsresistenten Prostatakrebs ein. Der neuroendokrine Prostatakrebs (NEPC) ist eine sehr aggressive Form des Prostatakrebses, die sich durch die Expression von neuroendokrinen (NE) Markern und fehlendem Ansprechen auf hormonablative Therapie vom Adenokarzinom unterscheidet.
Langfristig aktivierte Signaltransduktion über den Androgenrezeptor können zu Doppelstrangbrüchen der DNA führen und somit chromosomales „rearrangement" hervorrufen. Im Prostatakrebs wurden Genfusionen der ETS-Transkriptionsfaktoren beschrieben. Die T/E Genfusion ist die häufigste Genomveränderung im Prostatakrebs mit einer Prävalenz von 50% aller Tumore. Diese Genfusion resultiert aus der Fusion des Transkriptionsfaktors *ERG* mit dem androgensensiblen Gen *TMPRSS2* und begünstigt die Hochregulierung des ERG Proteins mit anschließender Aktivierung der ERG-Zielgene. Die Expression von Fusions-mRNA Molekülen von unterschiedlichen T/E Varianten ist assoziiert mit klinisch-pathologischen Parametern. Die molekularen Veränderungen, die als Folge der Expression von T/E Genfusionsvarianten auftreten, sind jedoch nicht ausreichend bekannt.

In **Kapitel 2** wurden die molekularen Veränderungen und funktionellen Auswirkungen der T/E Genfusion untersucht. Unter Verwendung eines Doxycyclin (Dox)-induzierbarem Überexpressionsmodel in LNCaP Zellen (LNCaP-T/E) konnte belegt werden, dass der TGF-β/BMP sowie der WNT/β-catenin Signalweg wichtige Regulatoren der T/E-vermittelten Epithelial-zu-Mesenchymal-Transition (EMT) in Prostatakrebszellen sind. Die Induktion der T/E Expression führte zur verstärkten Sekretion von TGF-β1 und -2 sowie erhöhter Expression von *ALK1*, einem Rezeptor der TGF-β Familie. ALK1 Hemmung in T/E exprimierenden Zellen blockierte die p38 Phosphorylierung und verringerte die Expression der TGF-β Zielgene *VIM*, *MMP1*, *CDH2* und *SNAI2*. T/E-Induktion führte auch zur verstärkten Zellmigration- und Invasion. Diese Ergebnisse deuten auf die ALK1-vermittelte TGF-β Signaltransduktion als onkogener Mechanismus in T/E positiven Prostatatumoren hin. Außerdem liefern diese Daten eine Grundlage für die Testung von ALK1-Inhibitoren bei der Behandlung von T/E positiven Prostatatumoren. Das lösliche rekombinante ALK1-Fc Fusionsprotein Dalantercept wird zurzeit in verschiedenen Krebsarten getestet und zeigte bereits Antitumorwirkung in unterschiedlichen Therapie-refraktären soliden Tumoren in Phase 1 (NCT00996957, NCT02024087) und Phase 2 Studien (NCT01642082, NCT01727336, NCT01720173), beschrieben in **Kapitel 5**. Des Weiteren konnten wir in **Kapitel 2** erhärten, dass der WNT/β-catenin Signalweg in T/E exprimierenden Zellen über den Frizzled Rezeptor FZD4 vermittelt wird. Die FZD4-

Inhibition hatte eine Reduktion der p38 Phosphorylierung zur Folge. Interessanterweise wurde eine Hochregulierung der microRNA *miR-503* ausschließlich in T/E Variant VI exprimierenden Zellen gefunden. Eine Überexpression der *miR-503* führte zur Reduktion von *SMAD7*, da als negativer Rregulator der TGF-β und WNT/β-catenin Signalwege bekannt ist. Die *miR-503*-vermittelte Reduzierung von *SMAD7* könnten ein 'escape' Mechanismus sein, der hemmenden Wirkung von SMAD7 auf TGF-β und WNT/β-catenin zu entkommen. Eine therapeutische Hemmung des FZD4-vermittelten Signalweges ist zurzeit nicht Gegenstand von klinischen Studien. Unterstützende Belege zur Möglichkeit einer FZD4-gezielten Therapie können abgeleitet werden von Studien, welche die selektiven Inhibitoren gegen FZD7 (Vantictumab) und FZD8 (Ipafricept) an HER2-negativen Brusttumoren (NCT01973309), Bauchspeicheldrüsenkrebs (NCT02005315), nicht-kleinzelligem Lungenkrebs (NCT01957007), und Eierstockkrebs (NCT02092363) testen.

In **Kapitel 3** wurde eine Analyse der epigenetischen Veränderungen als Folge der T/E Genfusion durchgeführt. Durch Überexpression der T/E Varianten zeigte sich ein globales Hypomethylierungsmuster. Die differentiell methylierten CpG-Orte befanden sich überwiegend in Gen-Körper Regionen. Eine integrative Analyse der epigenetischen und Genexpressionsveränderungen in LNCaP-T/E Zellen wies auf eine T/E-induzierte Hochregulierung von *FZD4* und *HLA-DMB*, die mit einem Verlust von DNA Methylierung einhergehen könnte. Ein direkter Zusammenhang zwischen DNA Hypomethylierung und mRNA Hochregulierung sowie eine Bestimmung der zugrundeliegenden Mechanismen der T/E-vermittelten epigenetischen Veränderungen konnte in der vorliegenden Analyse nicht erbracht werden. In Ergänzung zu den in **Kapitel 2** aufgeführten Diskussionspunkten könnte ein Zusammenhang zwischen der *FZD4* Hypomethylierung und mRNA Hochregulierung eine Basis sein für weitere Analysen zu der „druggability" von T/E fusionspositiven Tumoren.

In **Kapitel 4** wurde der Transkriptionsfaktor *INSM1* als Regulator einer neuroendokrine (NE) Differenzierung in Prostatakrebszelllinien identifiziert. Der neuroendokrine Prostatakrebs (NEPC) ist ein hochaggressives Karzinom, welcher oft in Kombination mit dem klassischen Adenokarzinom auftritt. In Patientenproben und in Zelllinien konnte ein Zusammenhang zwischen *INSM1* und der T/E Genfusion beobachtet werden. Experimentell führte die T/E Überexpression zur Hochregulierung von *INSM1* sowie zur verstärkten Expression von den NE Markern *TUBB3*, *SCG3*, *ASCL1*. Dies deutete daraufhin, dass die T/E Genfusion mit NEPC assoziiert sein könnte. Die gewebespezifische Expression und etablierte Funktion von *INSM1* in neuronalem und endokrinem Gewebe könnten von Vorteil sein bei der histologischen Diagnose von neuroendokrinem Prostatakrebs und als spezifisches ‚target' in der gezielten Therapie des NEPC. Die Re-Expression von *INSM1* in NE Tumoren erhielt Aufmerksamkeit in der ‚suicide' Gentherapie als tumorspezifische Behandlung des kleinzelligen Lungenkrebses und Neuroblastoms. *INSM1* Promoter-Konstrukte könnten potentiell Anwendung finden in der Diagnose und Verlaufskontrolle von NE Tumoren *in vivo*. In Ergänzung zu vorangegangen Studien, die auf beachtliche Ähnlichkeiten der Gensignaturen verschiedener NE Tumore hinweisen, zeigte auch die vorliegende Arbeit, insbesondere **Kapitel 4**, Übereinstim-

mungen in den genetischen und molekularbiologischen Veränderungen zwischen NEPC und bekannten NE Tumormodellen, wie zum Beispiel die Reelin Signaltransduktion. Dies lässt vermuten, dass weitere Erkenntnisse über die Mechanismen des NEPC abgeleitet werden könnten von den molekularpathologischen Mechanismen anderer NE Tumore und dass die ‚suicide' Gentherapie eine potentielle Strategie der gezielten Therapie im NEPC sein könnte.

Abschließend gilt für Prostatakrebserkrankungen, dass Marker für die verfeinerte Risikoabschätzung eines progredienten Tumorverlaufs benötigt werden. Verschiedene gewebsbasierte Multi-Genexpressionstests für die Einschätzung des aggressiven Prostatakrebses stehen bereits zur Verfügung. Ihre standardisierte Anwendung wird allerdings erschwert von den bekannten Herausforderungen der Prostatakrebsforschung, wie Heterogenität, Multifokalität und das eingeschränkte Probenvolumen aus der Stanzbiopsie. Die genetische Instabilität im Prostatakrebs erhöht die Komplexität der somatisch genomischen Aberrationen, welche zu spezifischen Kombinationen von ‚driver' Mutationen in einem Tumor führen. Die molekulare Pathologie ist jedoch ein schnell wachsendes Forschungsfeld, immer mehr ‚targets' werden entdeckt, die mit einer aggressiven Tumorbiologie korrelieren, wie zum Beispiel *AR* Spleißvarianten und Differenzierungsmarker einer neuroendokrinen Manifestation (zum Beispiel *INSM1* oder *L1CAM*). Letztere könnten zum Beispiel eine Einschätzung des Therapieansprechens auf eine hormonablative Behandlung ermöglichen. Aktuelle Studien zu neuen molekularen 'targets' werden in Kapitel 5 besprochen. Individuelle genetische Veränderungen können durch next generation sequencing erhoben werden und Anwendung finden für einen personalisierten Ansatz in der klinischen Praxis. Die molekularbiologische und genetische Klassifizierung am Biopsiematerial ist aktuell kein Bestandteil der Prostatakrebsrichtlinien. Sie könnte in Zukunft jedoch Einfluss haben auf die Standardtherapie des Prostatakrebses, wie es bereits am Beispiel des Brustkrebses, Melanoms und kürzlich auch des Lungenkrebses umgesetzt wurde. Gleichzeitig ist ein breiteres Spektrum an therapeutischen ‚targets' (in Ergänzung zur hormonablativen Therapie) dringend notwendig, damit die Behandlungsmaßnahmen für metastasierten Prostatakrebserkrankungen verbessert werden. Die funktionelle und mechanistische Untersuchung von genetischen Markern, wie in der vorliegenden Promotionsarbeit erarbeitet wurde, ist die Basis für die Entwicklung von neuen Diagnoseverfahren und könnte die Ausrichtung zukünftiger Forschungsvorhaben beeinflussen.

ACKNOWLEDGEMENTS

Most of the time, working on my thesis has been both a challenge and a pleasure. Always, collaborating with my mentors and colleagues has been a very special privilege. This part is about expressing my gratitude towards a number of people who have played a key part in my professional and personal life in the past years. Finishing my thesis with these notes of thanks is actually the nicest part, because it makes me rembering all the good things that happened.

With this, my first thank you goes to **Holger Sültmann**, for supervising my research: I cannot say how much I benefited from your scientific expertise and broad experience. Your constructive support and criticism helped me a lot to grow professionally and personally. You provided most valuable input that helped me constantly reflect on my research and to deal with all obstacles that came along the way. Under your supervision, I finally grew from a student to a reseacher.

I am more than thankful to **Frans Ramaekers**, who has been my first and most important mentor from my first days as a young A-KO on to the final revision of this thesis. Thank you for being a constant source of inspiration and motivation. I will not forget your visits to Heidelberg; after our TAC meetings, you always found the time for a friendly chat in a local pub.

Another big thank you goes to my co-supervisors **Sabine Klauck** and **Peter Altevogt**.
Sabine, you provided me the best possible support in terms of organizing my work and myself. Your eye for details has helped me to deliver results in a professional and productive manner. Your ingenious solutions saved many experiments and turned them into a success.

Peter, thank you for being such a inspiring mentor and coach. When I first came to Heidelberg, your warm hospitality made my start as a researcher in your group together with **Uwe**, **Nico**, **Kai** and **Natalie** an entirely pleasant and positive and experience. Your endless experience in so many different fields contributed to actually all subjects of my research. Your overwhelming enthusiasm about a promising result was very motivating and contagious to me. Sometimes, you knew better about the message of my results than I did.

I would also like to thank the members of the **Assessment committee**, **Prof. Manon van Engeland**, **Prof. Jack Schalken**, **Prof. Sascha Pahernik**, and **Prof. Marc Vooijs**, and **Supervisory committee** for investing the time and efforts to read this thesis and for giving me encouraging feedback. And also **Ralf Bischoff**, as a member of my Thesis Advisory Committee, you have given very valuable input which I am most thankful for.

Thank you, **Toon Van Gorp**, for opening many doors for me to my PhD studies and for bein such a reliable contact person in Maastricht.

Working with my **lab group** at the DKFZ in Heidelberg **– the awesome B063 –** has been a rewarding professional experience and a wonderful time of my personal life. Thank you, **Sabrina**, **Simon**, **Uwe**, **Steffen**, **Julia**, **Arlou**, **Sebastian**, **Doreen**, **Anja**, **Sabrina M.**, and **Simone**, thank you for all the laughing during lunch time, for the riddles, games and radio music that shortened hours of incubation time; for barbecues and selfmade Glühwein in the lab kitchen. With you, even the annual lab cleaning was fun. **Sabrina** and **Simon**, thank you for trembling with me for the countless qPCRs, migration assays or Western blots, and for being there for me when I got stuck in a huge cell culture experiment or when one of the machines did not wanted to work.

I was always happy about a distraction from the lab work by pub crawling with **Noemi**, **Micha**, **Uwe**, **Kay**, **Kathrin** any many others. Thank you for all the nights in O'Reilleys or the French corner pub that we did not want to end. **Lisa**, what a pleasure that I met you during my remaining months in Heidelberg at the PhD retreat. It was such a fun dancing with you all night long.

And I found more welcome distraction with my wind quintet **Kristina**, **Christa**, **Martin** and **Renate**, as well as with the Collegium Musicum Orchestra in Mannheim. Thank you for the nice chats. Playing with you gave my thoughts a break from research. And after some exciting pieces I was refreshed to return to the lab life. **Timmy** and **Karolina**, thank your for being loyal visitors of our concerts in Mannheim.

Kevin, **David** and **Caro**, thank you for your friendship and for your encouraging words that kept me going my way.

Helmut and **Annette**, thank you for your genuine interest in my research, and for your support with proofreading the German summary.

Alex, Tali, and **Nora**, while you live remotely, I still feel that we are close whenever we manage to meet. Thank you for this!

My dear family: my parents, **Edda** and **Michael**, with your support and your love I have made it so far. My sisters and my brother, **Saskia**, **Mirjana**, and **Nicolai**, thank you for your patience and your confidence in me. **Christian**, **Tim**, and **Hans**, **Judith**, and **André**, for me it is a big gift having you as part of our family. **Tante Schmitzi**, thank you for your love and care.

And finally, a very special thank you to **Tobias**. Thank you for all the moments we can share, your advice, patience, especially during this last, most stressful year, and your love.

CURRICULUM VITAE

Leonie Ratz was born on the 23rd of March 1987 in Cologne, Germany. After finishing her pre-university education (Abitur) at the Kaiserin-Augusta School in Cologne in 2004, she pursued her bachelor studies in 'Molecular Life Sciences' at the Maastricht University in the Netherlands.
Her fascination about the combination of scientific research and medical care encouraged her to enroll in the master program 'Medical Doctor and Clinical Resarcher' (A-KO) at Maastricht University. After finishing her studies, she performed a scientific internship at the German Cancer Research Center (DKFZ) in Heidelberg, Germany. In 2013, she started her PhD studies in the field of cancer genome research under supervision of Prof. H. Sültmann and in collaboration with Prof. F.C.S. Ramaekers at GROW, Maastricht University. During her PhD research, Leonie worked on the identification of novel driver genes in aggressive prostate cancer with special emphasis on the role of the *TMPRSS2:ERG* gene fusion. She now works as resident physician at the department of Gynecology and Obstetrics in the Augustinian hospital in Cologne.

PUBLICATION LIST

J.M.A. Pickl, D. Heckmann, **L. Ratz**, S.M. Klauck, H. Sültmann. Novel RNA Markers in Prostate Cancer: Functional Considerations and Clinical Translation. Biomed Res Int. 2014: 765207.

L. Ratz, P. Altevogt, S. M. Klauck and H. Sültmann. The biology of aggressive prostate cancer: Implications for innovative diagnostics and therapy. *In preparation for submission as review*.

L. Ratz, M. Laible, L.A. Kacprzyk, S.M. Wittig-Blaich, Y. Tolstov, S. Duensing, P. Altevogt, S.M. Klauck, and H. Sültmann. *TMPRSS2:ERG* gene fusion variants induce TGF-β signaling and epithelial to mesenchymal transition in prostate cancer cells. Oncotarget. 2017; 8(15):25115-25130.

L. Ratz, S. Bauer, P. Altevogt, S. M. Klauck and H. Sültmann. *INSM1* induces a neuroendocrine phenotype in prostate cancer cells. *TMPRSS2:ERG* overexpression induces changes in the epigenetic signature of human prostate cancer cells. *In preparation*.

L. Ratz, P. Altevogt, S. M. Klauck and H. Sültmann. *INSM1* induces a neuroendocrine phenotype in prostate cancer cells. *In preparation*.